The Influence of Magnetic Field on Wear in Sliding Contacts

A thesis submitted for the degree of Doctor of Philosophy

By

Yutaka Makida

Mechanical Engineering School of Engineering and Design

Brunel University

September 2010

Abstract

The influence of the horizontal magnetic field has not been sufficiently studied in contrast to study activity on the influence of the vertical magnetic field by researchers. The reason was that the influence of horizontal magnetic field to change the wear mass loss of ferromagnetic materials is smaller compared to the vertical magnetic field. However, the influence of horizontal magnetic field on rolling contact changes the subsurface crack initiation point toward surface is postulated by a researcher. Therefore, it is significance finding out how the horizontal magnetic field influences the tribological characteristics. This thesis presents a study on the influence of the horizontal magnetic field on wear in sliding contacts contributes for ascertainment the effect and mechanism of horizontal magnetic field on tribological characteristics of sliding contacts, through the experimental approach.The static magnetic field with densities of 0 and 1.1 Tesla and different orientations was applied to different contact conditions, different surface modifications and two sliding frequencies, using a ball-on-plate contact configuration. In conclusion, the presence of magnetic field enhances the chemical adsorption between iron or oxide iron and oxygen, and causes the transition of adhesive wear to oxidative wear. Besides, the presence of magnetic field combined with low sliding frequency forms the bulging on the wear surface and weakens the prevailing wear mechanism due to the low frictional temperature. On the other hand, the presence of magnetic field combined with high sliding frequency induces the transition to the oxidative wear mechanism and reduces the wear. Also, distinctly different appearances of wear surface are created by different magnetic field orientations. In the lubricated sliding contact, the magnetic field causes

the reduction of wear and induction of oxide. It is postulated that the presence of magnetic field enhances the oxygen adsorption on the wear track by iron wear particles and hence varies the tribological behaviour. The influence of magnetic field on carbon steel coating consists in changes of oxide iron layer and steel layer, alterations of mechanical properties of the coating, and decrease in the mass loss and the surface roughness on the dry sliding contact. All these could be suggested the influence of adhesive strength of the interface between the base material and coating.

ACKNOWLEDGEMENTS

I would like to express my sincere gratitude to supervisor Professor T. A. Stolarski for his assistance in creating this thesis. I would also like to express my deepest gratitude to Professor Shogo Tobe, who has been a university professor in Ashikaga Institute of Technology, for supply of test samples coated in thermal spray process. This study would not have been possible without their advices, knowledge and assistance.

Thanks to all of my colleagues. In particular, I would like to acknowledge Dr M. Yamane's contribution in the form of test samples and analysis data. Also, I would like to thank Dr P. Vongbandit for his valuable advices.

I would like to express my gratitude to Mr Keith A. Withers for his assistance and advices in the laboratory works. Moreover, I would like to thank Paul and other technicians in the workshop for their help in modifying test jig.

I would like to thank members of staff working in the ETC team for their operational assistance in analysis and observation by SEM and XRD. Particularly, I would like to express my deepest appreciation to Nita Verma and Lorna Anguilano.

Finally, I would like to express my immense gratitude to my family and friends for their support. I cannot express in words gratitude to my parents Katuyosi and Mihoko for

calmly awaiting me in Japan. Then, I am indebted to my big brother Masayoshi for his unwavering support. Also, I would like to thank my younger sister Hisako for her hopeful smile. I would also like to express deepest gratitude to my grandfather Eisaku and grandmother Harue who financed me during their life.

I dedicate this thesis to my grandparents who have been called to heaven.

Table of contents

List of Figures

Chapter 5

List of Tables

Nomenclature

Chapter 1

H_s	alternating magnetic field
σ_0	flow stress
σ_i	Internal stress
H	magnetic field of strength
P	total load
v	sliding velocity
t	sliding time
H_0	no magnetic field
H_{ver}	vertical magnetic field
H_{hor}	horizontal magnetic field
D	sliding distance

Chapter 2

a	contact area dimensions as circle
W	total load
P_{max}	maximum contact pressure
$P_{average}$	average contact pressure
δ	maximum deflection at the centre of the contact
τ_{max}	maximum shear stress
z	depth at which maximum Shear Stress Occurs
E'	reduced Young's modulus
R'	reduced radius of curvature
E_A, E_B	young's moduli of the contacting body A and B
ν_A, ν_B	Poisson's ratios of the contacting bodies A and B
R_x, R_y	reduced radii of curvature in x- and y-axis direction
R_{ax}, R_{ay}	radius of the sphere and the flat surface
σ	principal normal stress
τ	principal shear stress
P	the total normal load
P_0	maximum pressure is given by the Hertz theory
ϕ	Angle
μ	friction coefficient
q	stress normal to the interface
k	shear yield stress of the material (the maximum shear stress)
h_c	central film thickness
h_0:	minimum film thickness
U	entraining surface velocity
η_0	viscosity at atmospheric pressure of the lubricant
R'	reduced radius of curvature
h_c	central film thickness

α	pressure-viscosity coefficient
K	ellipticity parameter defined
$\sigma_{A,B}$	root mean square roughness values of body A and B
h_0	minimum film thickness
Λ	parameter characterizing the ratio of minimum film thickness to the composite surface roughness
B	magnetic flux density
μ_0	Permeability
I	intensity of magnetization
K	magnetic susceptibility,
Tc	curie point
Br	the remanent flux density and is the residual
BHc	coercive force

Chapter 3

V_t	thermal velocity
η	Viscosity
ρ	density of fluid
r	radius of the ball
m	weight of ball
g	gravitational acceleration, 980.7 cm/s2
y	distance of tall large measuring cylinder
$t_{average}$	measured velocity average
P	contact load
P_m	attractive force
P_l	normal load
d	diameter of ball
l	length, dimension of the plate specimen
w	width, dimension of the plate specimen
t	thickness, dimension of the plate specimen
μr	relative Permeability
F	magnetic force
B	magnetic flux density
H	coercive force
F_1	effect force and is the attractive force which calculated from Equation (3.5.1)
F_2	load (force)
l_1	distance from load force to fulcrum
l_2	distance from effect force to fulcrum
F_3	dead load
F_4	total load on contact
l_3	distance from total load to fulcrum

List of abbreviations

Chapter 1

SEM	scanning electron microscope

Chapter 2

EHL	elastohydrodynamic lubrication

Chapter 3

APS	atmosphere plasma spray
EHD	Elastohydrodynamic
FEA	finite Element Analysis
RMS	root mean square roughness
XRD	x-ray diffraction

Chapter 1 Introduction

1.1 General introduction

Wear occurs when one surface moves over another. Wear is a common phenomenon which occurs due to rubbing of two surfaces and is causing decrease in the volume of the materials. The phenomena of wear are studied by Tribology which is one of the new sciences established in 1967 by a committee of the Organization for Economic Cooperation and Development (OECD). The studies of tribology include the technology and science which relate to a surface phenomenon or process of interaction by bodies in relative motion. It is well recognized that the results of tribological research have contributed to the improvement of performance of rotary and reciprocating motion machines and are important for the reduction of natural resources and energy savings.

In the studies which took place half a century ago, a number of researchers noticed the influence of the magnetic field existing around a magnet and a coil on tribological behaviour. It has been confirmed that the mass loss by wear is affected by the existence of the magnetic field. (Muju and Radhakrishna 1986; Zaidi et al., 2001; Iida, 2007) These results also mean that the control of the tribological behaviour with magnetic fields is possible. In other words, it will be possible to reduce the wear loss and prolongs the service life of machines. Therefore, this study has potential application to improve wear residence of railway rails and railway wheels and to improve performance of bearings. However, the influence of horizontal magnetic field on tribological behaviour is not fully understood at present.

This thesis presents results of a study on the influence of the horizontal magnetic field on the performance of sliding contacts. Few researchers have studied the influence of

this type of magnetic field on tribological behaviour. Three types of wear tests were carried out under the presence of horizontal magnetic field, for dry sliding contacts, lubricated sliding contacts and high frequency sliding contacts.

1.2 Background

The influence of the magnetic field on friction has been studied by a number of researchers using various experimental methods in order to clarify its effect on material properties and material behaviour. This section reports on the effect of the magnetic field described in published experimental research.

1.2.1 Influence of magnetic field on material characteristics

According to Chikazumi (1964), the magnetization is insensitive to the applied low stress in the demagnetised state where the ferromagnetic material is not magnetizing. Besides, the magnetic field influences the plasticity of a ferromagnetic material according to Muju and Ghosh (1977), refer to Figure 1.1.

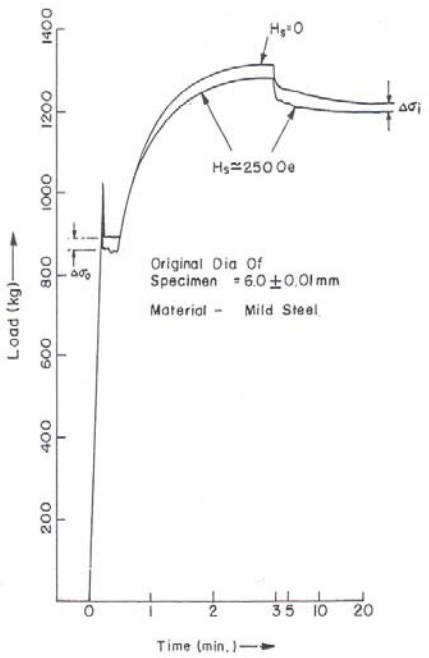

Fig 1.1 Stress relaxations in mild steel by application of magnetism (Muju and Ghosh, 1977)

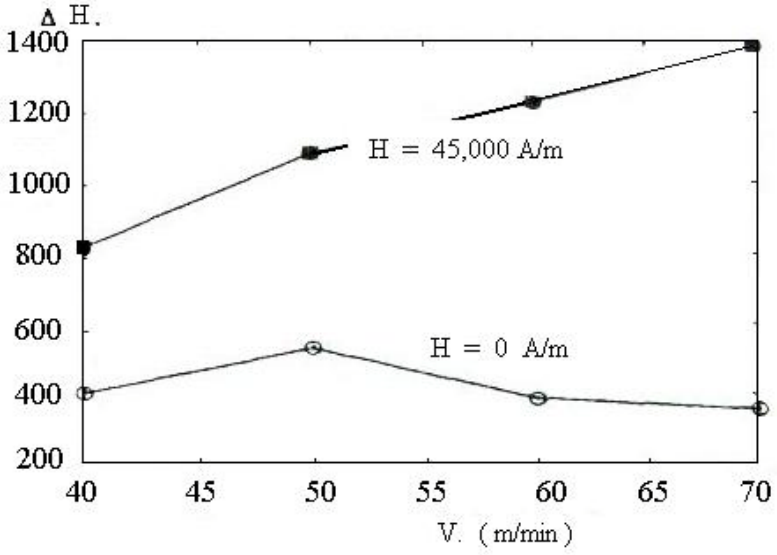

Fig 1.2 Micro hardness of sliding surface of XC48 disc in a copper pin on XC48 disc; P = 8 N; sliding time t = 60 min. (Mansori et al., 1996)

Also, it is confirmed by several researchers that the magnetic field changes the micro hardness and mechanical properties of a material. The micro hardness of the wear surface is an important factor for the tribological behaviour. Mansori et al. (1996) performed Vickers micro hardness measurements for the sliding surface of the ferromagnetic materials under the conditions of the magnetic field of H=4.5x10^4 A・m^{-1} and no magnetic field. The results are shown in Figure 1.2, where it is seen that the presence of vertical magnetic field to sliding surface increased micro hardness. Not only Mansori but also Zaidi et al. (2001) reported that the vertical magnetic field to sliding surface increased micro hardness of sliding surface.

1.2.2 Comparison of Effects Created by Vertical Magnetic Field and Horizontal Magnetic Field

A number of researchers have reported that vertical type of magnetic field reduces wear amount of ferromagnetic materials. For instance, Kanji and Pal et al. (1969) observed reduction of the mass loss of a tool. They studied the effect of external superimposed current while making a hole by a drill. Hiratsuka et al.（1986） presented the difference of the effects caused by two kinds of external magnetic field. The experiment was performed with a ferromagnetic pin sliding against a ferromagnetic disc at atmospheric environment. As shown in Figure 1.3 and 1.4, the wear mass loss increased when a horizontal magnetic field was applied. This is in contrast to the total wear for no magnetic field H_0 and that for vertical magnetic field H_{ver}. Besides, the reason for reduced mass loss when a vertical magnetic field H_{ver} was applied is that in an early period of sliding wear behaviour changed from a severe wear to a mild wear. When a horizontal magnetic field H_{hor} was applied the severe wear continued. The same was found to be true for no magnetic field. The wear surfaces of the pin and the disc to which the horizontal magnetic field H_{hor} was applied, are shown it Figure 1.5 and it could be seen that the severe wear took place.

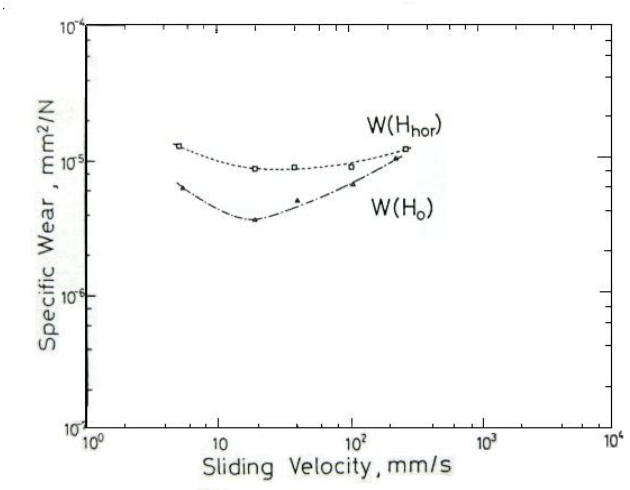

Fig 1.3 Comparison of specific wear with the effect of horizontal magnetic field and no magnetic field to sliding surface, Ferromagnetic materials of nickel in air was used in the wear test in air, P = 9.8N; D = 200 m

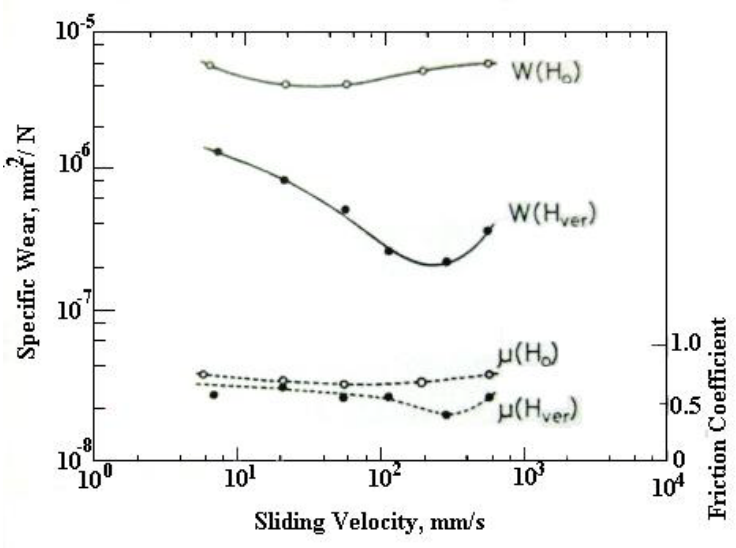

Fig 1.4 Comparison of specific wear and friction coefficient, when vertical magnetic field H_{ver} to sliding surface was applied and no magnetic field H_0

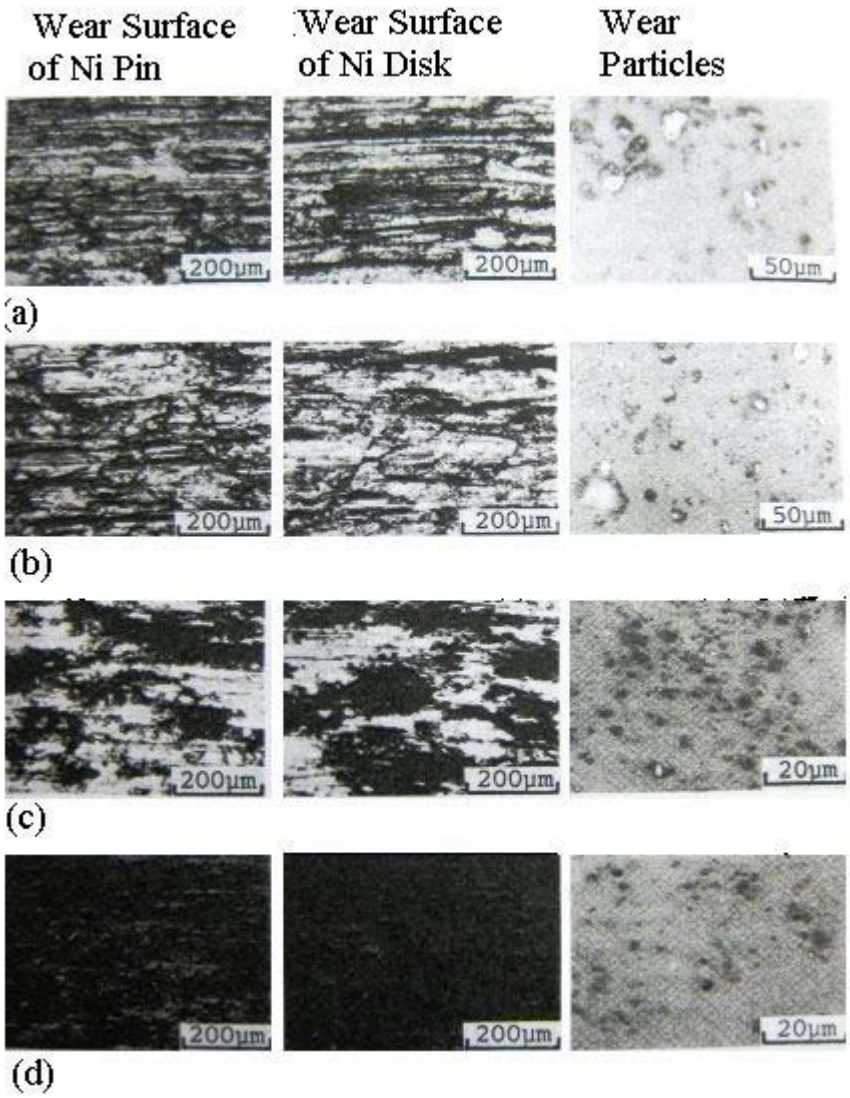

Fig 1.5 Comparison of wear surface of the pin, disk and wear particles, with (a) no magnetic field H_0, v=55.0 mm・s^{-1}; P= 11.0 N, (b) horizontal magnetic field H_{hor} v=39.0 mm・s^{-1}; P= 9.8 N, (c) vertical magnetic field H_{ver} v=6.59 mm・s^{-1}; P= 11.0 N and (d) vertical magnetic field H_{ver} v=290 mm・s^{-1}; P= 11.0 N in air. Materials are nickel. (Hiratsuka et al., 1986)

1.2.3 Oxidization Activity by Magnetic Field

Yamamoto and Gondo (1987) concluded that the surface activation energy was increased by magnetization. Contrary to their report, Muju and Radhakrishna (1980) stated the decrease of the wear activation energy with a magnetic field. Kumagai et al. (1993) reached the conclusion that a magnetic field reduced the wear activation energy.

In addition, they expressed the view that magnetization promoted generation of the minute particles and oxidization of the wear particles because the wear debris were attracted by magnetic force and were held in the contact area.

1.2.4 Effect of Magnetic Field on Wear Mass Loss

Iida (2007) investigated the effect of horizontal magnetic field on rolling contact of steel discs operating under several contact conditions using a two discs type machine. He clarified the mechanism of crack initiation and suggested a crack initiation model in a Hertzian contact with magnetic field. He also investigated magnetization of ferromagnetic material and its relation to energy status. He examined the relation between the debris thickness and the location of crack initiation due to rolling and arrived at the conclusion that there were certain relations between them.

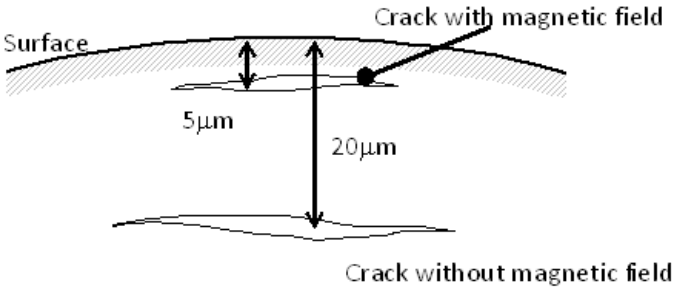

Fig 1.6 Differences in crack initiation location at undersurface with and without magnetic field (Iida 2007)

1.3 Aim and Objectives of the Thesis

The aim of this thesis was to examine the effect of horizontal magnetic field on sliding contact wear and to clarify the mechanism of magnetic field action.

Specific objectives of this research were to experimentally investigate the effect of horizontal magnetic field on sliding contact performance. In particular, the effect of the direction of magnetic field, its influence on lubricated contact, its consequences for two different magnetic coating materials and two sliding frequencies were examined. The experiments are carried out using a ball-on-plate sliding contact machine.

1.4 The Outline of the Thesis

Chapter 1 Introduction

Chapter 1 presents a brief introduction to the concepts of tribology, and the importance of the influence of magnetic field on tribological behaviour. It also discusses the relevant background of recent research pertinent to the influence of magnetic field. Additionally, this chapter summarizes the objectives and presents a brief overview of the thesis.

Chapter 2 Mechanisms

This chapter presents the mechanism of dry and lubricated sliding contact. Also, it explains fundamentals of the magnetism, the physics of magnetism and the origins of wear.

Chapter 3 Methodology

This chapter describes two apparatuses, materials, loading conditions, experimental procedure and test techniques. Firstly, it describes the main parts of friction machines A and B and samples used in experiments. Next, it describes the loading conditions under the influence of magnetic field, and results are shown. Then it describes initial influence of the static magnetic field estimated through FE analysis. Finally it gives details on experiment procedures and experiment techniques.

Chapter 4 Experimental Results

This chapter presents the experimental results obtained during sliding contact experiments in the presence and absence of the magnetic field. It is divided into the introduction and three main sections. Firstly, it presents the influences of magnetic field on dry sliding contact experiment. Also, it presents the influences of the orientation of

magnetic field. Moreover, it compares the influence of the magnetic field on two types of thermal spray coating. Secondly, it presents the effect of different magnetic field strengths on lubricated sliding contact. Finally, it presents the influences of magnetic field on high frequency sliding contacts formed by various materials.

Chapter 5 Discussions

This chapter discusses the complex questions of magnetic field effects on sliding contacts raised by experimental results, and it suggests the wear mechanism of sliding contacts in the presence of magnetic field. Firstly, it presents introduction of chapter 5 and describes the whole effect of magnetic field on sliding contacts. Secondly, it compares the effect of magnetic field on sliding contact with that on rolling contact. Thirdly, it presents the effect of magnetic field on the carbon steel coating. Then, results of lubricated sliding contact experiments are outlined. Finally, it discusses the relationship between oxidative wear and the effect of magnetic field.

Chapter 6 Conclusions and Future work

Chapter 6 presents the conclusions of the thesis and recommendations for future work.

References for chapter 1

Chikazumi, S., (1964) *PHYSICS OF MAGNETISM*: John Wiley & Sons, Inc., pp.433-434

Kanji, M. and Pal, K., (1969) Proceedings of the 3rd AIMTDR conference, Bombay

Kumagai, K., Suzuki, L. and Kamiya, O., (1993) "Study on Reduction in Wear due to Magnetisation", *Wear*, vol. 162-164, pp. 196-201.

El Mansori, M., Zaidi, H., Kardiri, K, E. and Paulmier, D., (1996)"Surface modifications of a non-ferromagnetic copper/ferromagnetic steel XC48 couple in magnetized sliding contact", *Surface and Coatings Technology*, vol. 86-67, pp. 511-515.

Hiratsuka, K., Sasada, T. and Norose, S., (1986) "THE MAGNETIC EFFECT ON THE WEAR OF METALS", *Wear*, vol. 110, pp. 251-261.

Iida, Y., Stolarski, T, A. and Sato, K., "Surface damage resulting from rolling contact operating in magnetic field", PhD. Thesis, University of Brunel, 2007 pp.109-110, 120-122

Muju, M, K. and Ghosh, A., (1977) "A model of adhesive wear in the presence of a magnetic field", *Wear*, vol. 41, pp. 103-116.

Muju, M, K. and Radhakrishna, A., (1980)"Wear of non-Magnetic materials in the Presence of a Magnetic Field", *Wear*, vol. 58, pp. 49-58.

Yamamoto, Y. and Gondo, S., "Effect of a magnetic field on boundary lubrication", Tribology International, Vol. 20, (1987), pp. 342-346.

Zaidi, H., Chin, J, K. and Frene, J., (2001) "Analysis of surface and subsurface of sliding electrical contact steel/steel in magnetic field", *Surface and Coatings Technology*, vol. 148, pp. 241-250.

Chapter 2 Mechanisms

2.1 Introduction

Sliding contact usually results in damages of surface and subsurface regions of contact area and produces wear particles. Also, high frequency reciprocating motion induces chemical phenomena such as rusting of wear debris and surface interactions of ferro-material. Finally, lubrication of a sliding contact induces decrease of wear due to separation of interacting surfaces by a lubricating film.

It is known that vertical magnetic field affects mechanical, physical and chemical properties of ferro-materials. Therefore, it is important to understand the fundamental knowledge relating to sliding contact and magnetic field action. This chapter presents the fundamental knowledge concerning the influence of magnetic field on sliding contact.

2.2 Mechanism of dry sliding contact

2.2.1 Contact stresses

Interaction of surfaces is in the finite area and results in plastic or elastic deformations and a high contact pressure is produced because the contact region is small. Hence, it causes damage within the contact region in the form of crack initiation and propagation. The stress analysis of the concentrated contact can be carried out using Hertz theory (1881). The geometry used during testing consists of a contact between a sphere and a flat plate, as shown in Figure 2.1 (Stachowiak 2005). The contact area between two bodies is enveloped by a circle or an ellipse, and the formulae for the main contact

parameters of the sphere and the flat surface in contact, as shown in the figure, are summarized as follows:

$$a = \left(\frac{3WR'}{E'} \right)^{1/3} \tag{2.1}$$

$$P_{\max} = \frac{3W}{2\pi a^2} \tag{2.2}$$

$$P_{average} = \frac{W}{\pi a^2} \tag{2.3}$$

$$\delta = 1.0397 \left(\frac{W^2}{E'^2 R'} \right)^{1/3} \tag{2.4}$$

$$\tau_{\max} = \frac{1}{3} P_{\max} \tag{2.5}$$

$$z = 0.638a \tag{2.6}$$

where

a ; the contact area dimensions as circle
W ; the total load
P_{max} ; the maximum contact pressure
$P_{average}$; the average contact pressure
δ ; the maximum deflection at the centre of the contact
τ_{max} ; the maximum shear stress
z ; the depth at which maximum Shear Stress Occurs
E' ; the reduced Young's modulus
R' ; the reduced radius of curvature

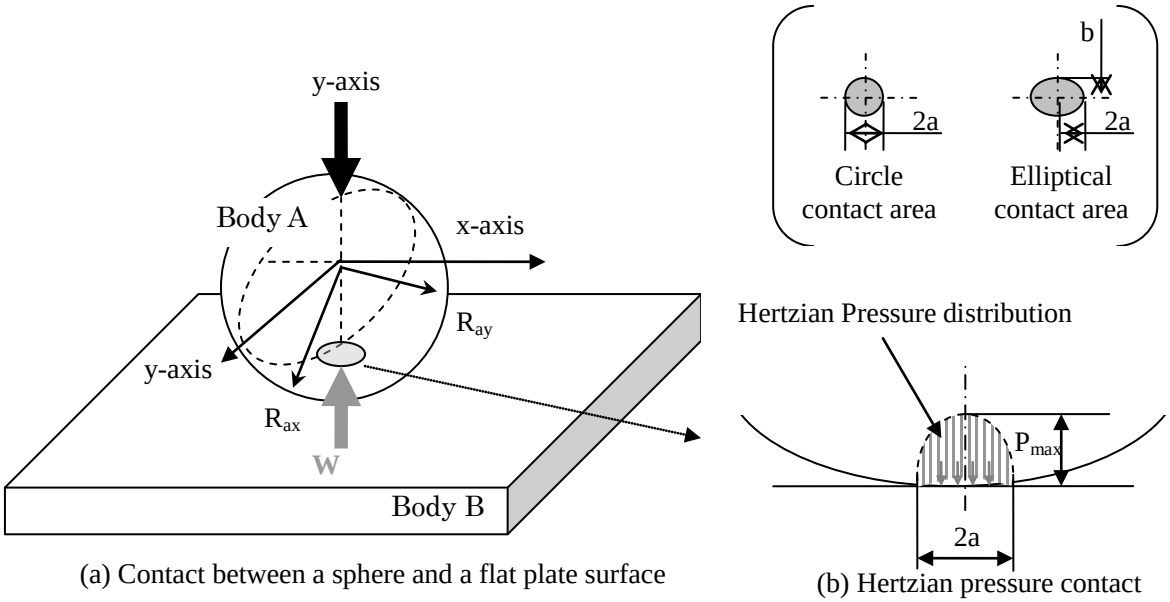

(a) Contact between a sphere and a flat plate surface

(b) Hertzian pressure contact

Fig 2.1 Hertzian pressure contact between a sphere and a plate surface

Reduced Young's modulus for contact between the sphere and the flat surface is expressed as:

$$\frac{1}{E'} = \frac{1}{2}\left[\frac{1-\nu_A^{\ 2}}{E_A} - \frac{1-\nu_B^{\ 2}}{E_B}\right] \tag{2.7}$$

where

E_A, E_B; young's moduli of the contacting body A and B
ν_A, ν_B; Poisson's ratios of the contacting bodies A and B

Since the radii of body A and body B applies so that $R_{ax}=R_{ay}=R_A$ and $R_{bx}=R_{by}=\infty$, respectively, the reduced radii of curvature in x- and y- axis are given by:

$$\frac{1}{R'} = \frac{1}{R_x} + \frac{1}{R_y} = \frac{1}{R_{ax}} + \frac{1}{R_{bx}} + \frac{1}{R_{ay}} + \frac{1}{R_{by}} = \frac{1}{R_A} + \frac{1}{\infty} + \frac{1}{R_A} + \frac{1}{\infty} = \frac{2}{R_A} \tag{2.8}$$

where

$R_x = R_y = R_A$
R_x, R_y; reduced radii of curvature in x- and y-axis direction
R_{ax}, R_{ay}; radius of the sphere and the flat surface

According to Lawn (1998), subsurface stress contours can be depicted as in Figure 2.2 for a contact of ceramic ball on a ceramic flat plate. It is assumed to be similar to subsurface stress contours at frictionless initial sliding contact.

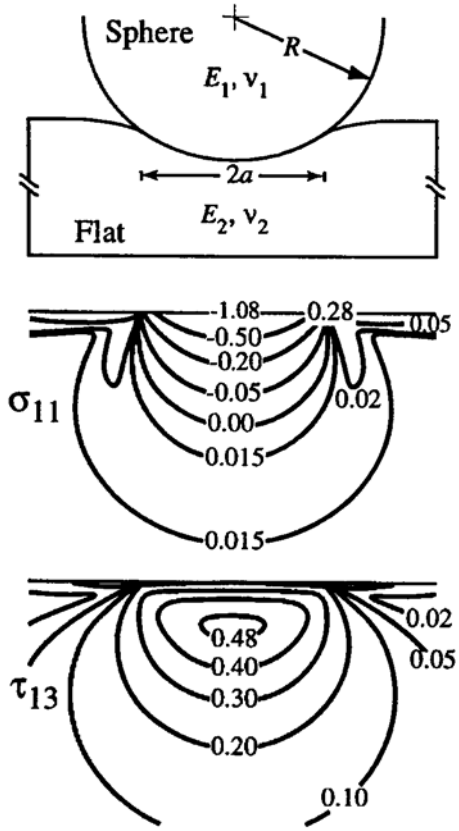

Fig 2.2 Subsurface stress contours for a ceramic ball on the ceramic plate is principal normal stress σ and principal shear stress τ (after Lawn 1998)

2.2.2 Sliding contact

Basically the friction of material surface is produced by rubbing a loaded spherical slider over a flat of the material being tested in absence of magnetic field, and it generates a quasi-static stress field (see Figure 2.3). Hence, the tangential traction *q(r)*, which is due to sliding parallel to the x-axis everywhere in the contact area, is expressed by Amontans' law of friction as below;

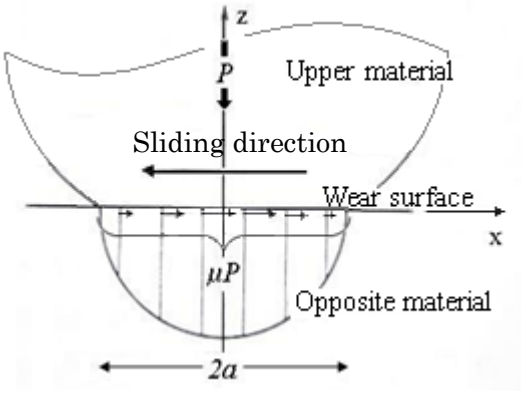

Fig 2.3 Illustration of a circular sliding contact

$$q(r) = \frac{3\mu P}{2\pi a^3}\left(a^2 - r^2\right)^{1/2}, \quad r < a \tag{2.9}$$

Where

a; the size of the circular contact area
P; the total normal load
μ; the friction coefficient ($\mu \neq 0$)

Besides, the Hertz pressure that is exerted between two frictionless elastic bodies of revolution in contact, is given by Hertz theory as follows,

$$P(r) = P_o \frac{\left(a^2 - r^2\right)^{1/2}}{a} \tag{2.10}$$

where

P_0; the maximum pressure is given by the Hertz theory

Crack formation

The tangential traction causes a shear stress exerted along the interface of body B, as shown in Figure 2.4. The action on subsurface stress field is related to crack formation and the subsequent surface failure. It is important that the effect of sliding on the subsurface stress distribution and crack initiation is considered. The frictional force causes a shear stress to be exerted along the plane of interface but it is rotated by an angle ϕ. The magnitude of the angle ϕ is given by the follows equation;

$$\phi = \frac{1}{2}\cos^{-1}(\mu q / k) \qquad (2.11)$$

where

μ; the friction coefficient
q; the stress normal to the interface
k; the shear yield stress of the material, (the maximum shear stress)

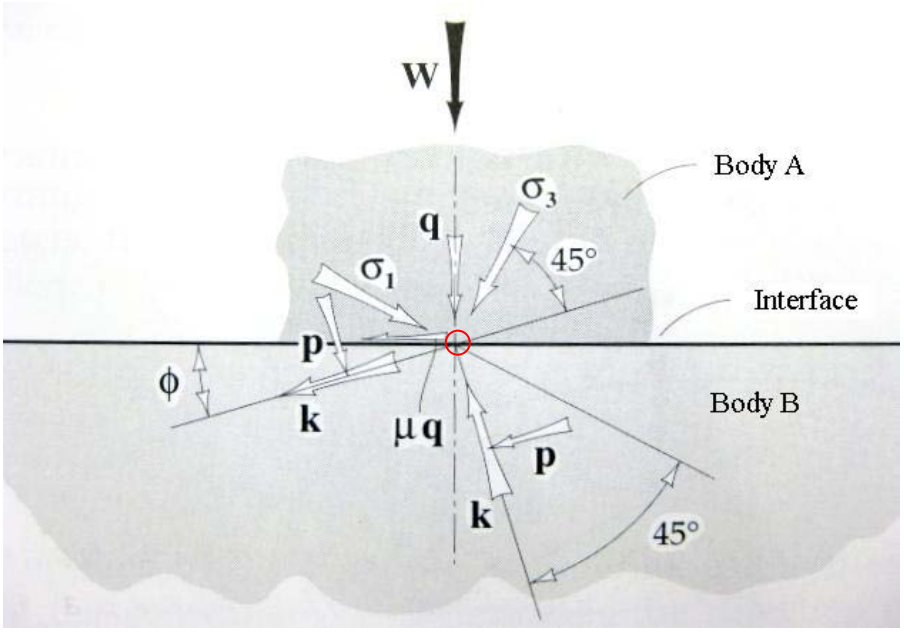

Fig 2.4 Angle ϕ of stress in a contact with sliding (Stachowiak 2005 p.291) σ_1 and σ_3: the principal stresses p: the hydrostatic pressure

2.3 Mechanism of lubricated sliding contact

In lubricated sliding contact, it is interposed lubricating oil between two contacting bodies. Additionally, lubricating oil separates the opposing surface of a concentrated contact and prevents direct contact. However, under concentrated contact condition, high load is applied over an extremely small contacting area hence the elastic deformation cannot be ignored. (Dowson and Higginson 1977: Hamrock and Dowson 1981: Gohar 1988) Therefore, it is necessary to calculate the film thickness, in order to find out the ratio of minimum film thickness to composite surface roughness. The end constriction to the EHL film is for a 'point' contact. The minimum film thickness in a point contact is found at both ends of the 'horseshoe' and at these locations the film thickness is only about 60% of its central value (see Figure 2.5). Figure 2.5 shows a case of two steel balls in contact to get an overview of the minimum film thickness, the central film thickness and the pressure distribution. Equations (2.11) and (2.12) are Elastohydrodynamic Film Thickness Formulae, provide the information about EHL (Stachowiak 2005 p.318). The formulae are substituted and the reduced Young's modulus *E'* is given by Equation (2.7).

$$\frac{h_c}{R'} = 2.69\left(\frac{U\eta_0}{E'R'}\right)^{0.67}(\alpha E')^{0.53}\left(\frac{W}{E'R'^2}\right)^{-0.067}\left(1-0.61e^{-0.73k}\right) \tag{2.11}$$

$$\frac{h_0}{R'} = 3.63\left(\frac{U\eta_0}{E'R'}\right)^{0.68}(\alpha E')^{0.49}\left(\frac{W}{E'R'^2}\right)^{-0.073}\left(1-e^{-0.68k}\right) \tag{2.12}$$

where

h_c; the central film thickness
h_0; the minimum film thickness
U; the entraining surface velocity, i.e., U= (U_A+U_B)/2, where the U_A and U_B refer to the velocities of bodies A, B
η_0 ; the viscosity at atmospheric pressure of the lubricant

R'; the reduced radius of curvature
α ; the pressure-viscosity coefficient
W; the contact load
K; the ellipticity parameter defined as k=a/b, where 'a' is the semi axis of the contact ellipse in the transverse direction and 'b' is the semi axis in the direction of motion

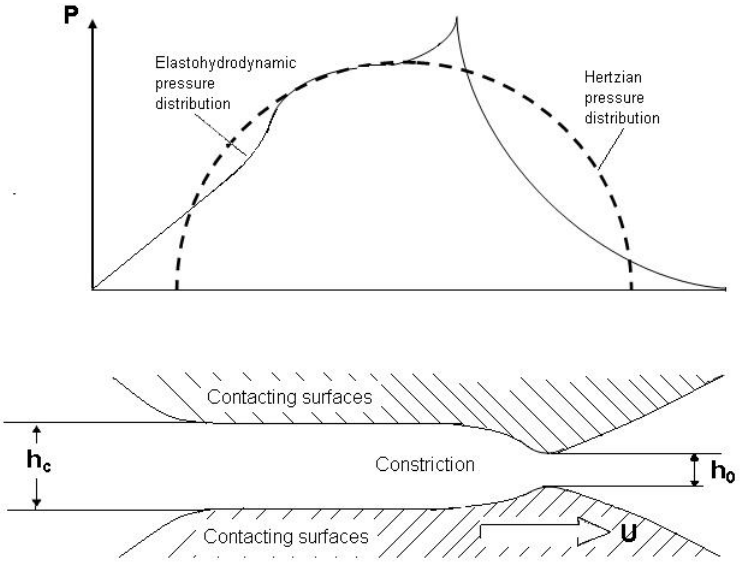

Fig 2.5 Elastohydrodynamic pressure distribution and illustration of film thickness h_c and h_0 (Stachowiak 2005 p.317)

To evaluate effectiveness of EHL film thickens, parameter λ is used as shown in Figure 2.6 (Tillian, 1967). The condition of two RMS surface roughnesses of bodies in contact affects the ratio of the minimum film thickness to the roughness of contacting surface, and is given by the following equation:

$$\lambda = \frac{h_0}{\left(\sigma_A{}^2 + \sigma_B{}^2\right)^{0.5}} \tag{2.13}$$

where

$\sigma_{A,B}$; the root mean square roughness values of body A and B
h_0 ; the minimum film thickness
λ ; the parameter characterizing the ratio of minimum film thickness to the composite surface roughness

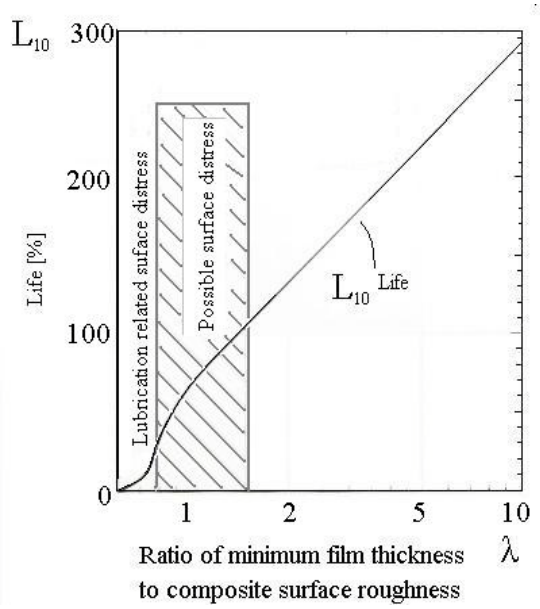

Ratio of minimm film thickness to composite surface roughness

Fig 2.6 Relationship of Ratio of minimum film thickness and contact fatigue life (Tallian 1967)

2.4 Magnetism

2.4.1 Magnetization

When ferromagnetic material is in a magnetic field of strength H magnetic flux density B is given in the following expressions:

$B=I+\mu_0 H$

where

μ_0; the permeability,

I ; the intensity of magnetization, magnetic moment per the unit volume

The magnetic moment is expressed as:

$I=\kappa H$

κ is a substance-specific constant called the magnetic susceptibility. It classifies materials roughly into diamagnetic materials (κ: 10^{-6}), paramagnetic substance (κ: $10^{-3} \sim 10^{-5}$), and ferromagnetic materials (κ: $10^{2} \sim 10^{4}$). Paramagnetic material and ferromagnetic material are attracted in the magnetic field. The ferromagnetic materials which are α-Fe, Co and Ni, are characteristic of magnetic maintenance of the magnetism known as permanent magnet. The ferromagnetic materials placed in the influence of a magnetic field are magnetized, and the intensity of magnetized ferromagnetic materials I reach the saturation state by increasing applied magnetic field. In addition, when the ferromagnetic materials are heated above the Curie point temperature Tc, they lose properties of ferromagnetic substance and exhibit properties of paramagnetic substance.For example, the Tc of α-Fe is supposed 768 degrees (A2 transformation). The internal structure which is not magnetised, is composed of small magnets which

have differently-oriented spins to provide totally zero magnetic moment. The internal structure of the magnet is called a magnetic domain. And by the magnetic field, the spins are aligned parallel to a single directional vector along axis of magnetic poles. In addition, it is postulated that the magnetic moment approaches a saturation value. The magnetization is saturated in the domains and is determined saturation state by the temperature. The size of the magnetic domain is10^{-1}～10^{-3} mm is nothing like the crystalline grain size, and the single crystal consists of many magnetic domains (see Figure 2.7). A domain wall which is the border of magnetic domains differs from a crystal grain boundary and has thickness of around 100 nm which a magnetization direction changes into continually.

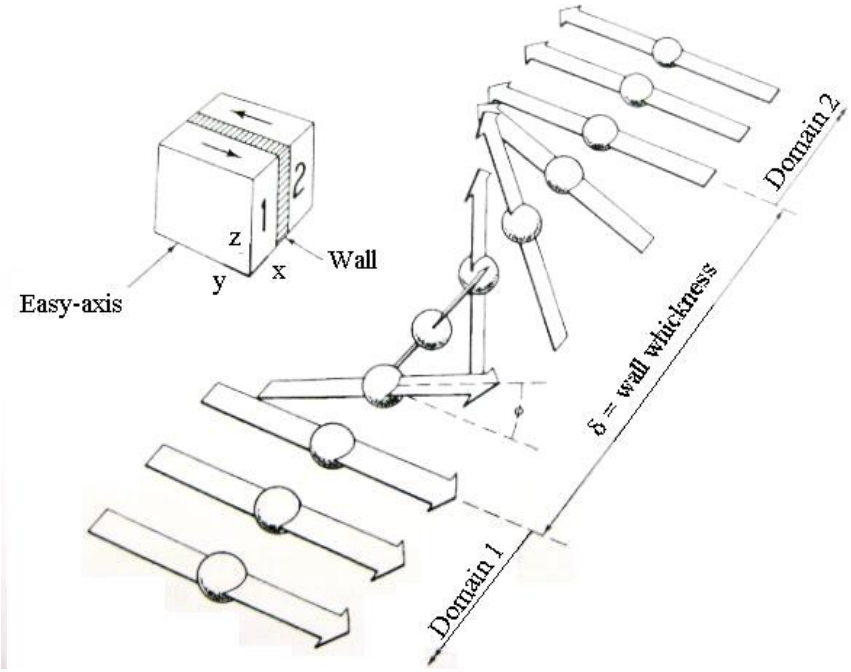

Fig 2.7 Spin rotation interaction in 180 degrees domain wall (Cullity 1972)

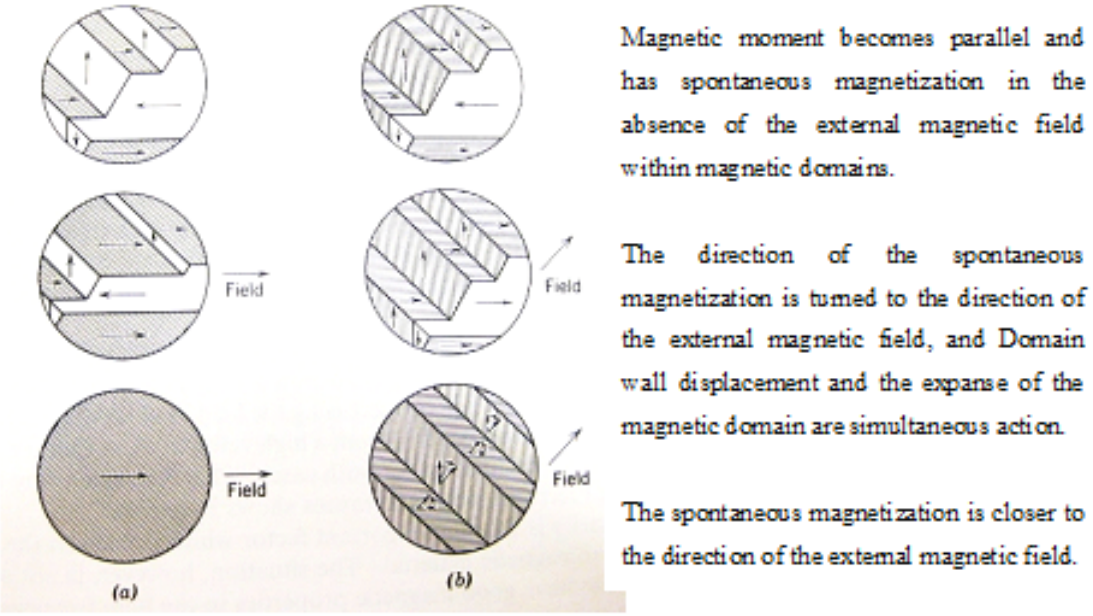

Fig 2.8 Domain wall displacement of Ferromagnetic material, Fe-Si crystal
(a) <001>surface (b) <110> surface (Chikazumi, 1964)

In the magnetic domain magnetised, the electron behaves as Bohr magneton by the magnetic moment to be caused by an electronic spin even if it is without magnetic field as shown in Figure 2.8. The magnetization direction of magnetic domains turns and rotates to the magnetic field direction so that the spontaneous magnetization direction is rotated to the direction of the external magnetic field. In the magnetic domain, domain wall displacement is generated with increase at a volume particularly, as shown in the middle illustrations.

The spontaneous magnetization finally is closer to the direction of the external magnetic field and reaches the saturation as shown in the above illustrations. Then, the magnetic anisotropic exists at the ferromagnetic single crystal which has magnetic domain structure. In fact, the directions that are easily magnetised of by the crystal orientation are different. For instance, the axis of easy magnetization of Fe is in the order corresponding to <100>, <110> and <111>. However, the magnetization is inhibited by

the internal strain of materials and the existence of impurities.

2.4.2 Hysteresis curve

Ferromagnetic materials can magnetise and demagnetise, as distinguished from a permanent magnet as shown in Figure 2.9. Even if induced magnetic flux density *B* by magnetic field *H* removes magnetic field, residual magnetism *Br* is left. Coercive force *Hc* is removed if *I* adds it to the opposite direction and produce high magnetic flux density with the low value of the magnetic field as shown in Figure 2.9(a). Additionally, it can be demagnetised by low coercive force. B-H curve is indicated to illustrate decrease or increase in magnetic field, and energy equivalent to the loop area lose energy in the form of heat. Additionally, when the ferromagnetic materials magnetise, the external of the magnetic bodies slightly is deformed so that the lattice parameter spontaneously varies along the direction of internal magnetization. This is called magnetostriction. (Chikazumi, 1964)

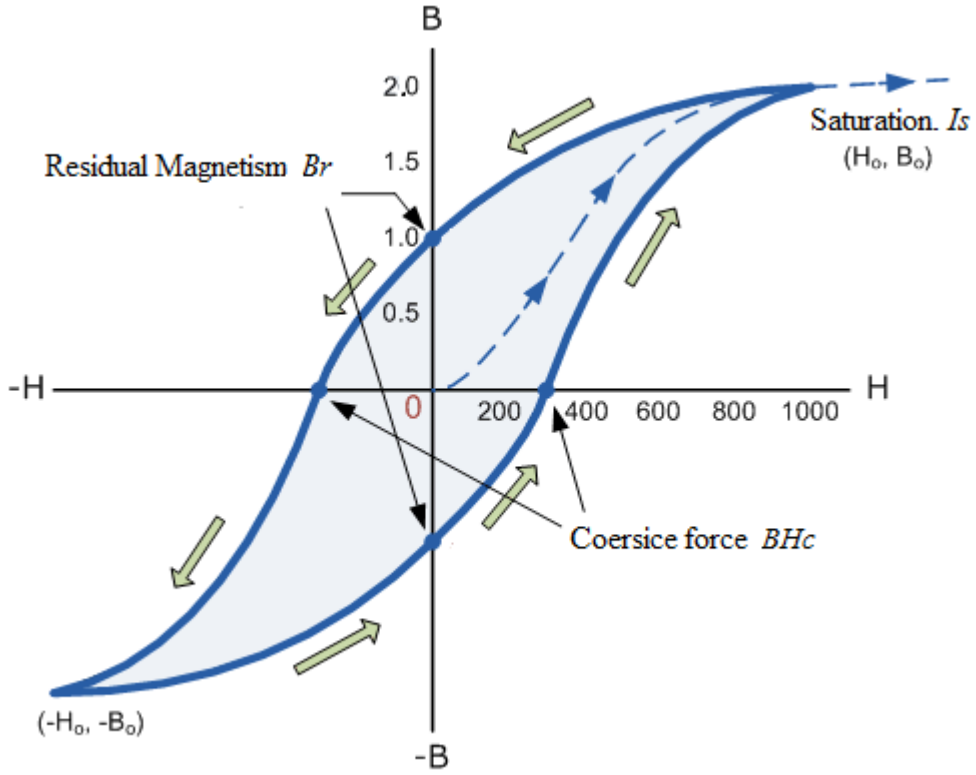

(a) Ferromagnetic material

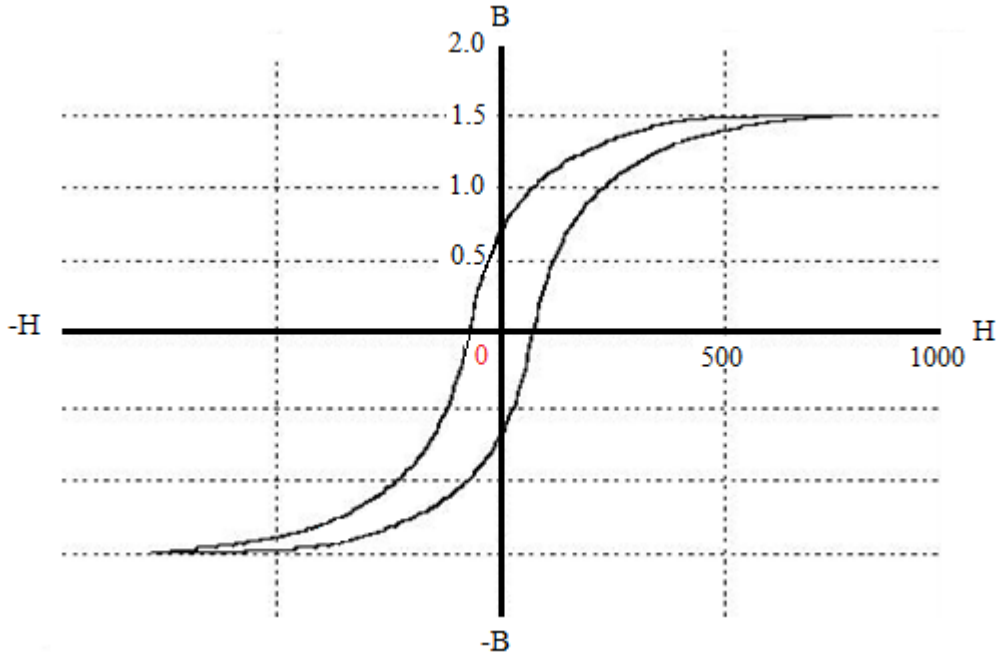

(b) Permanent magnet

Fig 2.9 Magnetic hysteresis loop
(Electronics-tutorials.ws 2001, Groom 2000)

The cause is because a crystal in the internal structure of the magnetic domain is distorted to the magnetization direction. Thus, it is hard to be made magnetised and material's hardness increases. By magnetostriction, it extends in the axial direction and contract at right angles to the axial direction when it is axially magnetised, or it expands and contracts in the opposite direction. The ferromagnetic materials are sensitive to stress, and permeability is different due to strength of the stress. The kinetic energy of domain wall moves the kinetic energy of dislocation, and dislocation motion produces the promoted phenomenon (Takahashi and Seiki 2007). The phenomenon is a dynamic interaction. The shear stress from the outside is added to dislocations which are pinned by obstacles. However, the phenomenon in Fe has negligible small effect because the magnetostriction constant is small. Furthermore, Craik and Wood (1970) state the characteristic of magnetization changes induced by stress in a constant applied field from the results caused by the stress. It is identified that discontinuous changes of domain structure occur by stress to the oriented materials and the isotropic polycrystalline materials. Therefore, it is important that the influence of magnetization under stress is considered.

2.5 Fundamentals of Wear

2.5.1 Fatigue wear and Surface Crack Initiation by Fatigue Wear

The fatigue wear during high frequency sliding in a reciprocating sliding wear tests is characterized by occurrence of the minute defects (cracks and fissures) on a worn surface. An initiation and the propagation of a crack is illustrated diagrammatically in Figure 2.10. The initiation of a crack occurs toward downward at weak points of the

contact area. In addition, the primary crack propagates along a slip plane or dislocation cell boundaries. Then, the primary crack develops and connects with a subsurface crack; it is the secondary crack. Some of the developing cracks reach the surface and a wear particle is released (Buckley 1981).

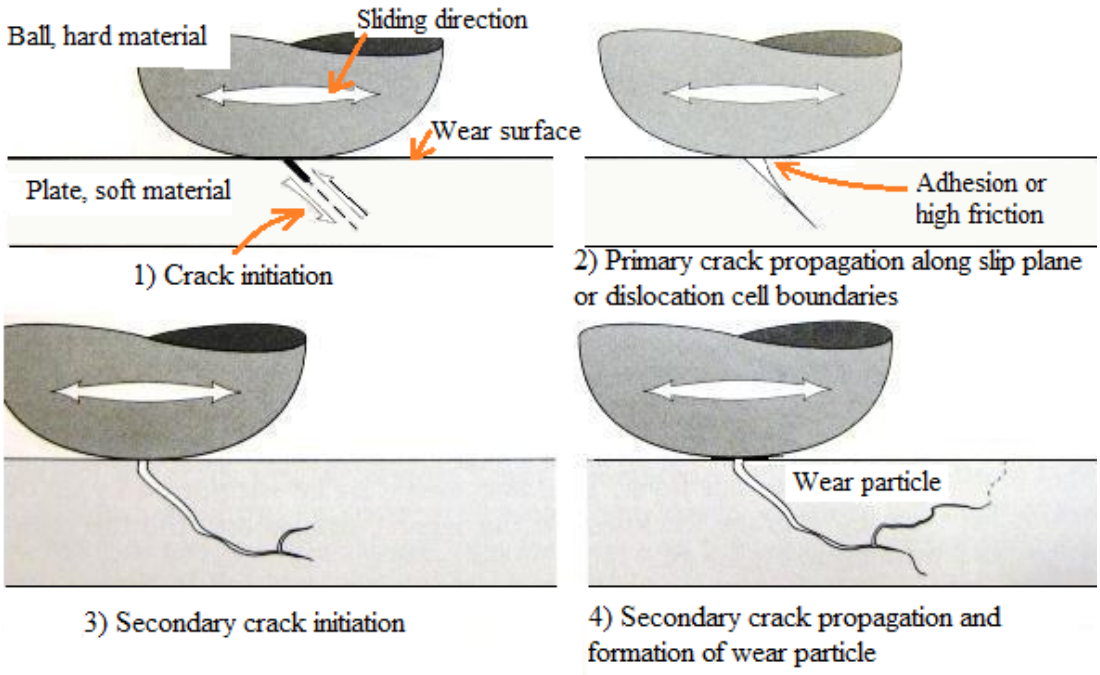

Fig 2.10 Crack initiation and propagation (Stachowiak 2005 p.597)

2.5.2 Other fundamental types of wear

Definition of wear can be as “the ultimate consequence of interaction between surfaces which is manifested in gradual removal of material”. Generally, four types of wear process can be distinguished (Mair, et al., 1996). However, this section deals with two types of wear only that is abrasive and adhesive wear processes as shown in Figure 2.11.

A. Adhesive wear

Adhesive wear is due to asperities contact which does not produce wear debris instantaneously. It undergoes the process of the mutual asperity deformation and the formation of adhesive bond. Finally, it moves to the brittle fracture stage or the ductile fracture stage during asperity separation.

B. Abrasive wear

Abrasive wear is caused by shear stress at the contact interface by harder asperities ploughing the surface of softer material. It is continued as the formation and delamination of the bulge and ends by the creation of wear debris.

C. Oxidative wear

The oxidative wear occurs for the metals which are in contact under a dry condition and the presence of the air. It has clear features that produce the smooth wear surface and small oxidized wear debris, afterwards it undergoes a process of change from a severe wear to a mild wear process. The occurrence of the oxidative wear is connected with a level of sliding speed and the perpendicular load. During oxidative wear of sliding contact at high frequency, a thin oxide film on the natively-oxidized steel plate is worn away or removed due to a fatigue process, before it can form thick oxide plateaus on the worn surface (see Figure 2.12 (a)). On the other hand, sliding contact at low frequency does not expose contact asperities on the worn surface to high flash temperature (Figure 2.12 (b)). However, an oxide film is rapidly worn away during a severe wear process, and then on adhesive wear process occurs. Produced oxide debris migrates along surface and pile up at asperities. As a result, oxide plateaus are formed on the contact surface. The developed oxide plateaus are accompanied by a progressive reduction in

the friction coefficient. The top of oxide plateaus is smooth and consists of large and fine oxide particles.

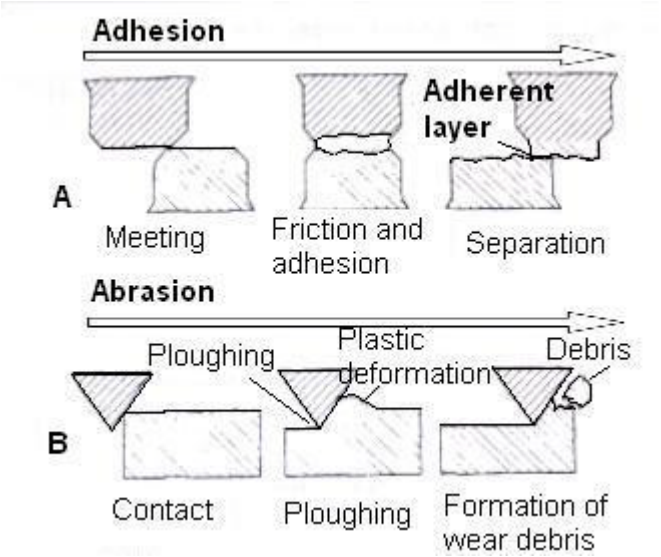

Fig 2.11 Fundamental mechanisms of wear related to the effect of magnetic field (A) adhesion: Adhesive wear (the brittle fracture during asperity separation), (B) Abrasion: Abrasive wear (Mair, et al., 1996)

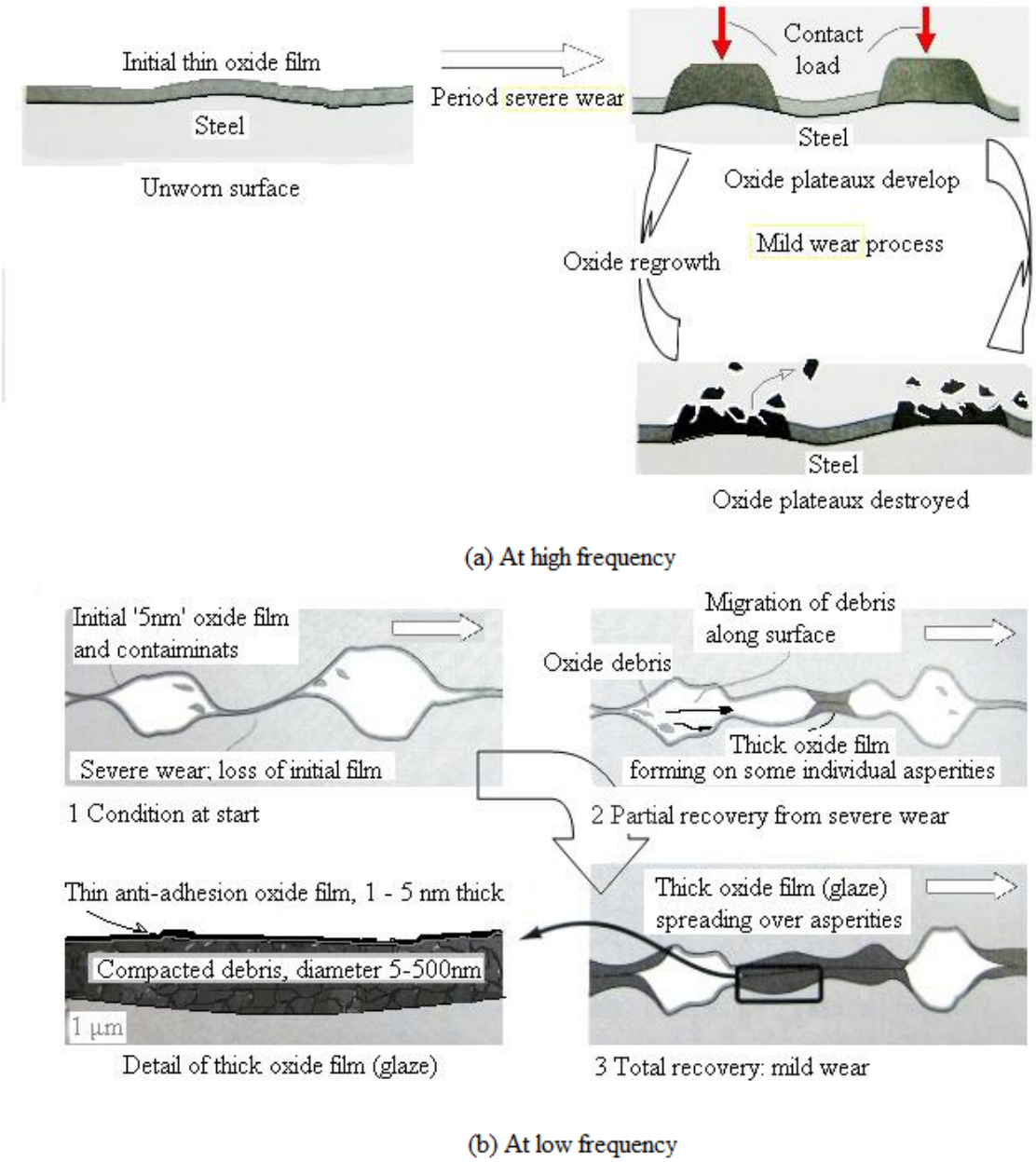

Fig 2.12 Fatigue process of oxidative wear on sliding contact
(Stachowiak 2005 p.584, 586)

2.6 Calcium carbonate characteristic in lubricant

The calcium carbonate is added to lubricant oil as antioxidant, and is classified as the over-based dispersants. It is shown schematically in the accompanying Figure 2.13. The calcium carbonate consists of metal, sulphonate and carbonate complexes. The calcium sulphonate is formed on the outer surface of the calcium carbonate core. When it is in contact with dirt particles in acidic oxidation products, dirt particles are wrapped by the colloidal particles. The wrapped dirt particles have a negative charge and to repel other dirt particles. Furthermore, as for colloidal particle of the calcium carbonate, the acidic oil oxidation products are neutralized by Ca^{2+} and $CaCO^{3}$ on the outer surface of the carbon carbonate core. In results, the fluidity of the oil is continued because of the wrapped dirt particles repel other dirt particles. Calcium carbonate is expressed as ion product:

$$CaCO_3 \rightleftharpoons Ca^{+2} + CO_3^{-2}$$

It ionizes in a positive ion and a negative ion, and it reaches the equilibrium. The positive ion binds together solvent to proton. And the negative ion is pulled up from the solvent.

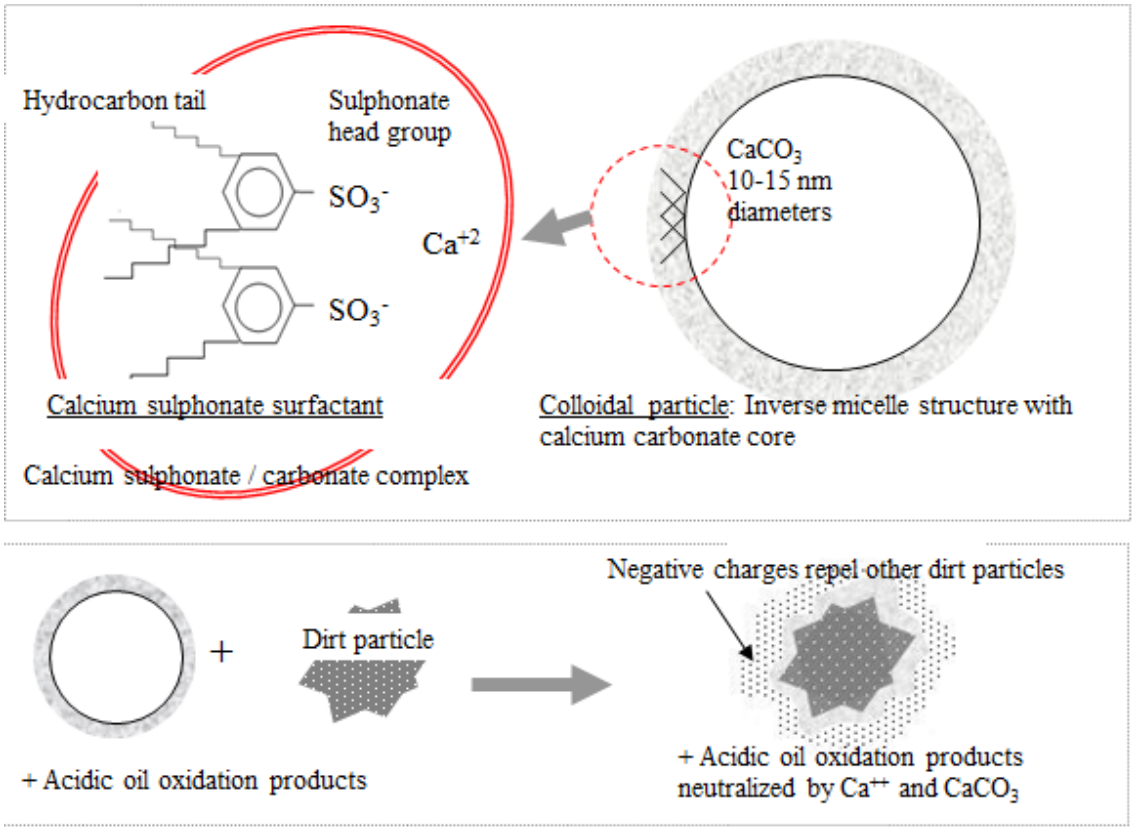

Fig 2.13 Synthesis and function of sulphonate detergents (Stachowiak 2005 p. 95)

2.7 The feature of thermal spray coating

Atmosphere plasma spraying is classified as a kind of thermal spraying techniques. It is a coating process in which melted powder material is sprayed onto a surface. The thermal spray coating has a lamellar microstructure consisting of splats. The molten metals may be oxidized on the top surface in flight and on the surface. Thus, the thermal spray coating has a sandwich structure of a thin oxidation layer and the splat. When the thermal spray coating is precipitated out of the molten materials, the process makes micro pores and may confine a gas to the pores. According to Edrisy et al. (2001), quoting the report by Hartfield-Wunsch et al., the thermal spray coating is prone to delamination from oxidation layer, which is thought to be a "weak point", in the sliding wear. They conclude that the low carbon steel coating main wear mechanism is the formation of Fe_2O_3. The magnetic effect on calcium carbonate precipitation is identified that it increases the precipitate formation and the total precipitate amount of resources (Madsen 2004: Fathi et al 2007).

References for chapter 2

Basic Electronics Tutorials by Wayne Storr., (2011) Electronics-Tutorials.ws, April 2011. **http://www.electronics-tutorials.ws/electromagnetism/magnetic-hysteresis.html**

Buckley, D, H., (1981) Surface Effects in Adhesion, Friction, Wear and Lubrication, Elsevier, Amsterdam, 1981

Chikazumi, S., (1964) *PHYSICS OF MAGNETISM*: John Wiley & Sons, Inc., pp.114, 125

Cullity, B., (1972) Introduction to Magnetic Materials, Addison-Wesley, Reading, MA

Craik, D, J. and Wood, M, J., (1970) Magnetization changes induced by stress in a constant applied field, *J. Phys. D: Appl. Phys.* **3** 1009

Dowson, D. and Higginson, G, R., (1977) Elastohydrodynamic Lubrication, Pergamon

Edrisy, A., et al. (2001) wear of thermal spray deposisted low carbon steel coatings on aluminum alloys, *wear 251*, pp1023-1033

Fathi, A., Mohamed, T., Mohamed, B, N., Claude, G. and George, M., (2007) Influence of magnetic field on calcium carbonate precipitation, *Desalination*, Volume 206, Issues 1-3, 5 February 2007, Pp.163_168.

Gohar, R., (1988) Elastohydrodynamic, Ellis Horwood

Groom, Nelson, J., (2000) A Comparison of Analytical and Experimental Data for a Magnetic Actuator, NASA/TM-2000-210328, September 2000. **http://www.tpub.com/content/nasa2000/NASA-2000-tm210328/NASA-2000-tm2103280001.htm**

Hamrock, B, J and Dowson, D., (1981) Ball Bearing Lubrication, John Wiley & Sons

Hertz, H, J., Reine and Angew., (1881) Math. 92, pp.156-171

Lawn, B, R., (1998) Indentation of ceramics with spheres: a century after Hertz. *J. Am. Ceram. Soc*. 81, 1977_94

Madsen, H, E, L., (2004) Crystallization of calcium carbonate in magnetic field ordinary and heavy water, J. Crystal Growth, 267, pp.251-255.

Mair, L, H., Stolarski, T, A., Vowles, R, W., and Lloyd, C, H., (1996) "Wear: mechanisms, manifestation and measurement. Report of a workshop" Journal of Density, vol.24, pp141-142.

Stachowiak, G, W., (Gwidon W.) (2005) Engineering tribology / Gwidon W. Stachowiak and Andrew W. Batchelor. 3rd ed. Oxford : Butterworth-Heinemann, pp.95, 288-310, 318, 317, 597

Tallian, T, E., (1967) On Competing Failure Modes in Rolling Contact, *ASLE Transactions*, Vol.10, pp.418-439

Takahashi, S., (2007) Magnetism and dislocation, kensagizyutu-v12n2p59-63.pdf Inspection technology, Vol. 12, the second, (2007), p59-63 http://ir.iwate-u.ac.jp/dspace/handle/10140/2065

Takahasi, N., Asada, H. and Yukawa, N., (1989) Metallic materials, Third edition, Morikita

Shuppan Co., Ltd. pp19_21.

Chapter 3 Methodology of Experiments

3.1 Introduction

The dry sliding contact experiment and the lubricated sliding contact experiment were carried out with ball-on-plate contact configuration. The ball-on-plate test apparatus is shown in Figure 3.1. Two permanent magnets were installed in the direction same as the ball sliding over the plate specimen. Besides, each part of the apparatus is shown schematically in the illustrations of Figure 3.2. The testing machine was used for the comparison of the effects created by the magnetic field for the different kinds of materials and coatings. In the high frequency sliding contact wear experiment, a smaller testing machine was used and is shown in Figure 3.3.

In this section, the mechanical properties of the plates, balls and other vital characteristics for experiments are described. The flow of the magnetic field inside the test plate was analysed using Finite Element Analysis (FEA).

Test procedure and test conditions are described in each section. The tests performed and presented in this thesis include hardness measurements, optical microscope observations, mass loss measurements, surface profile and roughness measurements, scanning electron microscope (SEM) observations, and X-ray diffraction (XRD) analyses.

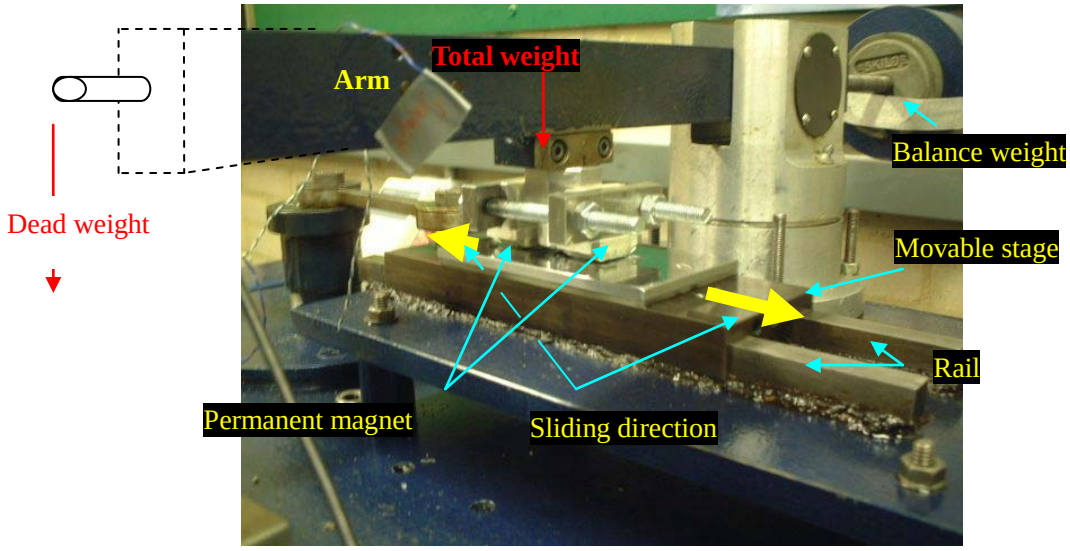

Fig 3.1 Illustration of the dry sliding wear experiment apparatus

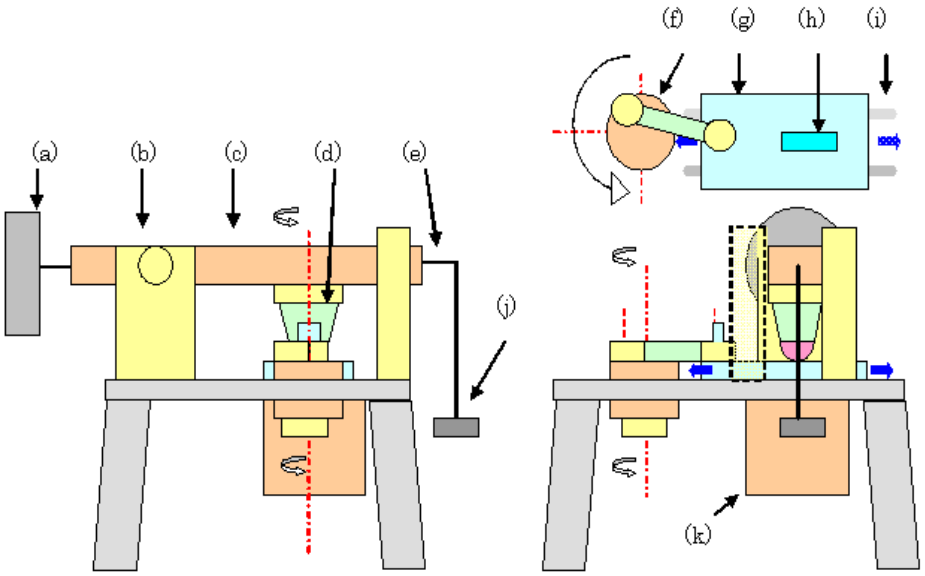

Fig 3.2 Explanation of a friction machine A
(a) Balance weight, (b) Fulcrum point, (c) Arm, (d)Point of application of force, ball, (e) Hook to hang dead weight, (f) Drive shaft,(g) Movable stage and frame of test piece,(h) Test piece of the plate type,(i) Rail,(j) Dead weight,(k) Motor

Operation of the Wear Testing Machine

With reference of Figure 3.2 the following is applicable: (a) balance weight is used to keep the arm horizontal, (b) fulcrum point of the loading arm (c), (f) drive shaft and (g) movable stage makes reciprocating motion. Amplitude can be adjusted by changing the position of the crank pin. The details of test samples and holder for permanent magnets are described in the next section. In Figure 3.3 timer (d) was connected to (c) operation control box, which was used to control start and stop of the wear test machine B. Test specimens and the permanent magnets were set up on (f) ball-on-plate sliding contact stage.

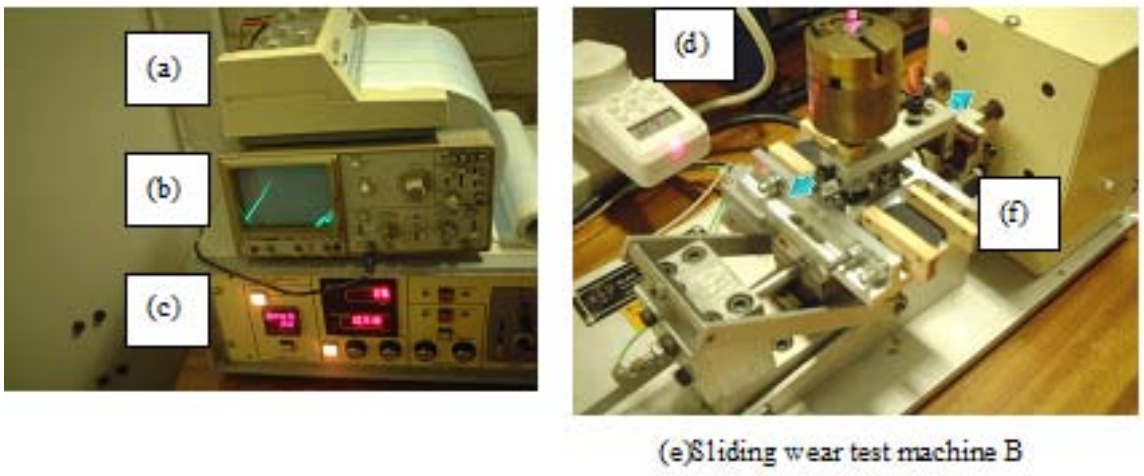

Fig 3.3 Illustration of high frequency sliding contact testing apparatus
(a) Recorder, (b) Oscilloscope, (c) Operation control box, Adjustment of frequency and the amplitude, (d) Timer, (f) Ball-on-plate sliding contact test apparatus which fixes permanent magnets and the plate specimen. Red arrow is dead weight. Blue arrows show sliding direction.

3.2 Test apparatus

3.2.1 Ball-on-plate sliding contact wear test machine A

Photograph of the ball-on-plate sliding contact test apparatus is show in the centre of Figure 3.1. As shown in Figure 3.4 (b), the ball holder consists of three parts and the bracket to which the permanent magnets are attached is shown in yellow. The three parts of the ball holder are a connector component, a fixation screw and a holder. The brackets and the connector component are fixed by two metal blocks that can be moved together by turning bolts as shown in Figure 3.4 (a). Two plates are fastened by screws to the movable stage in order to fix the test sample. The connector component consists of the shape of circular cylinder and the octagonal prism. The circular cylinder side fixes the welded fixed holder. On the other hand, the octagonal prism side has a hollow structure to insert the holder. The octagonal prism side has three screw holes to hold the holder by turning three hexagon socket set screws on three sides. A scale is marked to the side of the fixed holder, the connector component and the holder to be able to possess the fixed position.

The installation angles of the magnets can be changed to 0, 45 and 90 degree relative to the sliding direction as shown in Figure 3.5. For instance, brackets are arranged on the both sides where red shown in Figure 3.5(a) was painted in to fix the installation angle of the magnets to 90 degrees. 0 degree conespaonds to a direction perpendicular to the sliding direction, 90 degree means the same direction as the sliding direction. And 45 degree means 45 degree to the sliding direction.

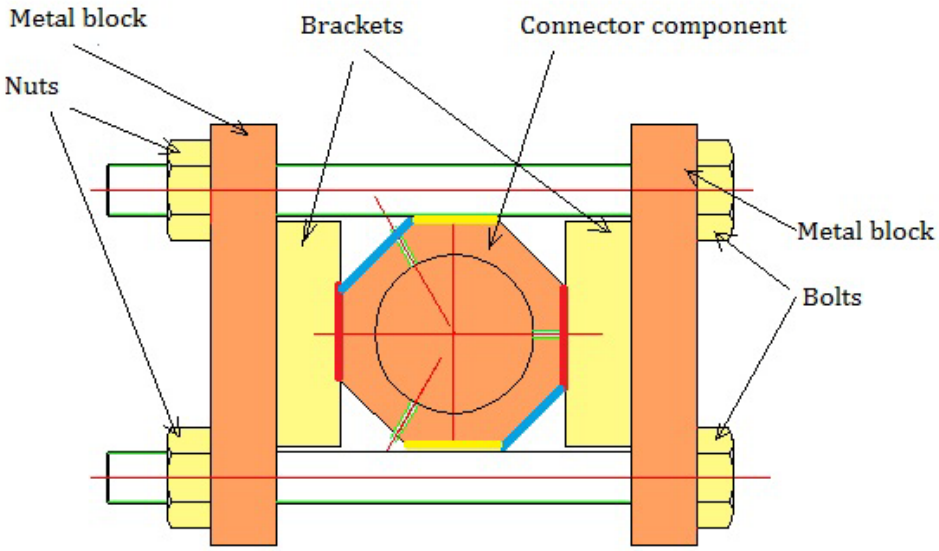

(a) Top view indicated by red arrows

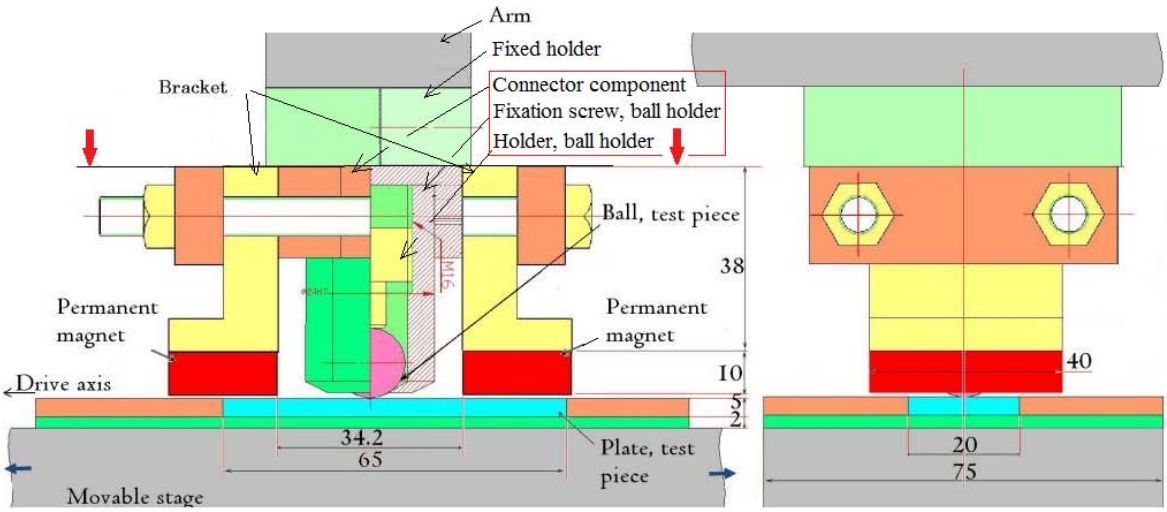

(b) Outline view of ball-on-plate sliding contact test apparatus

Fig 3.4 Dimensions of ball-on-plate sliding contact test apparatus, the permanent magnets were set at 90 degrees to sliding direction

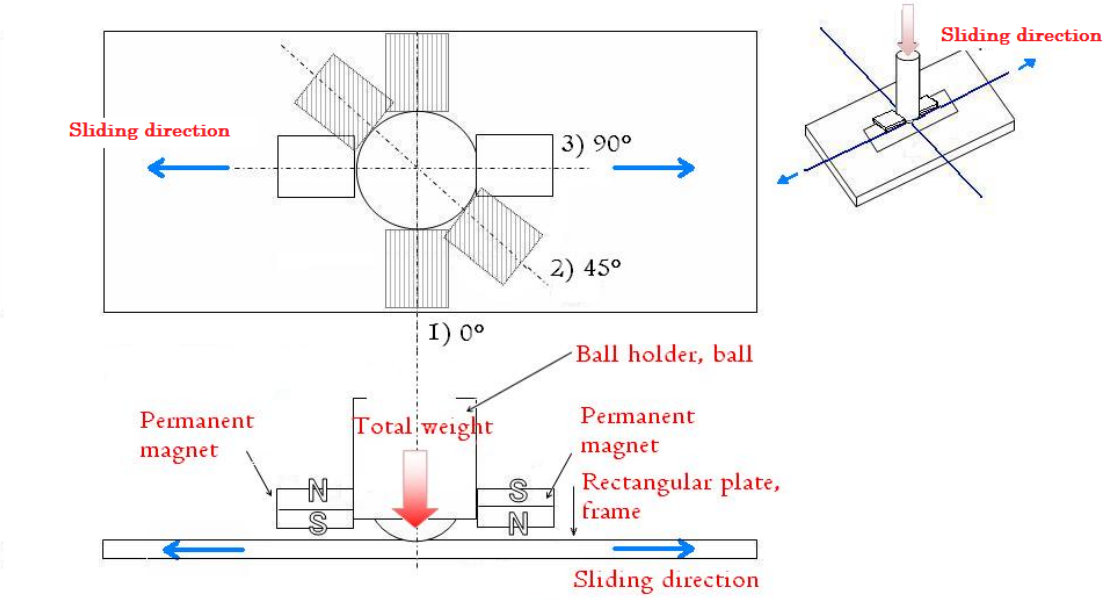

Fig 3.5 Illustration of setting of magnets, the magnets can be set at three angles

3.2.2 Ball-on-plate wear test machine B

A photograph of the apparatus is shown in Figure 3.6, Figure 3.7 presents schematic diagram of it. As illustrated in Figure 3.6, the permanent magnets and the plate specimen are installed on the stage and fixed to it. The specimen is installed with screws at the centre of the stage, and permanent magnets are fixed at both sides of the specimen on the stage. The permanent magnets are attached to the board of the paramagnetic material of 2 mm in thickness with four screws and a piece of wood on both sides. The reciprocating motion of the motor is transmitted to the ball through the arm. The ball and a weight are attached to the arm. To evaluate the direction of a magnetic field during the high frequency sliding contact experiment, the magnetic field direction was set by changing the installation angle of the stage to the sliding direction. The adjustment method of the angle of the magnetic field direction, it was rotated the ball-on-plate sliding contact stage 35 degrees to the sliding direction around on the centre of the contact area, and the ball-on-plate sliding contact stage was attached to the ball-on-plate sliding contact test apparatus with adhesive tape.

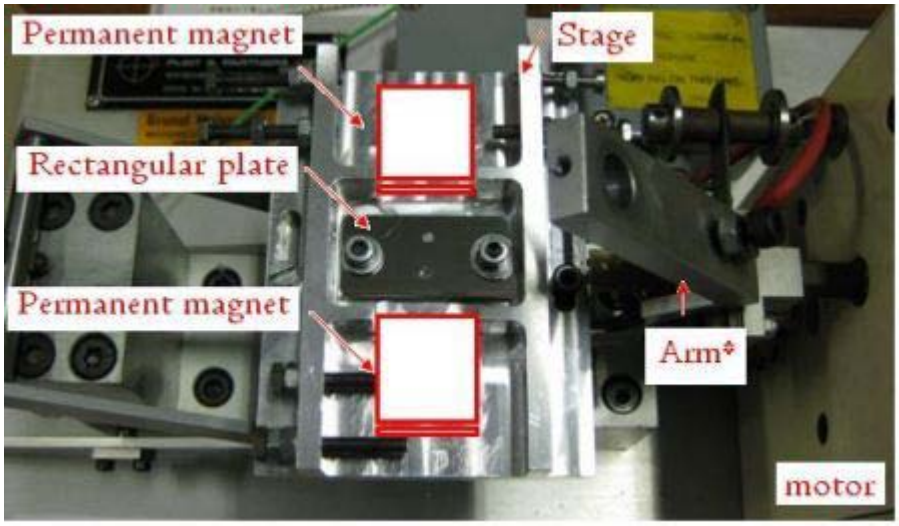

Fig 3.6 Overview of main part of the ball-on-plate sliding wear test machine

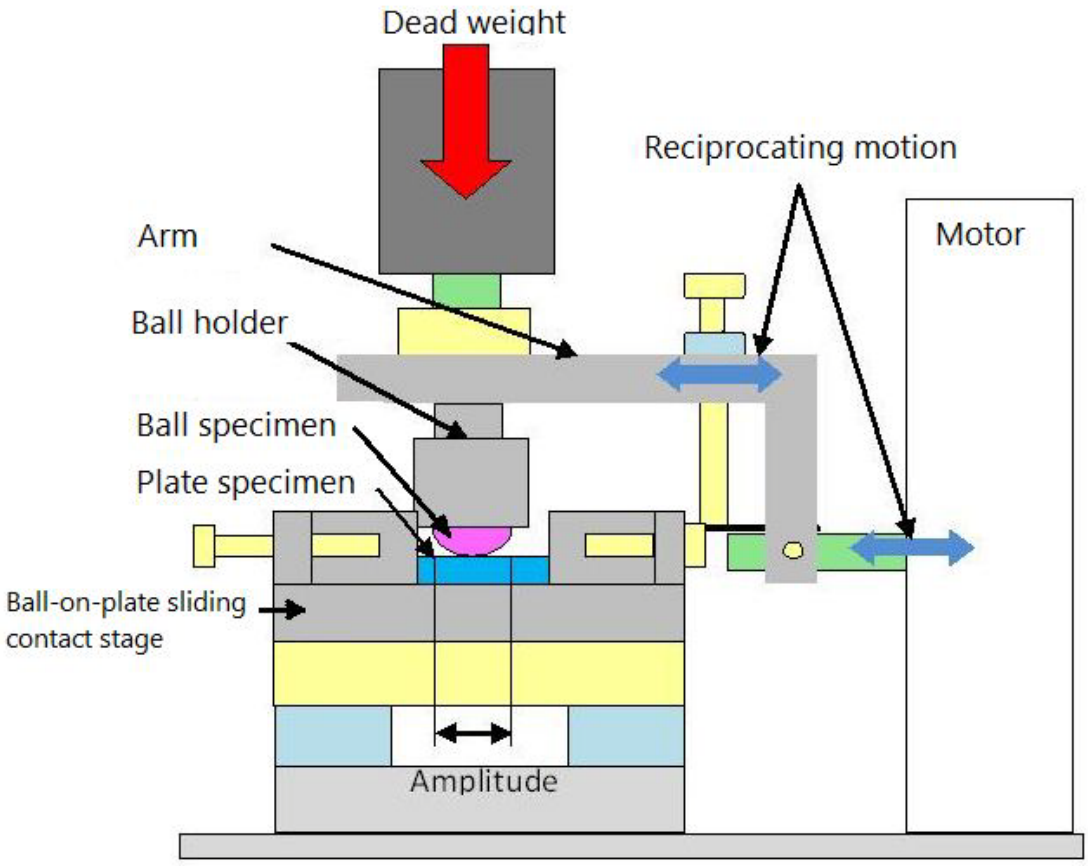

Fig 3.7 Side view of the machine

Test materials

To study the influence of magnetic field on the wear process, a plate specimen and a ball specimen were used. The test specimen was an uncoated rectangular plate made of mild steel (BS4360 43B). Its cross-section hardness was about 277 HV. The plate had dimensions of 65 mm in length, 20mm in width and 4mm in thickness and there were two holes at both ends of the plate. The rectangular plate was used for dry and lubricated sliding wear experiment. In addition, the plate was coated by carbon steel and an austenite stainless steel (316S31) under atmosphere plasma spray (APS) conditions and was used for the comparison of the magnetic field effect on ferromagnetic material and paramagnetic material. Thickness of both coatings was 250 μm. The hardness of the carbon steel coating was about 221 HV. The austenite stainless steel coating hardness was about 403 HV.

Test plate used for high frequency experiments had the dimension of 40 mm in length, 25 mm in width and 2mm in thickness.

The surface of all plate specimens were ground and polished with the abrasive paper of #300, #500, #1,200 and #2,400, respectively. The resulting roughness, Ra, of the surface was approximately 0.015 μm. Before the test, the specimen was cleaned with acetone. Mechanical properties of the rectangular plate are shown in Table 3.2.

On the other hand, balls which were used for a counter material were made of silicon nitride (Si_3N_4) and ball bearing steel 100Cr6 (AISI53100) and they had diameter of 6.35 mm. One type of Si_3N_4 balls was used for dry sliding wear experiment and high frequency sliding wear experiment and had gray colour. Its hardness was about 2019 HV. Another type of Si_3N_4 balls had black colour and its hardness was about 1404 HV. The black Si_3N_4 balls were used for lubricated sliding wear experiments and performance comparison of ferromagnetic coating with paramagnetic coating. The hardness of a

100Cr6 ball was about 700 HV. It was employed for the high frequency sliding experiments with a couple of ferromagnetic materials. Vickers hardness of the test materials is shown in Table 3.1.

Test materials mechanical properties and their chemical composition are shown in Tables 3.2 and 3.3. Chemical composition and characteristics of materials used for thermal spray coatings are shown in Table 3.4. Plate specimen had two countersunk holes at both ends as shown in Figure 3.8. The plate specimen was fixed to the stage by two flat head screws.

Lubricated sliding wear test it has less wear amount of the specimens than dry sliding wear test. In other word, it was expected that it is hard to evaluate the magnetic field influence due to the wear reduction. Thus, black colour Si_3N_4 balls were softer than gray colour Si_3N_4 ball were used in the lubricated sliding wear test to facilitate evaluating of the magnetic field influence. In addition, the black colour Si_3N_4 ball specimens were used in dry sliding wear test for coated plate specimen.

Table 3.1 Materials, sizes and micro hardness

Test specimen	Materials		Sizes mm[1]	Vickers Hardness Hv0.2	Notes: name of experiment
Plate	Mild steel (0.2C)	Ferro magnetic	l = 65, w = 20, t = 4	277	Dry[4], lubrication[5]
			l = 40, w = 25, t = 2	277	High frequency[6]
	Iron coating		t = 0.25	221	Dry
	Austenite stainless steel coating[2]		t = 0.25	403	Dry
Ball	Ball bearing Steel 100Cr6	Ferro magnetic	d = 6.35	700Hv0.5	High frequency
	Si_3N_4[3]	Para magnetic	d = 6.35	2019(gray), 1404(black)	Dry, Lubrication, High frequency

(1) d: diameter, l: length, w: width, t: thickness
(2) Austenite stainless steel: This is 316S31 in British Standards Institution.
(3) Si_3N_4 ball: Two types of balls were used for this study. A gray colour ball was used for dry sliding wear test, matched with uncoated plate black colour ball was used for other experiments.
(4) Dry: dry sliding contact experiment
(5) Lubrication: lubricated sliding wear experiment
(6) High frequency: high frequency sliding wear experiment

Table 3.2 Properties of materials at ambient temperature

Materials	Young's modulus (GPa)	Poisson's ratio	Yield strength (MPa)	Tensile strength (MPa)
Mild steel[(1)]	206	0.3	265 min	430-580
low alloy carbon steel	210	0.3	-	-
Austenite stainless steel	211	0.29	-	-
Si3N4[(2)]	315	0.26	-	700
Ball bearing Steel 100Cr6[(2)]	210	0.3	-	2500

1) (Iraj et al. 1996: Luxemotor "KEI" 2005)

2) (VIKRAM: ASM International 1997)

Table 3.3 Chemical Composition of test materials (VIKRAM)

Materials	Chemical composition, %								Type of Magnetism
	-	C	Si	Mn	P	S	Cr	Mo	
Mild steel (0.2C)	-	0.21 max	0.050 max	1.50 max	0.050 max	0.050 max	-	-	Ferromagnetic
Steel 100Cr	From – to	0.93-1.05	0.15-0.35	0.25-0.45	- 0.025	- 0.015	1.35-1.60	- 0.10	Ferromagnetic

Table 3.4 Thermal spray materials

Materials	Manufacturer	Product name	Chemical composition	Characteristic
Carbon steel powder	Sulzer Metco	SULZER 4052 Low Alloy Steel Powder	Fe 96% Cr 14% Mn 1.4% C 1.2%	Strongly magnetic
Austenite stainless steel powder	PRAXAIR	FE-101	Fe Cal. Cr 17% Ni 12% Mo 2.5%	Weakly magnetic

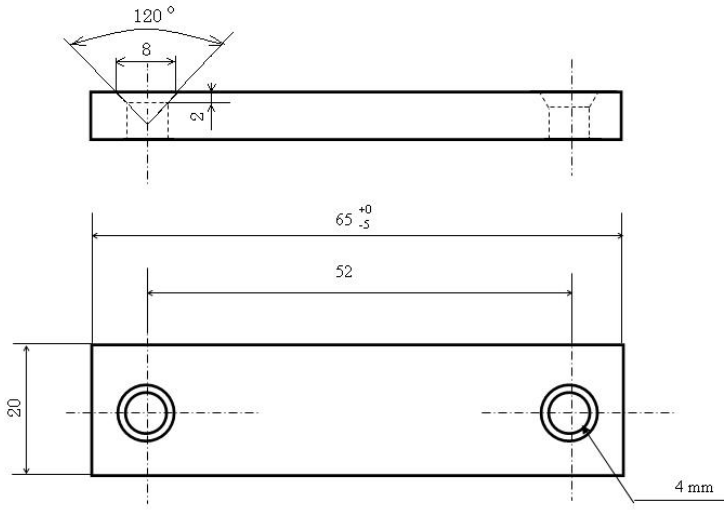

t = 5 mm

Fig 3.8 Shape and dimensions of plate specimen, Material is mild steel (0.2%C)

3.3 Lubricant

In the lubricated sliding wear test, engine oil Castrol GTD Magnatec 10W-40, was used. The oil prevents rubbing by soot particles of the exhaust gas in a diesel engine. The typical characteristics of the oil are shown in Table 3.5.

To obtain the central film thickness and the minimum film thickness of elastohydrodynamic pressure distribution, the viscosity measurement was carried out to determine the viscosity of the oil at room temperature (20 degree C).

The procedure was as follows; firstly, the measuring cylinder is filled with the oil. Secondly, one steel ball is dropped in the measuring cylinder and the time taken for the ball to travel from the surface of the oil to the bottom of the cylinder is measured with a stopwatch. Finally, the average of 10 measurements is calculated.

When the steel ball is falling in the oil, the ball reaches the bottom of a container the when the total of the buoyancy and the viscosity are equal to the gravity. In other words, viscosity was derived from the equations which are shown blow. (SEED Foundation 2008)

$$F_{buoyancy} + F_{viscosity} = F_{gravity} \tag{3.1}$$

$$F_b = \frac{4}{3}\pi r^3 \rho g \quad F_v = 6\pi\eta r V_t \quad F_g = m g$$

Substituting expressions of *Fb*, *Fv* and *Fg* to Formula (3.1) gives,

$$\frac{4}{3}\pi r^3 \rho g + 6\pi\eta r V_t = m g \tag{3.2}$$

Therefore,

$$\eta = \frac{9mg - 4\pi r^3 \rho g}{18\pi r V_t} \tag{3.3}$$

where

V_t ; *Thermal velocity*
η ; *Viscosity*
ρ ; *Density of fluid*
r ; *radius of the ball*
m ; *Weight of ball*
g ; $980.7 cm/s^2$

It was found that, the steel ball dropped at thermal velocity 0.097 m/s over the measurement distance 150 mm. The viscosity of the oil was derived by Formula (3.3) and the value was 0.019 Pas. The typical characteristics of the lubricant are shown in Table 3.5 and the viscosity measurement result of the oil in Table 3.6.

Table 3.5 Typical Characteristics of Castrol 10W-40 (OPIEoil.co.uk. 2006)

Test	Method(s)	Unit	Typical
Density @ 15C, Relative	ASTM D4052		**0.875**
Appearance	Visual		Clear & bright amber liquid
Viscosity, Kinematic100C	ASTM D445	mm²/s	14.5
Viscosity, Kinematic40C	ASTM D445	mm²/s	100
Viscosity, CCS -25C (10W)	ASTM D5293	cP	7000 max
Flash Point, PMCC	ASTM D93	°C	194
Ash, Sulphated	ASTM D874	% wt	1

Table 3.6 Characteristic of lubricant at room temperature

η, Viscosity (Pas)	y, Distance of tall large measuring cylinder (m)	$t_{average}$, Measured velocity average (s)	V_t Thermal velocity, (m/s)	ρ, Fluid of density (kg/l)	r, Sphere of radius (m)	m, Weight of ball (kg)
0.019	0.15	1.55	0.097	0.875	0.001	0.55×10^{-4}

3.5 Magnetic field

The horizontal magnetic field was produced by two types of permanent magnets, shown in Figure 3.5 and 3.6. Magnets were located near both ends of the contact area and were kept in the constant position from the contact area. The permanent magnets were fixed to the ball holder in the sliding wear test machine A as shown in Figure 3.4. Therefore, the formula for the total contact load P is as follows:

$$P = P_l + P_m$$

The contact load P is the total of the attractive force P_m due to the magnets and the normal load P_l produced by dead weight. The attractive force P_m acts at the interface between the frame and permanent magnet in the normal direction.

The primary effect of the magnetic field analyzed by FEA will be described below. This preliminary investigation becomes the important element, in discussion of the effect of the magnetic field on the sliding wear. In the FEA, data used are shown in Figure 2.9, Table 3.7 and 3.8. Two dimensional models of the fixed form were designed. Analysis of test specimens and two permanent magnets was carried out by the FEA. The FEA results are shown in Figure 3.10. Figure 3.10(a), depicts contact configuration to be solved and Figure 3.10(b) shows the analysis of the magnetic force, Figure 3.10 (c) shows magnetic flux density, and the analysis of the coercive force is shown in Figure 3.10 (d).

Additional effect of magnetic field on the contact point is given in this section because it is useful in discussion of the influence of horizontal magnetic field on wear. The properties of permanent magnets and mild steel are shown in Table 3.7, Table 3.8 and Figure 2.9.

Table 3.7 Properties of permanent magnets

Type of magnets	Size(1) (mm)	Br(2) (T)	BHc(3) (kA/m)
Rare earth magnet	*l = 40, w =20, t = 10*	1.1	877.5
Ferrite magnet	*l = 20, w = 20,t = 4*	0.4	319.1

(1)* *d*: diameter, *l*: length, *w*: width, *t*: thickness (2) Br: remanent flux density, T (3) BHc: Coercive force, A/m-1

Table 3.8 Relative permeability parameter of materials and magnetism (Kraus, 1984)

Substance	μr, Relative Permeability ($kg \cdot m \cdot s^{-2} \cdot A^{-2}$)	Magnetism
Air	1.0000004	Paramagnetism
Aluminum	1.00002	Paramagnetism
Mild steel	2,000	Ferromagnetism

3.6 Finite Element analysis of ferromagnetic material

Figure 3.10 shows two dimensional FEA results before wear test of uncoated plate specimen using the test machine A configuration. The two dimensional model is plane of section perpendicular to the sliding direction at contact area of the plate and the ball specimens. In particular, it focused on magnetic field potential at contact area of the ball and the plate specimens. The element models are air, an uncoated plate specimen, a ball specimen and two permanent magnets. Figure 3.10(a) shows zones of element models by using different colours. The arrows on Figure 3.10(b), (c) and (d) denote the direction of Magnetic force, Magnetic flux density or Coercive force. In addition, the colour of arrows The ball holder was made from aluminum which is the approximate value that was a relative permeability of air as shown in Table 3.8. Hence the ball holder is not incorporated in composition elements. In Figure 3.10(a), the coercive force from two permanent magnets is 877 and -877 kA/m. Magnetic force *F* did not reach the interface between the ball and the plate. The magnetic flux density *B* within the contact area was 0.92 T. In addition, the coercive force *H* was not found at the other side of the contact area. Analysis results are shown in Table 3.9.

FEA results for a plate worn out 50 μm due to the sliding wear test in machine B are presented in Figure 3.10. They show that the magnetic force *F* between two specimens was 0.86 N. Figure 3.11 shows the result of FE analysis for Si_3N_4 ball and the mild steel plate. The flow of the magnetic flux was found to take place between the steel ball and the mild steel plates as shown in Figure 3.11(b). Both Figure 3.11(a) and 3.11(b), confirm that magnetic flux density is flowing from the plate to the steel ball. Furthermore, the magnetic flux density on the side of the contact area was higher than at the bottom of contact area before the ball and the plate. In comparison to the contact

between Si_3N_4 ball and mild steel plate, the magnetic flux density *B* for the contact of the steel ball and mild steel plate was a bit higher and equal to 0.24 T.

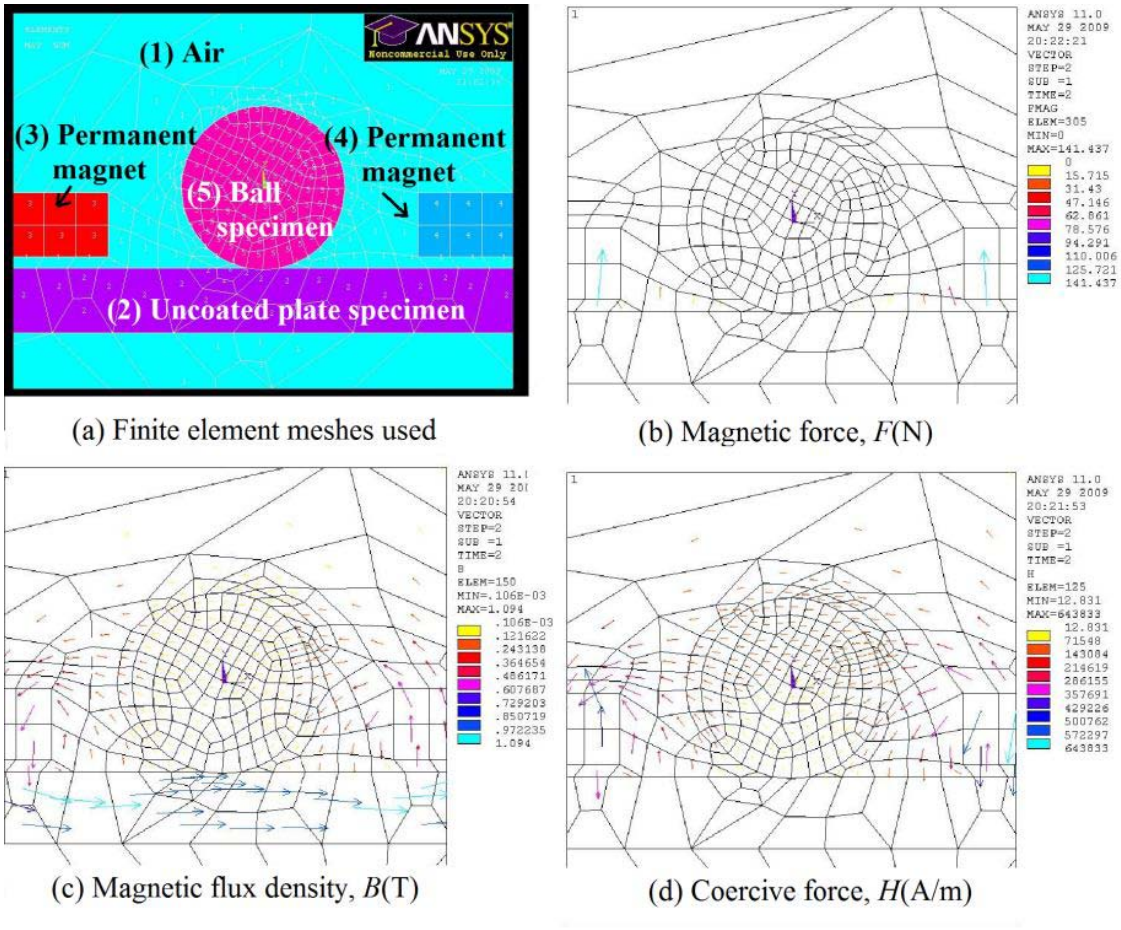

Fig 3.9 Finite element analyses (FEA) results of predefined at contact point in contour maps of magnetic field potential

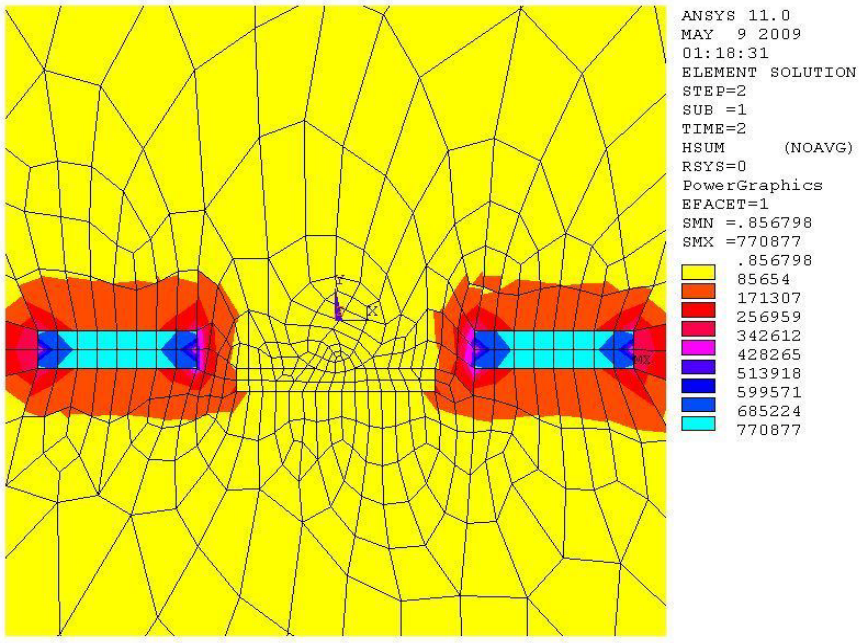

Fig 3.10 FE analysis result of magnetic force *F* (N)

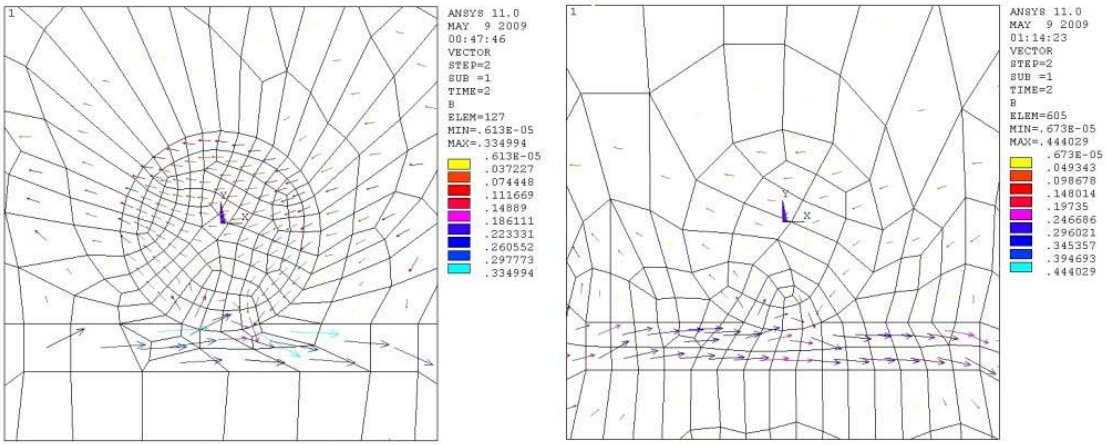

(a) Si_3N_4 ball vs. mild steel plate (b) Steel ball vs. mild steel plate

Fig 3.11 Magnetic flux density *B* of two kinds of combination, they are a couple of Si_3N_4 ball and mild steel plate and a couple of steel ball and mild steel plate.

Table 3.9 Magnetic field analysis results in the inferior region of the contact area under sliding wear test conditions which uses rare earth magnets

Sliding wear test machine	Combination of test specimen	*B* (T)	*H* (A/m)
A	Si_3N_4 ball vs. Mild steel plate	0.92	733.9
B	Si_3N_4 ball vs. Mild steel plate	0.20	159.5
	Steel ball vs. Mild steel plate	0.24	191.4

3.7 Loading under magnetic field

3.7.1 Attractive force measurement

A total load on the contact needs to be considered when the horizontal magnetic field and the dead load act simultaneously during sliding wear test in machine A. The magnetic field created by permanent magnets attracts the counter ferro-plates as described in the previous section. In order to calculate the Hertz contact stresses from the total load *P,* the attractive force between the permanent magnets and the counter ferro-plate has to be measured first. This section describes, therefore, the measurement of the attractive force.

3.7.2 Procedure to measure attractive force

To measure the attractive force, the sliding wear test machine A was used. The permanent magnets and additional dead weight were fixed to the ball holder. Then, the arm was kept horizontal with a balance weight. As shown in Figure 3.12, the attractive force is measured when the ball specimen is separated from the ferro plate by a load force F_2. Hence,

$$F_1 = \frac{l_2}{l_1} F_2 \qquad (3.5.1)$$

where

F_1; effect force, (attractive)
F_2; load, (force)
l_1; distance from load force F_2 to fulcrum
l_2; distance from effect force F_1 to fulcrum

In case of rare earth magnets, the ball specimen was detached from ferro plate when the

load force F_2, was equal to 40.9 N at the end of the arm at distance 215 mm from the fulcrum. The effect force F_1 was located at 170 mm from the fulcrum and was found to be 51.7 N. The value is 51.7 N. By the same procedure, the ferrite magnets produced attractive force of 29.7 N. Results are shown in Table 3.10.

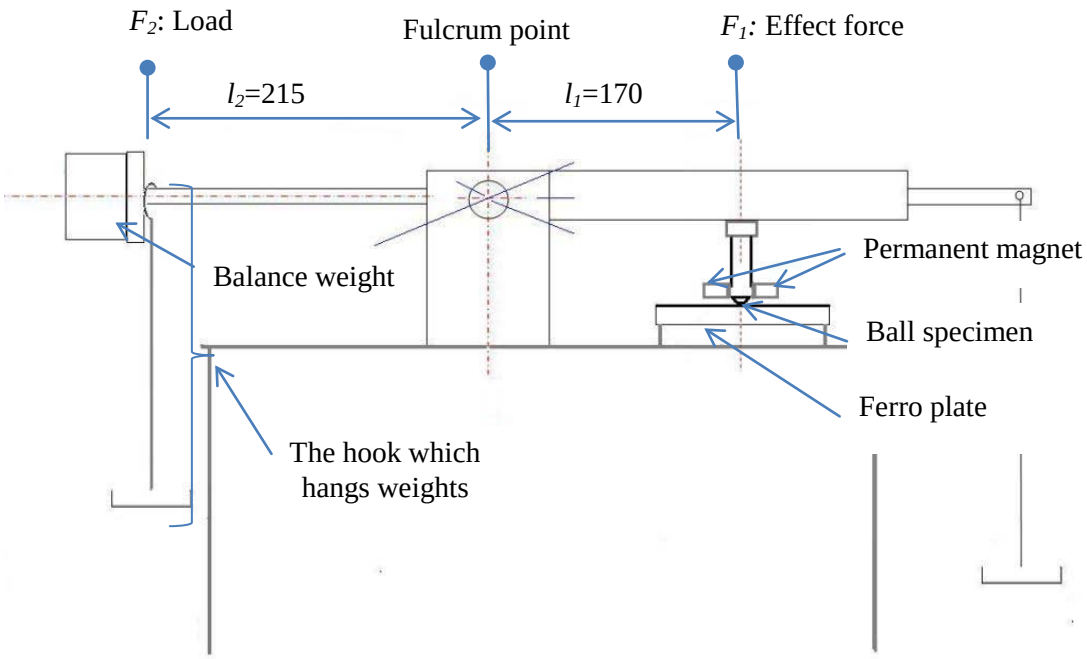

Fig 3.12 Measurement for attractive force

3.7.3 Total load on contact calculation

The state of static equilibrium can be expressed as shown in Figure 3.13.

$$F_4 = \frac{l_3}{l_1} F_3 + F_1 \qquad (3.5.2)$$

where

F_1; effect force and is the attractive force which calculated from Equation (3.5.1)
F_3; load force
F_4; total load on contact
l_1; distance from load force F_3 to fulcrum
l_3; distance from total load F_1 to fulcrum

When the magnetic field of the rare earth magnets is applied, a dead weight load F_3 of 1.2 N is applied at the point of 340 mm from the fulcrum. The effect force at 170 mm from the fulcrum is calculated by Formula (3.5.1) and the value is 55.2 N. On the other hand, the total load on the contact with the ferrite magnets is calculated so that the total load is to be 55.2 N the same as for the rare earth magnets. The dead weight load is given to be 8.5 N by Formula (3.5.2). Then, for the case of no magnetic field the dead weight load is 18.3 N in order to obtain total load of 55.2 N.

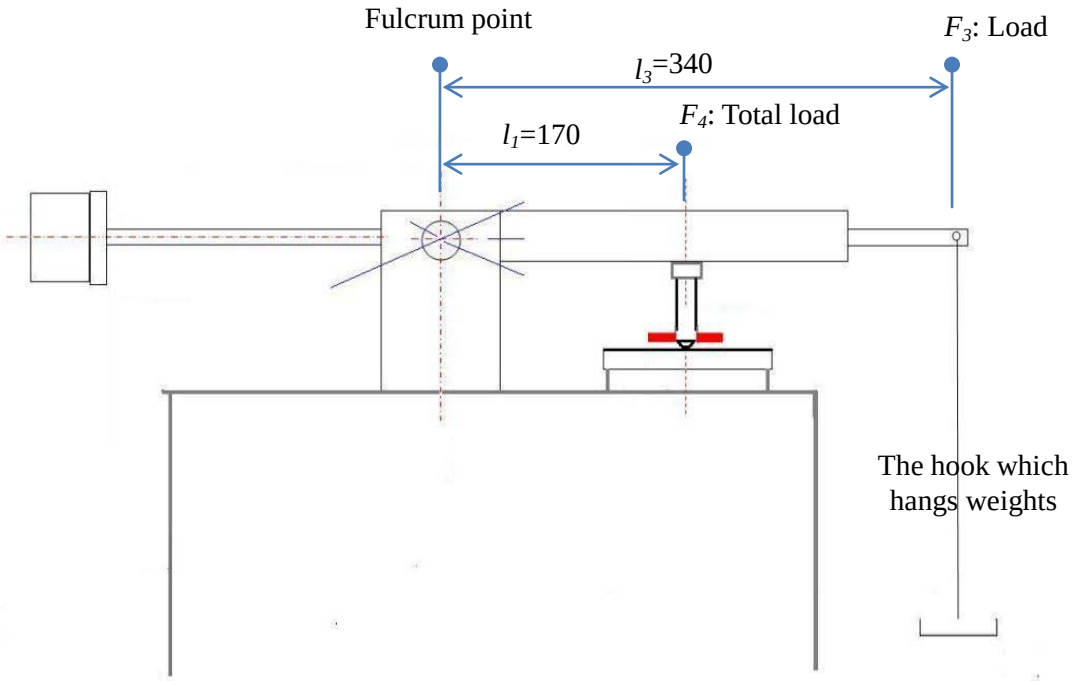

Fig 3.13 Force moment during sliding wear test

Table 3.10 Calculated total load and measurement results of magnetic field effect

	F_1, Attractive force (N)	F_2, load (N)	F_3, Dead load (N)	F_4, Total load (N)
Rare earth magnets	51.7	40.9	1.2	55.2
Ferrite magnets	29.7	22.3	8.5	55.2
No magnet	-	-	18.3	55.2

3.7.4 Lubrication regime

To estimate the thickness of the lubricating film, the film thickness between the contact surfaces and the lubrication regime were estimated using the classical elastohydrodynamic (EHD) formulae derived by Hamrock and Dowson (1981). The elastohydrodynamic film thickness was estimated by the substituting data parameters to EHD Formulae (2.11)-(2.12) (see Table 3.11). The central film thickness h_c and the minimum film thickness h_0 were 9.08×10^{-4} and 5.87×10^{-4} μm, respectively. The minimum film thickness h_c of the two real RMS surface roughnesses was substituted by

Formula (2.13), and the ratio of a minimum film thickness was 0.03. Hence, λ was less than 1 indicating plastic contact of the asperities. The calculation results and the RMS surface roughness of the two contacting bodies are shown in Table 3.12.

Table 3.11 Elastohydrodynamic film thickness and the operating conditions

α (mm^2/N)	k	η_0 (Pas)	U (mm/s)	E' (N/mm^2)	W (N)	R (mm)	hc (μm)	h_0 (μm)
$0.18x10^{-3}$	1	0.0189	8.59	$271.06x10^{9}$	55.24	6.35	$9.08x10^{-4}$	$5.87x10^{-4}$

Table 3.12 The calculated minimum film thickness and the ratio of minimum film

Sample	σ_A (mm) Si_3N_4 ball	σ_B (mm) mild steel plate	h_0 (mm)	λ
Before test	$0.30x10^{-5}$	$1.90\ x10^{-5}$	$5.87x10^{-7}$	0.03

3.7.5 Contact stresses

The dry sliding wear experiment was conducted under the total load of 55.2 N created by the attractive force and the dead load. In the case of uncoated plate, the width of the contact area a and the maximum contact stress P_{max} were calculated from Equations (2.1) - (2.2), and the values are 169 μm and 925.4 MPa, respectively. Besides, the calculation result for coated plate is different from the uncoated plate of calculation result. Therefore, two calculation results are shown in Table 3.13.

Table 3.13 Calculated Hertz contact stresses and depth of shear stress

	a (μm)	P_{max} (MPa)	$P_{average}$ (MPa)	δ (μm)	τ_{max} (MPa)	z (μm)
Uncoated	169	925.4	617	1.8	308.5	10.8
Coated	167	925.4	617	1.8	308.5	10.6

3.7.6 High frequency sliding contact stresses

The high frequency sliding wear experiment was conducted under a normal load produced by using dead weights, and was 3.5 N. In addition, the width of the contact area *a* and the maximum contact stress P_{max} are calculated by Formula (2.1) - (2.2), and the values are 0.67 μm and 370 MPa, respectively. Furthermore, the depth *z* at which maximum shear stress τ_{max} of 123.3 MPa occurs is 0.43 μm. Hertz contact stresses of sliding wear machine B, are not affected by the horizontal magnetic field.

Maximum contact pressure for 100Cr6 ball and mild steel plate combination is 370 MPa as well as for Si_3N_4 ball and mild steel plate combination. Then, contact area dimension *a* maximum shear stress τ_{max}, and the depth *z* were obtained from Formula (2.2)-(2.4)-(2.6). Finally, the dead weight is also obtained from Formula (2.2) and it is 5 N. The results are shown in Table 3.14.

Table 3.14 Calculated Hertz contact stresses and depth of shear stress

Combination	*a* (μm)	P_{max}, (MPa)	$P_{average}$ (MPa)	δ (μm)	τ_{max}, (MPa)	*Z* (μm)	*W* (N)
Si_3N_4/ mild steel plate	0.67	370	246.7	0.29×10^{-2}	123.3	0.43	3.5
100Cr6 ball/ mild steel plate	0.80	370	246.7	0.41×10^{-2}	123.3	0.51	5.0

3.8 Test procedure and test parameters

In this study two types of testing machines A and B were used. This section outlines experimental procedure and conditions used.

3.8.1 Friction machine A used in dry sliding wear testing and lubricated wear testing

3.8.1.1 Test procedure

I. The plate specimen and ball specimen were dried naturally after they were cleaned by acetone using an ultrasonic washing machine.

II. Before starting wear testing, weight measurements, surface roughness measurements and optical micro scope observations of the surface were carried out.

III. A plate specimen was fixed to the movable stage of ball-on-plate sliding wear test apparatus. The ball specimen was inserted to a ball holder.

IV. Permanent magnets were attached to a bracket with adhesive tape and cellophane tape. The bracket was fastened to the ball holder with bolts. The bracket had a gap of 1 mm at the interface between the frame and permanent magnet.

V. The arm of a wear testing machine was made horizontal with a spirit level.

VI. In the case of lubricated wear test, an enclosure was made in order to prevent the leakage of lubricant from the contact area. The enclosure was made by 0.5 mm

thick plate and was 30 mm in length and 10 mm in width. It is shown in Figure 3.14. The enclosure was filled with 0.2 ml of lubricant.

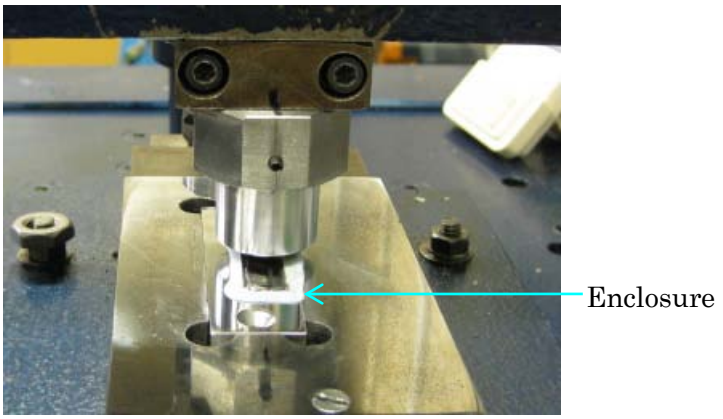

Fig 3.14 View of the enclosure

VII. Dead weight was applied as shown in Figure 3.2 and the preparation for testing was completed.

At the beginning of sliding wear experiment, the ball specimen was contacted with the plate specimen. The wear machine A was running when the ball was contacting the plate specimen. The plate specimen on the movable stage executed reciprocating motion.

3.8.1.2 Test parameters

The total load applied to the specimens is the sum of the magnetic force and dead load because permanent magnets attract the plate specimen. Resulting contact stresses were 925 MPa as shown in Table 3.14. The average sliding speed was 8.6 mm/s, and amplitude was 15mm; hence, corresponding frequency was 0.29 Hz. The total number of sliding stroke was approximately $213x10^3$ strokes requiring 23 hours of testing. To examine the magnetic field effect on wear, the tests were stopped every $24x10^3$ strokes and weight measurements, the surface roughness measurements and the optical microscope observations were carried out.

3.8.2 Friction machine B used in frequency sliding wear tests

3.8.2.1 Test procedure

I. The procedure for high frequency sliding wear test was same similar to that for wear test in low frequency sliding wear test.

II. A plate specimen was screwed on to the stage.

III. The permanent magnets were fixed to the stage. The permanent magnets were on both sides of the plate specimen and at a right angle to sliding direction.

IV. A ball specimen was inserted into the ball holder, and it was attached to the arm of wear test machine B.

V. The dead weight was applied to the ball holder.

VI. The preparations for the test were completed when the experimental parameters of time, frequency and amplitude were set up.

The adjustment of magnetic field direction could be performed by changing the position of the stage.

3.8.2.2 Test parameters

The experiments were carried out at 5.0 N normal load using dead weights. According to Hertz's theory, width of the contact area a and the maximum contact pressure p_0 were 8.0×10^{-5} m and 370×10^{6} N/mm^2 respectively. The load on contact was kept contact during the duration of the test. Three frequencies, namely 1.75 Hz (low), 14 Hz (intermediate) and 21 Hz (high) were used. The amplitude was set up to 1 mm. Inspection intervals were after 145 $\times 10^{3}$ strokes and the test finished after about 1,304 $\times 10^{3}$ strokes. Two types of permanent magnet were used, namely a rare earth magnet and a ferrite magnet.

3.9 Experimental techniques

Some additional post-test investigations experiments were carried out to evaluate the effect of magnetic field. They included hardness measurements, observations of the appearance on surface of test specimen, scanning electron microscope (SEM) observations and X-ray Diffraction (XRD) analyses. The distribution of wear debris on the plate specimen was investigated in order to find out the influence of magnetic field direction. SEM observations and SEM analyses were performed on wear particles. Moreover, the XRD analysis was attempted. The plate specimen was removed from the apparatus and washed using an ultrasonic cleaning device. Then weight measurement, optical micro scope observation, surface roughness measurement and surface profile measurement were carried out. The observation and measurements were carried out at the locations shown in Figure 3.15. Then, the specimen was cut and embedded in a resin and the cross section of the specimen was polished. The cross-section of the wear track was provided for an optic microscope observation and SEM observation. The wear track on the plate specimen which was tested in the high frequency sliding wear testing machine, was observed by an SEM.

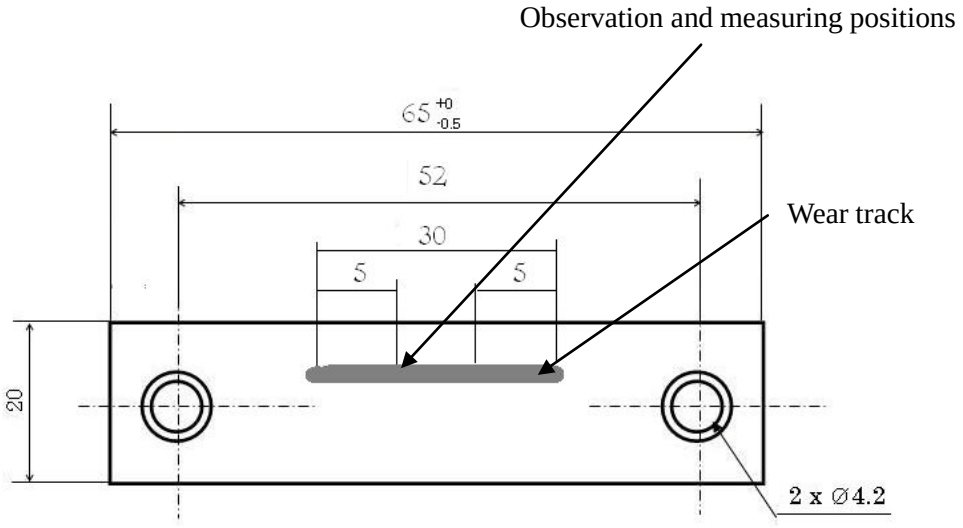

Fig 3.15 Illustration of measurement points

3.9.1 Hardness measurements

The hardness of the test specimens were measured with Vickers micro hardness tester, because hardness is an important characteristic of tribological behaviour. Thereupon, the hardness was employed to confirm the influence of the horizontal magnetic field to the mechanical property of materials. The plate specimen 5 mm in length and 20 mm in width and thickness of 5 mm was cut and embedded in a resin. The cross section was polished to make it ready for micro hardness measurements. In case of a plate specimen under magnetic field, the plate specimen was positioned halfway of the gap between two permanent magnets. Two permanent magnets were apart 34.2 mm. The results of micro hardness measurements were averaged and the maximum and minimum values were ignored. The arrangements are shows in Figure 3.16.

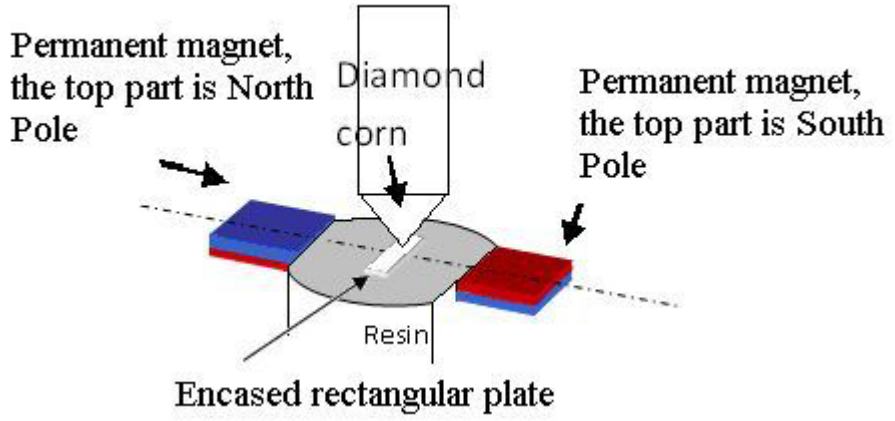

Attractive force is working on between permanent magnets.
Fig 3.16 Illustration of Vickers micro hardness measurement

3.9.2 Appearance of test specimen after testing

The optical microscope observations were carried out using OLYMPUS microscope, which magnification range is between 20 and 1000 times.

The surface profile and the surface roughness measurements were performed using Talysurf 2D surface profiler. The liner surface profiles can be measured by the Talysurf in which the stylus profilometer with a 2 mm/60 degree diamond tip is contacting the surface.

3.9.3 Scanning Electron Microscope (SEM) Observations

The distribution of wear debris around wear track was observed and some of them were collected for further analyses. Wear particles were examined by Back Scatter Electrons and Secondary Electrons techniques to examine their size and shape.

The search for subsurface cracks within the wear track was carried out using SEM on cross section of the contact area. Plates were cut through perpendicular to the sliding direction, polished and embedded in the resin for measurement and observations. ZEISS SUPRA 35VP type SEM and Joel 840 SEM were used.

3.9.4 X-ray Diffraction (XRD) Analysis

The wear debris and the wear surface were analysed by an X-ray diffraction machine (Bruker D8 Advance X-ray Diffractometer with Bragg-Brentano geometry). The instrument is used to study the crystalline structure of a wide range of materials.

References for chapter 3

ASM handbook. Volume 20, (1997) Materials selection and design / prepared under the direction of the ASM International Handbook Committee. Publication: Materials Park, OH : ASM International, 1997. Page 427

Hamrock, B, J. and Dowson, D., (1981) Ball Bearing Lubrication, The Elastohydrodynamics of Elliptical Contacts, John Willey Sons.

Iraj, H, P., Mamaghani, T, Usami. and Mizuno, E., (1996) Inelastic large deflection analysis structural steel members under cyclic loading, engineering structures, vol. 18, No.9, pp.659-668.

Kraus, D, J., (David, J.) (1984) Electromagnetics. New York; London: McGraw-Hill

Luxemotor"KEI". (2005). Steel%20BS4360%2043A [1]. [Online] available as: http://www.luxe-motor-kei.co.uk/documents/Steel%20BS4360%2043A.pdf (Accessed 10/11 /08)

Marui. en_100Cr6ing[1].pdf. [Online] available at: http://www.trafileriamauri.com/allegati/prodotti/en/en_100Cr6ing.pdf (Accessed 10/11 /08)

OPIEoil.co.uk. (2006) Castrol GTD Magnatec 10W40 data sheet, [Online] available at: 20th Jan. 2006. http://www.opieoils.co.uk/pdfs/castrol/Magnatec%20Range/GTD%20Magnatec%2010W-40.pdf#search (Accessed 10/11/08)

SEED Foundation. Viscosity. [Online] available at: http://www.sicenbyjones.com/viscosity.htm (Accessed 10/ 11/08)

VIKRAM. 3Hybrid [1] .pdf (SECURED). [Online] available as: http://www.vikramgmn.com/catalogue/3Hybrid.pdf (Accessed 25/09/07)

Chapter 4 Experimental Results

4.1 Introduction

This chapter presents experimental results obtained from three types of sliding contact test. The results include:

- Mass loss of a plate specimen and a ball specimen

  The mass loss of specimens is expressed by a total of the accumulation.
- Surface roughness *Ra* of the wore surface on plate specimen
- Appearance of wear surface and debris observation

Furthermore, SEM, XRD, FEA analyses and Vickers micro hardness measurements provides supplementary information for interpretation of experimental results. Table 4.1 summarizes parameters for magnets arrangements which based on magnetic flux density of magnets and the magnetic field orientation. For instance, when magnets of magnetic flux density 1.1 T were arranged to magnetic field orientation 90 degrees, the experimental arrangement for magnets is designated as 1.1T90.

Table 4.1 Experimental arrangements for magnets

Magnetic flux density (T)	Magnetic field orientation			
	θ=0º	θ =35 º	θ =45 º	θ =90 º
0	0T0	-	-	-
0.4	0.4T0	0.4T35	0.4T45	0.4T90
1.1	1.1T0	1.1T35	1.1T45	1.1T90

First, the influence of the magnetic field during dry sliding wear testing with low frequency is described. Then, the next section presents the effect of magnetic field observed during lubricated wear experiment. The final section deals with the magnetic field effect on the high frequency sliding wear test.

4.2 Dry sliding wear experiment

4.2.1 Different Magnetic Field Orientation

Figure 4.2.1 illustrates accumulated mass loss of uncoated plate specimen versus the number of sliding strokes under different magnetic fields. The accumulated mass loss was in proportion to the number of sliding strokes, and the tendency was a gradual rise. Unexpectedly, the mass loss at 0T0 was 1.19 mg after the first interval of sliding strokes and, raised about 0.1 mg in comparison with the mass loss under the influence of the magnetic field. In addition, the mass loss at 0T0 tended a plateau from $48x10^3$ to $72x10^3$ strokes. From $96x10^3$ strokes, it tended a steady increase to $192x10^3$ strokes for the accumulated mass loss. However, the mass loss at 0T0 after $48x10^3$ strokes was less than after $72x10^3$ strokes as indicated by a red arrow in the figure. Hence it is estimated that the accumulated mass loss is an error in the measurement. On the other hand, the mass loss at 1.1T90 obviously increased more than other at directions of the magnetic field from $120x10^3$ strokes. When the mass loss of the plate specimen was over 2.0 mg from $120x10^3$ to $144x10^3$ strokes, the highest mass loss of other magnetic field direction, 1.1T0 and 1.1T45 was about 1.6 mg. Thus, it is concluded that the magnetic field direction of 1.1T90 increases the wear amount of the plate.

Figure 4.2.2 presents the accumulated mass loss of the ball specimen. For all test conditions there was a steady increase until $216x10^3$ strokes. The mass loss shown in Figure 4.2.1 indicates that the accumulated mass loss at 1.1T90 was higher than for the other test conditions from $72x10^3$ strokes. Also the tendency at 1.1T45 was second highest for every test conditions used.

Surface roughness *Ra* of the wear track on uncoated plate specimen for different angles of magnetic field direction is presented in Figure 4.2.3. As indicated in the figure, the *Ra* at the

absence of magnetic field fluctuated within a range from approximately 0.5 to 0.8 μm. Whereas, the presence of magnetic field resulted in wider fluctuations of *Ra* values compared with the absence of magnetic field, and the fluctuation range was approximately 0.5 to 1.8 μm. In particular, the fluctuation range of *Ra* values at 90 degree orientation of magnetic field was largest (see Fig 4.2.1).

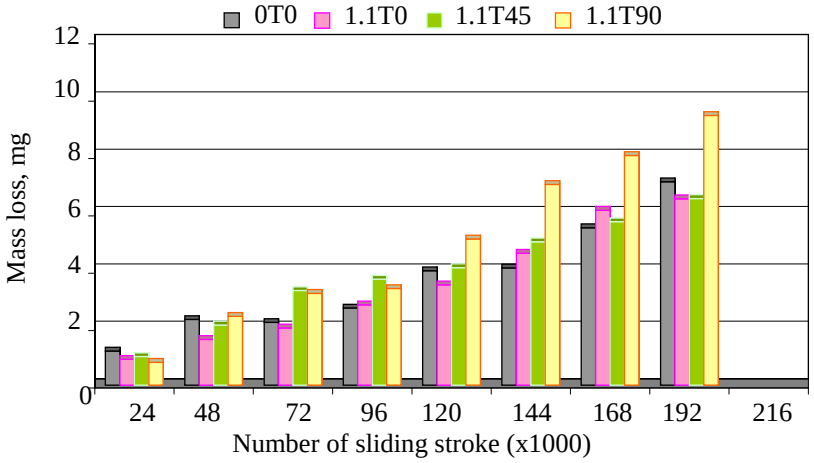

Fig 4.2.1 Accumulated mass loss of uncoated mild steel plate at three types of angle (Dry sliding contact wear test)

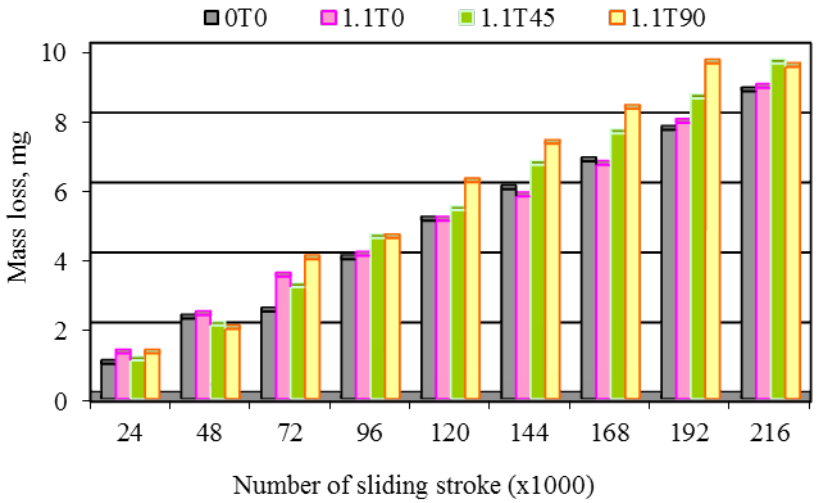

Fig 4.2.2 Accumulated mass loss of Si_3N_4 ball at three types of angle (Dry sliding contact wear test)

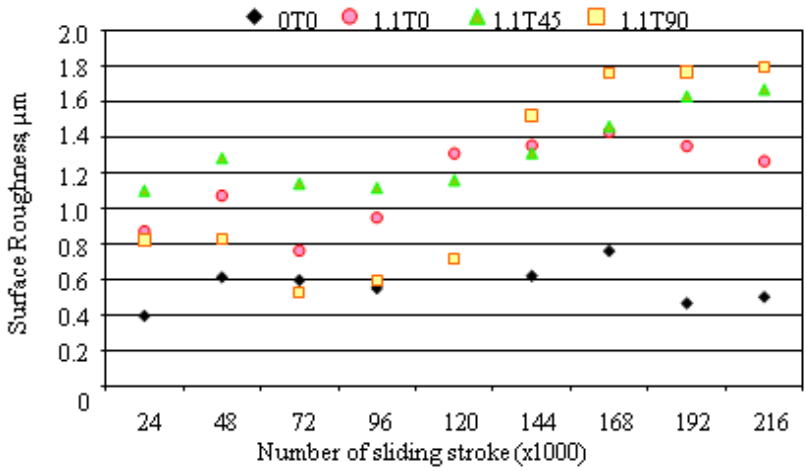

Fig 4.2.3 Surface roughness of uncoated plate in different angle of magnetic field direction

Topography on the surface of a plate and a ball specimen

Figure 4.2.4 shows the two-dimensional surface profiling for the outline of wear track on the plate specimen which was produced by the surface profile measurement. Optical microscope images depict wear tracks on the ball and plate specimens for created after $48x10^3$ and $192x10^3$. Table 4.2.1 shows the supplementary information concerning the width and the depth of the wear tracks.

- Surface profile of plate specimen

The wear surface created under the influence of the horizontal magnetic field has a jagged profile. In addition, deep grooves or pits were observed. Similar to results by Hirazuka et al. (1986), the wear surface presented an aspect of the severe wear. The grooves or the pits became clearly deep after $192x10^3$ strokes. The multiple grooves observed in Figure 4.2.4 (a-2) and (d-2) were deeper than 52 μm. In the wear surface shown in Figure 4.2.4 (b-2), such deep grooves were not observed.

- Wear surface on a ball specimen

Comparing wear surface of the ball after $192x10^3$ strokes with that after $48x10^3$ strokes using the width measured by a surface profile, it can be seen that significant increase of the width took plate.

- Wear surface on a plate specimen

In the wear track on the plate, fine scratches were observed and they were similar to the wear surface on the ball aligned in the sliding direction. After $192x10^3$ strokes, there was a delamination area which produced flakes in all images except Figure 4.2.4 (c -2).

- Summary

The tendency of the accumulated mass loss of the plate rose step-by-step. It was slightly

decreased after $48x10^3$ strokes because of the presence of magnetic field. In addition, the accumulated mass loss became stable between $96x10^3$ and $144x10^3$ strokes. Magnetic field direction resulting in the highest mass loss was 1.1T90 (θ =90°). Magnetic field direction 0T0 (θ =0°) produced the lowest mass loss. The mass loss was comparable to that of no magnetic field conditions.

The accumulated mass loss of the ball was stable unlike the accumulated mass loss of the plate which was gradually rising. In addition, the relationship between the surface roughness *Ra* and the mass loss probably affected the increase and decrease of the quantity of wear. The 2-D surface profiles of the wear surface produced without magnetic field and 1.1T90 show deep grooves. It was not observed in 1.1T0 and 1.1T45.

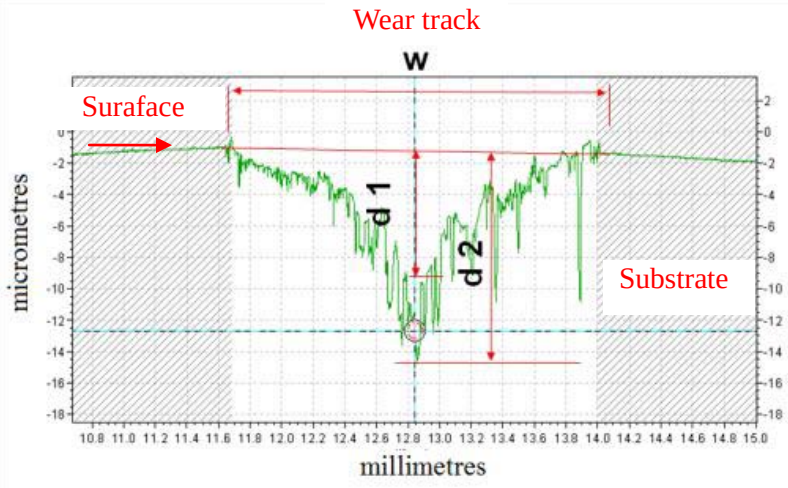

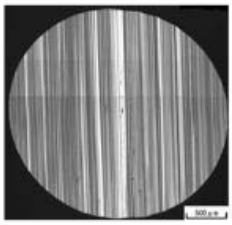
Ball

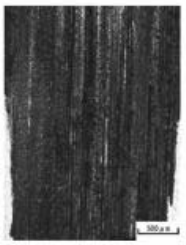
Plate

Fig 4.2.4 (a-1) 0T0, 48x10^3 strokes

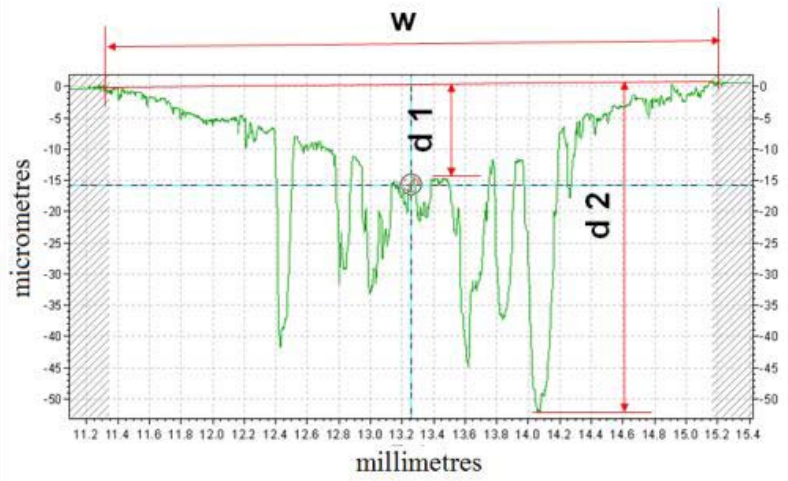

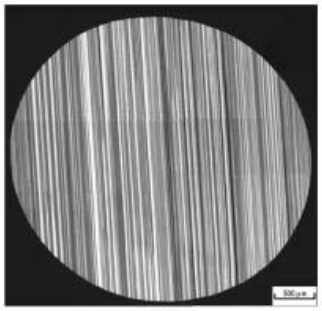
Ball

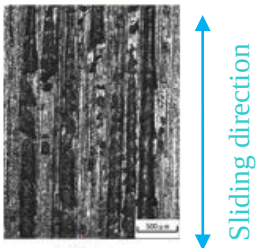

Plate

Fig 4.2.4 (a-2) 0T0, 192x10^3 strokes

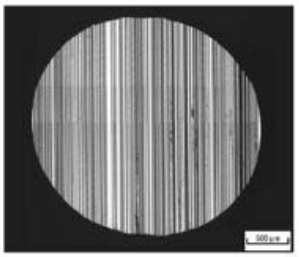
Ball

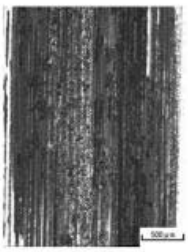
Plate

Fig 4.2.4 (b-1) 1.1T, 48x10^3 strokes

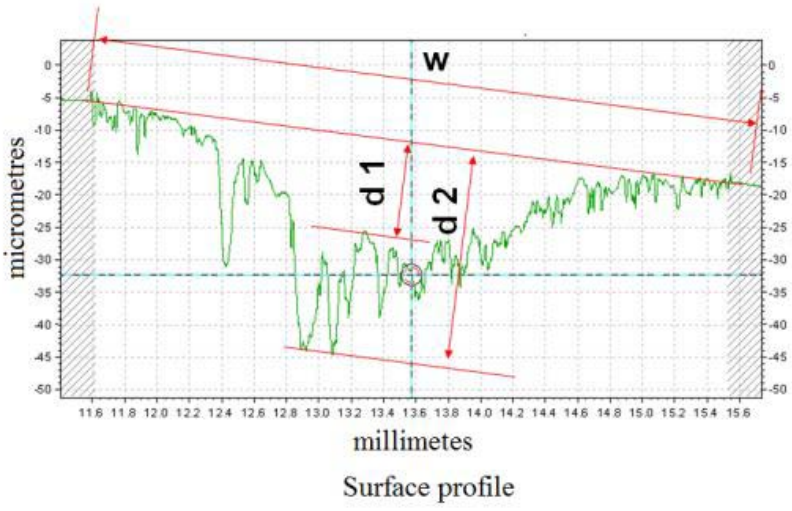

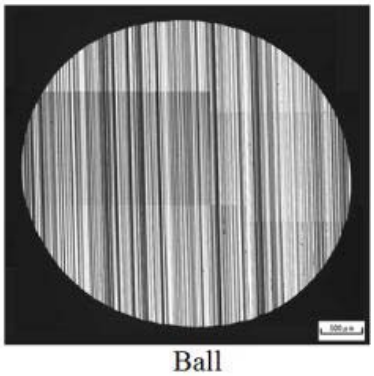
Ball

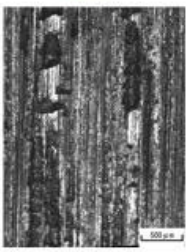
Plate

Sliding direction

Fig 4.2.4 (b-2) 1.1T0, 192x10^3 strokes

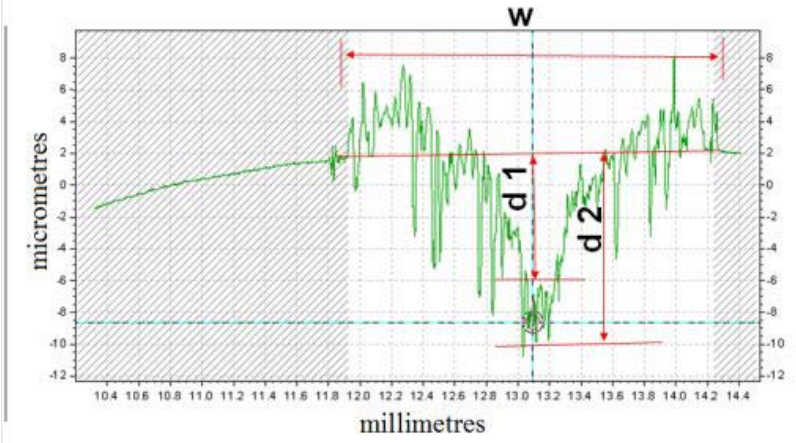

Surface profile

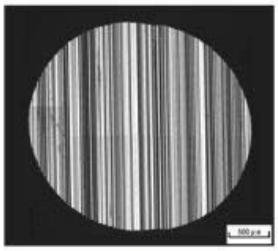

Ball

Plate

Fig 4.2.4 (c-1) 1.1T45, 48x10 ^{3} strokes

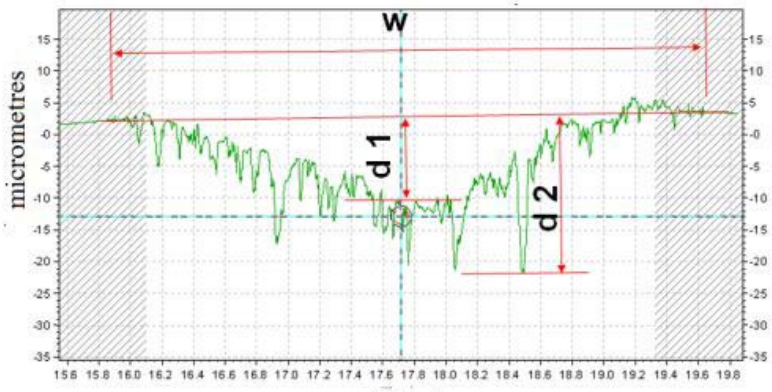

Surface profile

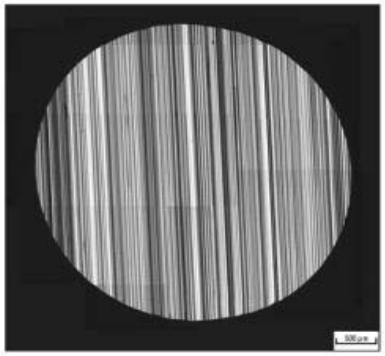

Ball

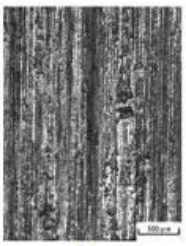

Sliding direction

Plate

Fig 4.2.4 (c-2) 1.1T45, 192x10^3 strokes

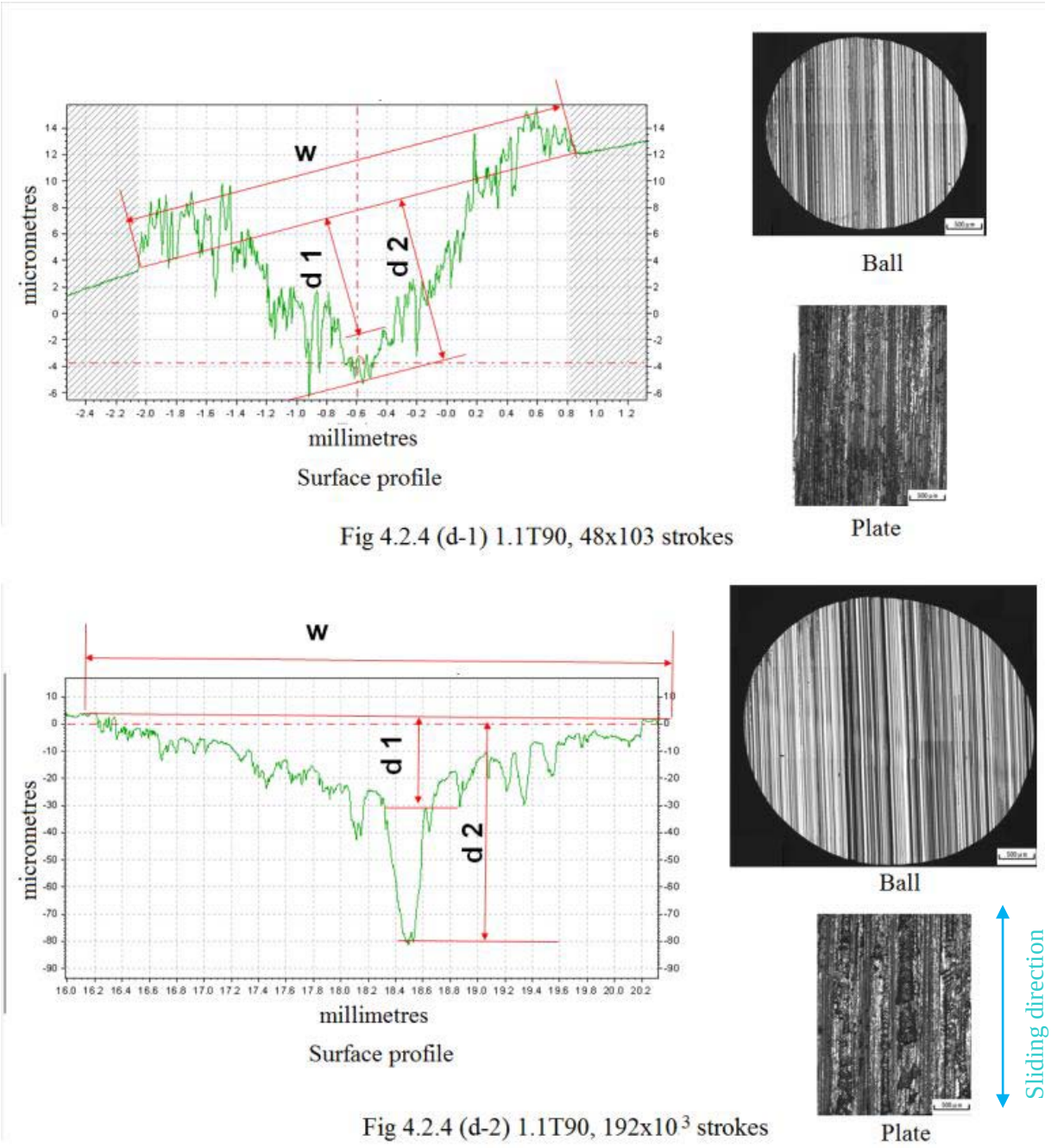

Fig 4.2.4 Surface profiling and surface observation of plate and ball specimen (50 x magnifications) note: The w is the width. The *d1* is the depth of wear track. And the *d2* is the depth of wear track however it is including the depth of pits.

Table 4.2.1 Size of wear track is indicated in Figure 4.2.3

	Size, μm		
(a-1)	w=2360,	d1=8.0,	d2=13.5
(b-1)	w=2220,	d1=7.0,	d2=9.5
(c-1)	w=2500,	d1=7.0,	d2=11.5
(d-1)	w=2950,	d1=10.0,	d2=12.5

	Size, μm
(a-2)	w=3900, d1=15.0, d2=52.0
(b-2)	w=4100, d1=15.0, d2=33.0
(c-2)	w=3770, d1=13.0, d2=25.5
(d-2)	w=4200, d1=24.0, d2=81.0

Observation of wear track appearance

The wear track on the plate was examined by an optical microscope (200 and 500 magnifications), 2-D surface profiling, and the SEM image of the track cross section. Additionally, the influence of no magnetic field and the presence of magnetic field with different directions were compared. Figure 4.2.5 shows the optical micrographs of the wear surface which were taken after $48x10^3$ and $216x10^3$ strokes. There are mainly fine scratches on all wear surfaces.

A coarse surface appeared in the wear area produced after $48x10^3$ strokes without the magnetic field, as indicated in Figure 4.2.5 (a-1). On the other hand, initial cracks, occasional pits, flaking and spalling were observed on wear surfaces produced after $48x10^3$ strokes with the magnetic field. An initial crack can be seen in Figure 4.2.5 (b-1) and (c-1), and the delamination area in the form of spalling and flaking is visible in Figure 4.2.5 (d-1). After $216x10^3$ strokes, delamination area was spread, and became very clear.

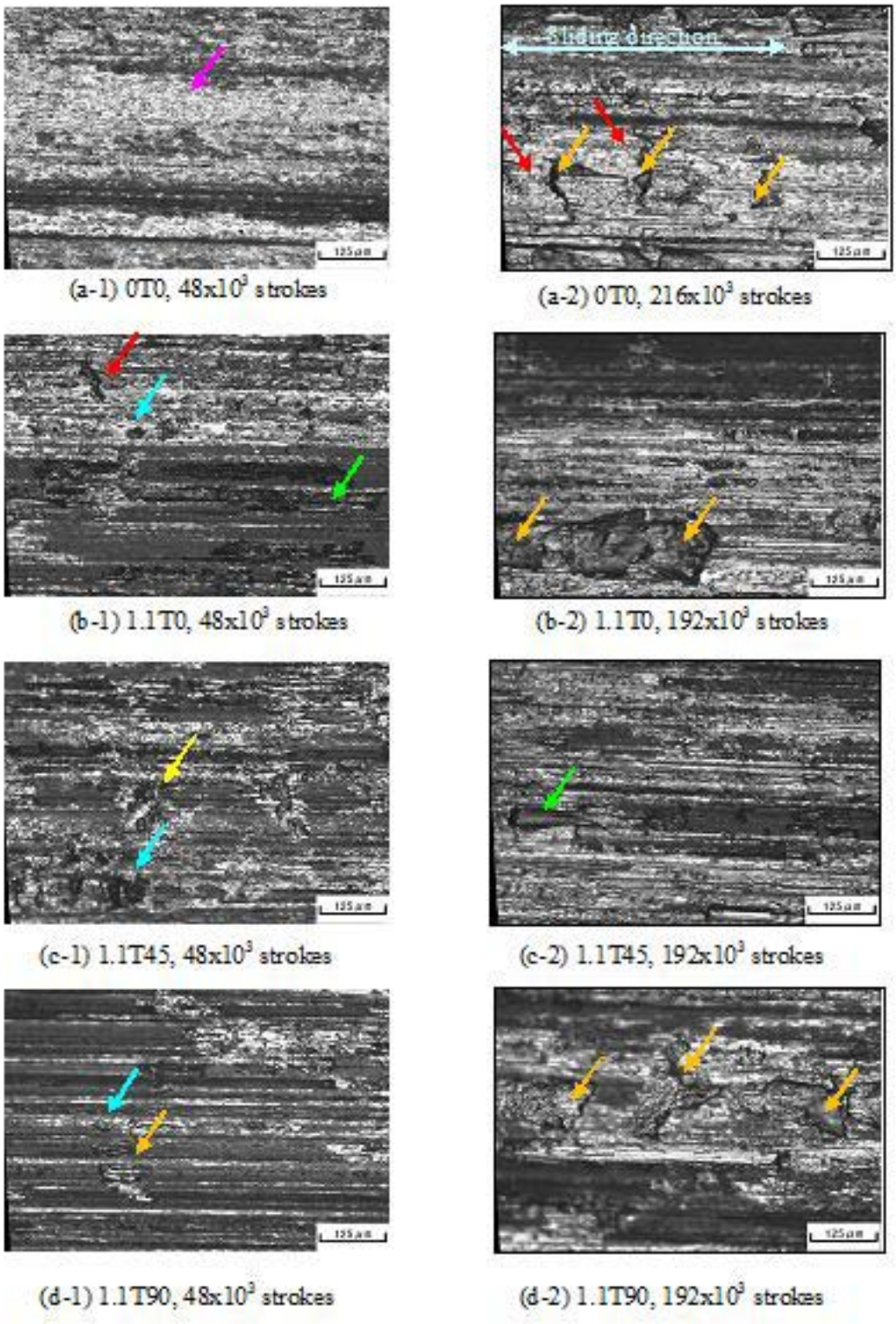

Fig 4.2.5 Surface observation of uncoated plate at $48x10^3$ and $216x10^3$ strokes (Optical Micrographs were taken at 200 times magnification, →: flaking, →: pitting, →: spalling, →: coarsing surface, →:spalling, →:crack)

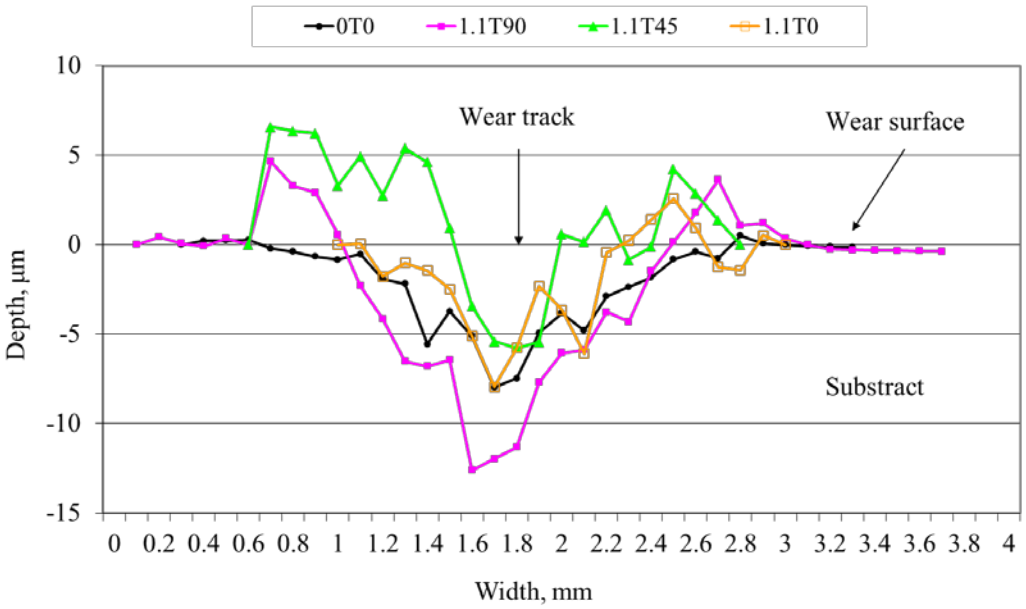

Fig 4.2.6 Comparison of 2-D surface profiling of uncoated plate specimen after $24x10^3$ strokes

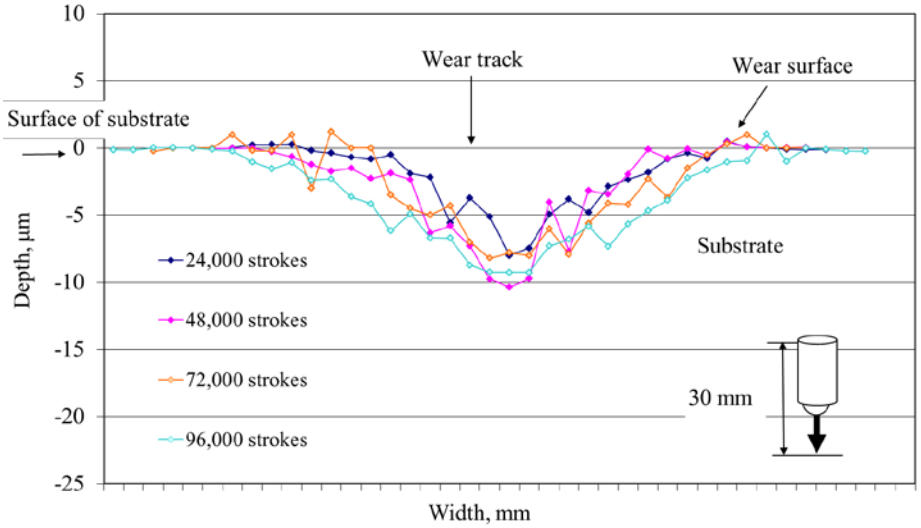

(a) 0T0

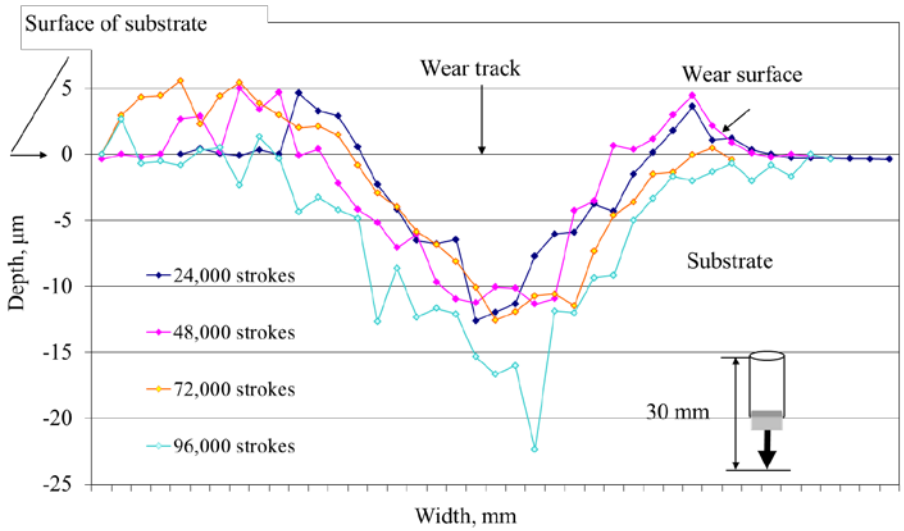

(b) 1.1T90

Fig 4.2.7 Relationship of number of sliding strokes and surface profiling

Figure 4.2.6 compares 2-D surface profiles of the wear track for 0T0, 1.1T0, 1.1T45 and 1.1T90 generated after $24x10^3$ strokes. The differences can be summarized as follows;

- Only as for wear track which was produced under the presence of magnetic field, the bulging was observed on both sides of wear track. For 1.1T0 it was about 3 μm in height, and for 1.1T45 it was larger than for any other magnetic field direction and equal to about 6 μm.
- Surface profile for 0T0 was deeper than that for 1.1T0 and 1.1T45. Furthermore, in the surface profile for 1.1T45, the bulging area was large in comparison to the area of the wear grove.

Figure 4.2.7 (a) and (b) show changes of the surface profile of the plate specimen with the number of sliding strokes. The surface profile of 1.1T90 after $96x10^3$ strokes shows that the bulging was rubbed off the surface.

Characteristic features of a delamination area beneath the interface are revealed by SEM observations of the cross section of the wear track. Figure 4.2.8 shows SEM-images of the cross section of wear track after $216x10^3$ strokes. The left figure is a bottom area of wear track and the light figure is a side area of wear track. The characteristic features are as follows:

- Multiple cracks of curved shape in the bottom of the delamination area are observed in Figure 4.2.8 (a-2) and (c-2).
- Small cracks originating at the bottom of the delamination area are observed in Figure 4.2.8 (b-1), (c-1) and (d-1).

- Surface asperities can be seen the surface of the bottom in Figure 4.2.8 (a-1), (b-1), (b-2) and (d-1).
- Smooth surface can be seen in Figure 4.2.8 (d-2).
- Visible fine crack is of horizontal direction. It is about 6 μm below the outer layer in Figure 4.2.8 (b-2) and in Figure 4.2.8 (c-2) it is about 2 μm below.

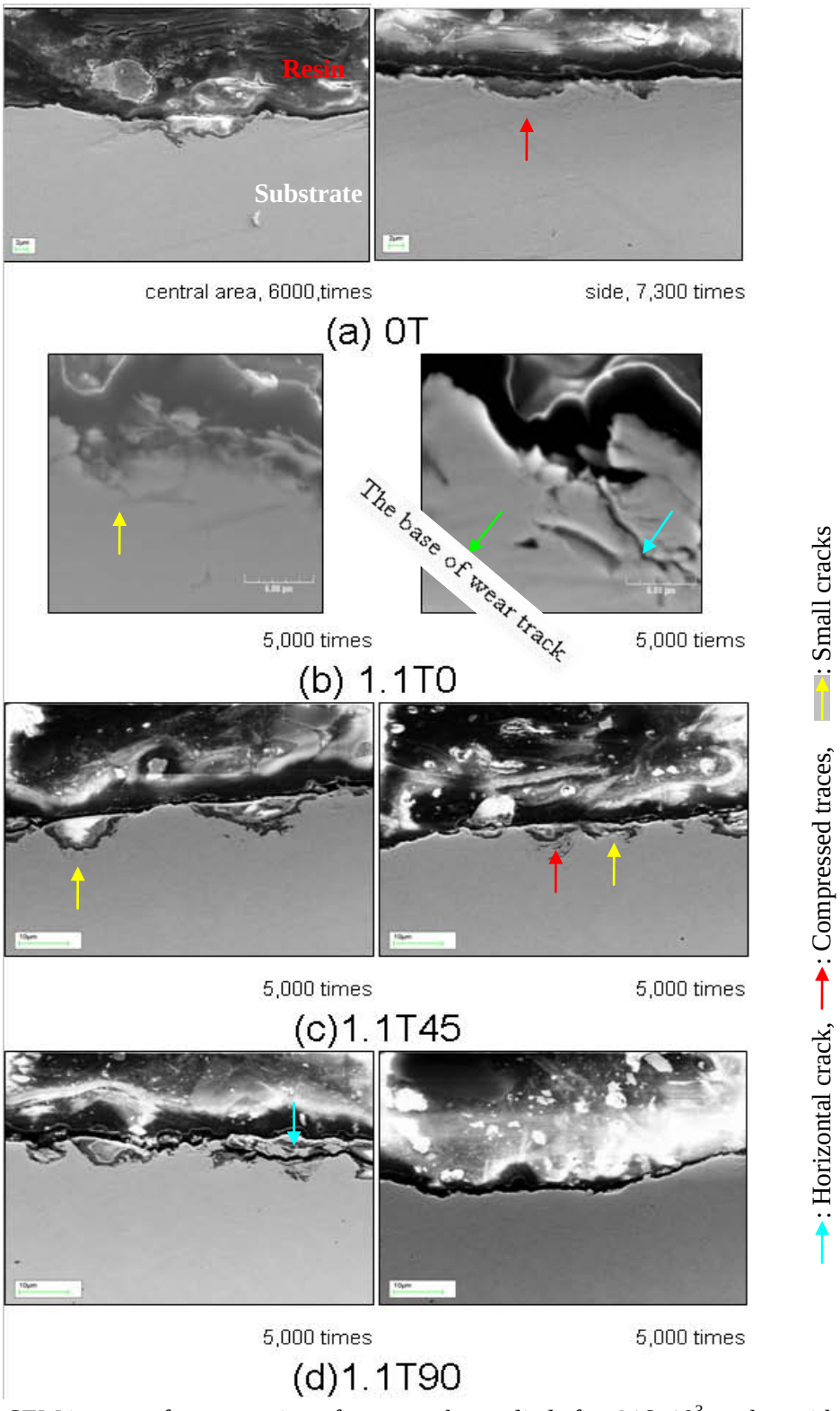

Fig 4.2.8 SEM images of cross section of wear track supplied after $216x10^3$ strokes with and without the magnetic field, left side of SEM images are the bottom of the wear track, and right side of SEM images are the side of the wear track.

4.2.1.1 Wear debris behaviour

Assessment of the magnetic field effect is based on arrangement of debris and observations of debris location just after a sliding wear test. Arranged wear debris around wear track are shown in Figure 4.2.9. Moreover, the right side drawings of Figure 4.2.9 illustrate the sliding direction and a magnetic field direction in a schematic way for each test conditions. In addition, Table 4.2.2 summarizes the arrangements of the wear debris.

Aligned wear debris at 1.1T0 differ from that for 0T0. In addition, a few wear debris at 1.1T90 accumulated on the surface of the plate specimen. Therefore it appears that the wear debris was removed from the wear track by the external of magnetic field.

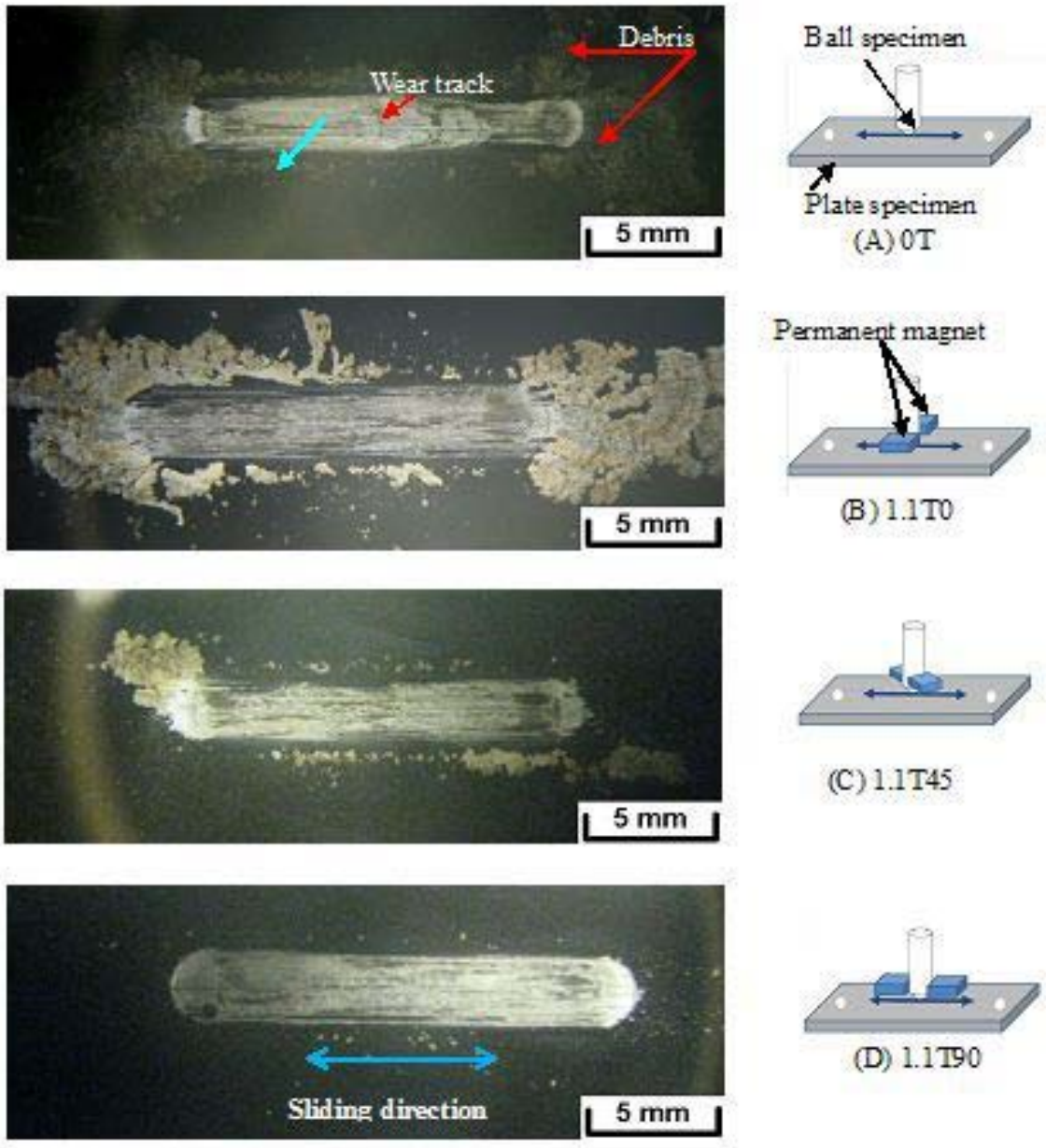

Fig 4.2.9 Location of wear debris around wear track after $24x10^3$ strokes

Table 4.2.2 Properties of debris location

	Both end of a wear track	Alongside a wear track
0T	Wear debris spread like a fan.	It accumulated alongside the wear track.
1.1T0	It accumulated beside of end of wear track.	It was spread out to vertical direction.
1.1T45	One side	Debris was scattered at random.
1.1T90	The white wear debris dotted	The white wear debris was dotted

Elemental composition of a small area on the wear debris is shown in Figure 4.2.10. The presence of the Ferro system debris revealed by backscatter electron image and secondary electron image ought to be noticed.

White particles and gray particles were observed in the backscatter image as shown in Figure 4.2.10 (a-1). The white particle contains mainly iron. Other particles contain silicon and oxygen. Figure 4.2.10 (a) shows ferro particle about 6 μm in diameter. The shape is close to a sphere. Besides same of Si-system particles were also observed around the ferro particles. On the other hand, the wear particle at 1.1T0 is an agglomerated particle including iron, oxygen and silicon as shown Figure 4.2.10 (b-1) and (b-3). Wear particle at 1.1T90 consists of long particles which as shown in Figure 4.2.10 (c-1). The magnetism of the large ferro particle was attracting the long wear ferro particle. The wear debris was not of a flat shape.

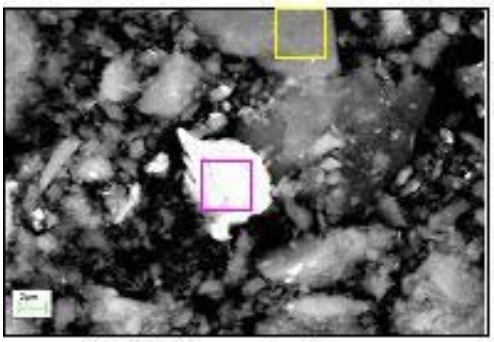

(a-1) Back-scatter image

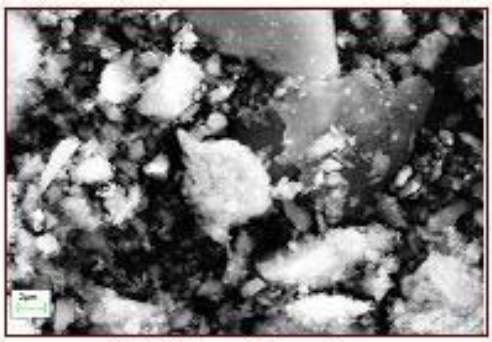

(a-2) Secondary image

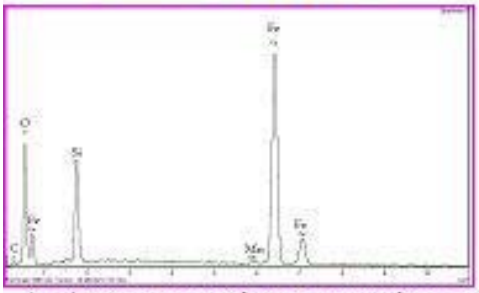

(a-3) SEM analysis result, white area

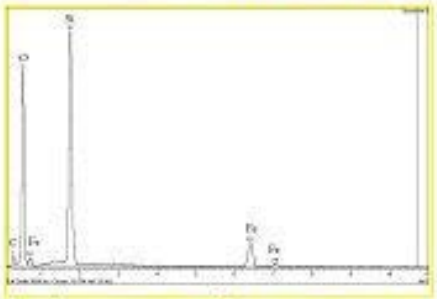

(a-4) SEM analysis result, gray area

(a) 0T0 was collected after $48x10^3$ strokes, 10,000 x magnifications

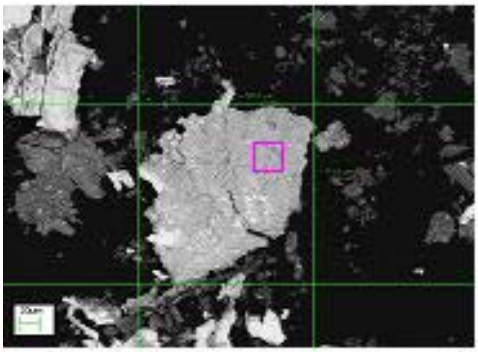

(b-1) Back-scatter image

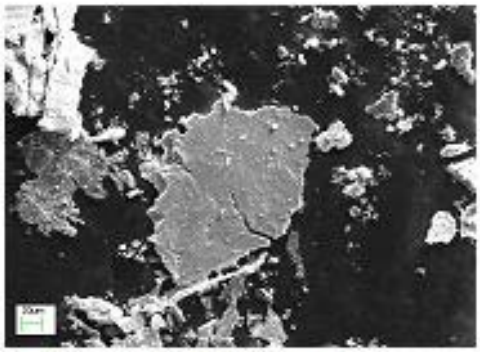

(b-2) Secondary image

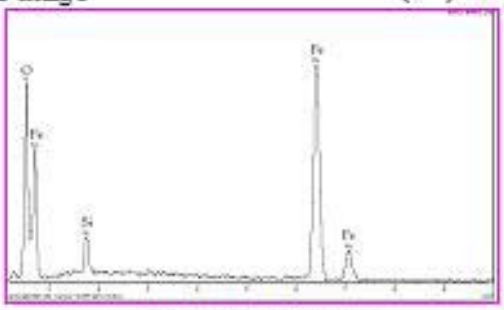

(b-3) SEM analysis

(b) 1.1T0 wa collected after $24x10^3$ strokes, 800 x magnifications

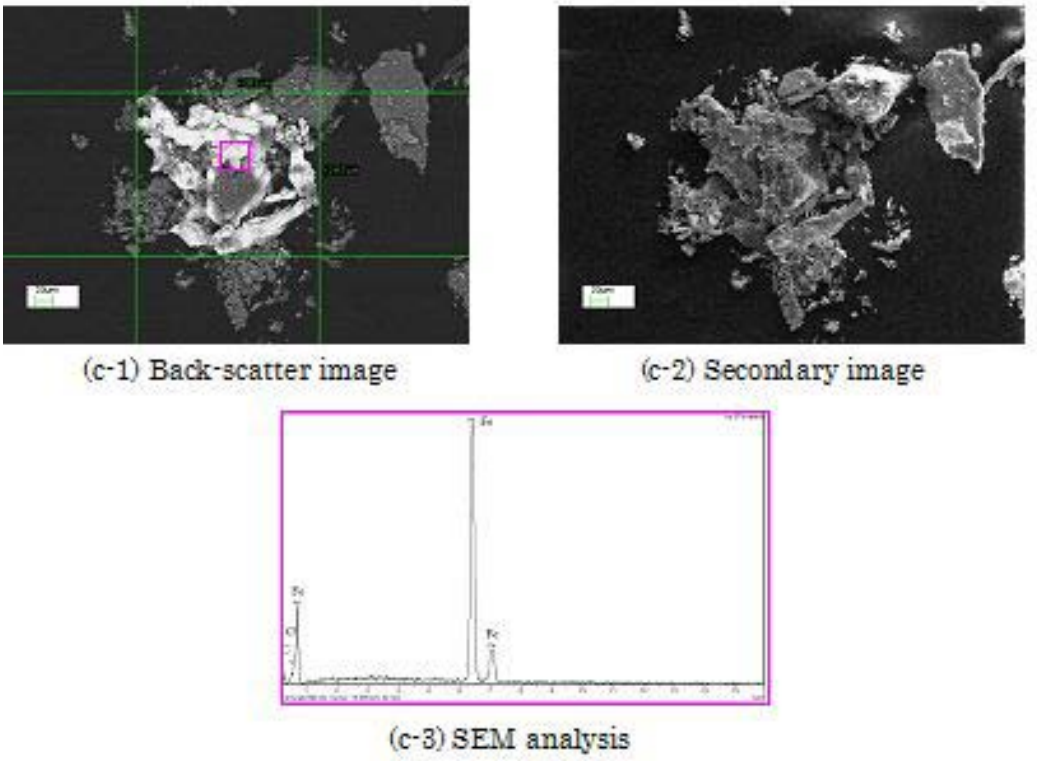

(c) 1.1T90 was collected after $48x10^3$ strokes, 680x magnifications
Fig 4.2.10 SEM analysis results for wear debris were supplied at 0T0, 1.1T0 and 1.1T90.

XRD analysis results of wear debris

Figure 4.2.11 shows XRD analysis results of the surface of the plate specimen. The XRD analysis revealed that the surface of the uncoated plate specimen contains iron (α -Fe).

XRD analysis also showed that the wear debris at 0T0 consist of iron (α -Fe), Wüstite (FeO) and silicon dioxide (SiO_2). In contrast, the wear debris at 1.1T90 consisted of Hematite (Fe_2O_3), including iron (α -Fe), Wüstite (FeO) and silicon dioxide (SiO_2). It is shown in Figure 4.2.12.

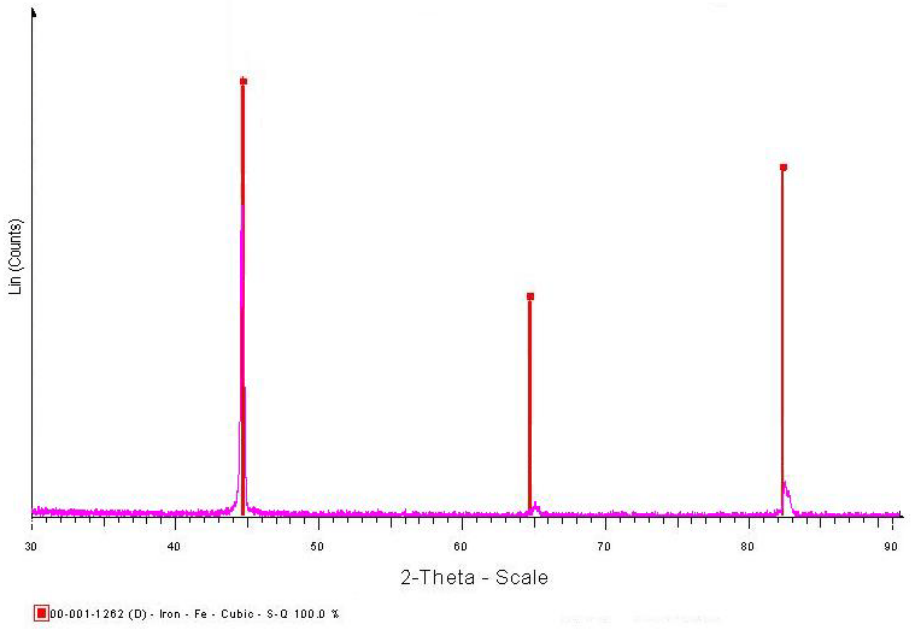

Fig 4.2.11 XRD analysis on the surface of the mild steel plate

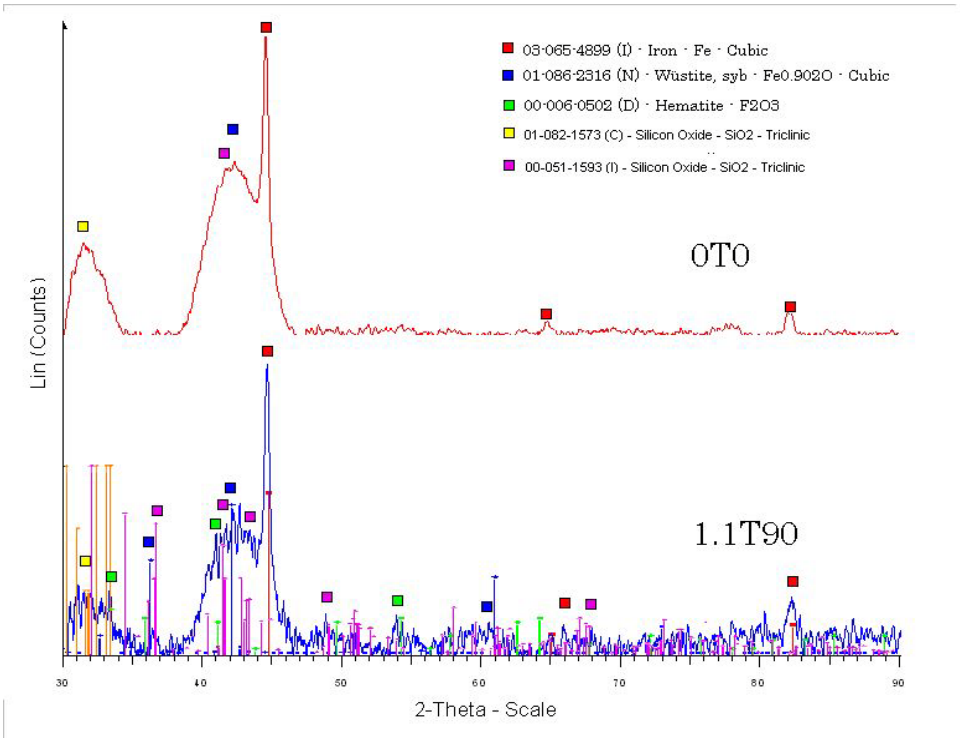

Fig 4.2.12 XRD analysis results of applied the wear debris at 0T0 and 1.1T90 after $24x10^3$ strokes

4.2.1.2 Influence of magnetic field on mild steel structure

Figure 4.2.14 shows micro Vickers hardness values of a mild steel plate at three conditions. The conditions are as follows:

- The mild steel plate before it was magnetised.
- The mild steel plate which was exposed to the horizontal magnetic field or the vertical magnetic field.
- The mild steel plate that was removed from a magnetic field.

Magnetic field condition for hardness measurements were similar to that for the sliding wear testing in horizontal magnetic field (see Figure 4.2.13).

At interval from 0 to 1 hour, the micro hardness in the horizontal magnetic field was a slightly increasing; reaching 308 Hv. After that, the micro hardness decreased to 302 Hv that is its value was same as the mild steel plate before it was magnetized. Furthermore, after the magnetic field was removed, the micro hardness value decreased to 290 Hv temporarily in one hour. Hence, horizontal magnetic field does not change mechanical properties significantly.

The micro hardness of the mild steel plate in vertical magnetic field decreased to about 260 Hv in two hours, and fluctuated in the range of 260 to 270 Hv under the influence of a vertical magnetic field. Thus, it decreased 14% in comparison with the mild steel which was not magnetised.

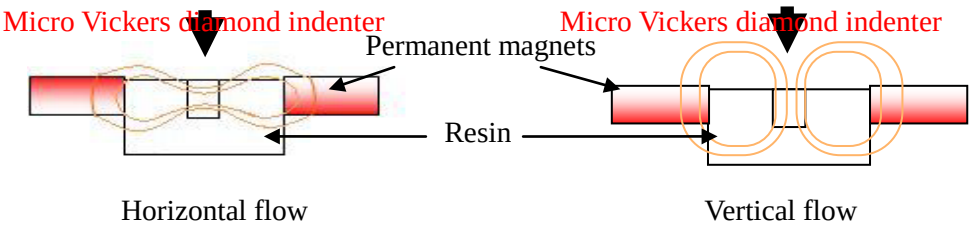

Fig 4.2.13 The flow of magnetic field act to a mild steel plate in the resin, the magnetic pole of permanent magnet is an S pole in the white side and an N pole in a red side.

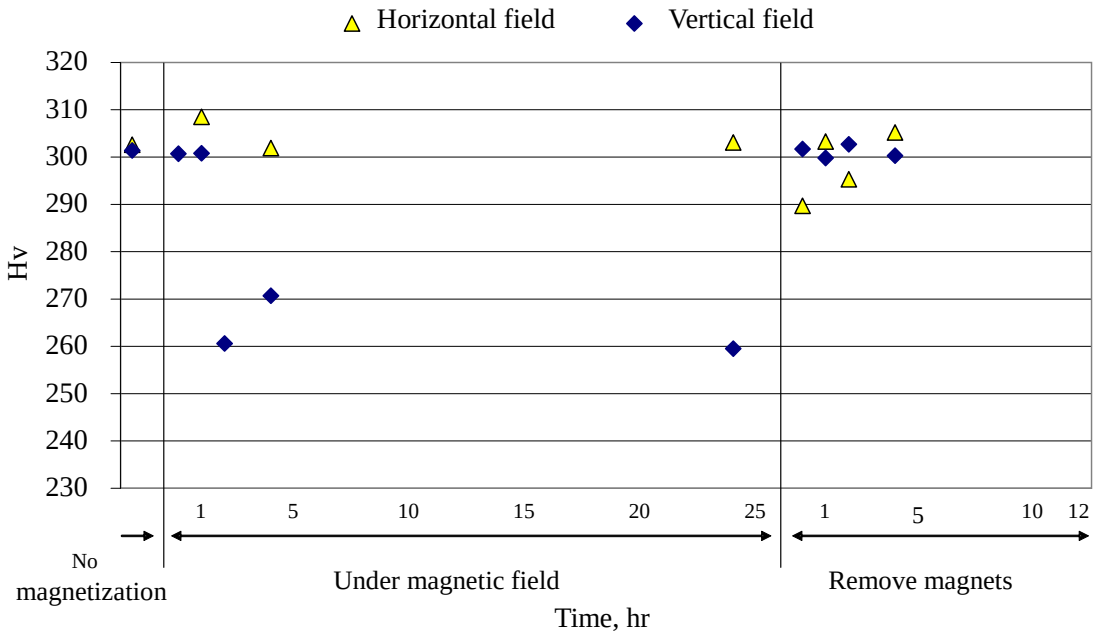

Fig 4.2.14 Change of the mechanical characteristic of the mild steel under a magnetic field, it was performed to evaluate the change of the mechanical characteristic with micro Vickers hardness measurement

4.2.2 Influence of the magnetic field on thermal spray coatings

The influence of horizontal magnetic field on the carbon steel coating and the austenite stainless steel coating was assessed by the mass loss of the test specimens, its surface roughness, and the surface observations. The influence of the magnetic field was set to 0 degree relative to the sliding direction during dry sliding wear testing with low frequency is described. This section is divided into four parts. Firstly, it presents the influence of magnetic field on the carbon steel coating which is ferromagnetic material. Next, it presents the influence of magnetic field on the austenite stainless steel coating which is paramagnetic material. Then, it compares influence of the magnetic field on two thermal spray coatings. It was found that the influence of horizontal magnetic field for ferromagnetic coating results in a remarkable change of mechanical properties. The final part highlights the properties of the wear debris of the carbon steel coating by using the SEM observation and the XRD analysis.

4.2.2.1 Carbon steel coating vs. Si_3N_4 ball

Accumulated mass loss of a carbon steel coating plate during dry sliding wear testing with and without magnetic field is shown in Figure 4.2.15.The accumulated mass loss at 1.1T0 was 2.2 mg at $24x10^3$ strokes and was about 6.6 mg lower compared to the mass loss at 0T0. Furthermore, the difference of accumulated mass loss between the amount 0T0 in $216x10^3$ strokes and the amount at 1.1T0 increased more and more and reached 16.1 mg. The amount of mass loss at 1.1T0 was slightly up but was 50% lower than that for 0T0.

Accumulated mass loss of ball specimens was steady increased for both 0T0 and 1.1T0 as indicated in Figure 4.2.16. In addition, the mass loss for both 0T0 and 1.1T0 was changed an approximate value to the number of sliding strokes.

Hence, the influence of magnetic field to mass loss of specimens features as follow: magnetic field has no influence of mass loss for Si_3N_4 ball specimen however it reduces the mass loss of the carbon steel coating plate.

Figure 4.2.17 shows surface roughness *Ra* of the wear track produced on the plate during sliding wear testing. Surface roughness *Ra* at 0T0 increased from about 0.7 to about 1.3 µm. However, surface roughness *Ra* at 1.1T0 slightly decreased from 1.2 to about 0.8 µm. Hence, it can be say that the influence of magnetic field increases slowly *Ra* value of wear track on carbon steel coating plate to the number of sliding strokes. However, in the first inter

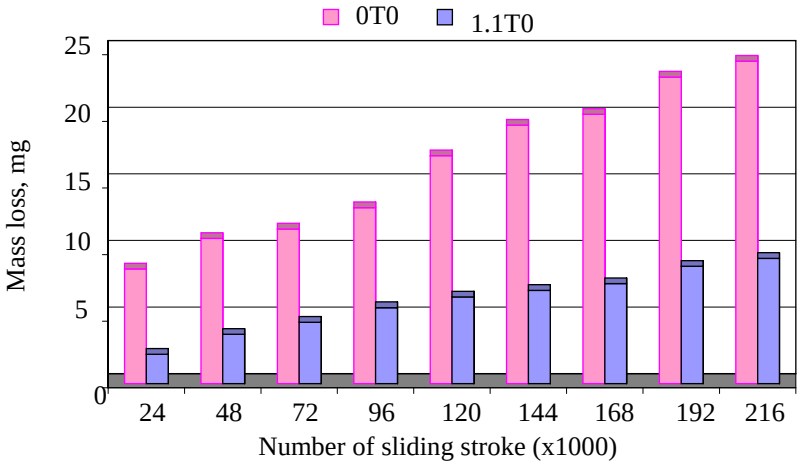

Fig 4.2.15 Accumulated mass loss of carbon steel coating

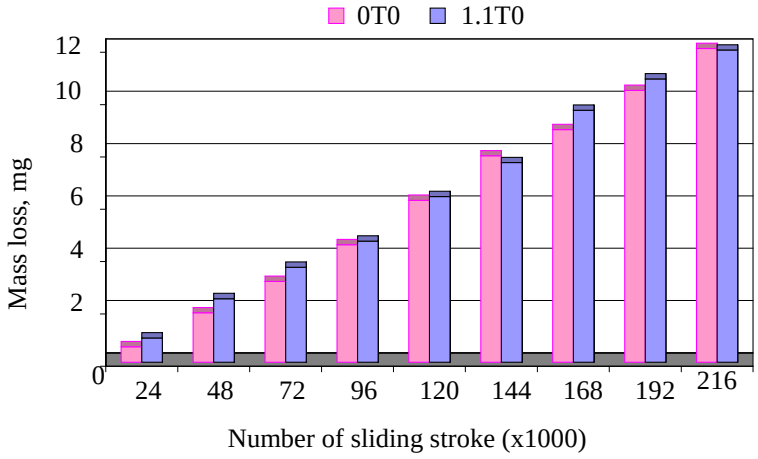

Fig 4.2.16 Accumulated mass loss of Si_3N_4 ball

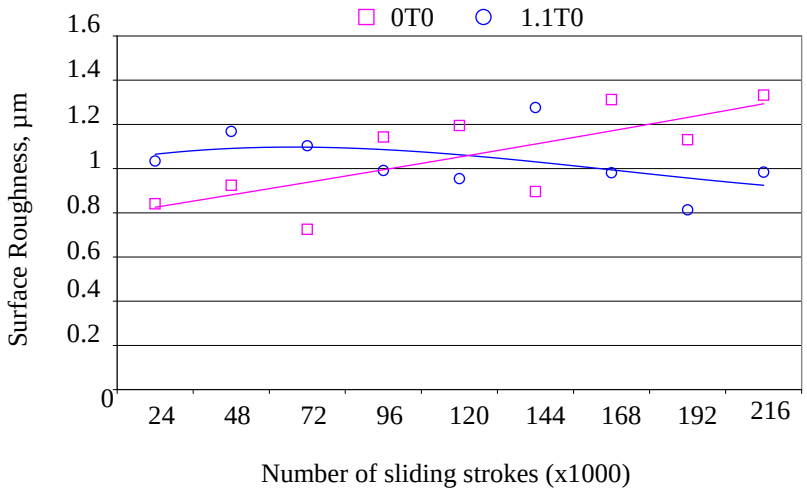

Fig 4.2.17 Surface roughness on the wear surface of the carbon steel coating

Mass loss and surface roughness respectively showed stable tendency. The surface observations are shown in Figure 4.2.18.

The width on the wear track in 1.1T0 was 2.60 mm and was more than 0.25 mm narrower for 0T0 after $24x10^3$ strokes decreasing further to 0.05 mm after $168x10^3$ strokes. Hence, it can be said that the horizontal magnetic field prevents growth of the width of the wear track. Furthermore, in Figure 4.2.18(B-1), the depth from the surface at 1.1T0 was 16.5 mm after $24x10^3$ strokes and was lower than 50% in comparison to 0T0.

Surface observations on the ball, revealed that there were mainly fine scratches. However, 1.1T0 was observed to produce two delamination areas as spalling after the sliding direction in $168x10^3$ strokes.

Surface observations of the carbon steel coating showed that the wear surface had mainly fine scratches and delamination areas. Figure 4.2.19(b) shows some blurred scratches.

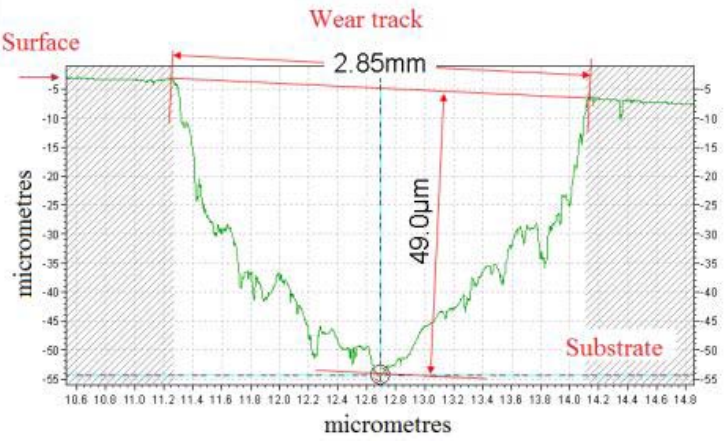

Surface profile

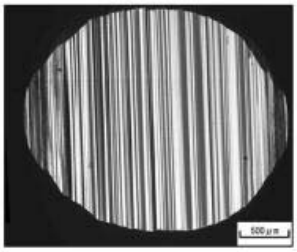

Ball

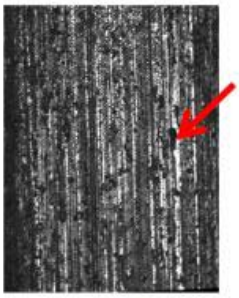

Plate

Fig 4.2.18 (b-1) 1.1T0, 24x10^3 strokes

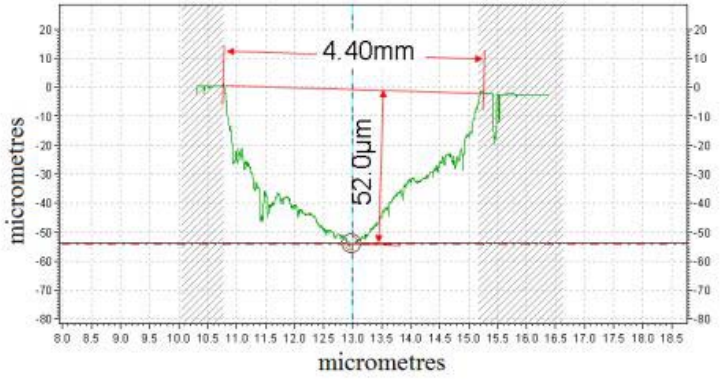

Surface profile

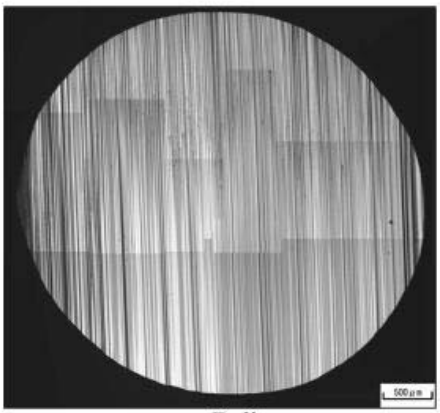

Ball

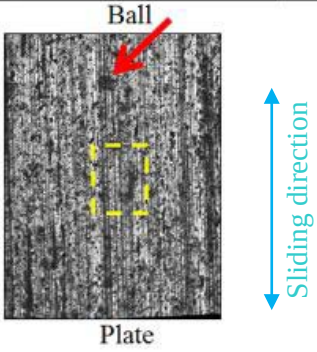

Plate

Fig 4.2.18 (a-2) 0T0, 168x10^3 strokes

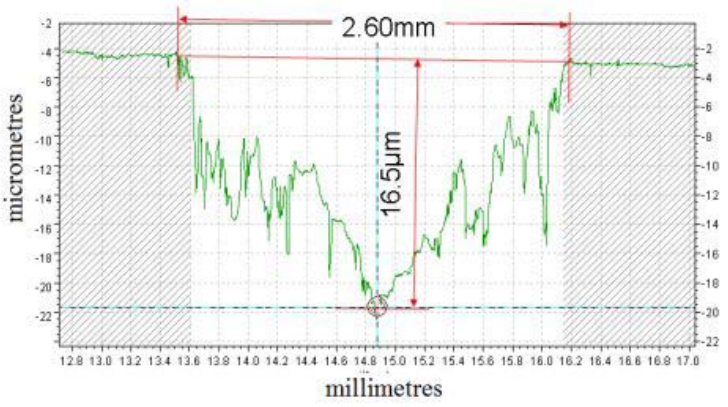

Surface profile

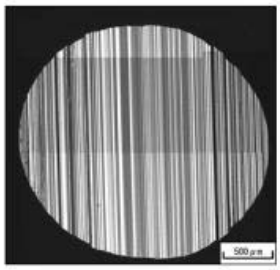

Ball

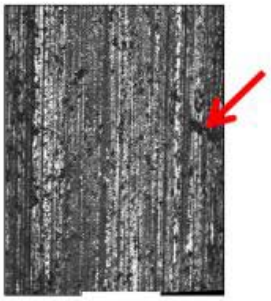

Plate

Fig 4.2.18 (b-1) 1.1T0, 24x10³ strokes

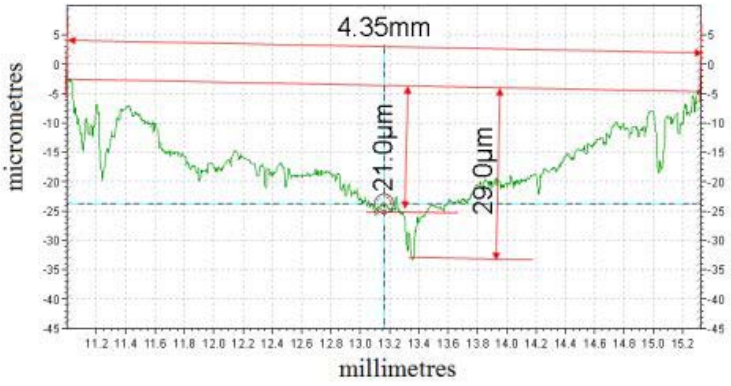

Surface profile

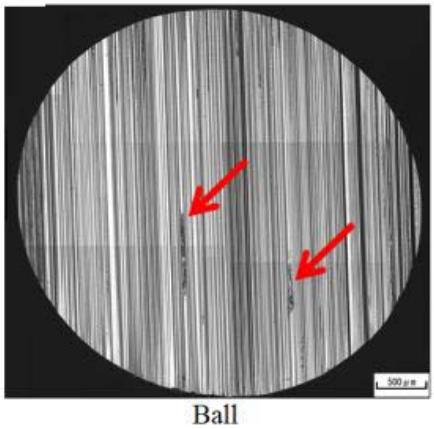

Ball

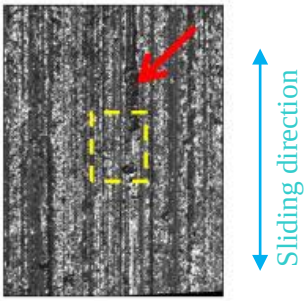

Plate

Fig 4.2.18 (b-2) 1.1T0, 168x10³ strokes

Fig 4.2.18 Appearance of the carbon steel coating optical microscope images of wear surface of a plate and a ball, a raw profile on the wore plate, 50 x magnifications
→: delamination area, the yellow frame of a and b are displayed in Figure 4.2.19.

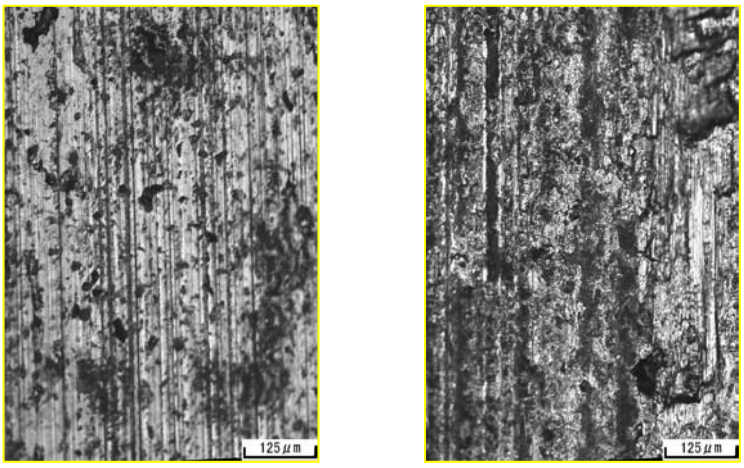

(a) 0T0 (b) 1.1T0

Fig. 4.2.19 Surface observation on the coated plate in $168x10^3$ strokes, 200x magnifications

Wear debris behaviour and the influence on mechanical property

Figure 4.2.20 illustrates the location and arrangement of wear debris after the sliding wear testing. At $24x10^3$ strokes, wear debris were spread widely around wear track. Besides, the amount of brown wear debris was few, compared to 0T0 in Figure 4.2.20 (a-1).

At $168x10^3$ strokes, the difference between the 0T0 and 1.1T0 became clear. As at the end of sliding path, brown wear debris is not seen. Thus, it is suspected that the attractive force of the permanent magnets has an influence on the brown wear debris.

Fig 4.2.21 illustrates micro hardness of the carbon steel coating with and without magnetic field. As for the micro-hardness of the carbon steel coating in the magnetic field, it decreased 12% from 300 to 2 64 Hv in 30 minutes. Besides, after 4 hours, it has returned to original value which was about 300 Hv. Hence, under the influence of the magnetic field mechanical properties are affected only for a short time after magnetization.

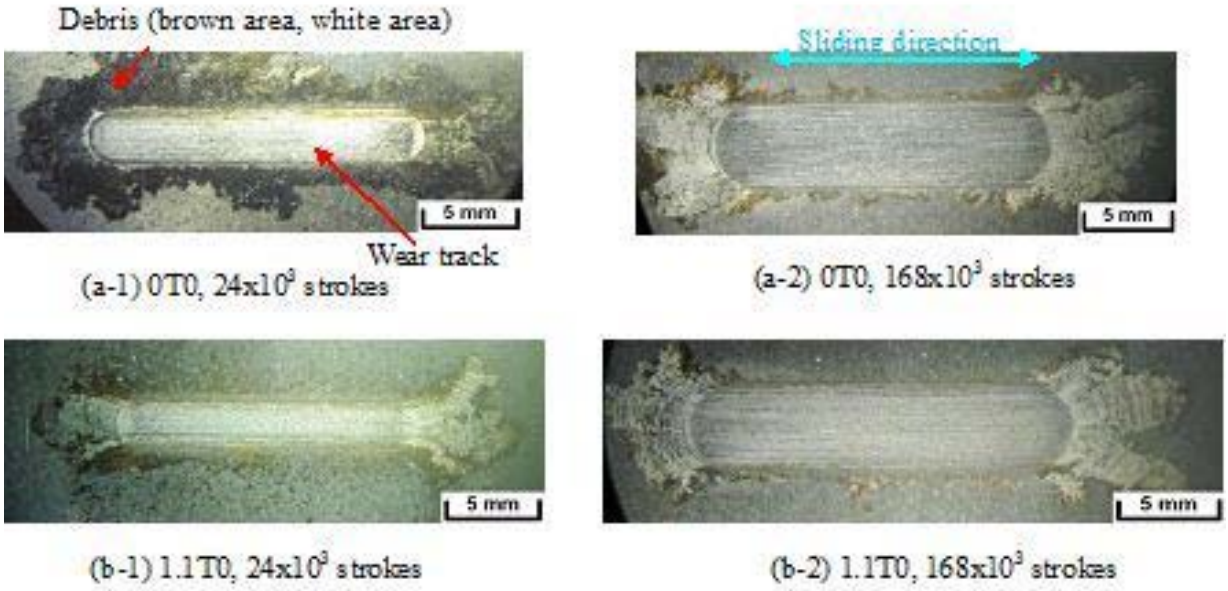

Fig 4.2.20 Location of debris on steel coating, 6.4x magnifications

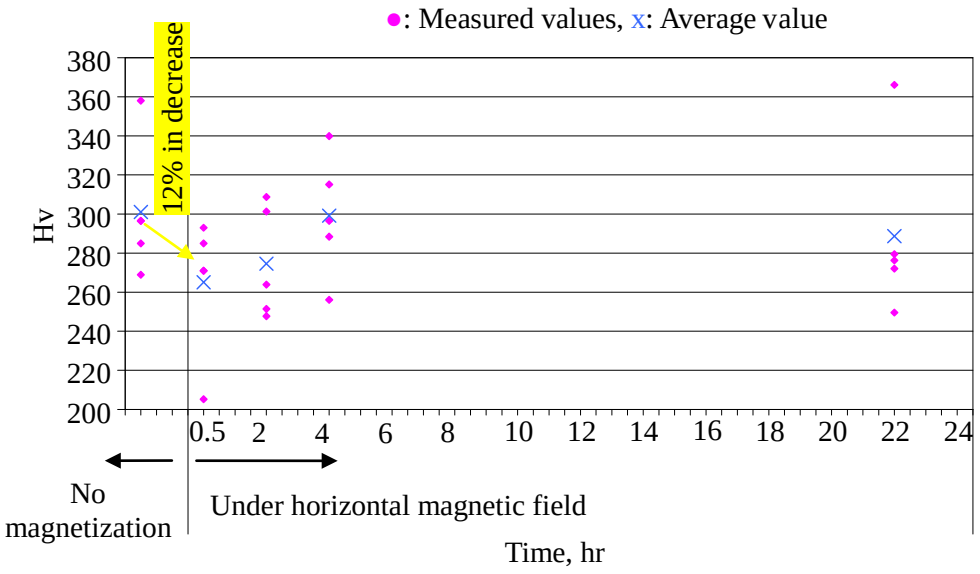

Fig 4.2.21 Micro-Vickers hardness of the carbon steel coating of no magnetization and the carbon steel coating under the horizontal magnetic field

4.2.2.2 Austenite stainless steel coating vs. a Si_3N_4 ball

Firstly, mass loss, surface roughness and surface observation of specimens are presented. Then, the wear debris behaviour and the influence on mechanical properties of austenite stainless steel coating are outlined.

Figure 4.2.22 illustrates accumulated mass loss of austenite stainless steel coating plate specimen versus the number of sliding strokes under different magnetic fields.

The accumulated mass loss at 0T0 was a gradual upward trend, while, for 1.1T0 it was in proportion to the number of sliding strokes and the tendency was a gradual rise. The mass loss at 1.1T0 was 1.0 mg from $96x10^3$ to $144x10^3$ strokes, and a difference between 0T0 and 1.1T0 peaked at $144x10^3$ strokes and it was 3.2 mg.

Figure 4.2.23 illustrates accumulated mass loss of Si_3N_4 Ball specimen versus the number of sliding strokes under different fields. The Figure 4.2.23 shows a slight increase in the accumulated mass loss for both 0T0 and 1.1T0 in proportion to the number of sliding strokes.

The mass loss for 1.1T0 was similar to the mass loss for 0T0 that was approximately 0.5 mg from $24x10^3$ to $216x10^3$ strokes. Therefore, it can be assumed that magnetic field does not influence the amount of the mass loss of specimens of austenite stainless steel coating and Si_3N_4 ball.

The surface roughness of the austenite stainless steel coating at 0T0 ranged from about 6 to 4.26 μm at $96x10^3$ strokes as indicated in Figure 4.2.24. In other words, the influence of magnetic field seems that it produced multitudes of delaminated area of the shallow, small size on the wear surface of austenite stainless coated plate specimen. On the other hand, the surface roughness for 1.1T0 was slightly increased from about 0.2 to about 0.5 μm and equalled that for 0T0 after $144x10^3$ strokes. Hence, it seems that magnetic field influences the value of the surface roughness of the wear track on the austenite stainless coating.

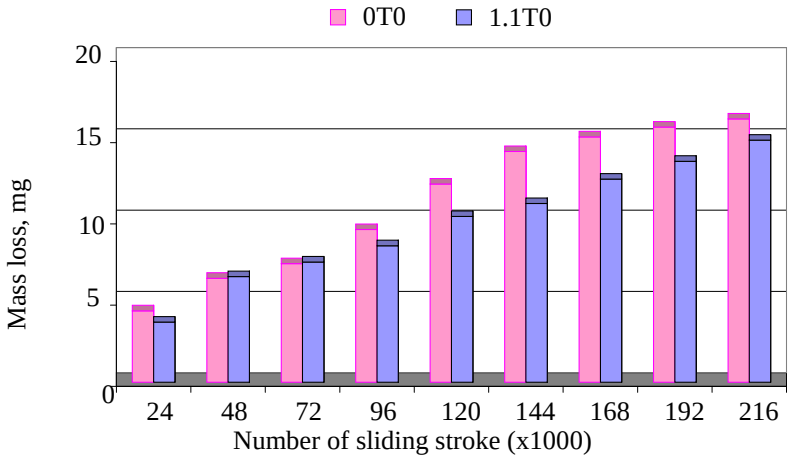

Fig 4.2.22 Accumulated mass loss of the austenite stainless steel coated plate

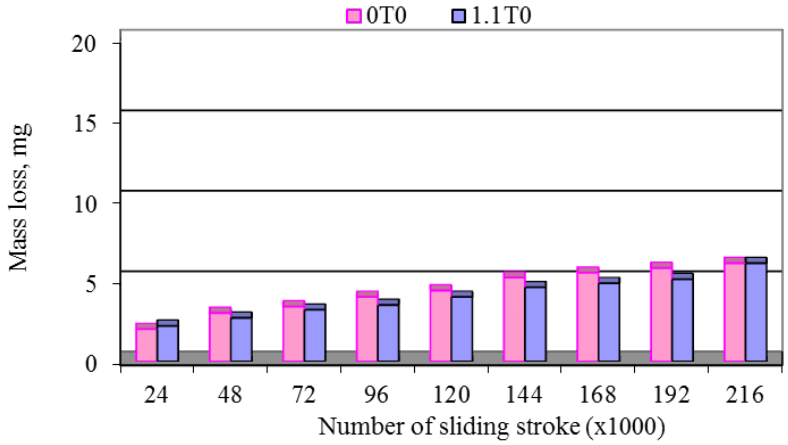

Fig 4.2.23 Accumulated mass loss of Si_3N_4 ball

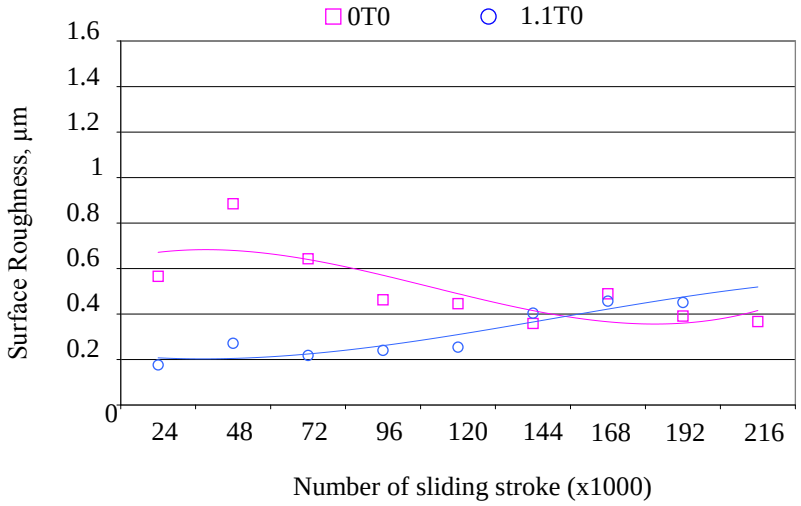

Fig 4.2.24 Surface roughness of the austenite stainless steel coated plate specimen

As can be seen from raw profiles shown in Figure 4.2.25, size of the wear track at 1.1T0 was estimated about 20% larger in comparison with 0T0. The wear track surface at 1.1T0 has deep grooves and was about 5 mm in depth. In addition, some delamination areas were observed on the wear track. The surface of ball specimen at 1.1T0 consisted mainly of fine asperities and scratches.

Figure 4.2.26 (a) shows some delamination areas on the wear track. In addition to these delamination areas, there are places looking similar to the unmelted particles observed in Figure 4.2.26 (b). It is assumed that these features resulted from coating process. Besides, additional delamination area was found around unmelted particles as shown in Figure 4.2.26 (b).

It is assumed that the unmelted particle is strongly magnetic material and the surrounding material may be sort of a permanent magnet.

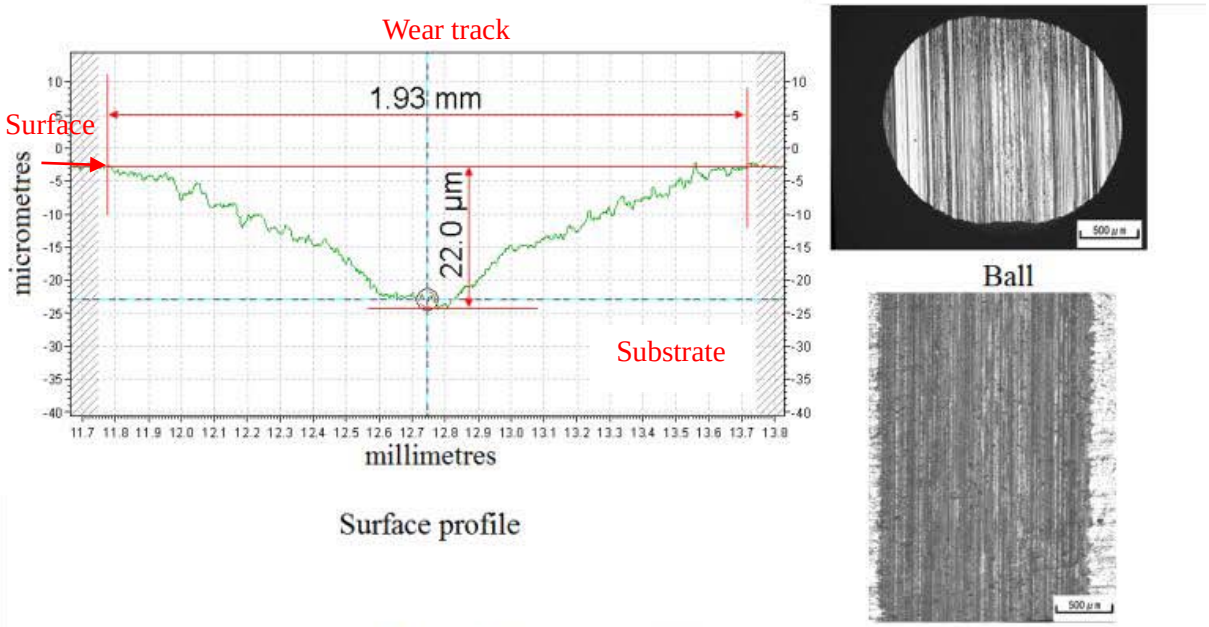

Surface profile

Fig 4.2.25 (a-1) 0T0, 24x10^3 strokes

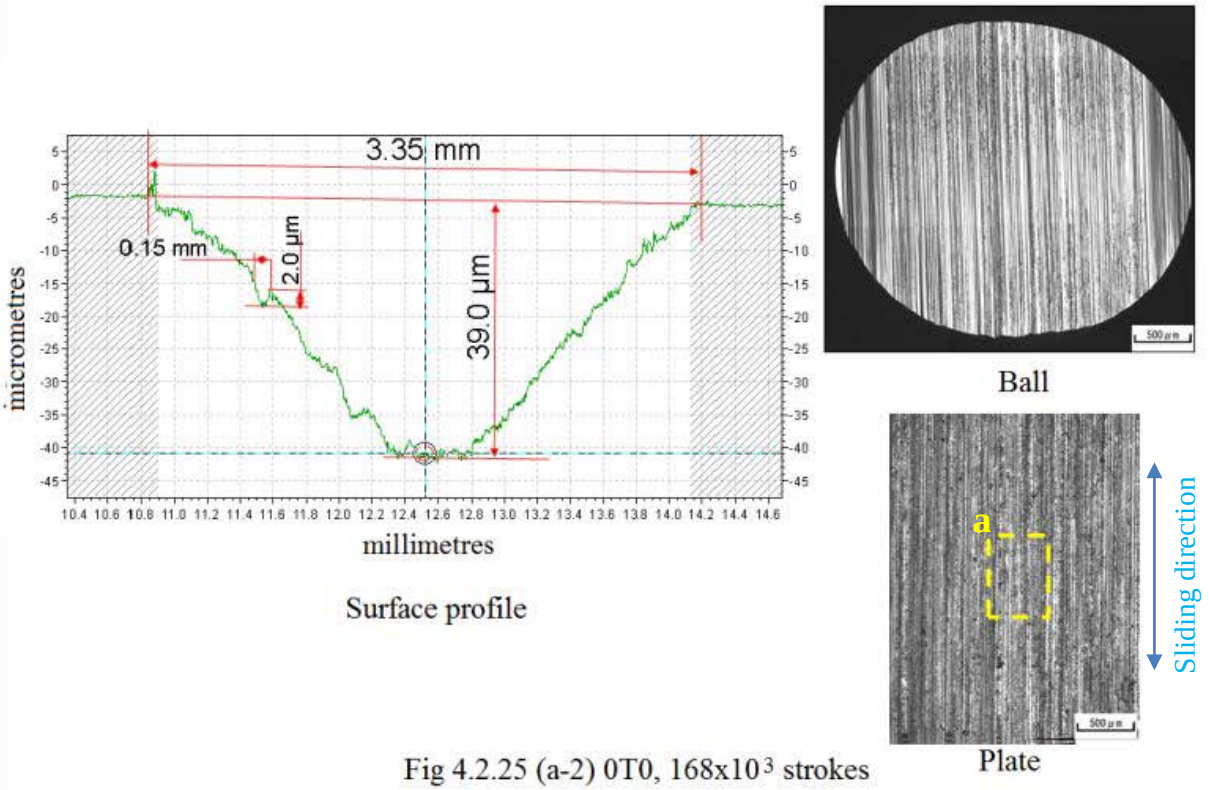

Surface profile

Fig 4.2.25 (a-2) 0T0, 168x10^3 strokes

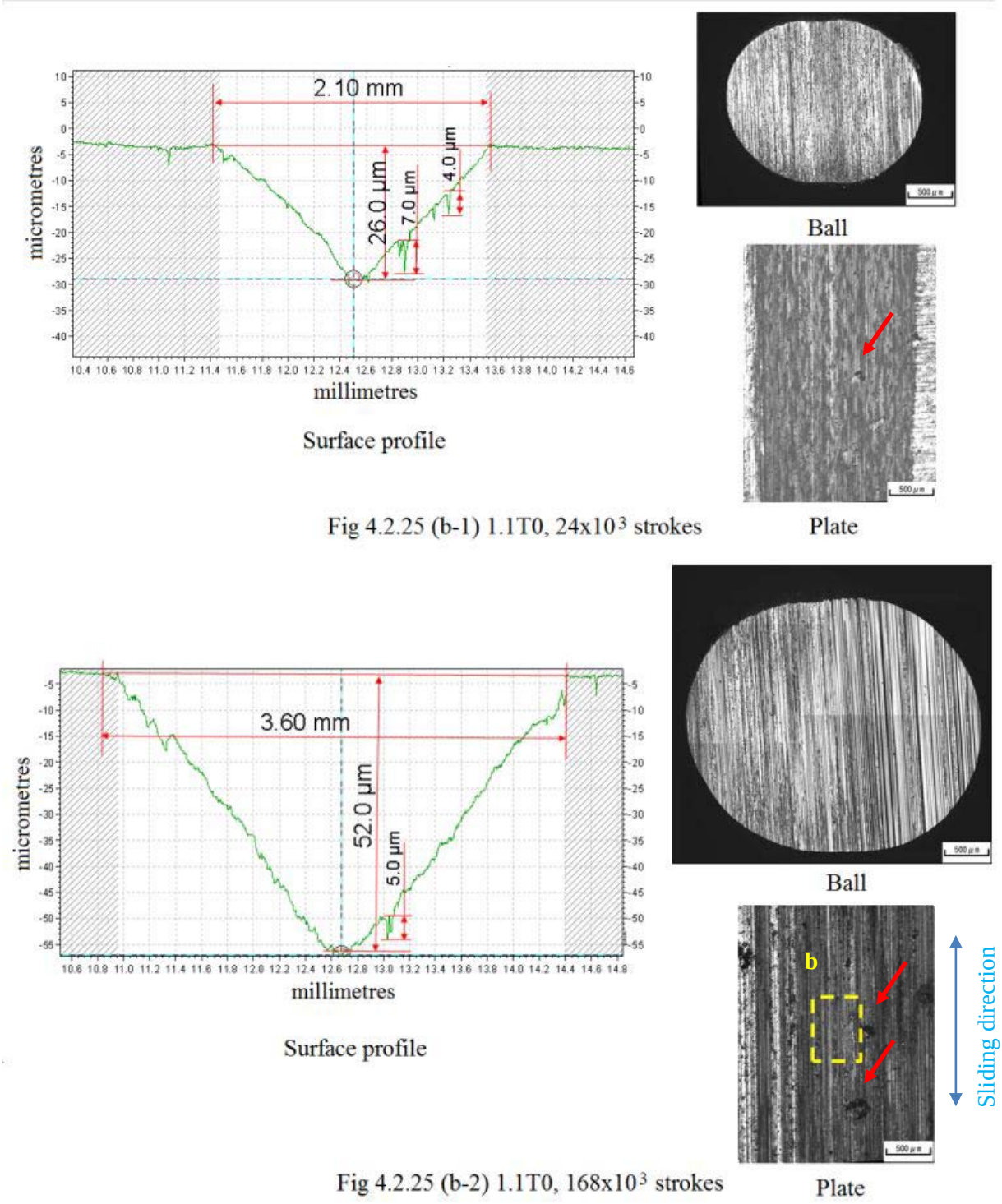

Fig 4.2.25 Appearance of the austenite stainless steel coating, optical microscope images of wear surface of a plate and a ball, a raw profile on the wore plate, 50x magnifications
→: delamination area, the yellow frame of a and b are displayed in Figure 4.2.26.

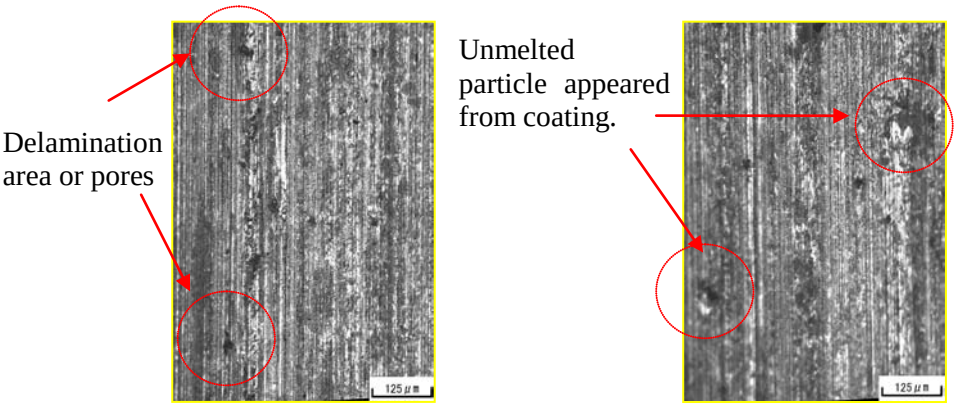

(a) 0T0 (b) 1.1T0

Fig 4.2.26 Surface observation on the coated plate in $168x10^3$ strokes, 200x magnifications

Wear debris behaviour and the influence on mechanical properties

Figure 4.2.28 illustrates the micro hardness of the austenite stainless steel coating without magnetic field and under the horizontal magnetic field. Hardness of the coating under magnetic field was very changeable. However, the average of micro hardness decreased about 5% after two hours and started to increase a little bit from three hours onwards and became similar to that of the coating without magnetic field.

Figure 4.2.29 shows results of XRD analysis. The spectrum consists of Fe_3O_4 and $NiFe_2O_4$ and $NiCrO_3$ other than Taenite (Fe, Ni). According to the Mineralogical Society of America (2001-2005):

Taenite is γ-(Fe,Ni) with a cubic structure and has strongly magnetic properties.

Fe_3O_4 is of orthorhombic structure and weak magnetic properties.

$NiFe_2O_4$ has a cubic structure.

$NiCrO_3$ has a rhombohedra structure.

In addition, it can be seen from Figure 4.2.27 (b-1), that wear debris were not attracted by the magnetic force. Hence, the austenite stainless steel thermal spray powder, which is the paramagnetic material, retained its magnetic properties even after it was coated by a thermal spray process.

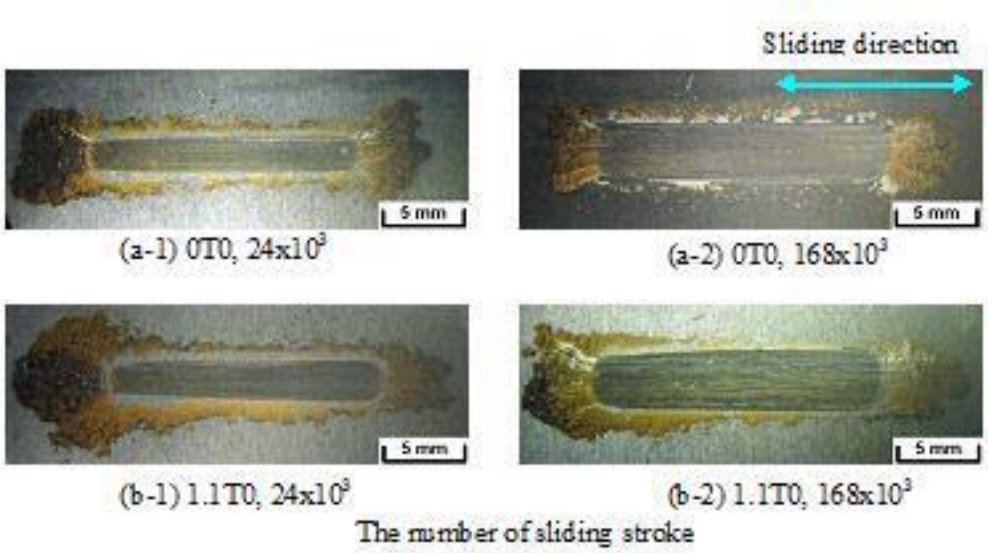

Fig 4.2.27 Location of wear debris around wear track, the austenite stainless steel coating, 6.4 x magnifications

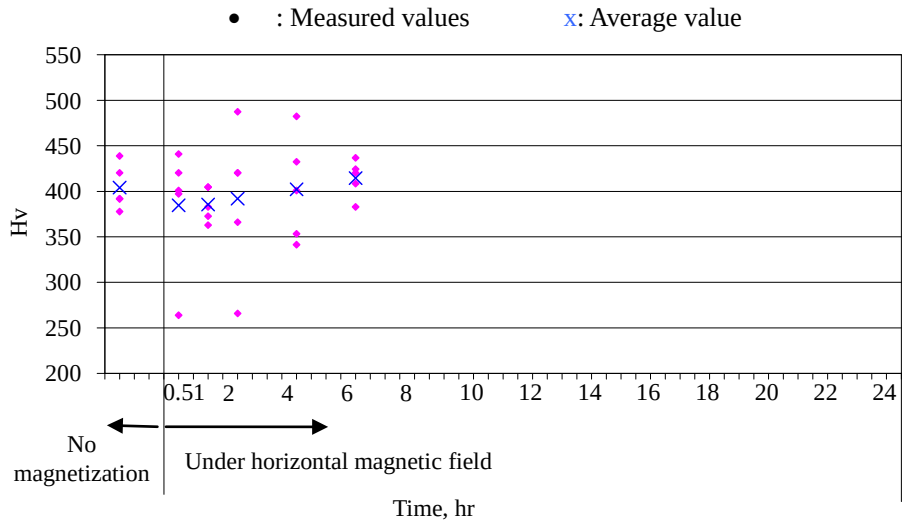

Fig 4.2.28 Micro-Vickers hardness of the austenite stainless steel coating of no magnetization and the coating under the horizontal magnetic field

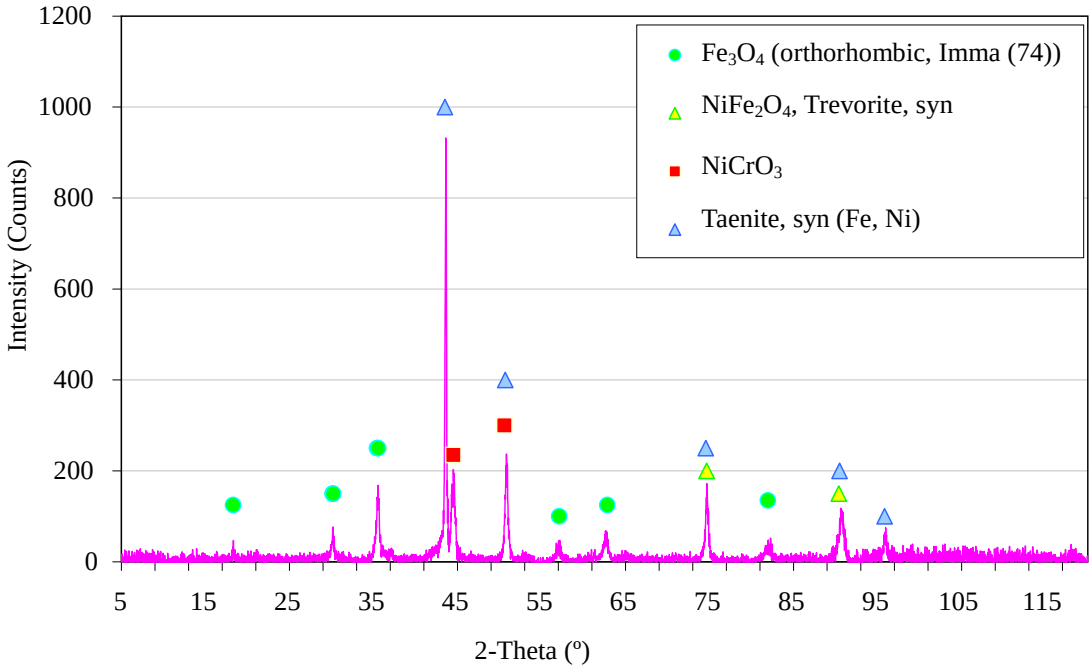

Fig 4.2.29 XRD pattern on the surface of the austenite stainless steel coating

4.2.2.3 Wear particle observations and analysis of carbon steel coating

In the case of the austenite stainless steel coating in the magnetic field, it was found that the influence of the magnetic field was weak. On the other hand, the magnetic field influenced the carbon steel coating by significant decrease of the mass loss and a fall of the surface roughness.

As shown in Figure 4.2.30 (a) and (b), which shows SEM images by backscatter electrons and secondary electron for wear particles, wear particles at 0T0 were flat and flake shaped. Besides the size of particles at the centre of SEM images were estimated to be as follows:

Width 166.4 μm; length 158.7 μm in Figure 4.2.30 (a)

Width 63.11 μm; length 69.21 μm in Figure 4.2.30 (b)

On the other hands, as shown in Figure 4.2.30 (c) and (d), the particles were elongated spheroids or flats with gently rounded shape. The elongated wear particle is presumably an aggregate of fine particles. Besides the size of particles at the centre of SEM images were estimated to be as follows:

Width 40.71 μm; length 26.9 μm in Figure 4.2.30 (c)

Width 83.57 μm; length 39.45 μm in Figure 4.2.30 (d)

When compared to the particle size generated at 0T0, the particles produced at 1.1T0 were relatively small. The particle size for each that condition used was calculated and shown in Figure 4.2.31. The numbers represents an average area of a typical wear particle. Particle size reached a peak value of about 25,000 μm^2 for both 0T0 and 1.1T0 after $168x10^3$ strokes. It can be said that the magnetic field retains wear particles within the contact area because the particles at 1.1T0 were of fine gentle round shape.

Figure 4.2.32 shows the XRD pattern on the surface of the carbon steel coating. Besides, the XRD pattern of wear debris can be seen in Figure 4.2.32. (Mineralogical Society of America

2001-2005):

The result clearly shows that Fe_3O_4 was not on the XRD spectrum for both 0T0 and 1.1T0 (see Figure 4.2.33). However, in the magnetic field, XRD spectrum does not contain oxidized iron, hence; the dry sliding wear testing did not produce high temperatures required to short oxidization process.

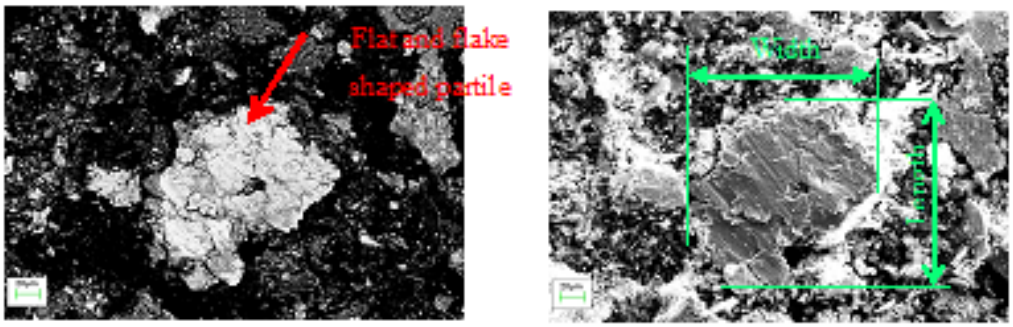

(a-1) Backscatter electron image (a-2) Secondary electron image

(a) 0T0, $24x10^3$ strokes, 1000x magnifications

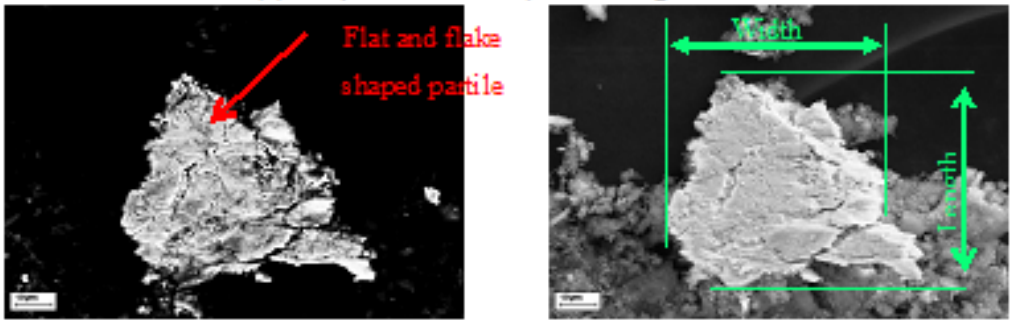

(b-1) Backscatter electron image (b-2) Secondary electron image

(b) 0T0, $120x10^3$ strokes, 3000x magnifications

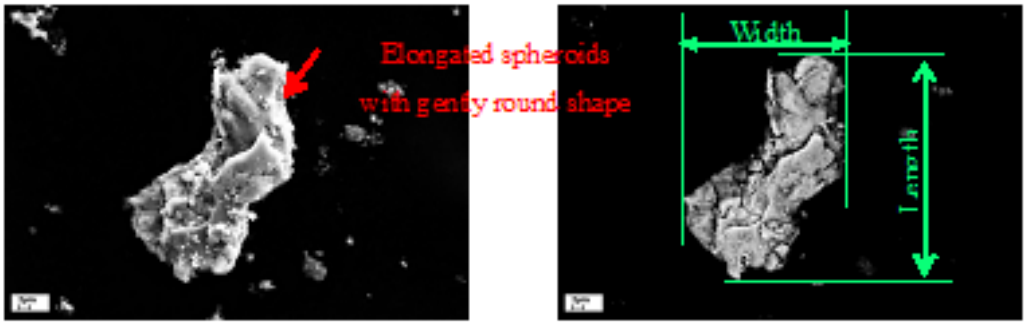

(c-1) Backscatter electron image (c-2) Secondary electron image

(c) 1.1T0, $24x10^3$ strokes, 5000x magnifications

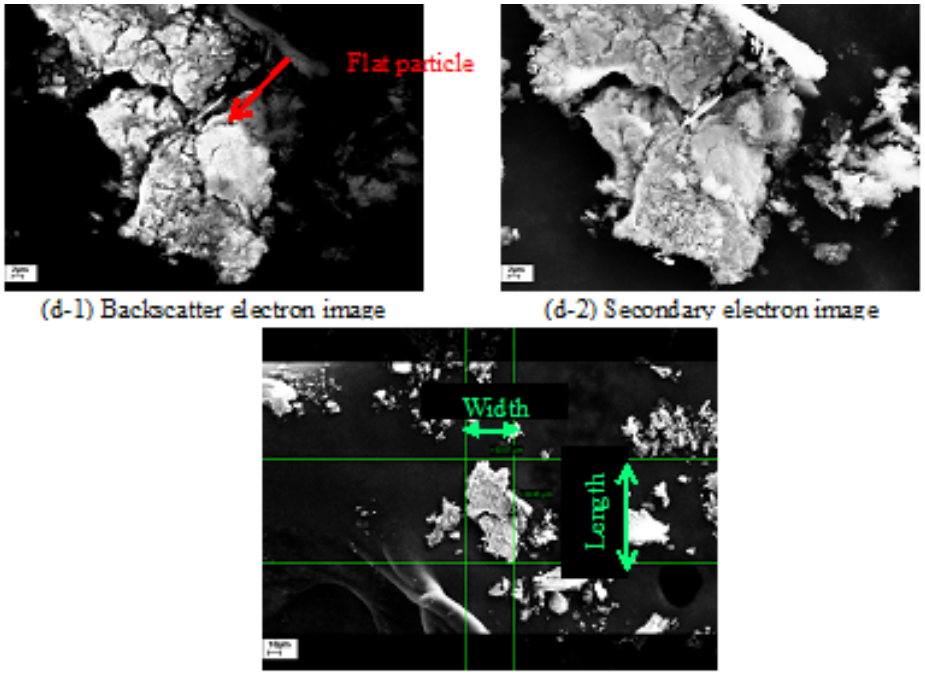

(d-1) Backscatter electron image

(d-2) Secondary electron image

(d-3) Secondary electron image to measure size, 1000x magnifications

(d) 1.1T0, 120x10³ strokes, 5000x magnifications

Fig 4.2.30 SEM observation by secondary and backscattered electrons for wear particles

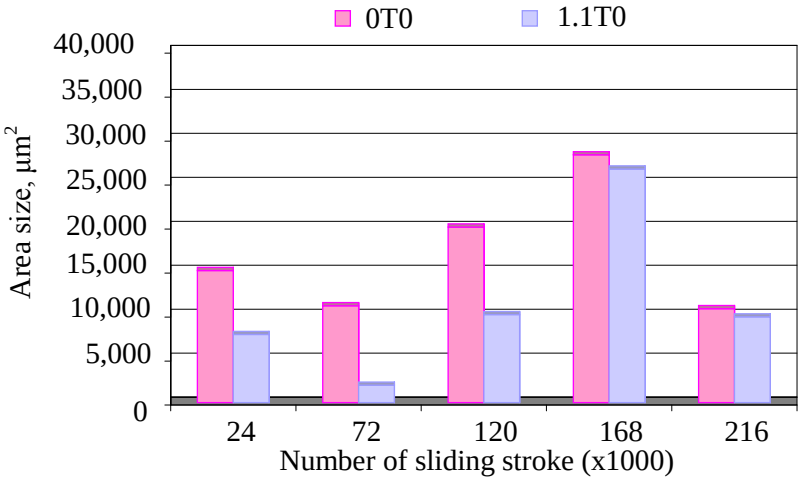

Fig 4.2.31 Area size of wear particles

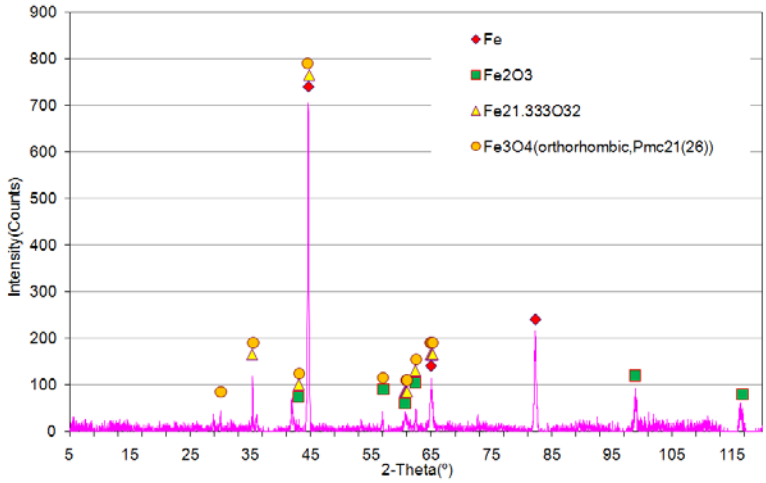

Fig 4.2.32 XRD pattern on the surface of the carbon steel coating

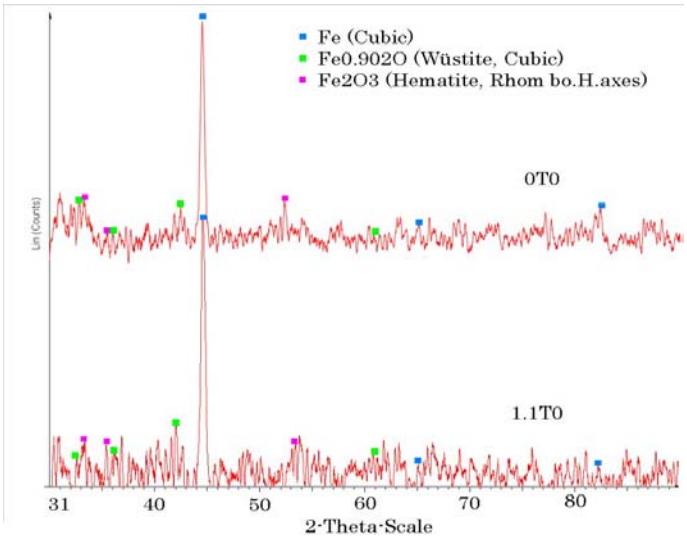

Fig 4.2.33 XRD pattern of wear debris at 0T0 and 1.1T0

4.3 Lubricated sliding contact experiments

4.3.1 The accumulated mass loss of the plate

Figure 4.3.1 illustrates accumulated mass loss of the plate specimen versus the number of sliding strokes under different magnet flux densities. The accumulated mass loss is proportional to the number of sliding strokes. In addition, the accumulated mass loss at 0T0 increases sharply from 8 to 184 mg approximately, while, the accumulated mass losses at both 0.4T0 and 1.1T0 increase steadily approximately from 5 to 118 mg. In detailed comparison between 0.4T0 and 1.1T0, the mass loss of 1.1T0 weighs more than 0.4 mg. Thus, it is concluded that the presence of the magnetic fields decrease the wear amount of the plate. In addition, the difference of the range from 0.4T to 1.1T has insignificant influence on the amount wear of the plate.

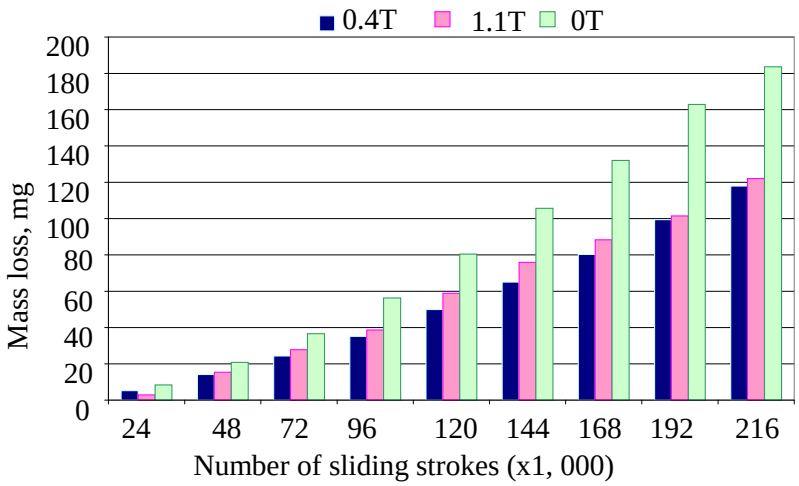

Fig.4.3.1 Accumulated mass loss of the plate in difference magnet flux densities

4.3.2 Surface roughness on the wear track of the plate

Figure 4.3.2 illustrates the surface roughness of the wear track for different magnetic flux densities. The surface roughness at 0T0 changes sharply from 0.17 to 0.32 μm during $72x10^3$ strokes. In the case of 1.1T0, the surface roughness increases gradually and it is fluctuating between 0.25 to 0.41 μm during $192x10^3$ strokes, while the surface roughness of 0.4T0 fluctuates approximately between 0.25 to 0.32 μm during $72x10^3$ strokes. After $96x10^3$ strokes, all *Ra* values range from 0.25 to 0.42 μm, and increase slightly until $168x10^3$ strokes. Unexpectedly, surface roughness of 0T0 and 0.4T0 decreases after $216x10^3$ strokes. On the other hand, the surface roughness at 1.1T0 considerably changed approximately from 0.19 to 0.36 μm. Thus, it can be said that the range of the surface roughness change is narrowed in the presence of the magnetic field.

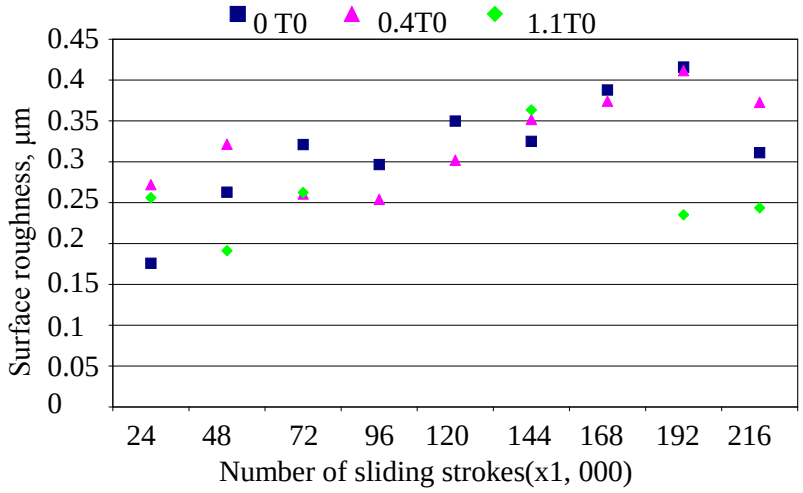

Fig.4.3.2 The surface roughness on the plate in different magnet flux densities

4.3.3 Appearance of the wear track on the plate and ball

Figure 4.3.3 shows the two-dimensional surface profiles and optical microscope images of wear tracks generated after $24x10^3$ and $184x10^3$ strokes.

- Surface profile of plate specimens

The wear surface generated under the influence of the horizontal magnetic field is a smooth arc like shape which is similar to the wear track produced in the absence of the magnetic field. However, the magnetic field produced the small jagged shape on the bottom area of the wear track after $24x10^3$ strokes. It is shown in Figure 4.3.3 (b-1) and (c-1).

The wear track of 0T0 was 1.81 mm in width and 62.0 μm in depth after $24x10^3$ strokes and grew to 5.1 mm in width and 510 μm in depth after $184x10^3$ strokes. While, in comparison both the depth and width of the wear track at 0.4T0 are almost same sizes as at 1.1T0 after $24x10^3$ and $184x10^3$ strokes. The comparison of the width and the depth of the wear track at 0.4T0 with 0T0 is as follows;

- After $24x10^3$ strokes; 92% in width and 85% in depth
- After $184x10^3$ strokes; 85% in width and 73% in depth

Therefore, it is concluded that the influence of a weak magnetic field (0.4T0) is significant and the magnetic field slightly decreases the wear of the plate.

- Wear surface of plate specimens

Fine scratches can be observed on the wear surface of 1.1T0 sample after $184x10^3$ strokes. The observation of the surface was carried out at 50 times magnification. Significant delamination is observed at the wear track of 1.1T0 sample and in some places spalling is also observed as shown in Figure 4.3.3(c-2). Figure 4.3.4 shows appearance of the wear track for 0.4T0 sample. Long and narrow unidirectional delamination areas can be observed. In addition, the delamination region of 1.1T0 sample covers a wide area. Furthermore, from

Figure 4.3.4 that shows the surface observation of test specimens under high magnification, delamination area can be observed on the wear track in the presence of magnetic field.

- Wear surface on the ball specimen

An elliptically shaped wear track is observed on the surface of the ball. In Figure 4.3.3 (a-2), (b-2) and (c-2), the elliptically shaped wear track can be seen as convex because it is out of focus including the centre area.

The appearance of the wear track of 0.4T0, which was created under the same conditions as 0T0, fine scratches are seen. However, 1.1T0 produced blurred scratches at the centre area. Figure 4.3.4, shows that fine scratches are generated on 0.4T0 and 1.1T0 samples. However, for 0T0 case a small pit in the coarse region is generated.

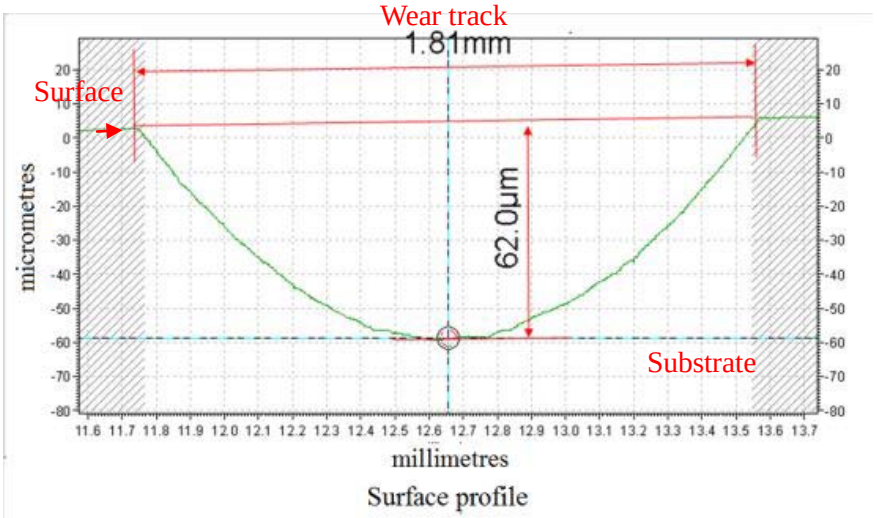

Surface profile

Fig 4.3.3 (a-1) 0T0, 24x10^3 strokes

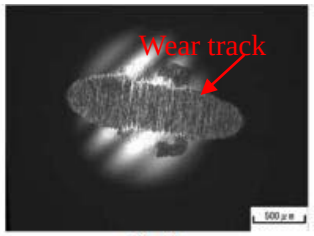

Ball

Plate

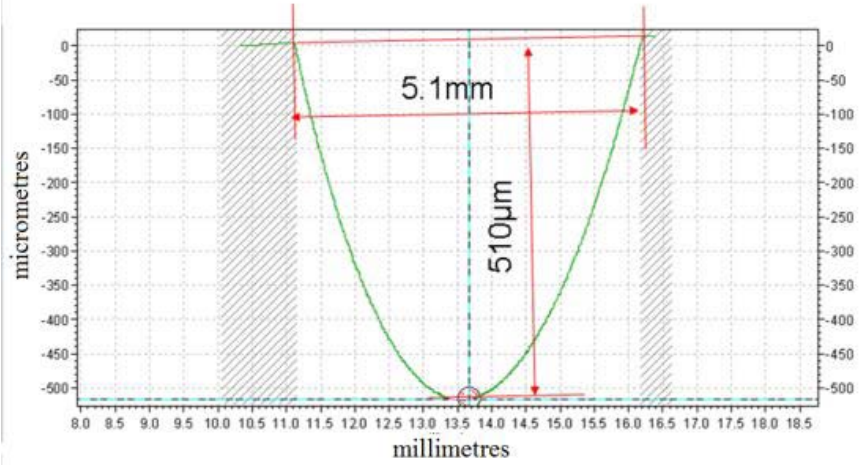

Surface profile

Fig 4.3.3 (a-2) 0T0, 184x10^3 strokes

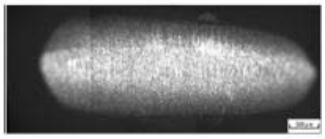

Ball

Sliding direction

Plate

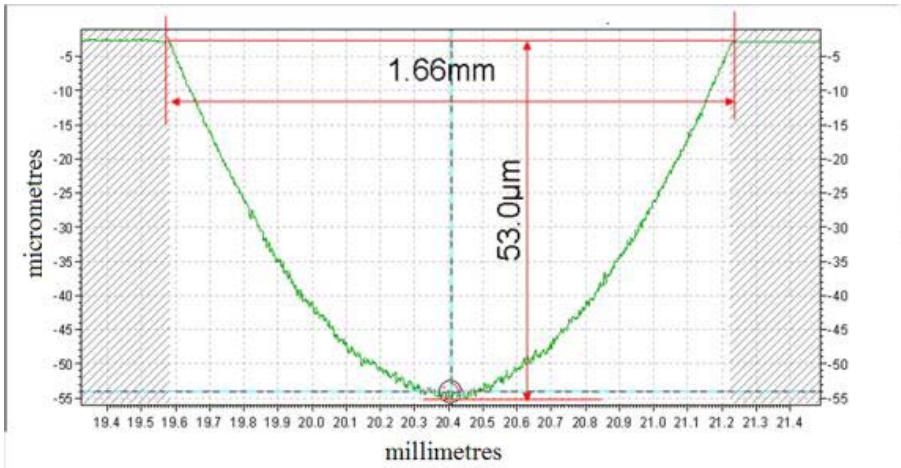

Surface profile

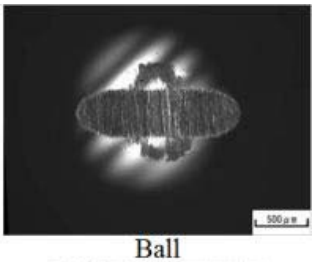

Ball

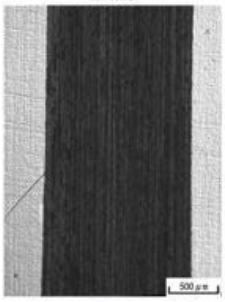

Plate

Fig 4.3.3 (b-1) 0.4T0, $24x10^3$ strokes

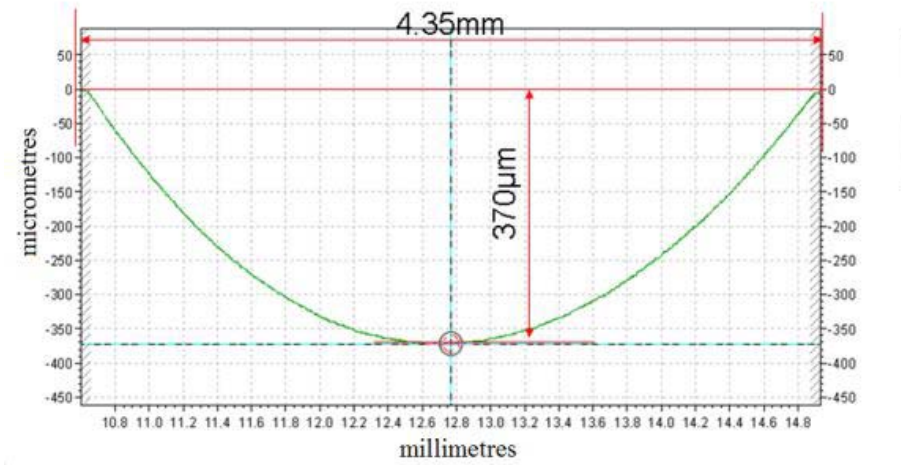

Surface profile

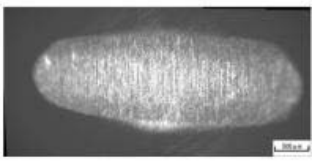

Ball

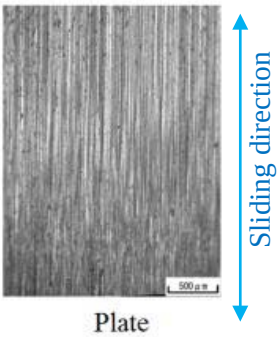

Plate

Fig 4.3.3 (b-2) 0.4T0, $184x10^3$ strokes

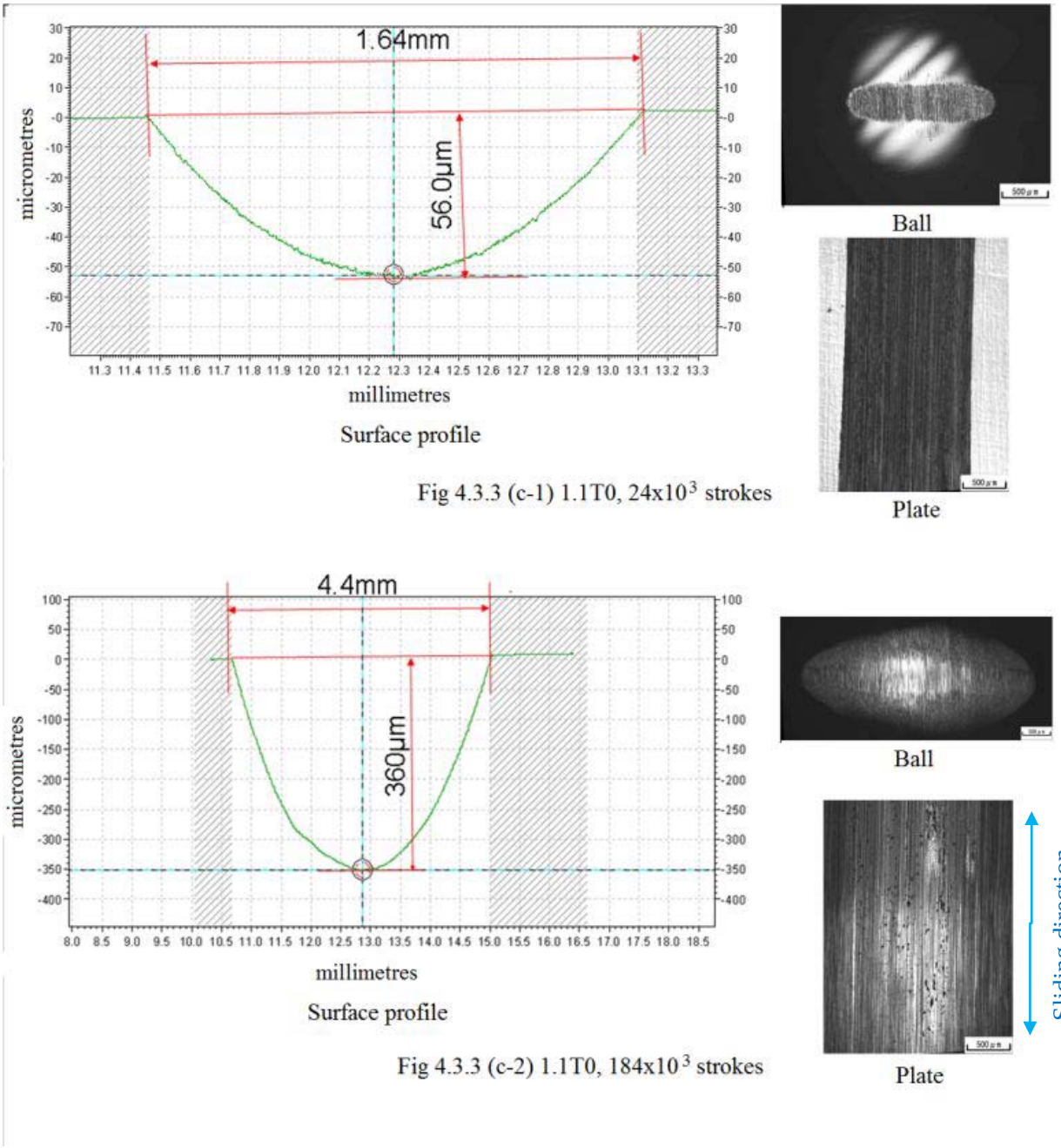

Fig 4.3.3 (c-1) 1.1T0, 24x10^3 strokes

Fig 4.3.3 (c-2) 1.1T0, 184x10^3 strokes

Fig 4.3.3 Appearance of the wear track on plates and balls, optical microscope images of wear surface of a plate and a ball, a raw profile on the wore plate, 50 times magnification

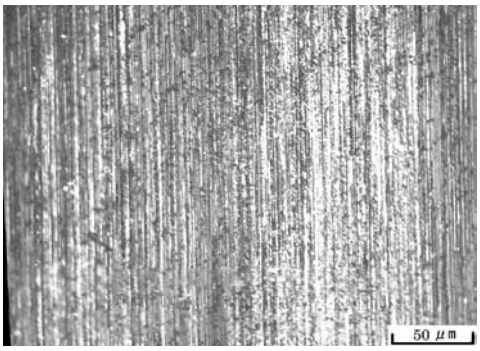

(a-1) Ball

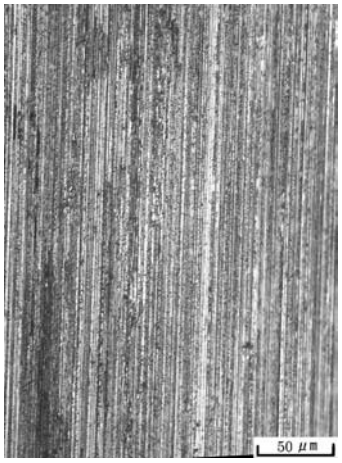

(a-2) Plate

(a) 0T0

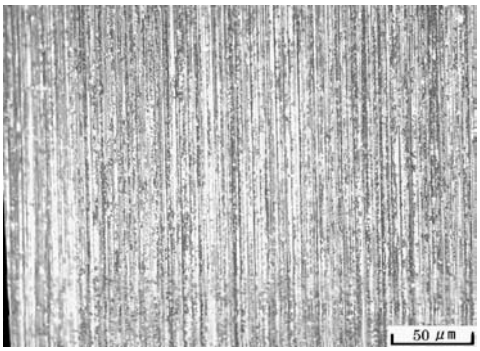

(b-1) Ball

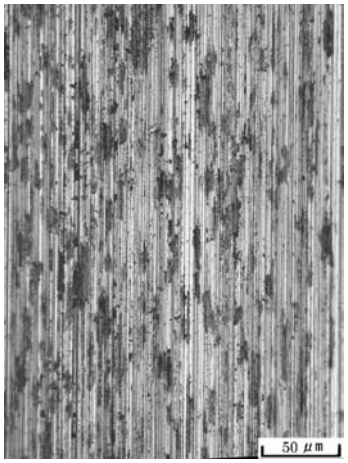

(b-2) Plate

(b) 0.4T0

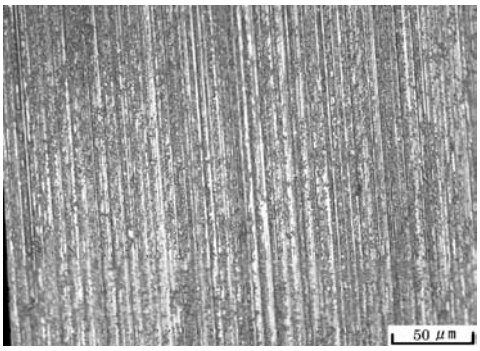

(c-1) Ball

(c-2) Plate

(c) 1.1T0

Fig.4.3.4 Appearances of the wear surface on plates and balls after $72x10^3$ strokes

4.3.4 Wear debris behaviour

Figure 4.3.5 shows lubricant under an optical microscope after lubricated sliding wear testing. The appearance of a normal lubricant is clear and bright amber liquid. However, lubricant containing wear debris at 0T0 is opaque black liquid after lubricated sliding wear test. The appearance of lubricant for both 0.4T0 and 1.1T0 is opaque brown liquid after lubricated sliding wear testing. Hence, it is concluded that the magnetic field influences the wear debris contained in the lubricant.

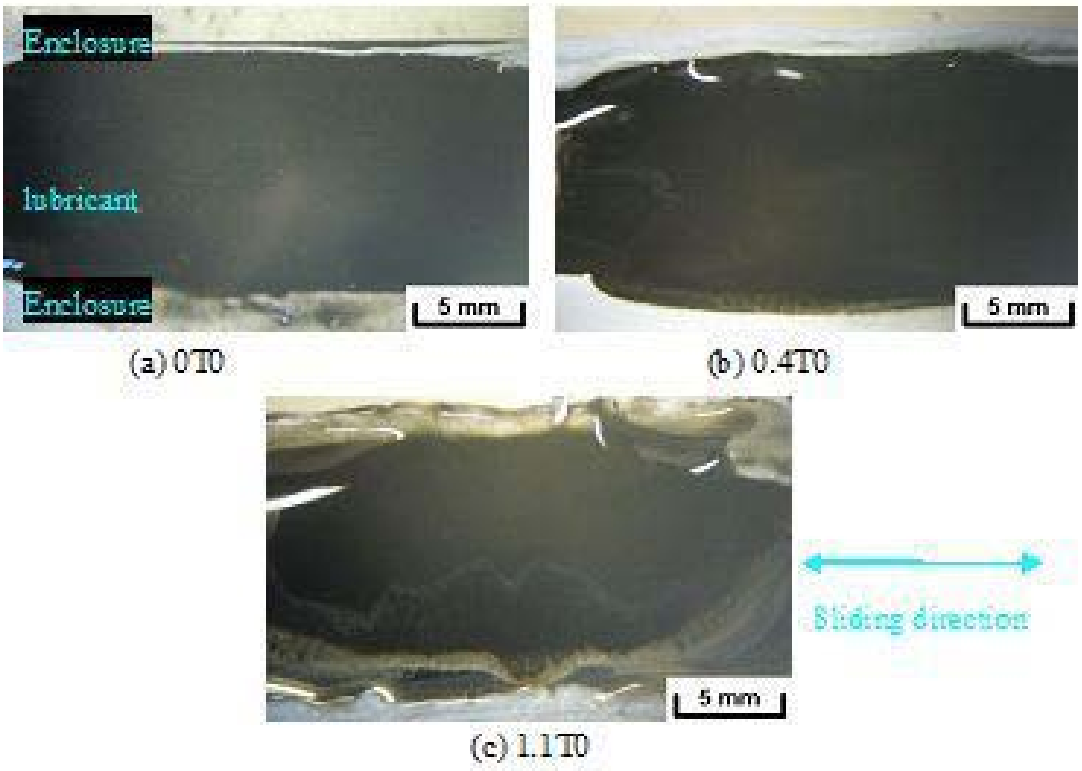

Fig 4.3.5 Lubricants observations after lubricated sliding wear testing in different magnetic fields

4.3.5 Wear debris observations

The obtained secondary electron images shown in Figure 4.3.6 show a varied different shapes and sizes of wear debris at a magnification of 500 times. After $24x10^3$ strokes, three common features for them generated at different magnetic flux densities include fine particles less than 10 μm in diameter. Besides, flaky particles with irregular shapes, exist as shown in Figure 4.3.6 (a-1), (b-1) and (c-1). However, the wear particles of both 0.4T0 and 1.1T0 feature split flaky marks which are indicated in Figure 4.3.6 (b-1) and (c-1). Additionally, there are aggregate particles, absent at 0T0, scattered and aligned with wear track. Hence, it can be said that the magnetic field produces split flaky particles together with fine particles. Finally, wear debris after $120x10^3$ strokes include differently shaped particles in comparison with wear debris after $24x10^3$ strokes. They are flat particles and at 1.1T0 they are of a size less than 40 μm in diameter.

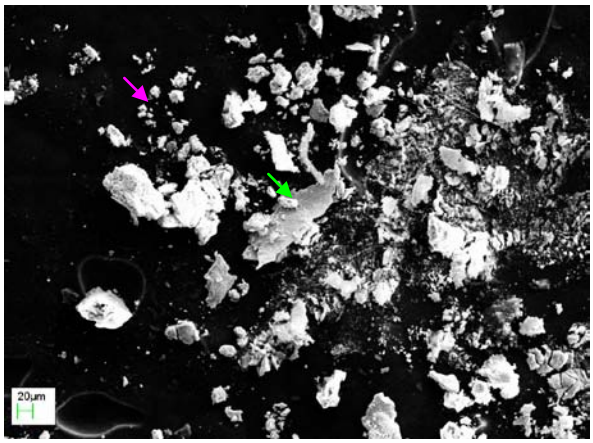

(a-1) 24x10³ strokes

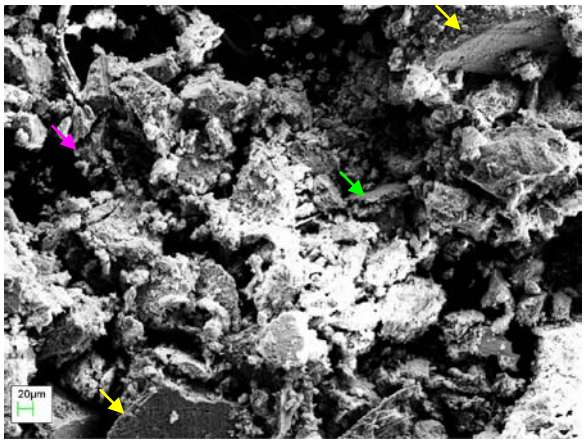

(a-2) 120x10³ strokes

(a) 0T0

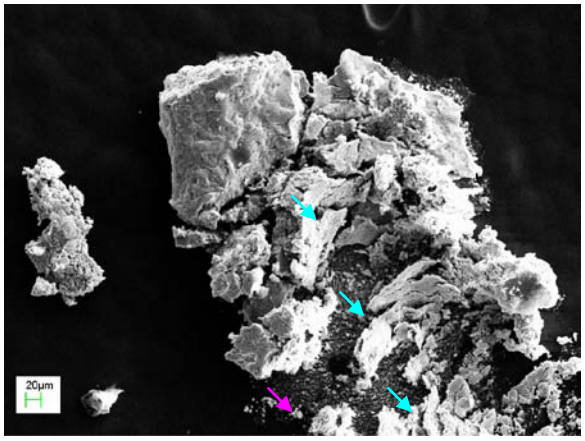

(b-1) 24x10³ strokes

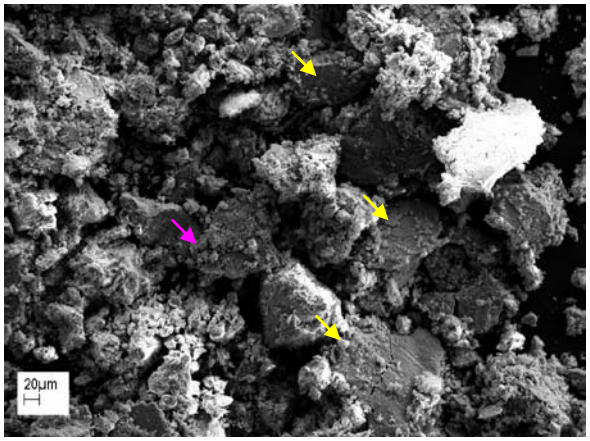

(b-2) 120x10³ strokes

(b) 0.4T0

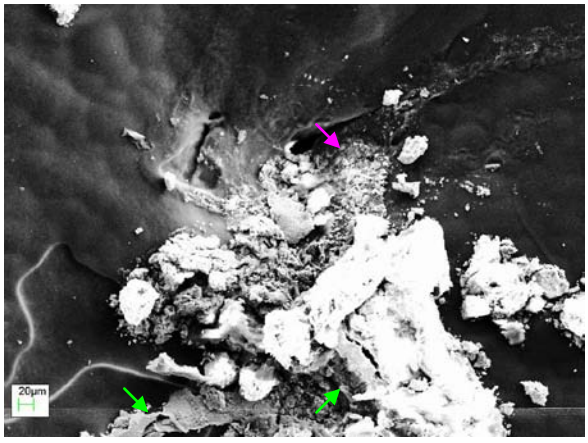

(c-1) 24x10³ strokes

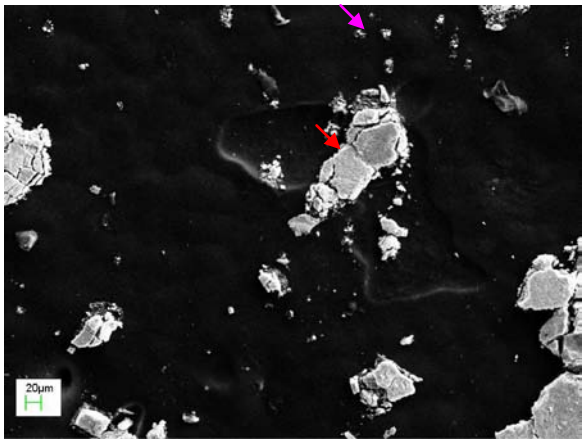

(c-2) 120x10³ strokes

(c) 1.1T0

Fig.4.3.6 General secondary images of wear debris, 500x magnifications
→: fine particles, →: flaky particle, →: flaky particle which has slits, →: flat particle (large), →: flat particle (small)

4.3.6 Analysis of wear debris

SEM analysis was carried out for ferro-particles with white colour in the backscatter electron images of Figure 4.3.7, 4.3.8 and 4.3.9. The element spectrum shows that the wear debris consists of C, Ca, Fe, O, S and Si. The Ca and S were additives for lubricant. Oxygen peaks of both 0.4T0 and 1.1T were obviously high in comparison with the peak at 0T0.

The XRD analysis in Figure 4.3.10 and 4.3.11 shows that wear debris under different magnetic flux density consist of α-iron and $CaCO_3$ (Calcium carbonate). The peaks of α-iron are at nearly 46º, 65.5º and 82.5º. Besides, other weak peaks, which are $CaCO_3$, are present at several points. Wear debris of both 0.4T0 and 1.1T0 increased the peak of $CaCO_3$ in comparison with wear debris at 0T0 (see Figure 4.3.10). Additionally, the analysis results at 1.1T0 indicate the high peaks of $CaCO_3$ comparing to that at 0.4T0. Figure 4.3.11, indicates that peaks of $CaCO_3$ were increased in the high magnetic field. It resembles results shown in Figure 4.3.10.

Therefore, SEM analysis suggests that the magnetic field enhances the oxidation of ferro-wear debris. Furthermore, the peaks of $CaCO_3$ are increased due to the influence of the magnetic field.

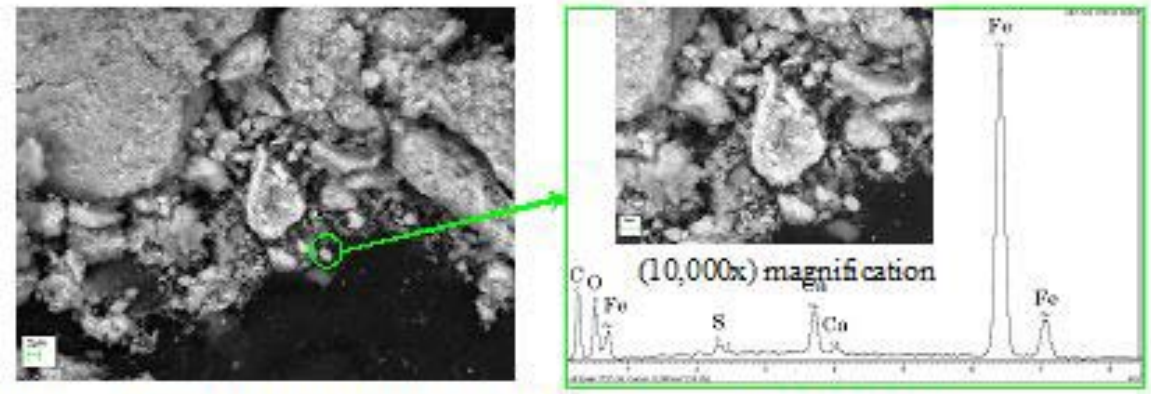

Back scatter images, 5,000x magnifications Element analysis

(a) 24x10^3 strokes

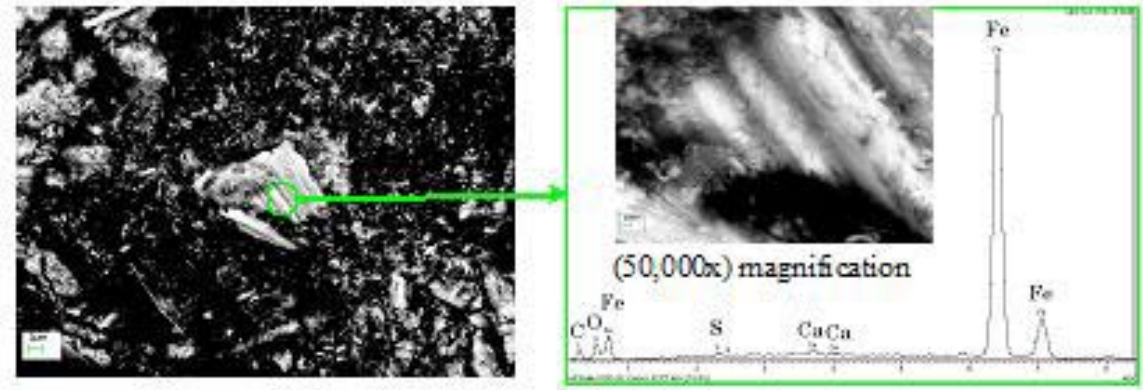

Back scatter images, 5,000x magnifications Element analysis

(b) 92x10^3 strokes

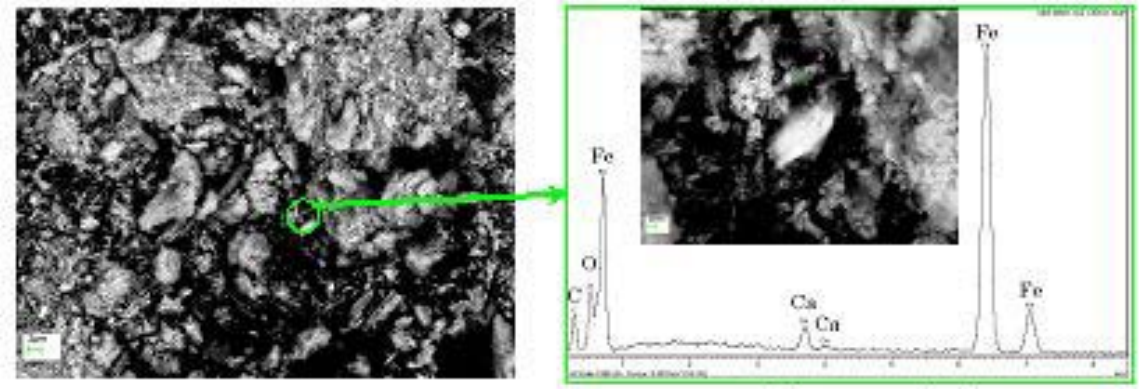

Back scatter images, 5,000x magnifications Element analysis

(c) 120x10^3 strokes

Fig. 4.3.7 Backscatter image and SEM analysis of particle at 0T0

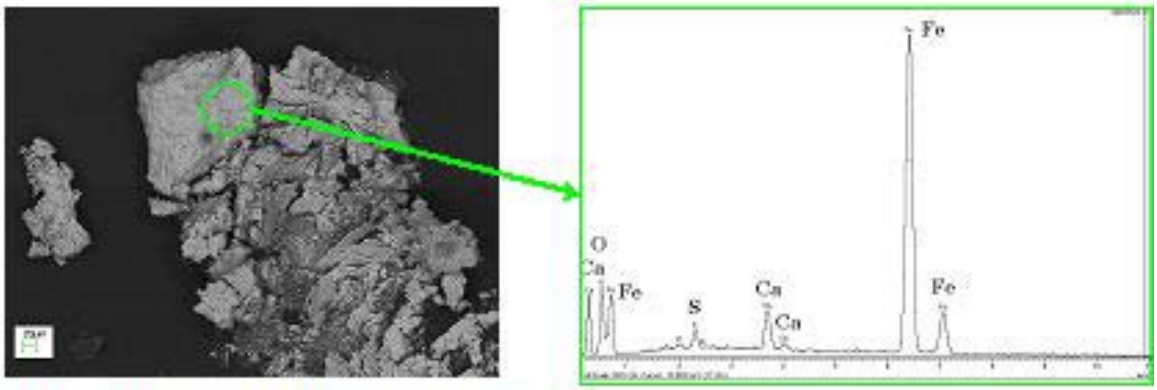

Back scatter images, 500x magnifications　　Element analysis

(a) 24x10^3 strokes

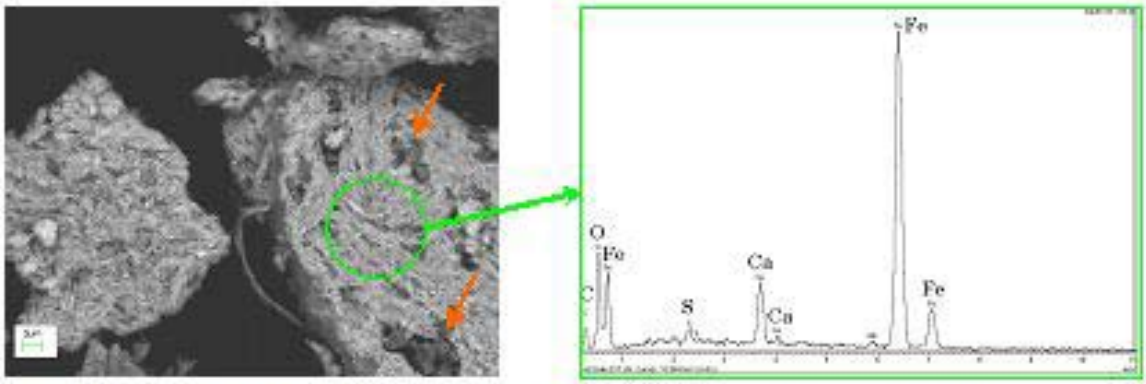

Back scatter images, 5,000x magnifications　　Element analysis

(b) 92x10^3 strokes

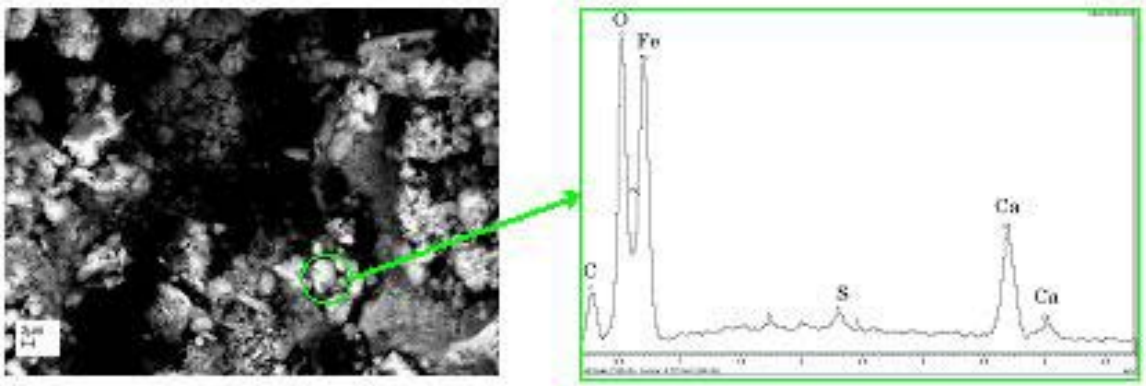

Back scatter images, 5,000x magnifications　　Element analysis

(c) 120x10^3 strokes

Fig 4.3.8 Backscatter image and SEM analysis of particle at 0.4T0 (→: Ca system particle)

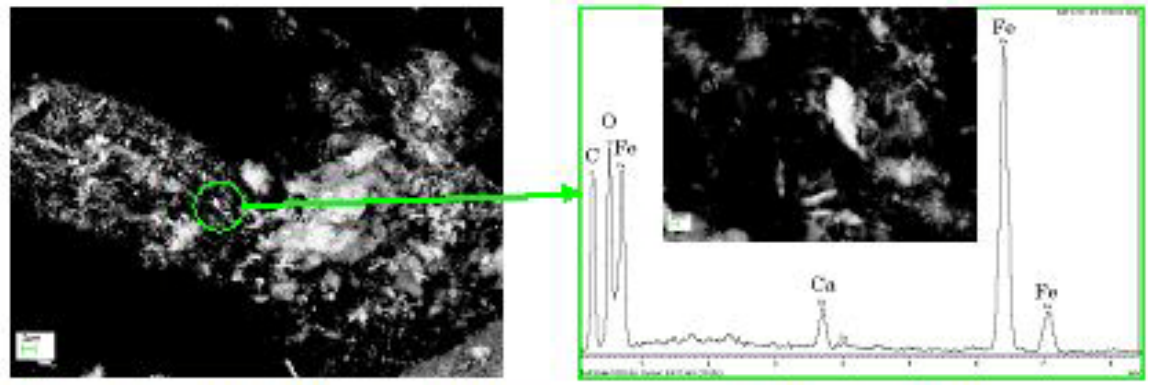

Back scatter images, 5,000x magnifications　　Element analysis

(a) $24x10^3$ strokes

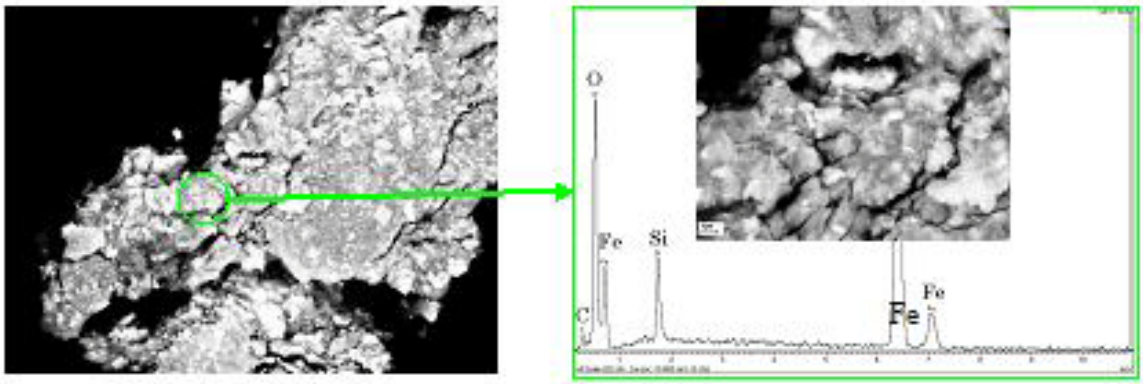

Back scatter images, 5,000x magnifications　　Element analysis

(b) $92x10^3$ strokes

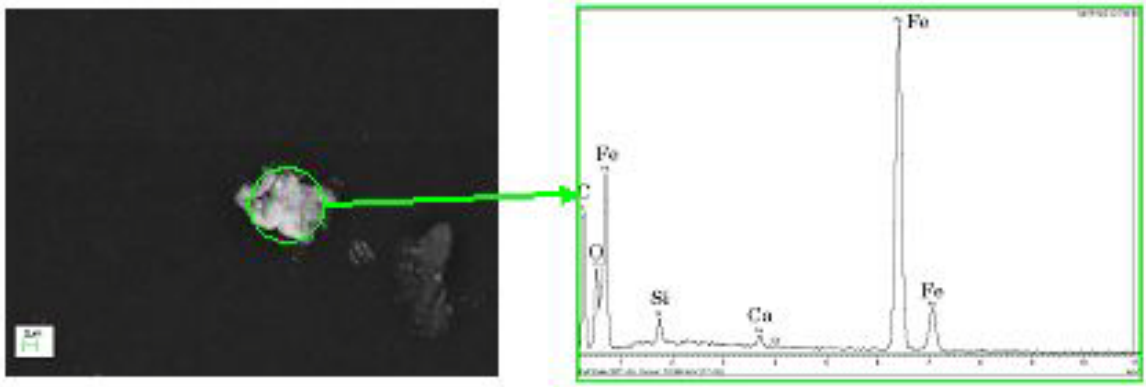

Back scatter images, 5,000x magnifications　　Element analysis

(c) $120x10^3$ strokes

Fig 4.3.9 Backscatter image and SEM analysis of particle at 1.1T0

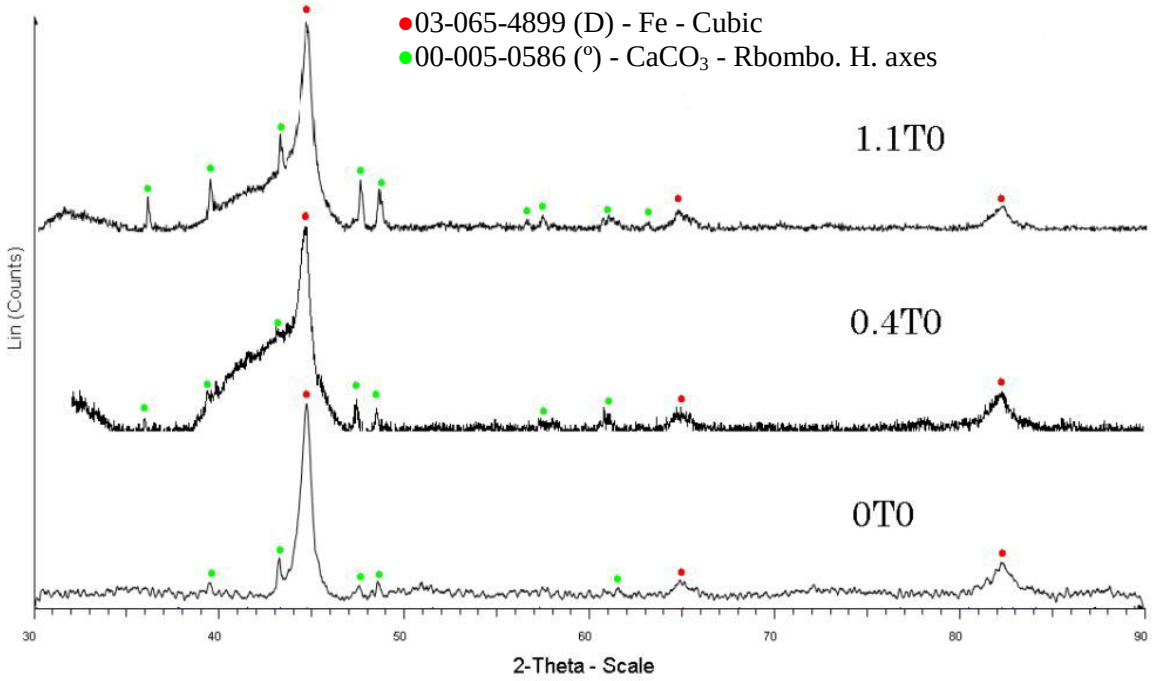

Fig 4.3.10 XRD analysis of wear debris after $24x10^3$ strokes

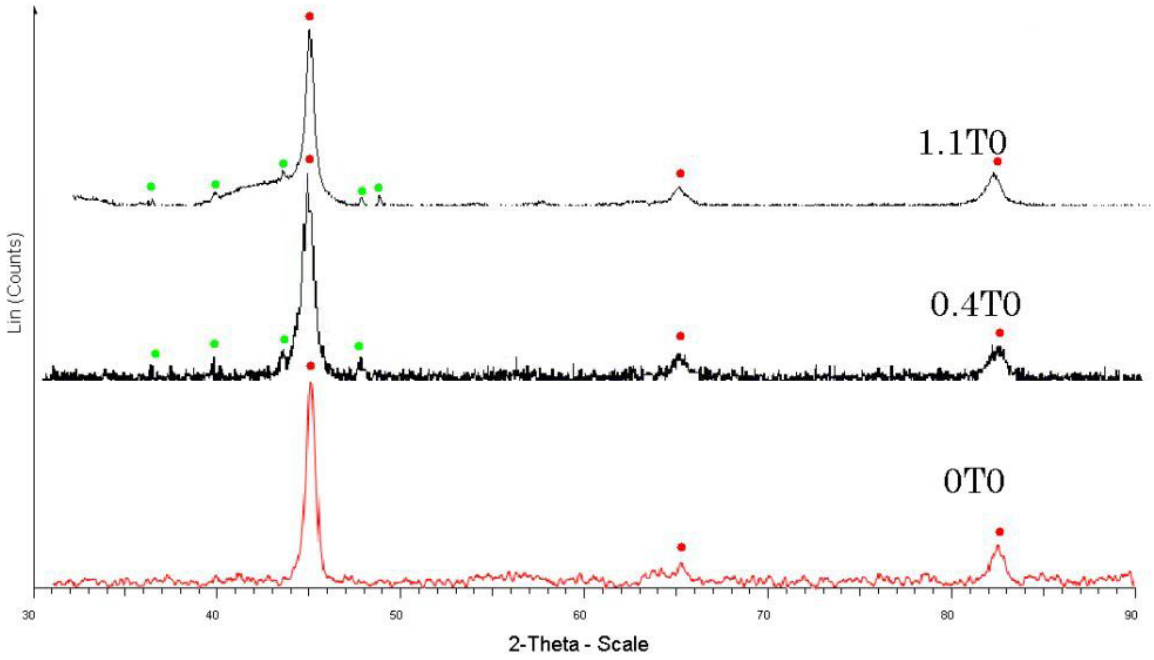

Fig 4.3.11 XRD analysis of wear debris after $120x10^3$ strokes

4.4 High frequency sliding contact

4.4.1 Paramagnetic material vs. ferromagnetic material

4.4.1.1 Magnetic field density

The weight measurements of both the plate and the ball were inconclusive due to extremely small mass loss (less than 1 mg). Thus, the influence of magnetic field was evaluated by other measurements.

Figure 4.4.1 illustrates surface roughness, Ra, of the wear track on the plate specimen for different magnetic field density angles. It shows that *Ra* range was less than 0.8 μm and had stable tendency. In addition, the *Ra* average, the maximum Ra, the minimum *Ra* and the *Ra* are more than 6 μm shown in Table 4.4.1. In Figure 4.4.1 (a), the *Ra* value at 1.1T0 is extremely high after $580x10^3$ strokes. From Figure 4.4.2, it can be seen that the cause of the high *Ra* value was a bulge from the surface of the wear track; therefore, the extreme *Ra* value was excluded from Table 4.4.1.

- Low frequency: *Ra* ranges were less than approximately 0.3 μm. Thus, the influence of the magnetic field has a negligible influence on the surface roughness of the wear track.
- Middle frequency: 1.1T0 caused less variability than 0T0 and 0.4T0. The maximum *Ra* at 1.1T0 was 0.913 μm which is approximately 0.2 or 0.4 μm less than for other test conditions.
- High frequency: When the maximum *Ra* values at 0.4T0 and 1.1T0 are compared with the maximum *Ra* value at 0T0, the difference is less than approximately 0.2 μm.

The bulge in the wear track area is clearly visible in surface profile in Figure 4.4.2. It was created in the presence of the magnetic field. It is most certainly created by wear debris piled

up by plastic deformations.

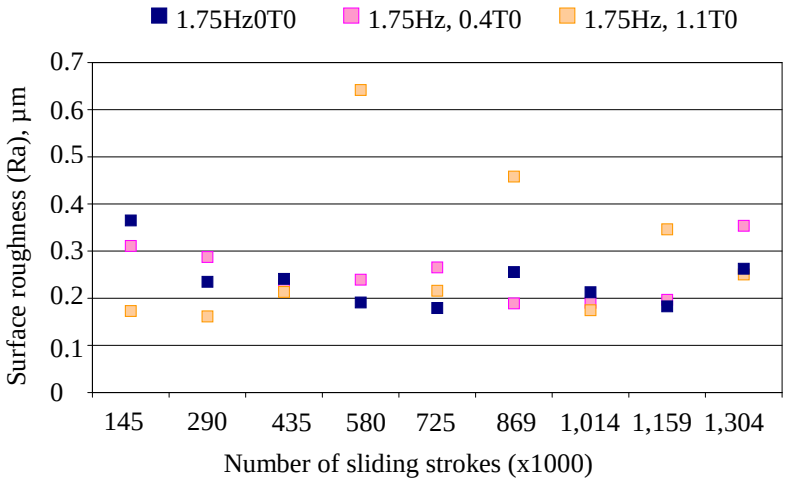

(a) Low frequency

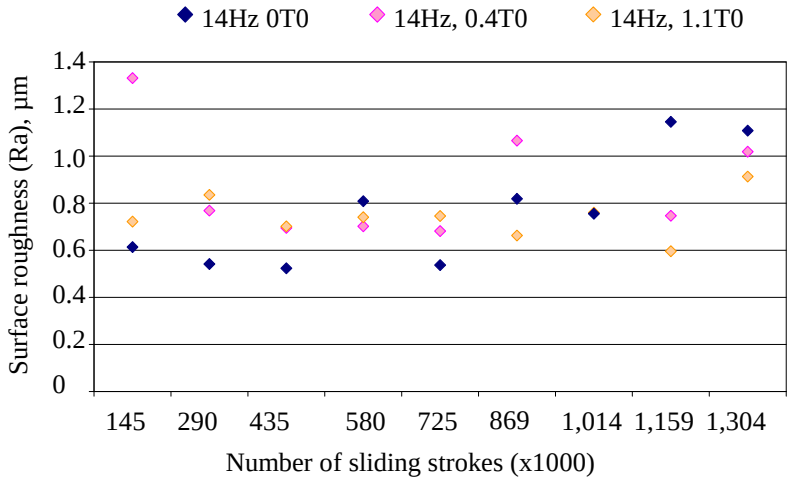

(b) Middle frequency

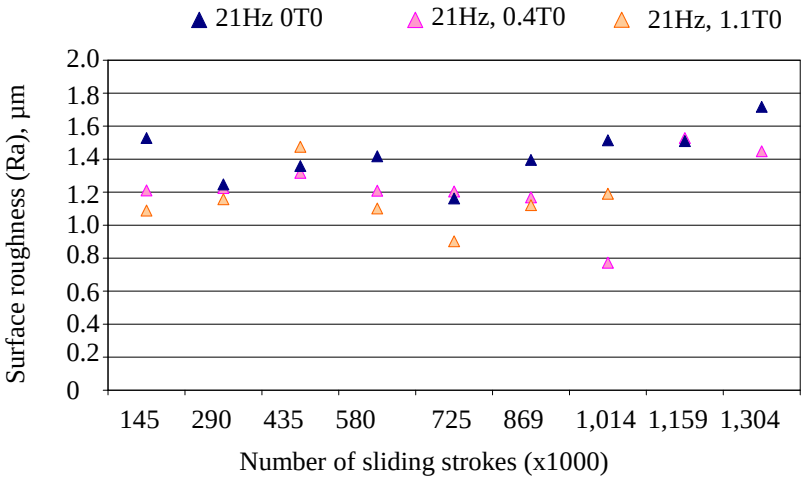

(c) High frequency

Fig 4.4.1 Surface roughness of plate in different magnet flux densities

Table 4.4.1 *Ra* values on the wear surface of plates

	1.75Hz			14Hz			21Hz		
	0T0	0.4T0	1.1T0	0T0	0.4T0	1.1T0	0T0	0.4T0	1.1T0
Max (μm)	0.37	0.35	0.46	1.15	1.33	0.91	1.72	1.53	1.47
Min (μm)	0.18	0.19	0.16	0.52	0.68	0.60	1.16	0.77	0.90
Ra range (μm)	0.19	0.16	0.30	0.62	0.65	0.32	0.56	0.76	0.57
Average (μm)	0.24	0.25	0.25	0.76	0.88	0.74	1.43	1.23	1.15

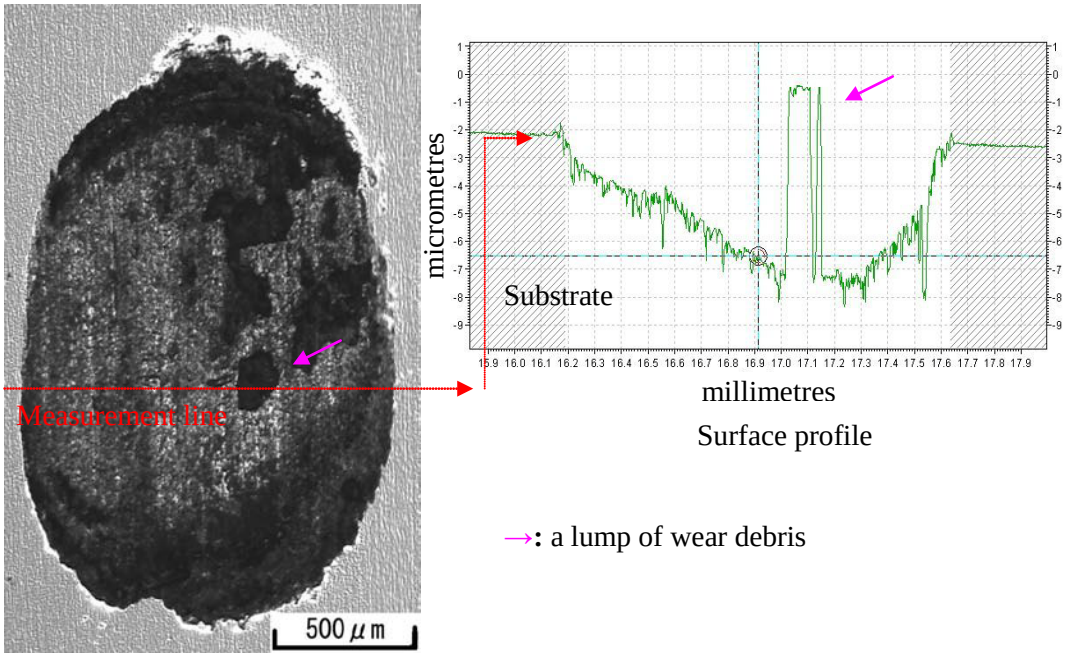

Fig 4.4.2 View of the wear track and the profile of the plate at 1.1T0 in 1.75 Hz after 580×10^3 strokes

Figure 4.4.3 shows the two-dimensional surface profiling and optical microscope images of wear tracks created after $1{,}304x10^3$ strokes.

Figure 4.4.3, in addition, shows that the depth of wear track increased due to the influence of the magnetic field at low frequency sliding condition. While, middle frequency sliding wear condition increased amount of wear in the presence of the magnetic field. Finally, a combination of high frequency and magnetic field produced shallow wear track with depth of 19 μm.

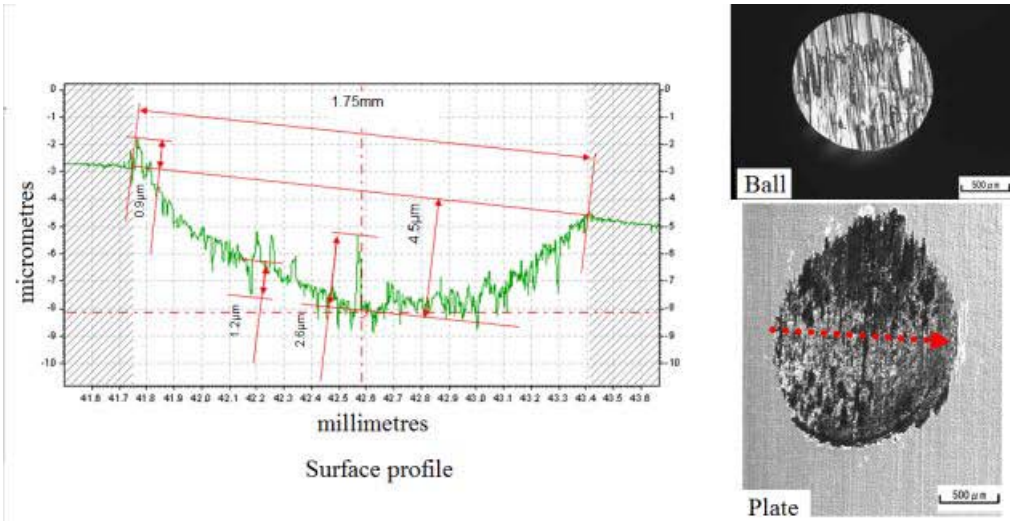

Fig 4.4.3 (a-1) 1.74Hz, 0T0

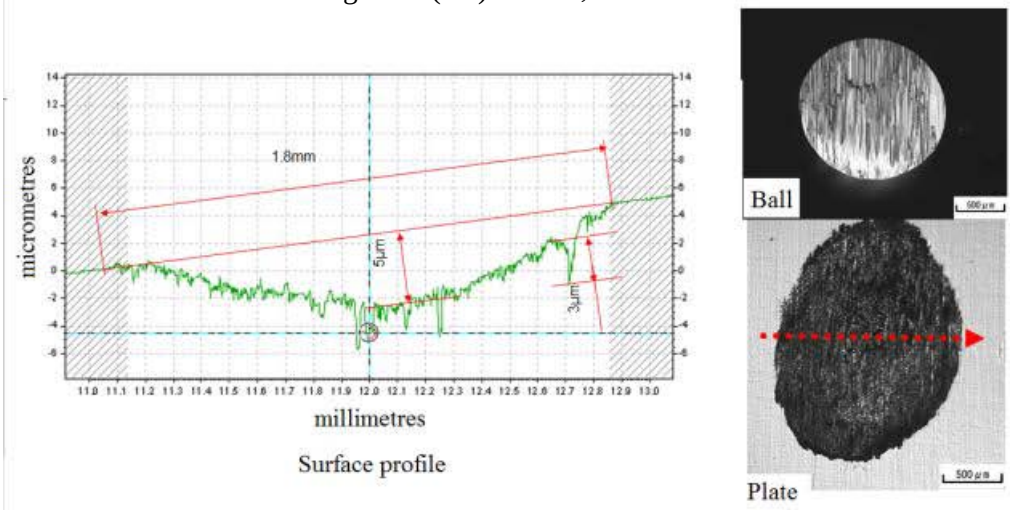

Fig 4.4.3 (a-2) 1.74Hz, 0.4T0

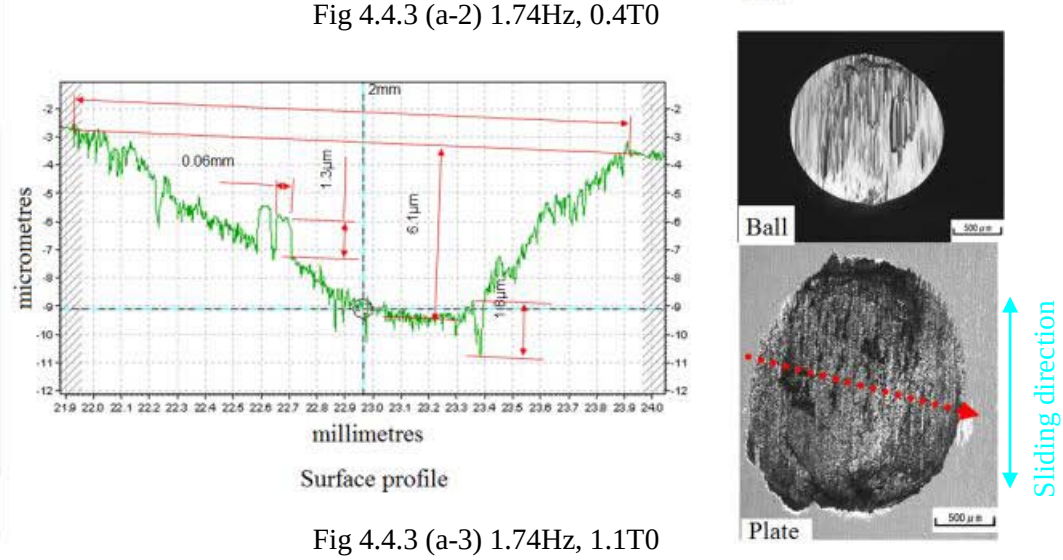

Fig 4.4.3 (a-3) 1.74Hz, 1.1T0

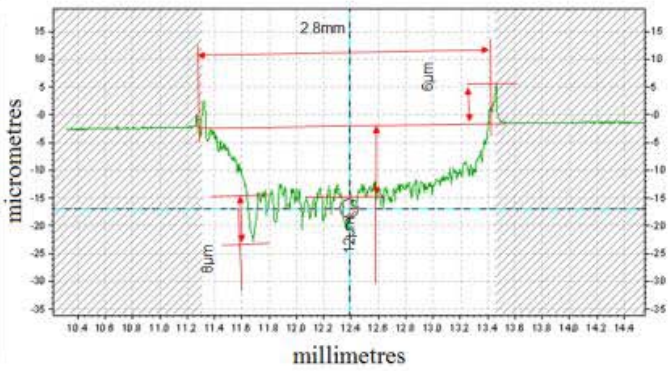

Surface profile

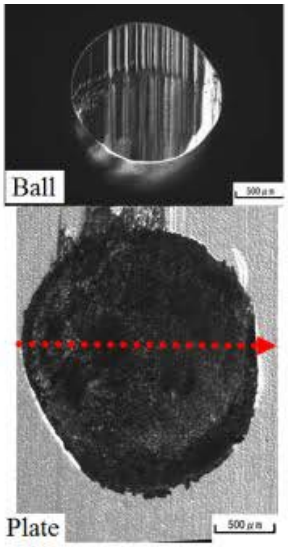

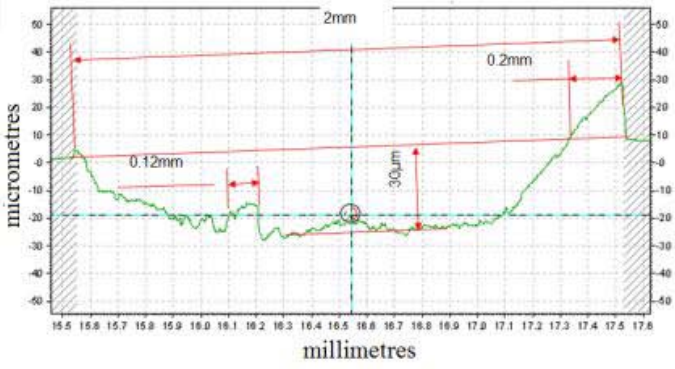

Surface profile

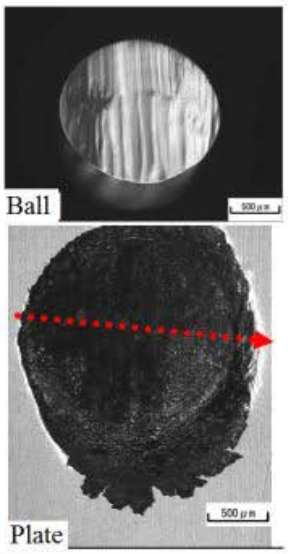

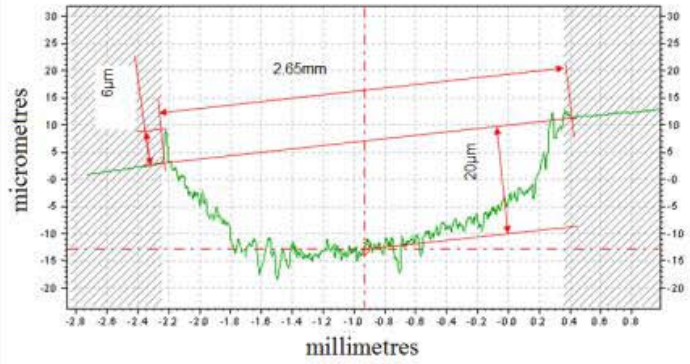

Surface profile

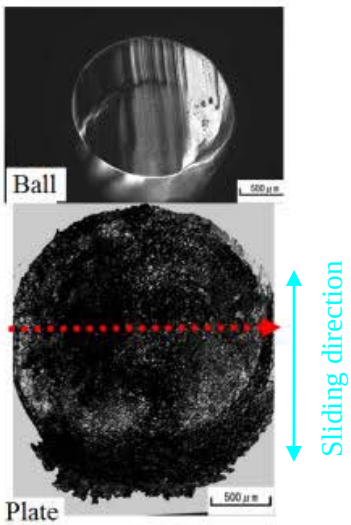

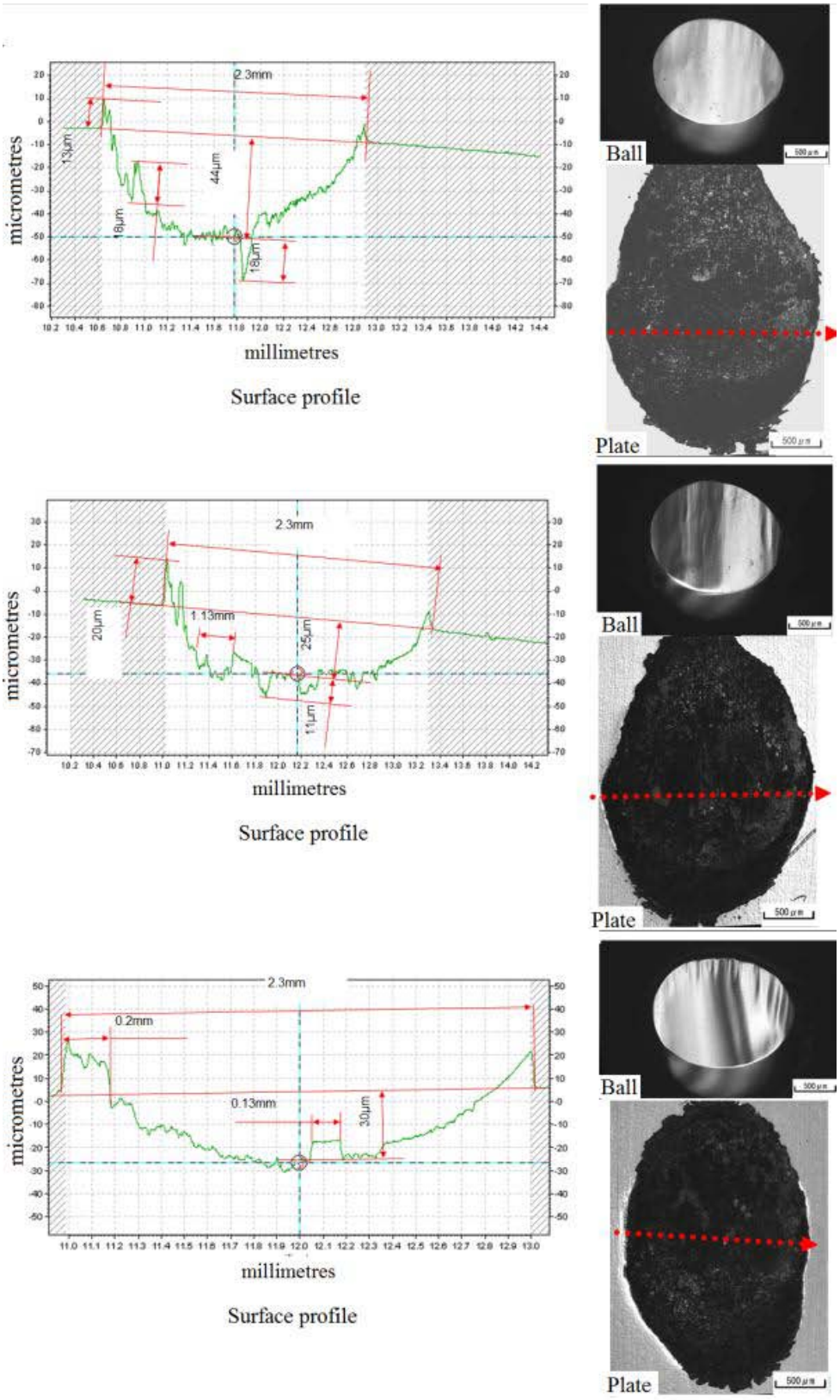

Fig 4.4.3 Surface profiling and surface observation of plate and ball specimen after 1,304 x10^3 strokes, 50x magnifications, →: Measurement line

Observation of wear track appearance

Figures 4.4.4, 4.4.5 and 4.4.6 show SEM images of the wear track on the plate after 1,304 $x10^3$ strokes. The chemical composition at locations indicated by different colour arrows in these figures is shown in Figure 4.4.7. Additionally, Table 4.4.1 contains *Ra* values for SEM images of the wear track.

- Low frequency: The scratches or traces in (a) and (c) of Figure 4.4.4 were oriented in the same direction as the sliding direction. Besides, pits were observed on the wear track shown in Figure 4.4.4. The pits at 1.1T0 were in the form of a shallow hole and the bottom area of the hole is flat.
- Middle frequency: The appearance of the wear track in Figure 4.4.5 is mainly uneven flat surface. However, the wear track at 0T0 has very bumpy surface. The high magnification image shows that silver area was dotted with iron and silicon. Additionally, by the rise of the magnetic flux density, the spread of the silver area was observed to increase. From the low magnification image of Figure 4.4.5(a), it is seen that the gray small particles adhered to the surface of wear track. In the case of 1.1T0, Figure 4.4.5 (c) shows two or three small particles attached to the side of wear track.
- High frequency: The appearance of wear track in Figure 4.4.6 points to a bumpiest surface in comparison with other frequencies.

Finally, the SEM analysis is shown in Figure 4.4.7. The composition elements are indicated by arrows in SEM images.

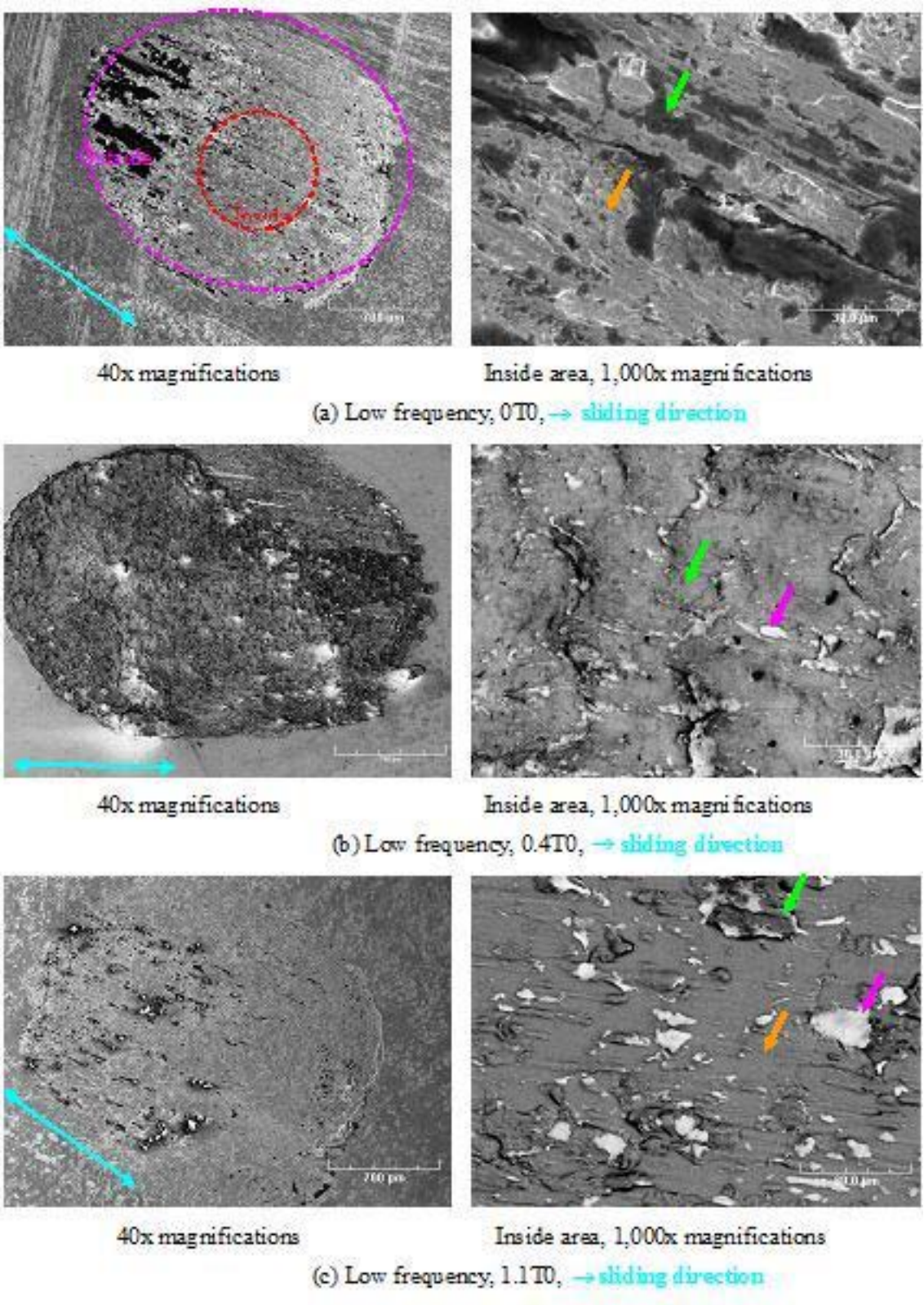

Fig 4.4.4 SEM images of the plate, low frequency, after $1{,}304 \times 10^3$ strokes

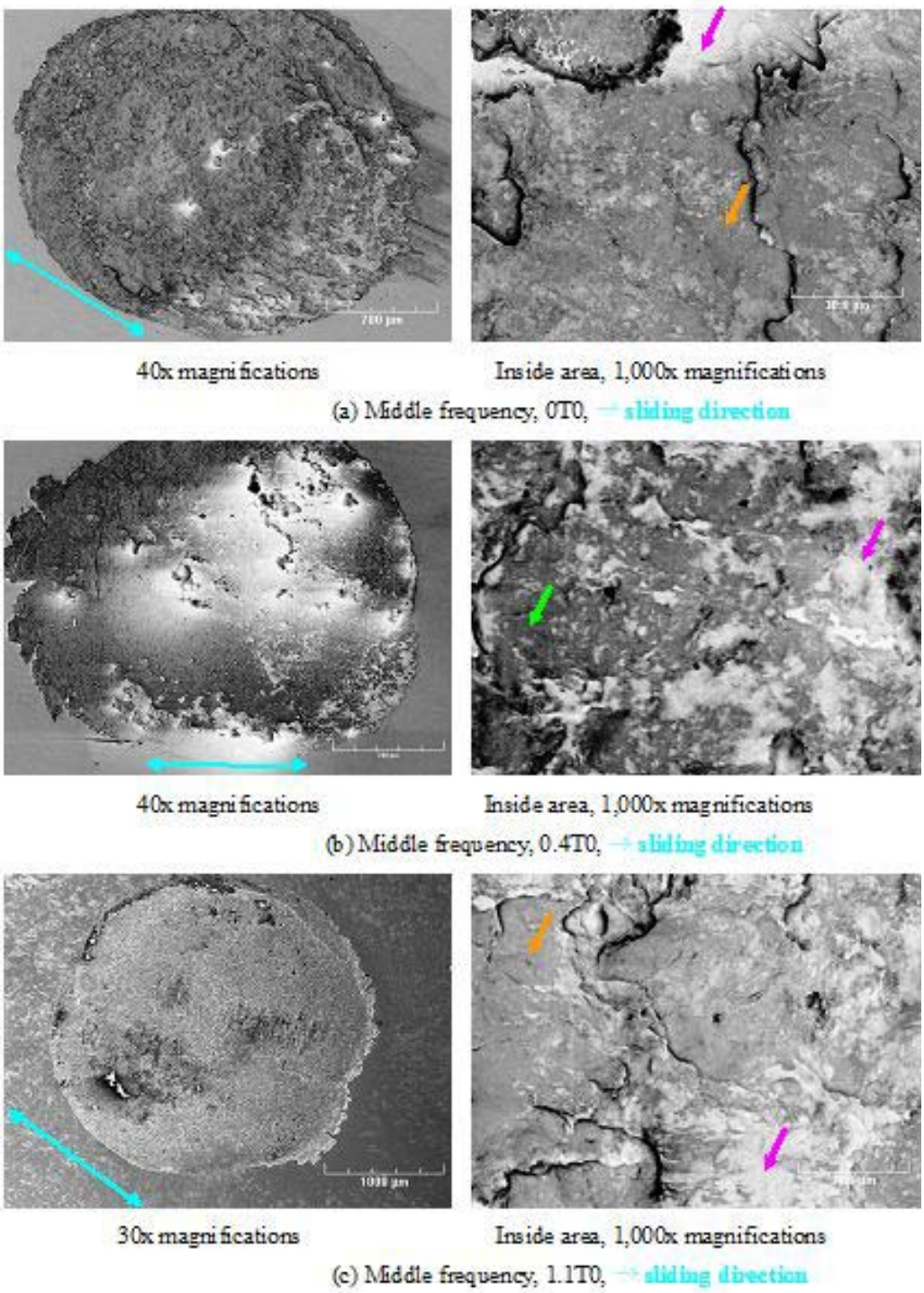

Fig 4.4.5 SEM images of the plate, middle frequency, after $1{,}304 \times 10^3$ strokes

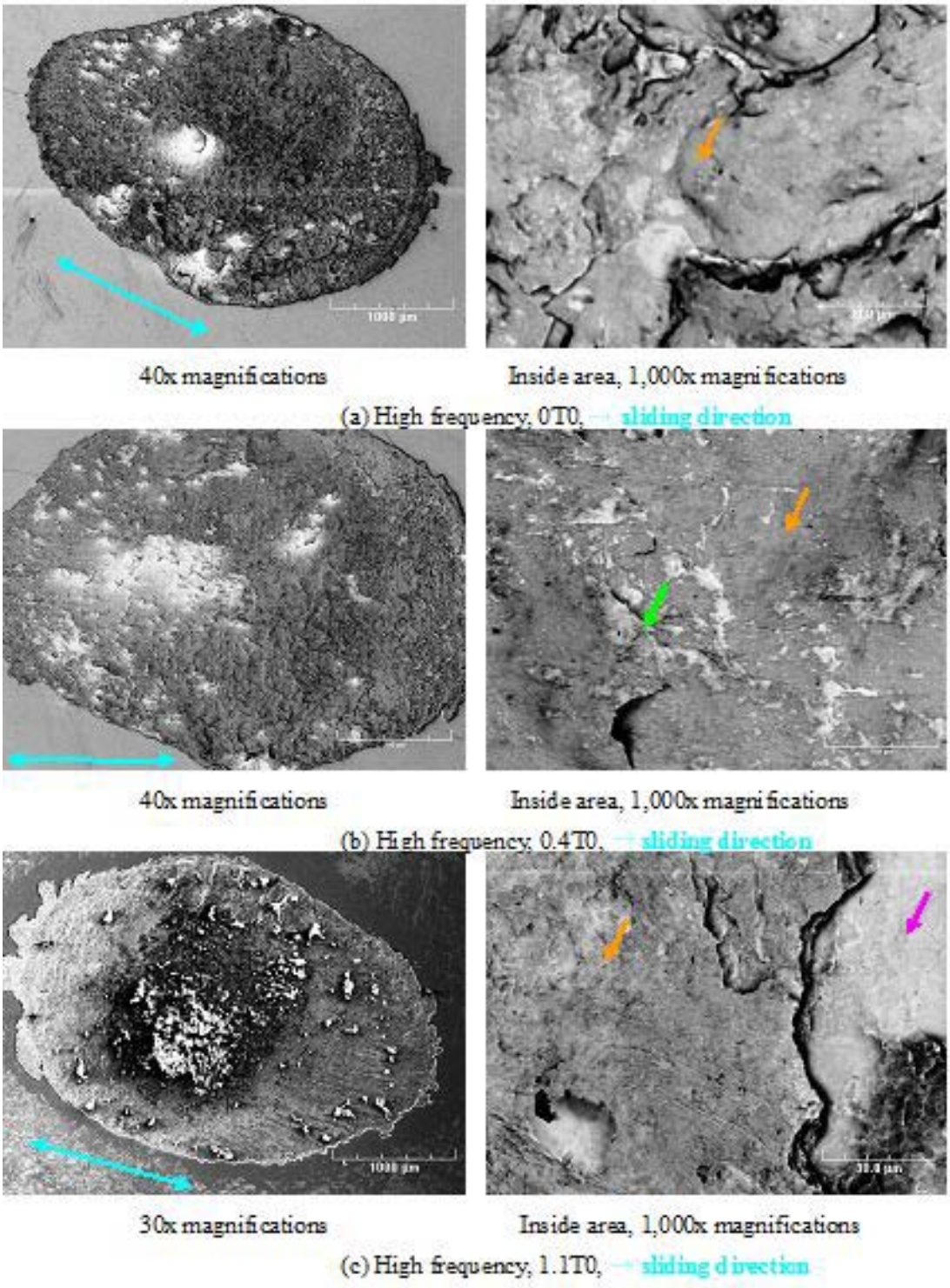

Fig 4.4.6 SEM images of the plate, high frequency, after $1{,}304 \times 10^3$ strokes

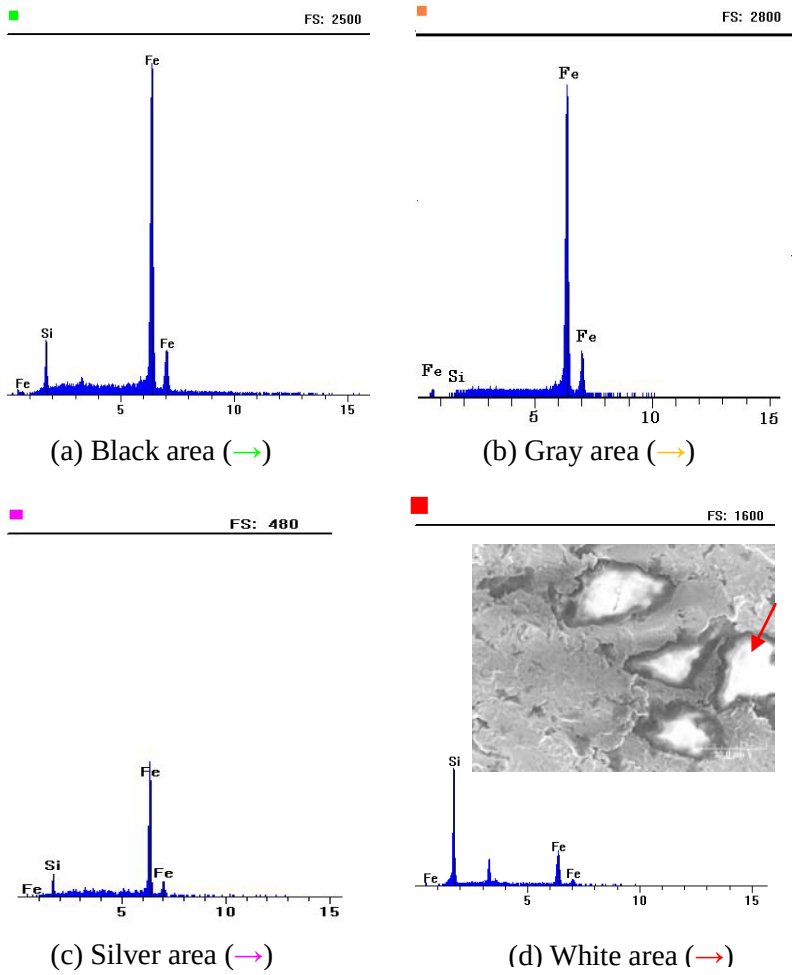

(a) Black area (→) (b) Gray area (→)

(c) Silver area (→) (d) White area (→)

Figure 4.4.7 SEM analysis was indicated by arrows in Figure 4.4.4, 4.4.5 and 4.4.6, White area (d) is the outside of Figure 4.4.4(a).

Table 4.4.2 the explanation of the wear track shown in Figure 4.4.4, 4.4.5 and 4.4.6

		Appearance	Pit	Crack etc.
Low	0T0	Scratches (12 μm in width)	Pits, 6 μm in diameter	A way of sliding direction
	0.4T0	Uneven	Pits, 3 μm in diameter	Difference in rank, it is a vertical direction in the sliding direction.
	1.1T0	Flat	Hollow, 6 μm in diameter	A short trace, it is a vertical direction in the sliding direction.
Middle	0T0	Uneven	-	Difference in rank (a vertical direction)
	0.4T0	Uneven and flat	-	
	1.1T0	Flat	-	
High	0T0	Uneven	-	
	0.4T0		-	
	1.1T0	Uneven (centre), flat (outer area)	Hollow, 18 μm in diameter	

4.4.1.2 Wear debris behaviour

Figure 4.4.8 shows aligned wear debris after 1,014x10^3 strokes. Two types of wear debris namely aggregated wear debris and particulate wear debris, can be seen in the figure. The aggregated wear debris were produced during low frequency sliding wear, and their colour is light silver. On the other hand, the particulate wear debris were produced in high frequency sliding wear, and their colour is light brown or dark brown.

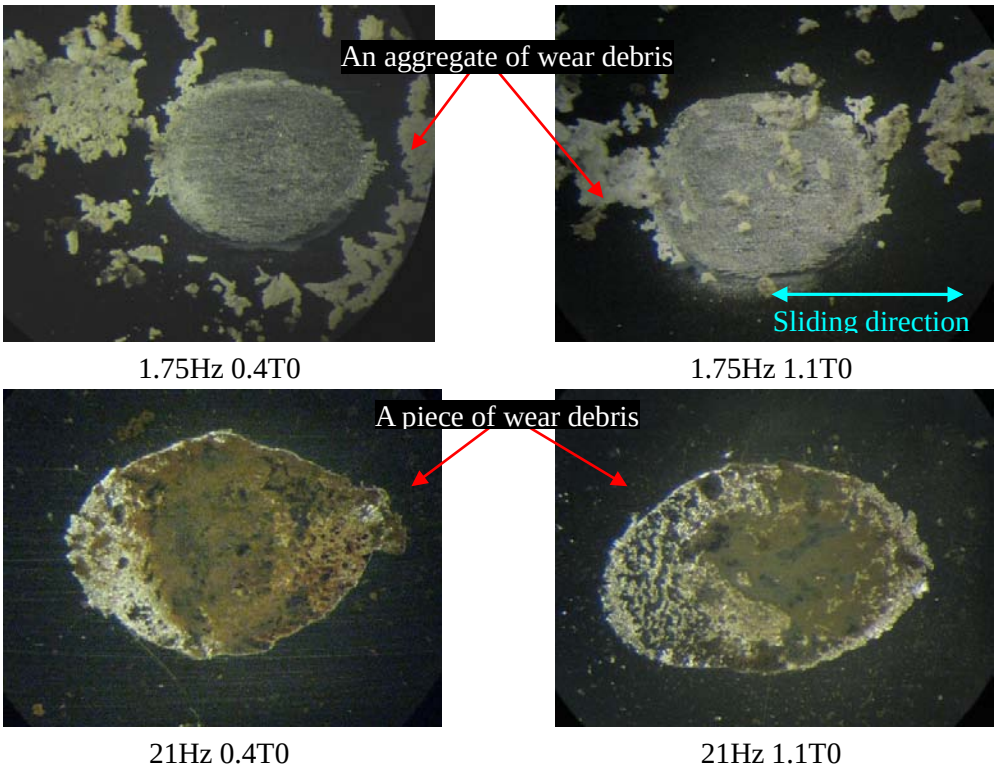

Fig 4.4.8 Aligned wear debris observation after 1,014x10^3 strokes

4.4.1.3 Different magnetic field orientation

Figure 4.4.9 illustrates the difference between surface roughness for magnetic field directions of 0 and 35 degree. Points in the figure represent the results of subtraction of *Ra* for 0.4T35 from that of 0.4T0. Magnetic field with direction of 35 degree increased the surface roughness of the plate excluding 1.1T35. The case of 1.1T35 with middle and high frequency reduces the surface roughness of the plate.

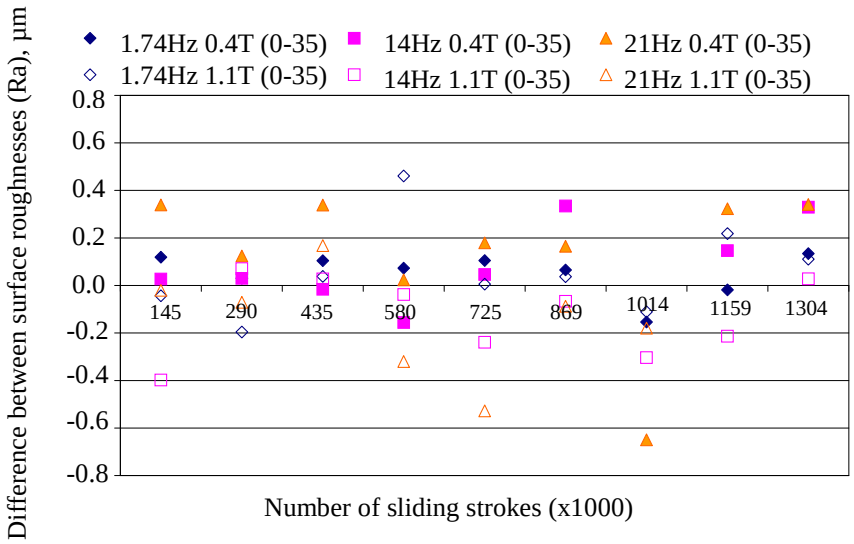

Fig 4.4.9 Difference of between surface roughness in magnetic field directions of 0 and 35º

4.4.1.3.1 Topography on the surface of the plate and a ball test specimens

Figure 4.4.10 shows the two-dimensional surface profiles and optical microscope images for wear tracks are produced after $1{,}304x10^3$ strokes.

The depth and the width of wear track at 1.1T35 are compared with that for 1.1T0. The difference between magnetic field directions at low frequency is negligibly small, which, the test conditions at middle and high frequencies produced a visible change in contact area dimensions. For 1.1T35 sample wore out 32 μm increasing depth by 10 μm. In addition, the bottom area of the wear track is a rough and has a deep groove or bulge.

The wear spot on the ball specimen of 1.1T35 has even surface.

Therefore, it can be said that wear debris produced at 1.1T35 are fine particles aligned in the same direction.

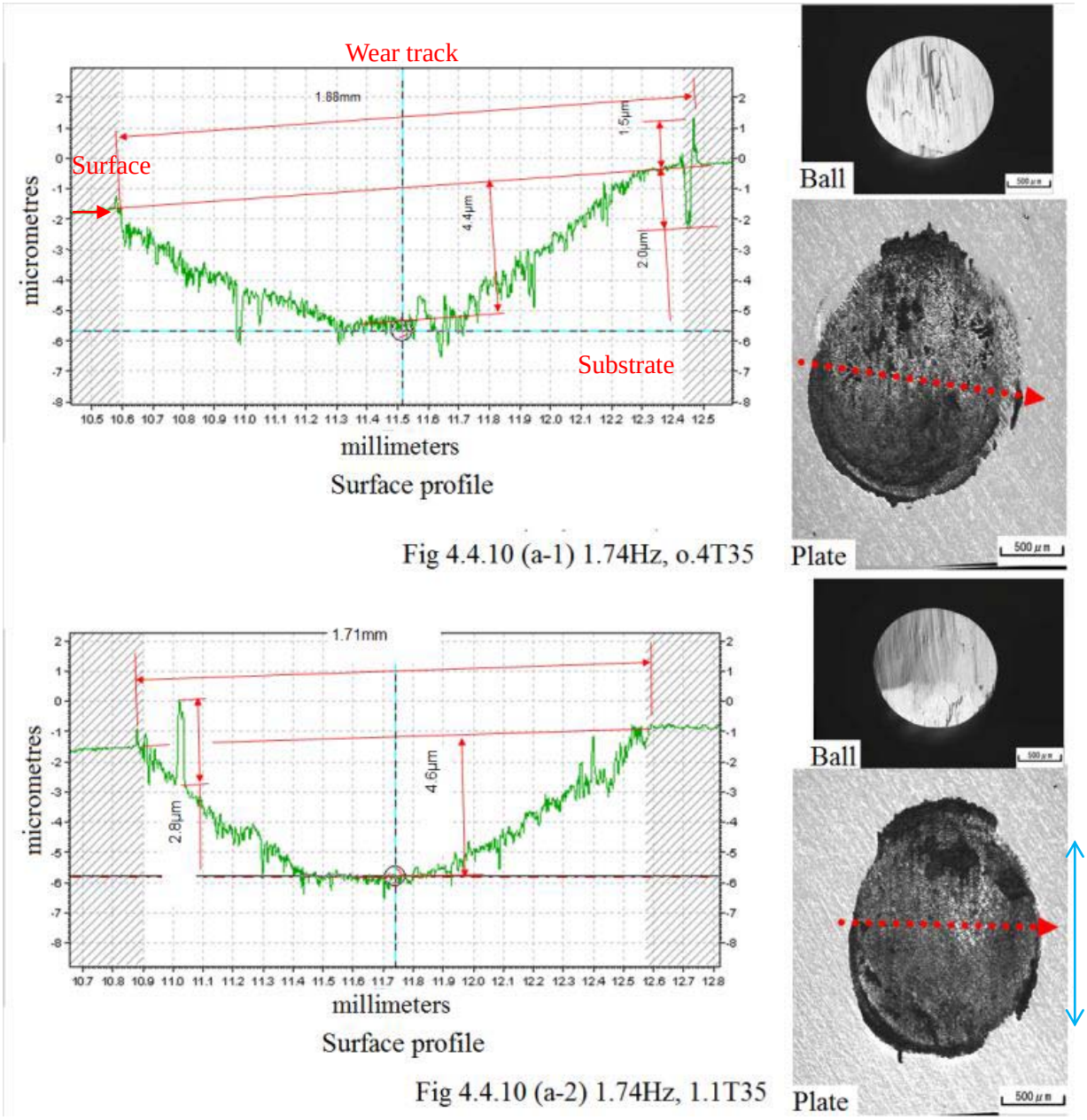

Fig 4.4.10 (a-1) 1.74Hz, o.4T35

Fig 4.4.10 (a-2) 1.74Hz, 1.1T35

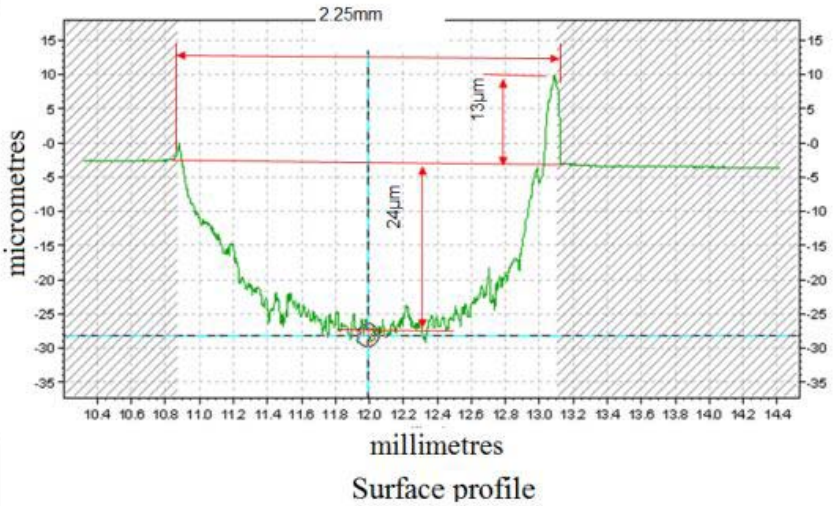

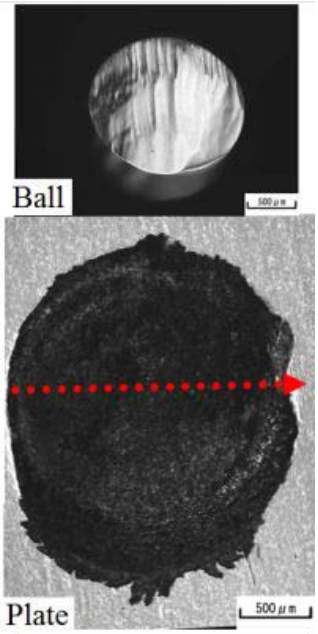

Fig 4.4.10 (b-1) 14Hz, 0.4T35

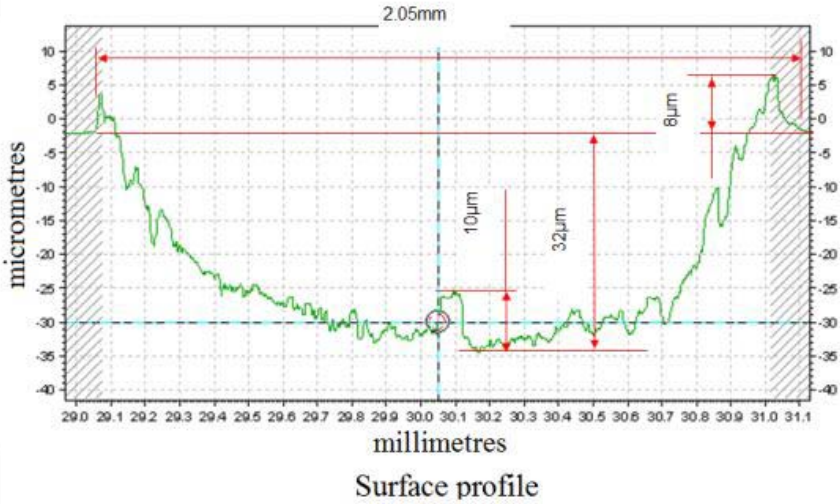

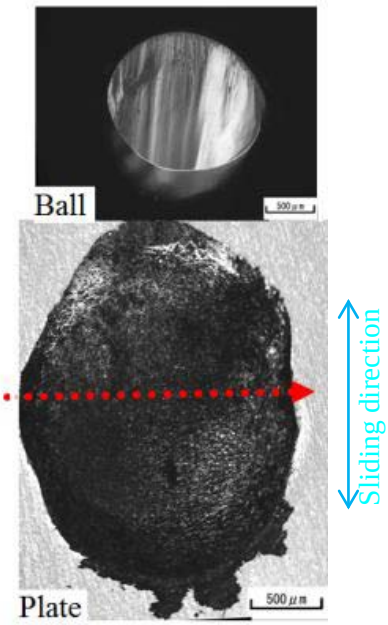

Fig 4.4.10 (b-2) 14Hz, 1.1T35

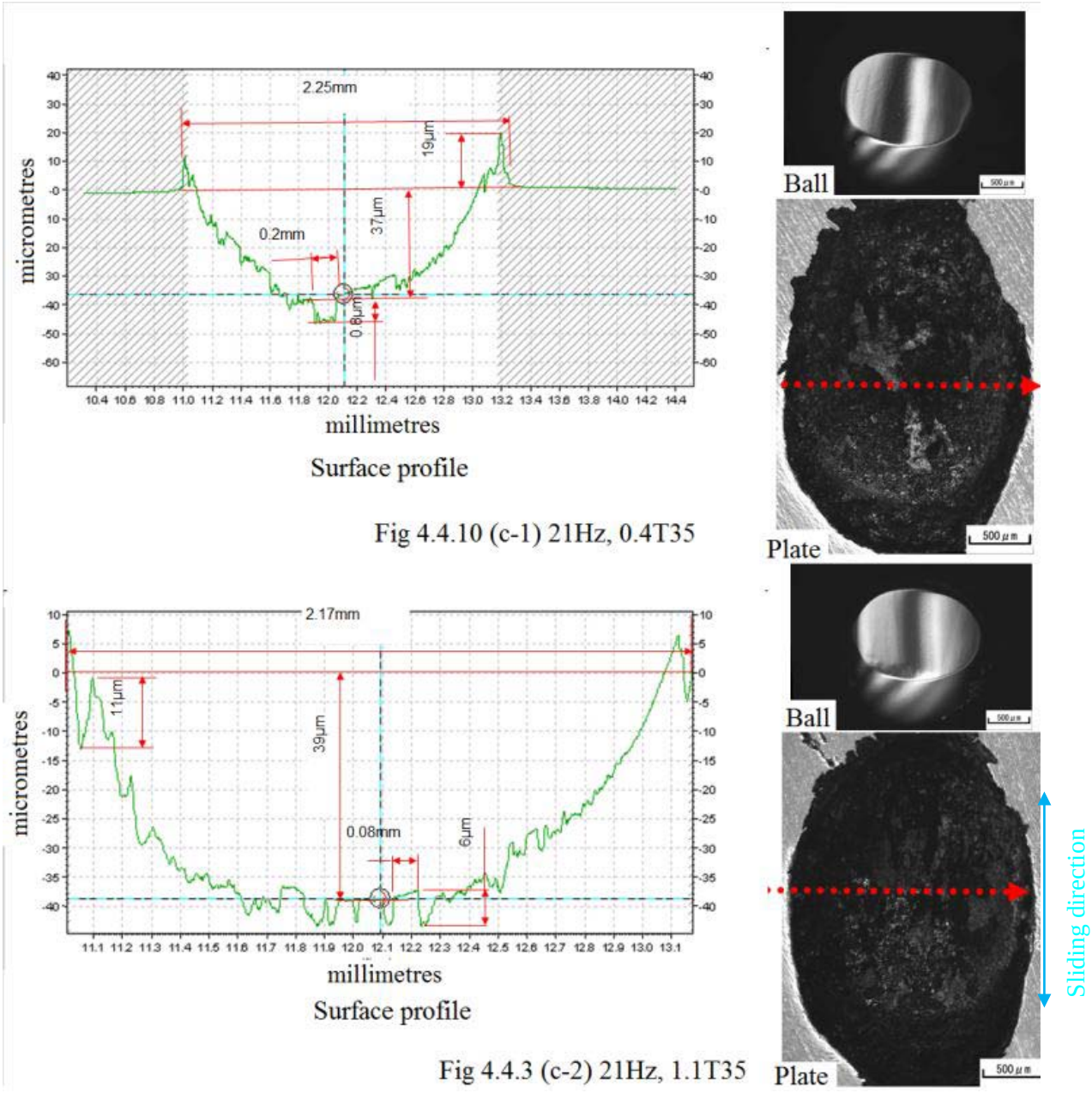

Fig 4.4.10 2-D surface profiling and optical microscope images of wear tracks supplied in 1,304x10^3 strokes

4.4.1.3.2 Observation of wear track appearance

SEM images of the wear track on plate specimens for different angles of magnetic field direction are shown in Figure 4.4.11, 4.4.12 and 4.4.13.

- Low frequency: Figure 4.4.11 shows SEM images of the wear track on plates for 1.1T0 and 1.1T35 at low frequency. 1.1T35 sample appears to have a rough surface which has dots in black region and is uneven. The dots in black region are wear debris of iron and silicon, as shown in Figure 4.4.7. In addition, the diameter of the dot is of the same size as that of the dot in a silver region, indicated in Figure 4.4.11 (c-1).
- Middle frequency: An outline of the wear track at 1.1T35 is of an ellipse shape, and the contact area appears as bumpy surface which has innumerable bulges. In addition, the black dots are scattered all over the surface, with prevailing diameter of 12 μm.
- High frequency: Features are aligned with the sliding direction with clear lines of the bulge, as shown in Figure 4.4.13 (a-2). The bulges mainly consist of iron. The main feature of the contact area at 1.1T35 is the scattered wear debris region, which consists of the iron and the silicon. It is a significant feature demonstrating the influence of the magnetic field on the contact area.

35°

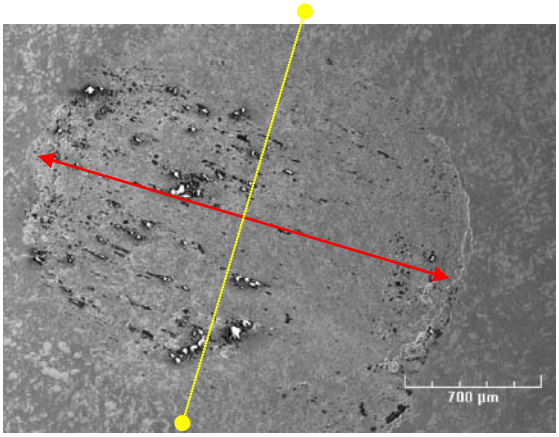

(a-1) 1.75Hz1.1T0, 40x modifications

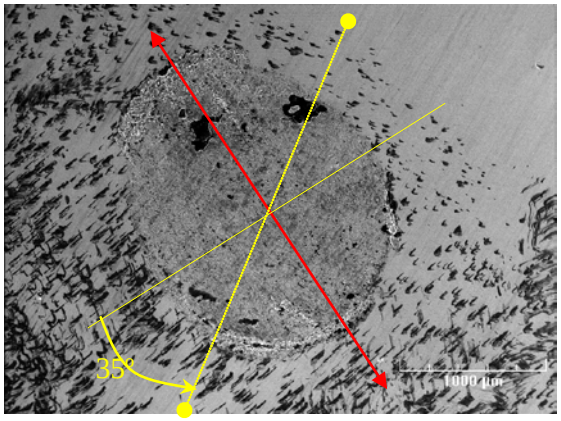

(a-2) 1.75Hz1.1T35, 30 x modifications

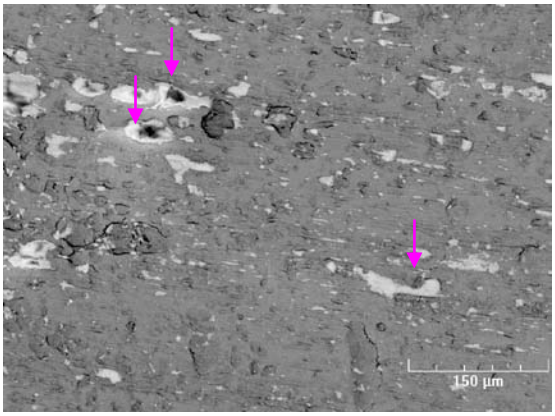

(b-1) 1.75Hz1.1T0, 200x modifications

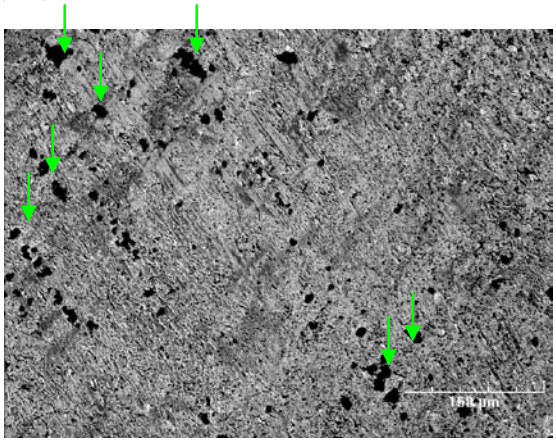

(b-2) 1.75Hz1.1T35, 200x modifications

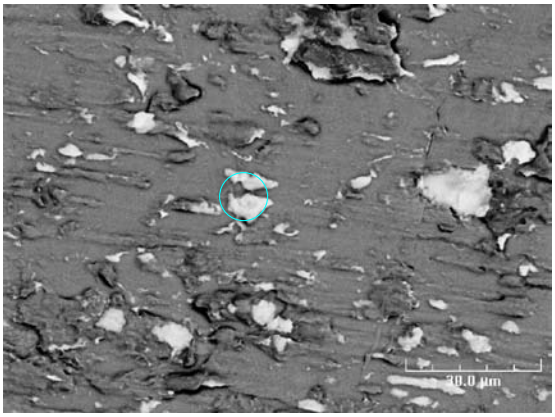

(c-1) 1.75Hz1.1T0, 1,000x modifications

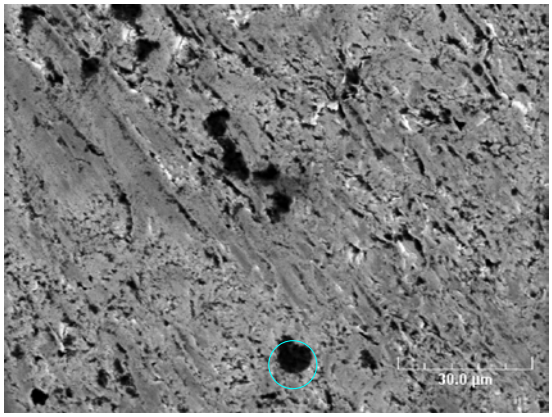

(c-2) 1.75Hz1.1T35, 1,000x modifications

↔: Sliding direction, ●—●: Direction with the permanent magnets
→: Black region (iron and silicon), →: Silver area (silicon and iron)

Fig 4.4.11 SEM images of plates for different angles of magnetic field direction with low frequency

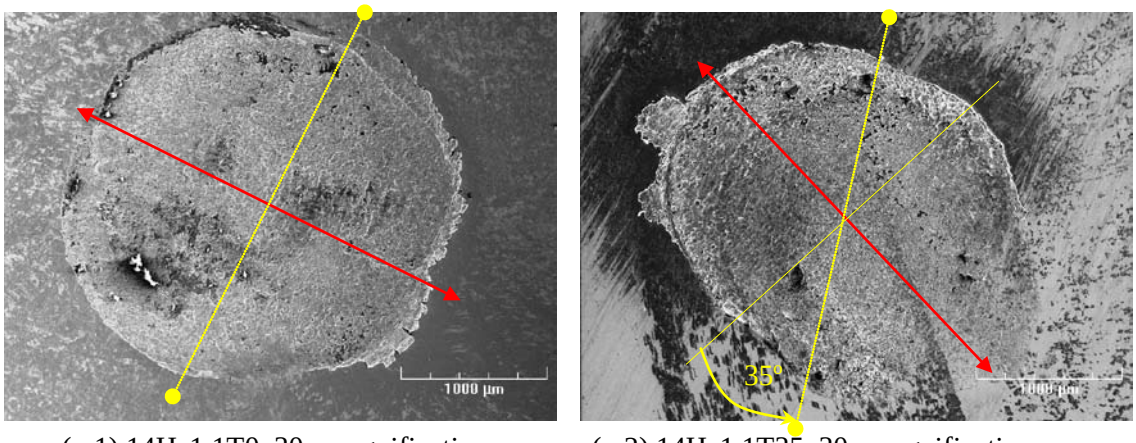

(a-1) 14Hz1.1T0, 30x magnifications (a-2) 14Hz1.1T35, 30x magnifications

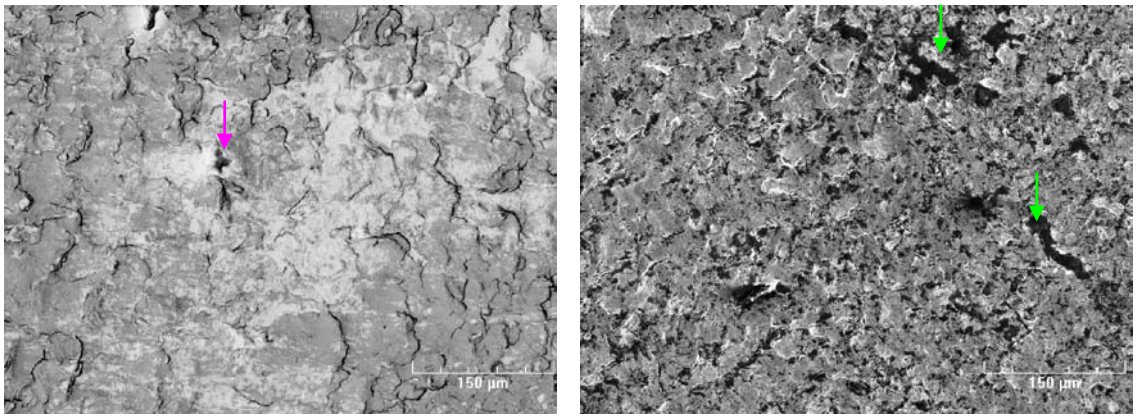

(b-1) 14Hz1.1T0, 200x magnifications (b-2) 14Hz1.1T35, 200x magnifications

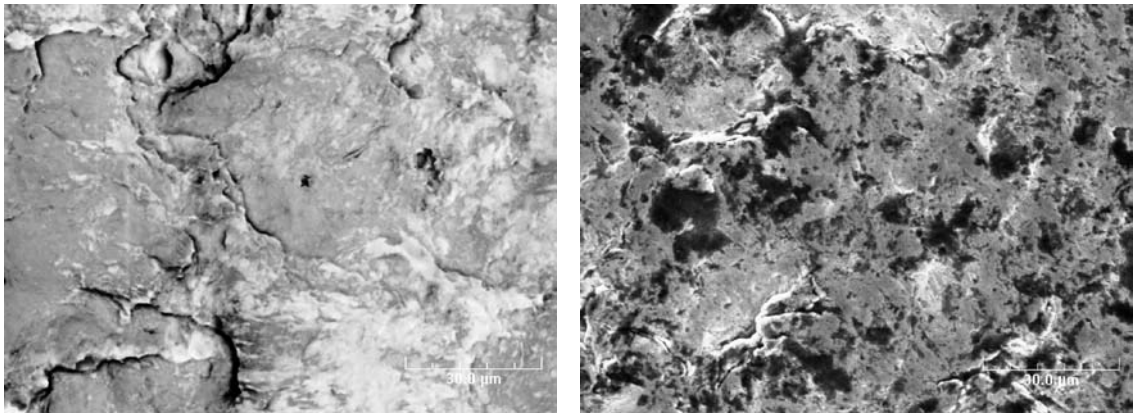

(c-1) 14Hz1.1T0, 1,000x magnifications (c-2) 14Hz1.1T35, 1,000x magnifications

↔: Sliding direction, ●–●: Direction with the permanent magnets
→: Black region (iron and silicon), →: Silver area (silicon and iron)

Fig 4.4.12 SEM images of a plate for different angles of magnetic field direction with middle frequency

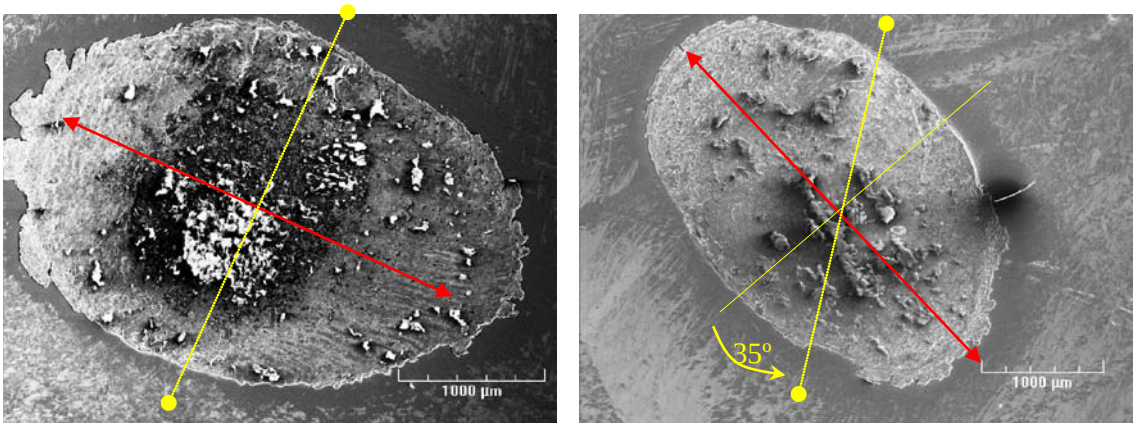

(a-1) 21Hz1.1T0, 30x magnifications (a-2) 21Hz1.1T35, 25x magnifications

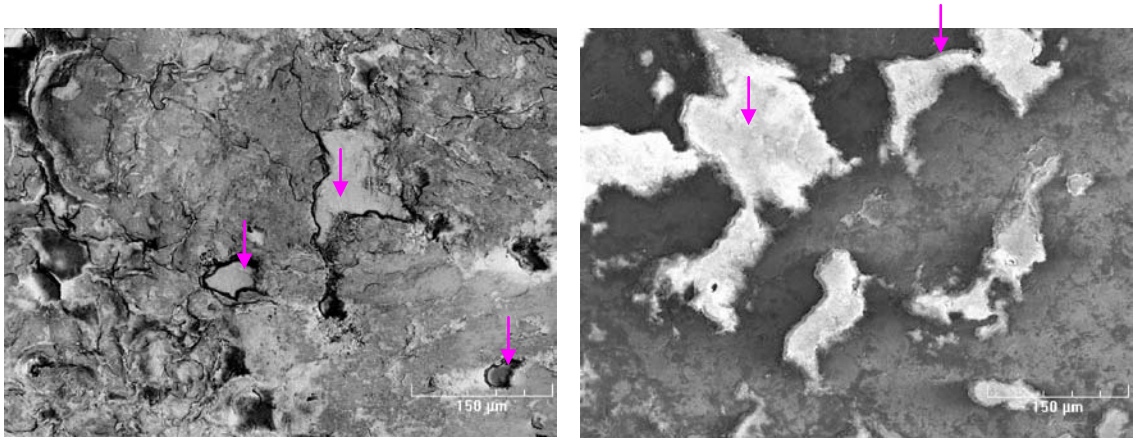

(b-1) 21Hz1.1T0, 200x magnifications (b-2) 21Hz1.1T35, 200x magnifications

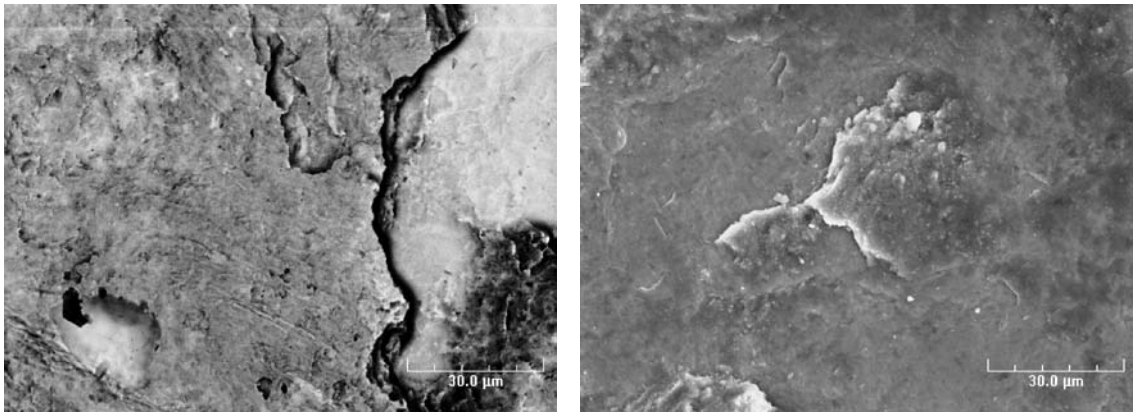

(c-1) 21Hz1.1T0, 1,000x magnifications (c-2) 21Hz1.1T35, 1,000x magnifications

↔: Sliding direction, ●—●: Direction with the permanent magnets
→: Silver area (silicon and iron)

Fig 4.4.13 SEM images of a plate for different angles of magnetic field direction with high frequency

4.4.1.3.3 Wear debris behaviour

Figure 4.4.14 shows wear debris arranged around wear track for different magnet flux densities. At low frequency, the common feature for 1.1T0 and 1.1T35, is the aggregation of wear debris. The feature for 1.1T35 is the brownish wear debris indicated by yellow circle in the figure. High frequency, however, produces wear debris spattered in all directions. The feature for 1.1T35 is dark brown wear debris in the wear track. Therefore, it could be said that the presence of the magnetic field is enhancing oxidation.

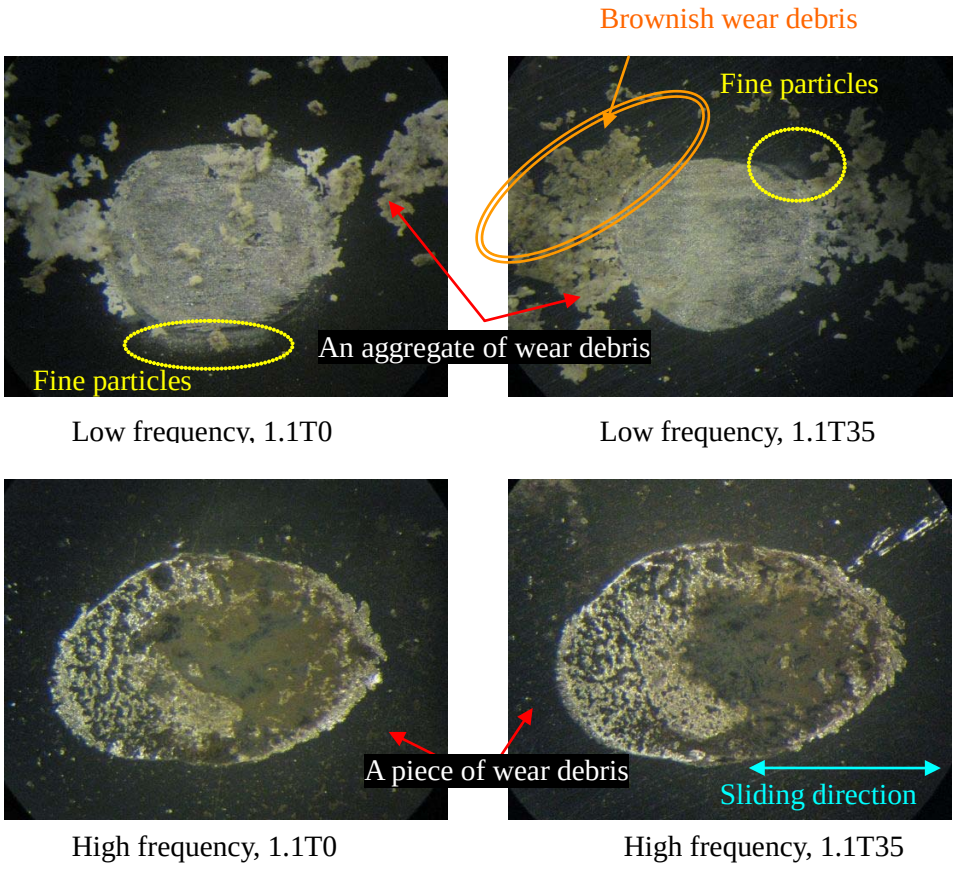

Fig 4.4.14 Aligned wear debris observation after 1,014x10^3 strokes

4.4.2 Ferromagnetic material vs. ferromagnetic material

4.4.2.1 Magnetic field density

The accumulated mass loss of test specimens

The accumulated mass loss of the plate for test conditions used follows a logarithmic curve (see Figures 4.4.15 and 4.4.16.).

- Low frequency: The accumulated mass loss for plates is a gradual increase until $801x10^3$ strokes. After that, the amount of loss weight in the presence of magnetic field maintains the gradual tendency. In addition, the amount of loss weight in the presence of magnetic field is about two-thirds of the accumulated mass loss for 0T0. Furthermore, accumulated mass loss at low magnet flux density changes very slightly approximately 1mg until $1,090x10^3$ strokes.
- High frequency: Accumulated mass loss at 0T0 is a steady increase and proportional to the number of sliding strokes. On the other hand, the tendencies in the presence of magnetic field are a slow upward curve and are approximately half the loss weight found in the absence of magnetic field.

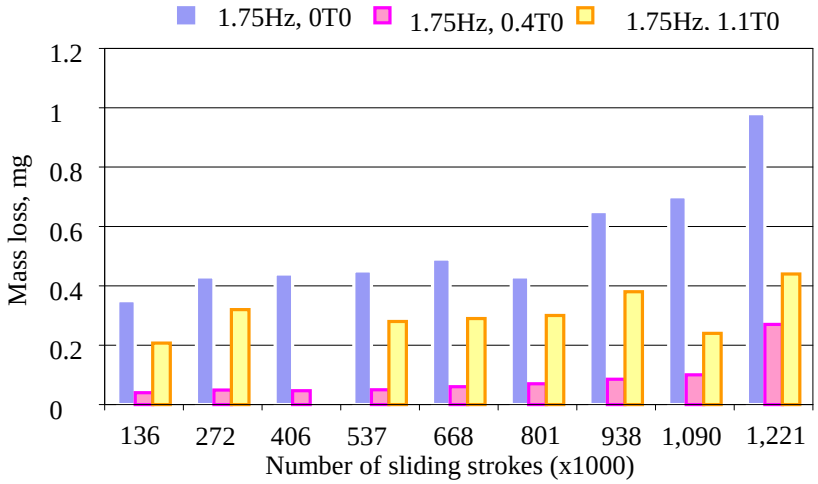

Fig 4.4.15 Accumulated mass loss of the plate in different magnet flux densities, low frequency

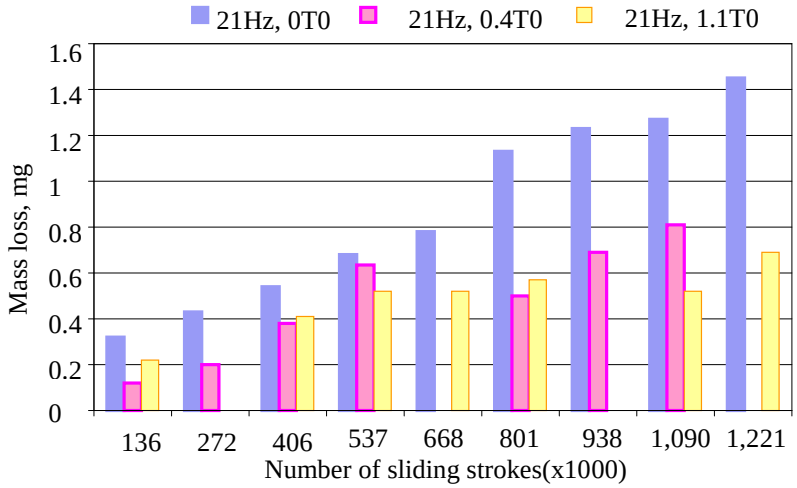

Fig 4.4.16 Accumulated mass loss of the plate in different magnet flux densities, high frequency

The accumulated mass loss of the ball for test conditions used also follows a logarithmic curve (see Figures 4.4.17 and 4.4.18.).

- Low frequency: The accumulated mass loss in the presence of magnetic field is less than half of that recorded for 0T0 and shows a slight increase.
- High frequency: The tendency of accumulated mass loss in the absence of magnetic field is a slight increase. However, the tendency in the presence of magnetic field is similar to that for low frequency.

Therefore, the presence of the magnetic field reduces the wear for the combination of ferromagnetic materials in sliding contact.

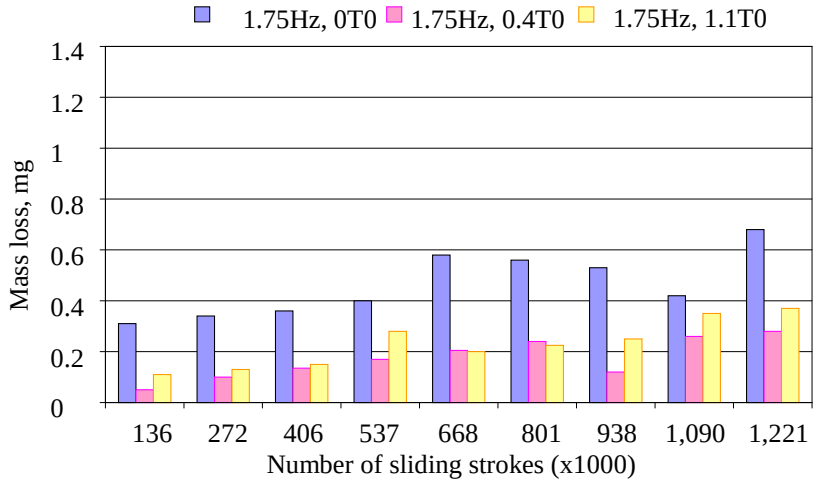

Fig 4.4.17 Accumulated mass loss of the ball in different magnet flux densities, low frequency

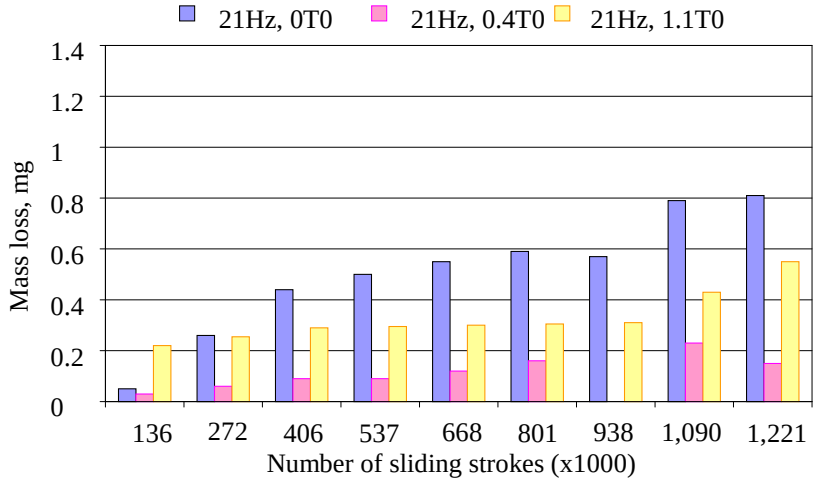

Fig 4.4.18Accumulated mass loss of the ball in different magnet flux densities, high frequency

4.4.2.2 Surface roughness in the wear track of the plate

Figure 4.4.19 illustrates surface roughness in the wear track of the plate for different magnet flux densities. Besides, Table 4.4.3 contains the principal numerical data for that figure. The fluctuation range of some *Ra* values is above 0.5 μm until $406x10^3$ strokes. However, fluctuation ranges are reduced to approximately 0.2 μm. *Ra* after that and show an overall trend toward stabilization. The influence of magnet flux densities on wear track roughness at low and high frequencies can be summarised as follows:

- Low frequency: Average *Ra* at 0.4T0 is 0.5 μm (low magnet flux densities) and approximately 0.3 μm in the absence of magnetic field. In addition, average *Ra* at 1.1T0 (high magnet flux density) is lower than that at low magnet flux density and is approximately 0.4 μm.
- High frequency: In the presence of magnetic field, the *Ra* values undergo wide fluctuations in contrast with the absence of magnetic field. However, the average *Ra* does not change.

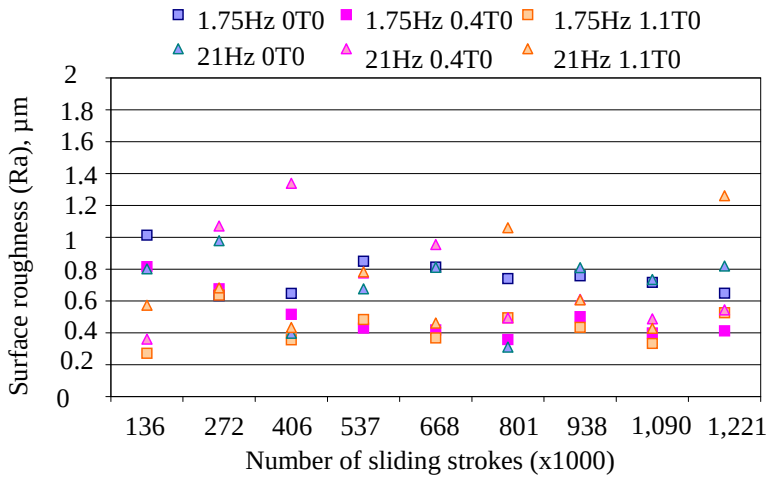

Fig 4.4.19 Surface roughness on the plate in different magnet flux densities

Table 4.4.3 *Ra* values on the wear surface of plates

	1.75Hz			21Hz		
	0T0	0.4T0	1.1T0	0T0	0.4T0	1.1T0
Average Ra, µm	0.76	0.50	0.43	0.70	0.74	0.70
Max, µm	1.01	0.82	0.64	0.98	1.34	1.26
Min, µm	0.63	0.36	0.27	0.31	0.36	0.43

4.4.2.3 Topography on the surface of test specimens

2-D surface profile of the plate specimen and optical micro photos of wear surface on test specimens are shown in Figure 4.4.20.

- Low frequency: The common features are the jagged surfaces in wear track of the plate. In the presence of the magnetic field, the wear track is shallow and narrow. In addition, it has slender bulges and narrow grooves. Besides, the contour of the contact area for the ball is an ellipse elongated in the sliding direction.
- High frequency: The wear track in the presence of the magnetic field is shallow and narrow. In addition, it is rather smooth as shown in the surface profile, compared with the wear track at the absence of magnetic field.

Therefore, it could be said that the magnetic field reduces the depth and width of the wear track.

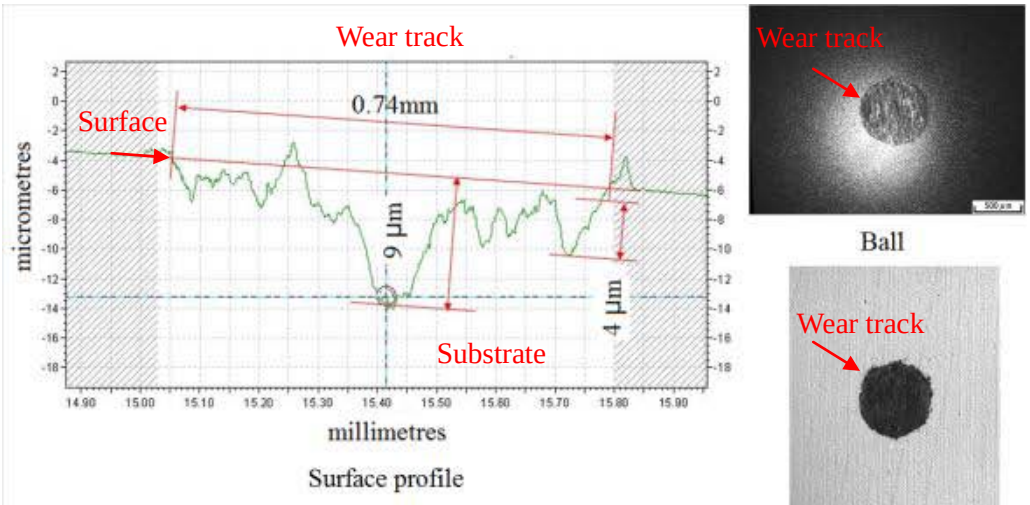

Fig 4.4.20 (a-1) 1.75Hz, 0T0

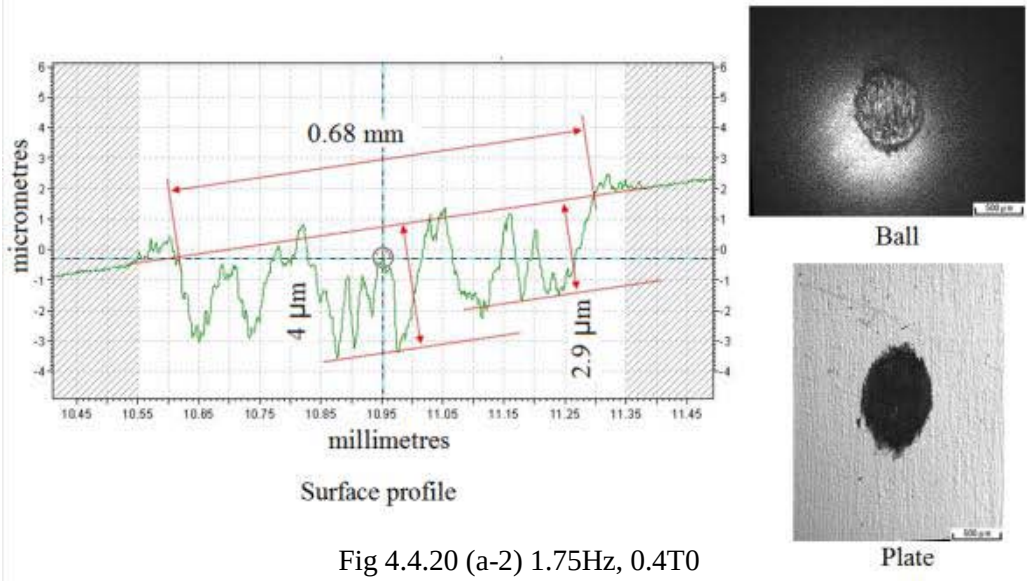

Fig 4.4.20 (a-2) 1.75Hz, 0.4T0

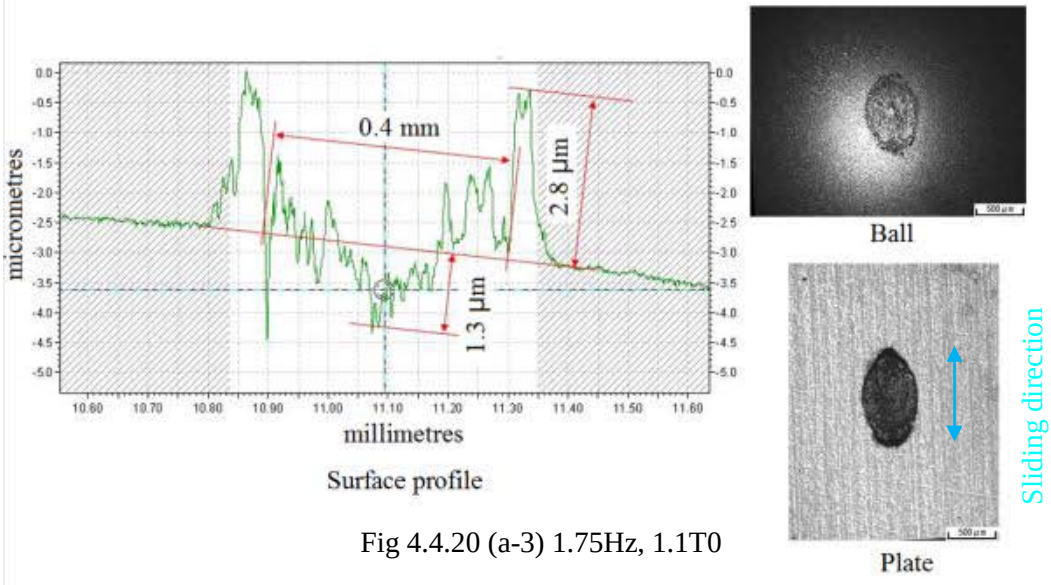

Fig 4.4.20 (a-3) 1.75Hz, 1.1T0

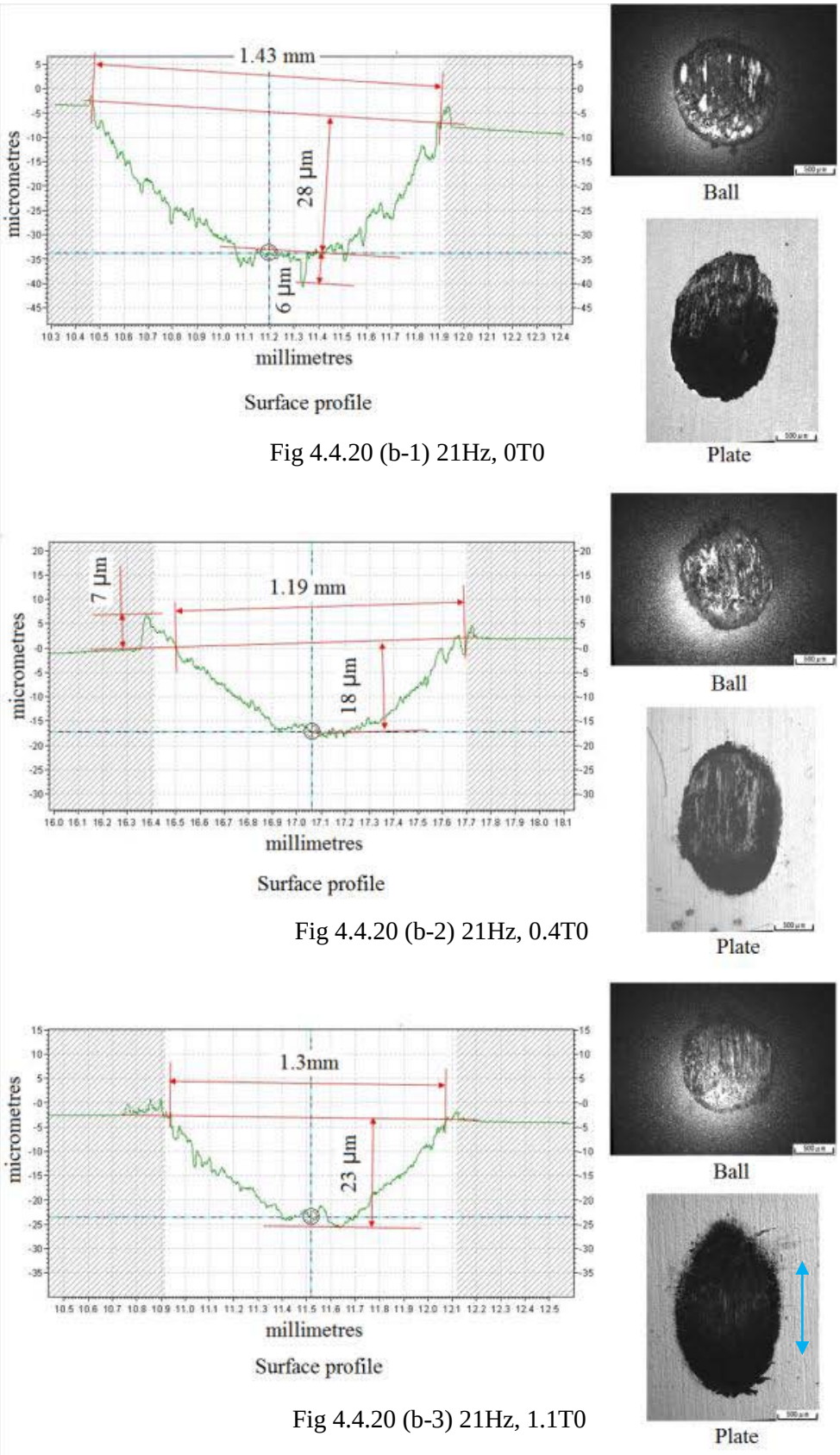

Fig 4.4.20 2-D surface profile on the surface of a plate, surface observation of the wear track on the plate and a ball after $136x10^3$ strokes

4.4.2.4 Wear debris behaviour and the observation

The expanse of the wear debris around the outline of the contact area is shown in Figure 4.4.21.

Low frequency: Wear debris are light brown and form the aggregate surround the outline of contact area.

High frequency: In contrast with that at low frequency, wear debris are dark brown and in the form of single particles.

Common points of low and high frequencies are as follow: wear debris are arranged over a wide area. However, in the presence of magnetic field, they are gathered and bundled around the contour of contact area. In addition, brown wear debris on the contact area can be seen.

Figure 4.4.22 shows the backscatter electron images for wear debris at 0T0 and 0.4T0. White region represents mainly iron, and gray region contains iron and oxygen; it is oxidised iron.

- Low frequency: Large particles are approximately 4 μm in diameter and were observed for both with and without magnetic field. The particles which the figure (b) shows are mainly particles of the iron.
- High frequency: In the absence of the magnetic field, wear debris consist of large particles of approximately 20 μm in diameter and small particles of approximately 1 μm in diameter. On the other hand, main wear debris in the presence of the magnetic field are uniformly approximately 2 mm in diameter.

Therefore, it could be said that magnetic field affects the size of wear particles.

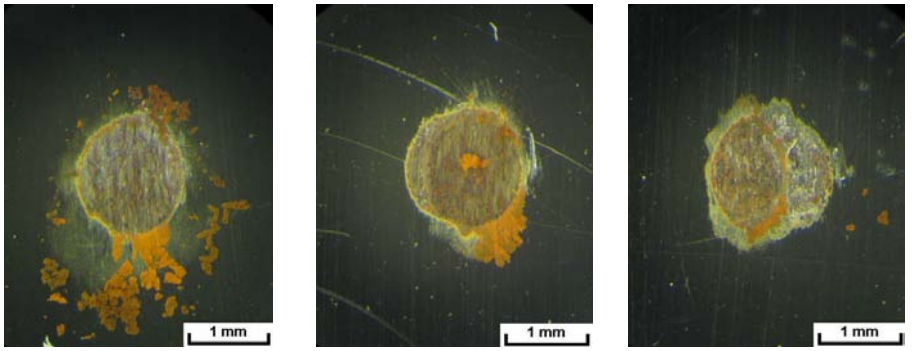

(a-1) 1.75Hz 0T0 (a-2) 1.75Hz 0.4T0 (a-3) 1.75Hz 1.1T0

(b-1) 21Hz 0T0 (b-2) 21Hz 0.4T0 (b-3) 21Hz 1.1T0

Fig 4.4.21 Aligned wear debris around wear track on the plate

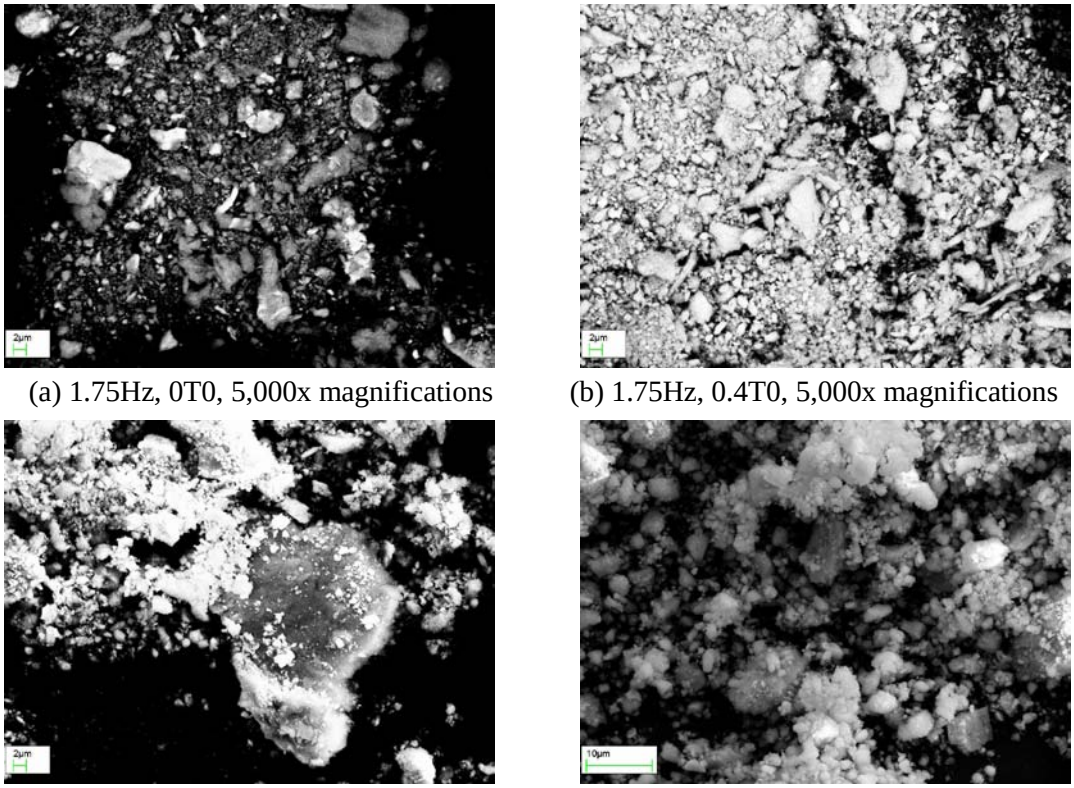

(a) 1.75Hz, 0T0, 5,000x magnifications (b) 1.75Hz, 0.4T0, 5,000x magnifications

(c) 21Hz, 0T0, 5,000x magnifications (d) 21Hz, 0.4T0, 5,000x magnifications

Fig 4.4.22 Back scatter electron images of wear debris

4.4.2.5 SEM observation and analysis of the wear track

Figures 4.4.23 and 4.4.24 show backscatter images of the surface of plate samples.

SEM images for a wear track are shown in a pattern made by black and white regions for horizontal with the sliding direction.

- Low frequency: The wear track at 0T0 is in a stripe pattern. Comparing 0.4T0 with the wear track at 0T0 it is seen that it is occupied main by black regions, and the white regions are rather thin. Furthermore, the wear track at 1.1T0 is occupied by the large black region.
- High frequency: The wear track at 0.4T0 is occupied by a black area with white patchy patterns.

Figure 4.4.25 illustrates the backscatter electron image and SEM analysis at locations where is indicated crosses by marks in figure (a). The gray region consists of iron and the black region contains iron and oxygen.

Therefore, the magnetic field covers the contact area of the plate with oxidised iron.

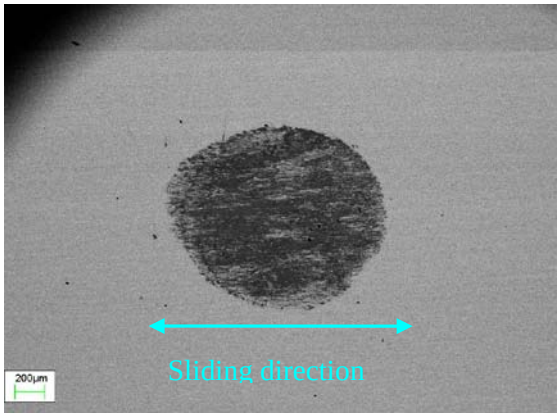

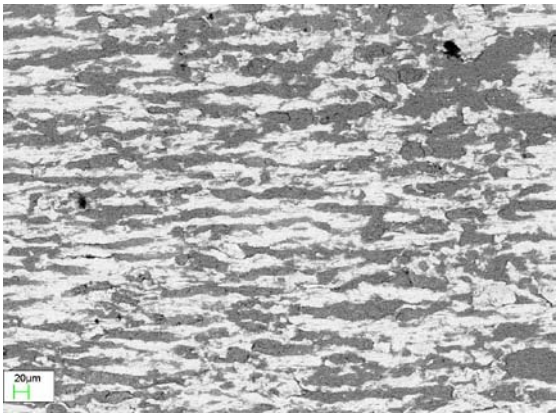

(a-1) 102x magnifications (a-2) 500x magnifications

(a) 1.75Hz 0T0

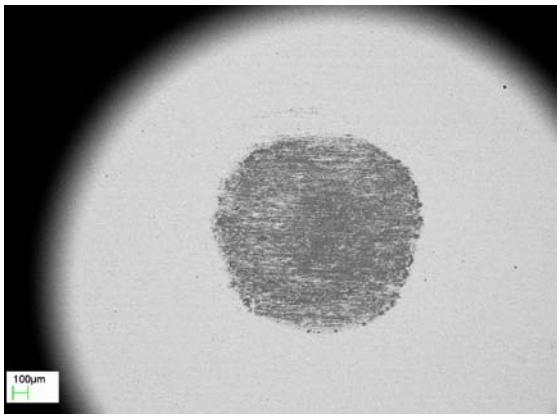

(b-1) 102x magnifications (b-2) 500x magnifications

(b) 1.75Hz 0.4T0

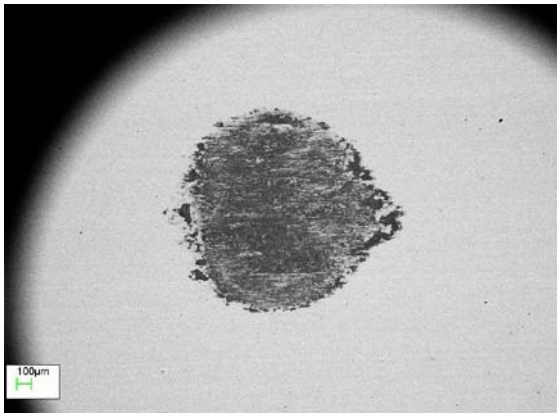

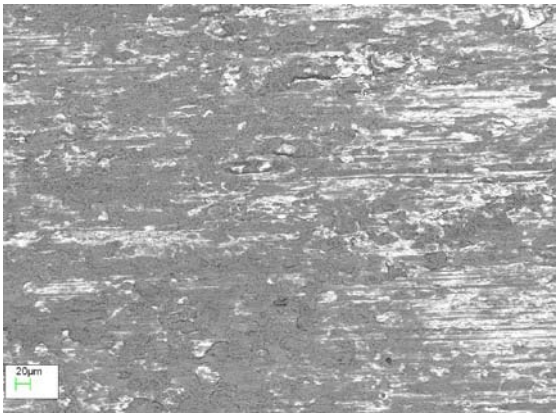

(c-1) 102x magnifications (c-2) 500x magnifications

(c) 1.75Hz 1.1T0

Fig.4.4.23 Backscatter images on the surface of plate samples, low frequency

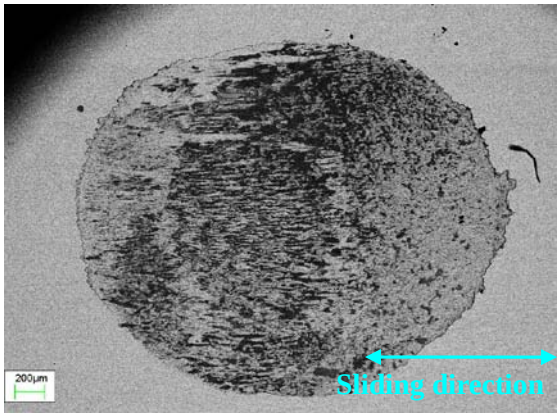

(a-1) 102x magnifications

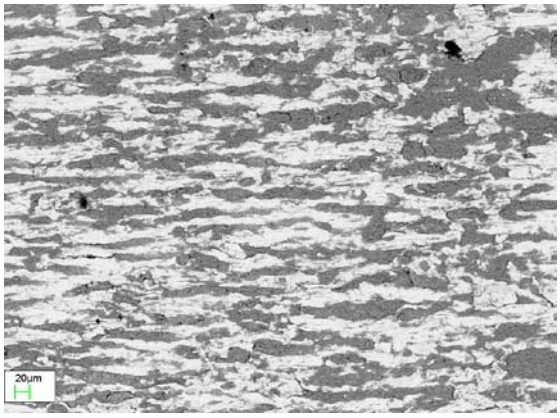

(a-2) 500x magnifications

(a) 21Hz 0T0

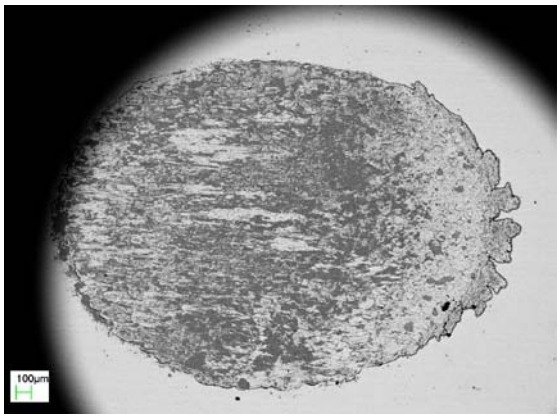

(b-1) 102x magnifications

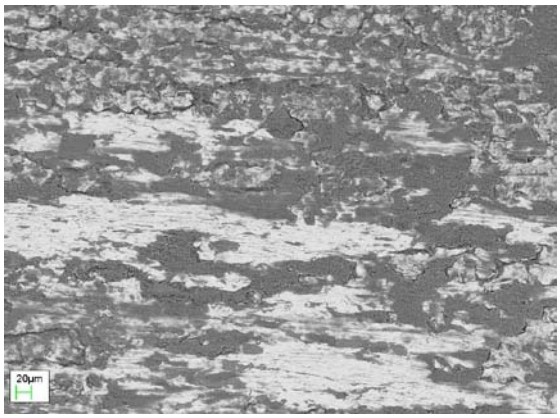

(b-2) 500x magnifications

(b) 21Hz 0.4T0

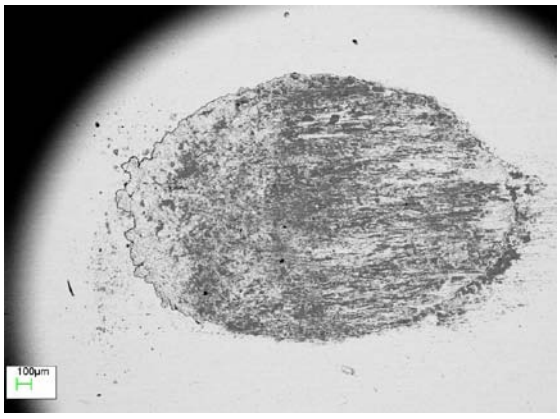

(c-1) 102x magnifications

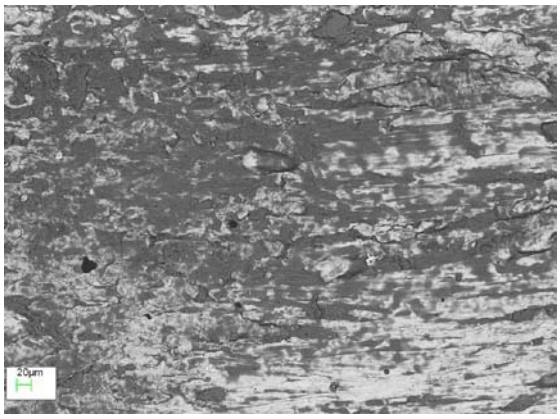

(c-2) 500x magnifications

(c) 21Hz 1.1T0

Fig.4.4.24 Backscatter images on the surface of plate samples, high frequency

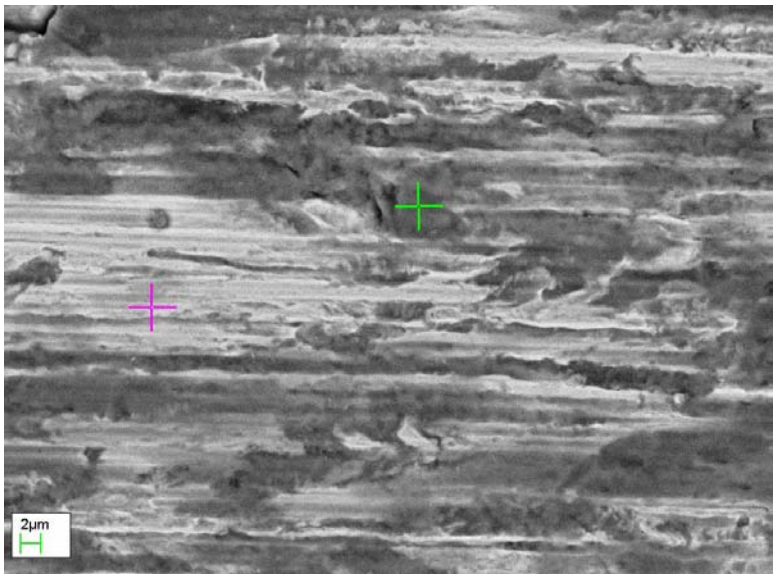

(a) 1.75Hz 0.4T0 5,000x magnifications

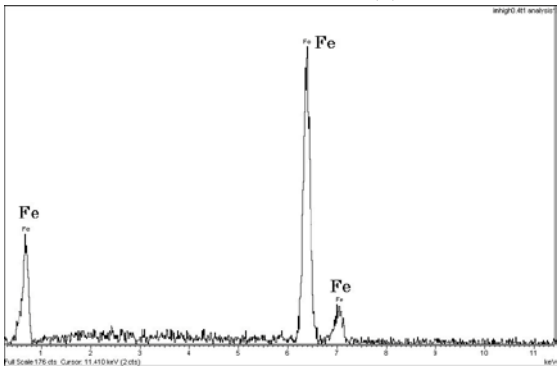

(b) Gray region (+)

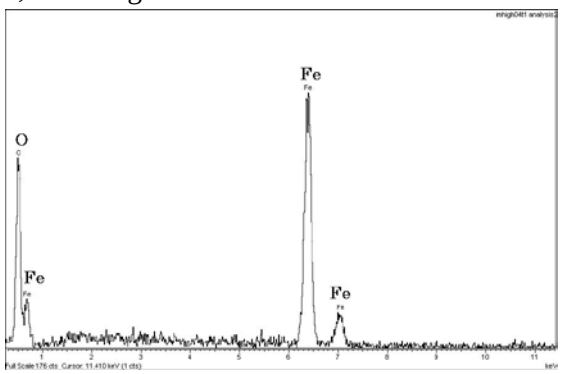

(c) Black region (+)

Fig 4.4.25 Backscatter electron image and SEM analysis where is indicated by marks into the figure (a)

References for chapter 4

Edrisy, A., et al. (2001) “Wear of thermal spray deposited low carbon steel coatings on aluminium alloys”, *wear* vol. 251, pp.1023-1033.

Hiratsuka, K., Sasada, T. and Norose, S. (1986) “THE MAGNETIC EFFECT ON THE WEAR OF METALS”, Wear, 110, pp. 251-261.

Mineralogical Society of America (2001-2005). *Iron pdf*, , [online] available at: http:www.handbookofmineralogy.org/ [Accessed 03/12/2008]

Mineralogical Society of America (2001-2005). *Kamacite pdf*, , [online] available at: http:www.handbookofmineralogy.org/ [Accessed 03/12/2008]

Mineralogical Society of America (2001-2005) *Maghemite pdf*, , [online] available at: http:www.handbookofmineralogy.org/ [Accessed 03/12/2008]

Mineralogical Society of America (2001-2005). *Magnetite pdf*, [online] available at: http:www.handbookofmineralogy.org/ [Accessed 03/12/2008]

Mineralogical Society of America (2001-2005).*Taenite pdf*, [online] available at: http:www.handbookofmineralogy.org/ [Accessed 03/12/2008]

Mineralogical Society of America (2001-2005). *Wüstite pdf*, , [online] available at: http:www.handbookofmineralogy.org/ [Accessed 03/12/2008]

Chapter 5 Discussions

5.1 Introduction

This chapter consists of five sections.

At the beginning, comparison with previous research is made to find out why the wear increased in the presence of the magnetic field. Model for a crack initiation under the surface in the magnetic field proposed by Iida (2007) is outlined. Also, wear mechanism for a combination of mild steel plate and Si_3N_4 ball is assessed. Next, an attempt is made to clarify the wear mechanism of the thermal spray coating in the presence of the magnetic field. Then, the mechanism for a wear decrease of plate specimen in the presence of the magnetic field and a lubricant is discussed. After that, the wear mechanism in the presence of the magnetic field and high frequency is presented using contact area images and analyses.

Before focusing on the main subjects of discussion, comparison of the experimental results obtained for each experimental condition used in the form of wear amount and *Ra* values is made, with the aim to identify related tendencies in experimental results.

Compared with the wear of the plate specimen in the absence of magnetic field, the presence of horizontal magnetic field does not affect the wear of a mild steel plate and the austenite stainless steel coating under the dry sliding contact at low frequency (see Figure 4.2.1 and Figure 4.2.22). However, it decreases the amount of wear of the carbon steel coating (see Figure 4.2.15). In addition, lubricated sliding wear also decreases the wear of the plate (see Figure 4.3.1).

The *Ra* value of the contact area is rather high or displays an increasing trend for Ferro

material under dry sliding contact at low frequency (see Figure 4.2.17). On the other hand, the *Ra* value of the contact area on a paramagnetic material of austenite stainless steel coating shows a slight increase (see Figure 4.2.24). Furthermore, the high frequency combined with the presence of magnetic field decreases *Ra* values for the combination of Si_3N_4 ball and mild steel plate (see Figure 4.4.1(c)).

For the 90 degree orientation of the magnetic field wear amount of the plate specimen increases (see Figure 4.2.1). Similarly, 35 degree orientation of the magnetic field combined with high frequency shows an increase in wear (see Figure 4.4.10(c)). However, the former orientation of magnetic field increases *Ra* value, in contrast, to that caused by the latter (see Figure 4.2.23 and Figure 4.4.9).

Therefore, it can be said that the influence of magnetic field changes in the mass loss and the surface roughness of a plate specimen on sliding contact. In addition, it is inferred from the conclusion that the control of the tribological properties is possible by magnetic flux density of magnets, the magnetic field orientation and a level of sliding speed.

Table 5.1.1 shows tendencies, in wear amount and surface roughness Ra. The presence of horizontal magnetic field is compared to the conditions without magnetic field. In addition, Table 5.1.2 also shows tendencies, caused by the effect of magnetic field orientation to the sliding direction.

Table 5.1.1 Tendencies of wear amount and surface roughness *Ra*, the presence of horizontal magnetic field is compared to the absence of the magnetic field

	Combination	Magnet flux density, 1.1T	
		Wear amount	Ra
Dry sliding contact, low frequency	Si_3N_4 ball and mild steel plate (Uncoating)	No change	High
	Si_3N_4 ball and carbon steel coating	Decrease	Increasing trend
	Si_3N_4 ball and austenite stainless steel coating	No change	Increase
Lubricated sliding contact, low frequency	Si_3N_4 ball and mild steel plate	Decrease	No change
Dry sliding wear, high frequency	Si_3N_4 ball and mild steel plate	---	Decrease
	Ball bearing Steel 100Cr6 and mild steel plate	Decrease	No change

Table 5.1.2 Tendencies of wear amount and surface roughness *Ra*, the effect of magnetic field direction as against zero degree orientation of magnetic field

Dry sliding contact	Combination	Magnetic field direction	Wear amount	Ra
Low frequency	Si_3N_4 ball and mild steel plate	45 º	No change	Increase
		90 º	Increase	Increase
High frequency	Si_3N_4 ball and mild steel plate	35 º	Increase	Decrease

5.2 Comparison of Magnetic field effects on sliding and rolling contacts

5.2.1 Effects of horizontal magnetic field on rolling contacts

The model of the crack initiation under the surface in the magnetic field suggested by Iida (2007) was verified by using two-disc rolling contact wear tests, as shown in Figure 5.2.1. Pure rolling is the contact between two parallel discs. Rolling with sliding contact was carried out at 0 degree and a twist angle of 57.1 degrees as shown in Figure 5.2.1(a).

The experimental results showed that the rolling contact under experimental conditions used creates initial cracks emanating from the subsurface. Moreover, the presence of horizontal magnetic field produces finer and thinner particles, as showed in Figure 5.2.2 (b), and reduces the surface roughness of the wear surface. In addition, the association between the crack initiation points and the thickness of wear particles is found and the number of cycles required to detach one layer can be calculated by evaluating the number of cycles required to detach one layer (Iida 2007). He provides the specific example that the influence of magnetic field created the crack initiation points to a quarter depths in case of no magnetic field. Finally, it is concluded that the influence of magnetic field on rolling contacts consists of initiation of cracks at the shallow point and to detachment of wear particles after a small number of load cycles.

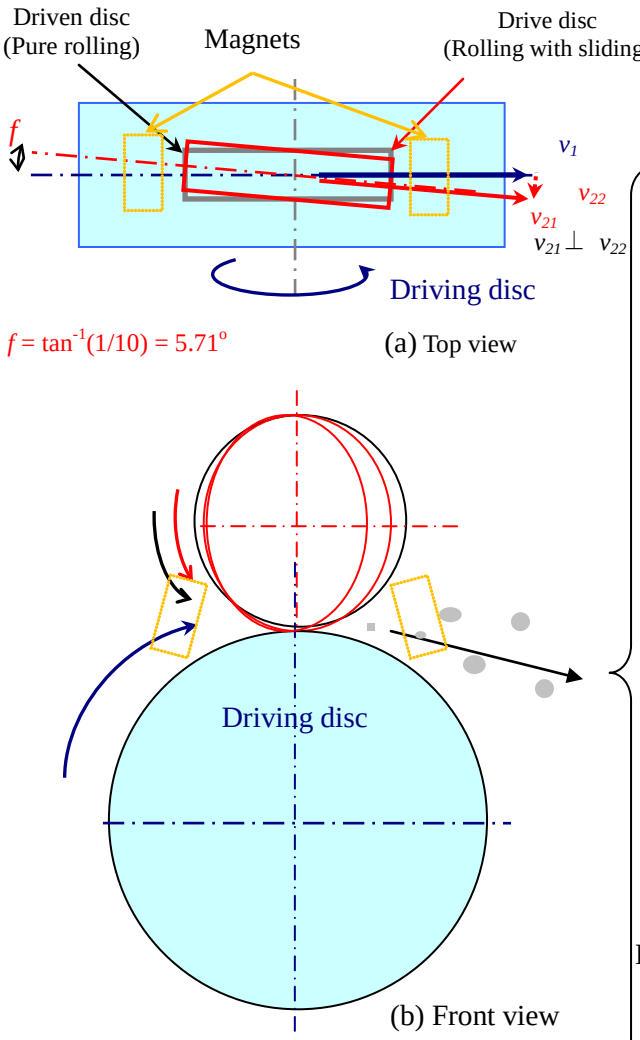

Fig 5.2.1 Illustration of pure rolling and rolling with sliding

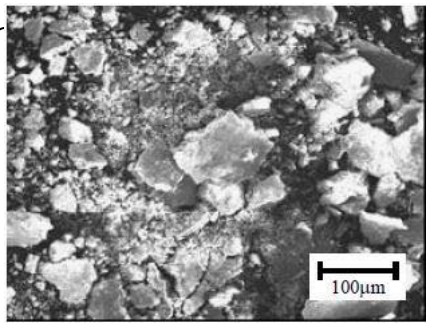

(a) Wear particles, 0 T

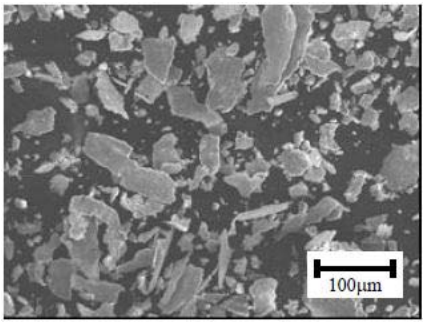

(b) Wear particles, 0.4T

Fig 5.2.2 Wear particle observation of mild steel discs (Pure rolling)(Iida 2007)

5.2.2 Comparison of magnetic field effects for sliding and rolling contacts

Reciprocating sliding contacts under the dry condition are characterised by different wear mechanism comparing to that for rolling contacts. It creates the flat wear debris or the hemispherical wear debris. The sliding contacts are with different initiation crack points to that of rolling contacts. Therefore, the influence of magnetic field cannot be evaluated using the thickness of wear debris and the same equation used for the rolling

contact. In addition, Hertzian contact pressure reduces rapidly in inverse proportion to the number of sliding strokes because the area of contact grows due to wear (see Figure 5.2.3).

The sliding contacts in the presence of magnetic field also have different wear mechanism comparing to the rolling contact, and the influences of the magnetic field on the sliding contact can be summarised as follows:

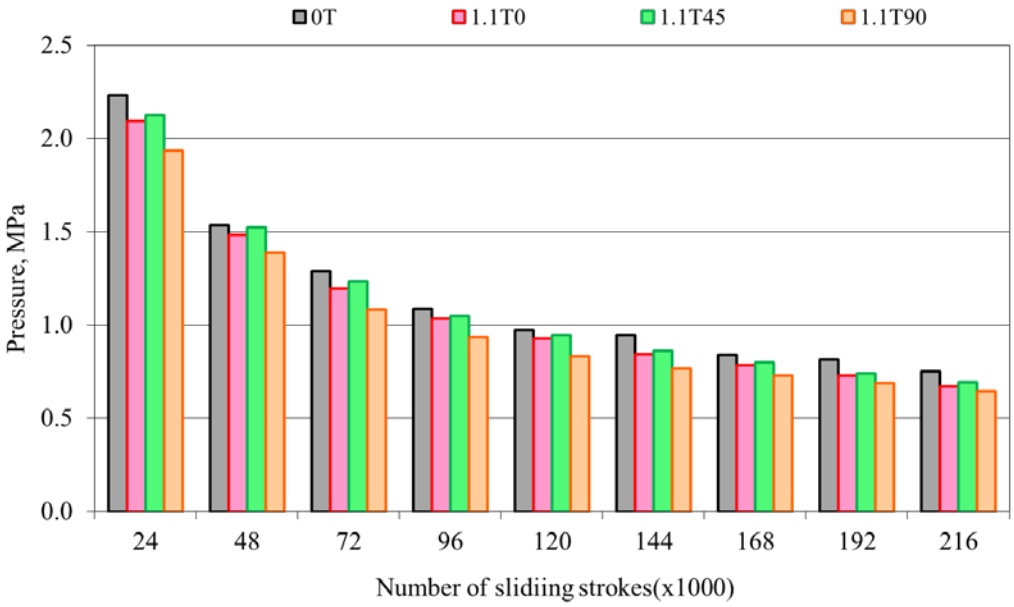

Fig 5.2.3 Predicted tangential traction, calculation from the contact area of a ball

- Magnetic field arranged at 90º, increases the mass loss of the plate after $48x10^3$ strokes and that is the contrary to the results obtained for pure rolling contacts.
- Delamination area is created on the wear track from the beginning of sliding strokes, and the surface roughness is increased substantially.
- Wear debris are produced and consist of the flat iron particles and the agglomerated particles including iron, oxygen and silicon. Moreover, magnetic field affects the enhanced oxidation of iron wear fine particles.

It is concluded that the magnetic field influences on the sliding contact are different to that observed for the rolling contacts.

Additional, influences of magnetic field on sliding contact characteristic are;

- An initial bulging is produced on the wear surface of the plate and it is on both sides of wear track. Its width corresponds to the contact area dimensions.

Horizontal magnetic field does not significantly affect mechanical properties of the mild steel test plate.

5.2.3 Effect of magnetic field on uncoated plate wear

The sliding contact test was carried out at the low frequency that does not cause an excessive oxidation of the wear surface of mild steel. Thus, the sliding contact test in the presence of magnetic field was assumed not to cause the oxygen adsorption. The presence of magnetic field promotes oxidation of the surface of the magnetised material because it attracts the oxygen and raises oxygen density around the material (Kumagai 1993; Sasada et al 1993). However, the experimental conditions caused brown spots distribution on the surface of wear track, even in the absence of magnetic field. As indicated in Figure 5.2.4, the brown spots distribution reduces and disappears before $96x10^3$ strokes, however in the presence of magnetic field brown spots exist after $96x10^3$ strokes. Furthermore, it reduces the surface area of the brown spots distribution and diffuses the whole surface area. Thus, it could be concluded that these experimental conditions induce the oxidation in the absence of magnetic field.

Turning now to the magnetic field effect on uncoated plate wear, first, the factors controlling mass loss of the plate specimen in presence of magnetic field are discussed. In surface observations just after sliding contact tests, the effect of the external magnetic field is discovered because the magnetic attractive force of the permanent magnets removes the iron wear particles from the wear surface of the plate specimen. In particular, 90º condition moves almost an iron wear particles from the area because the bottom plane of the permanent magnets faces the wear surface and the distance is close compared with other magnetic field directions. The wear mechanism is severe wear; without severe-mild wear transition (Hirazuka and Sasada 1986). Therefore, the real contact area is enlarged, and, the mass loss and the surface roughness are both increased. On the other hand, the other magnetic field directions did not remove iron wear particles

from the wear track in common with the absence of the magnetic field. The influence of magnetic field is estimated to produce the hemisphere iron particles and the agglomerated particles. Also it causes the transfer of wear particles to the surface of magnetised plate. Thus, it is estimated that the surface roughness of the test plate is increased more than in the absence of magnetic field. However, the mass loss continues to be almost as for the absence of magnetic field. The reason for that is the magnetic field enhances the adsorption of oxygen to the iron wear particle, and they temporarily protect the surface of the plate from wear.

Therefore, it can be assumed that the main factors of the influence of magnetic field are the removal effect of iron wear particles and enhancement of adsorption of oxygen to the sliding contact.

Next, the discussion is focused on the following main factors.

- In the enhancement of the adsorption of oxygen to the iron wear particles, they may be piled up on the wear track as described in next section 5.2.4.
- In the removal effect of the wear debris from the wear track, the different magnetic field directions affect discharge quantity of wear debris because the distance of the permanents and the wear surface is different as described in Section 5.2.5.

In conclusion, it can be said that the effect of magnetic field weakens the prevailing wear mechanism.

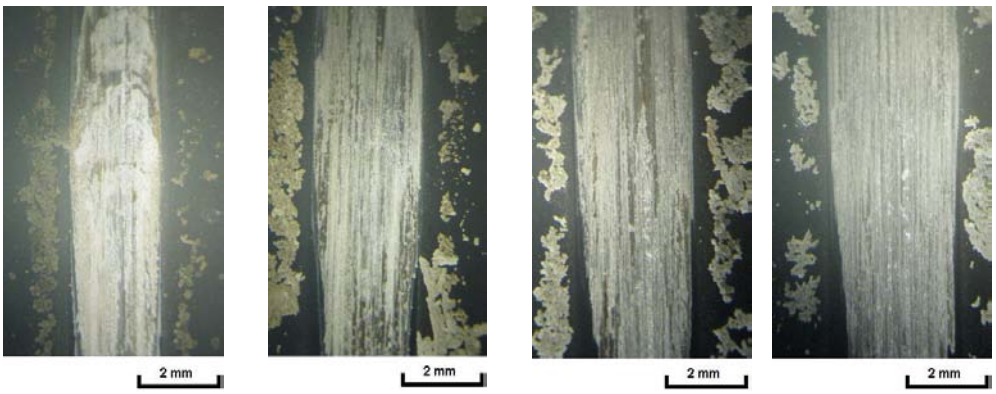

24 strokes 48 strokes 72 strokes 96 strokes

(a) 0T0, the absence of magnetic field

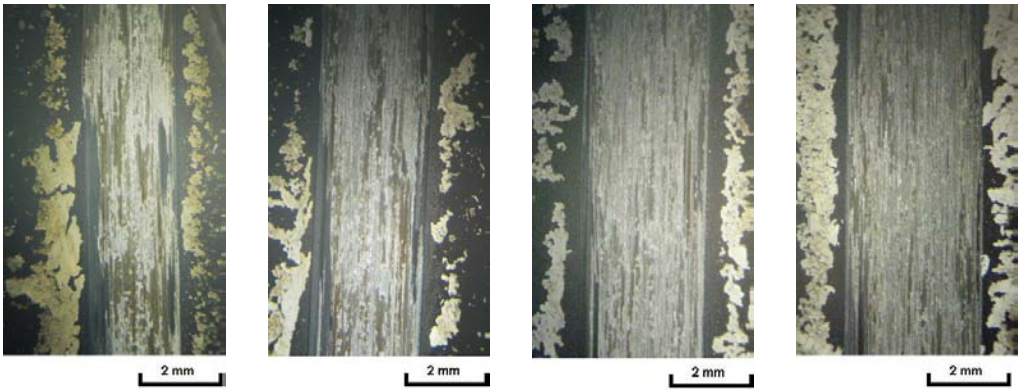

24 strokes 48 strokes 72 strokes 96 strokes

(b) 1.1T0, the presence of magnetic field

Fig 5.2.4 Brown spots distribution on the wear track

5.2.4 Bulge formation on wear surface in the presence of magnetic field

It is suggested that the bulging on wear surface is formed in the presence of magnetic field. Furthermore, the height of the bulging is approximately 4 μm, and that height is kept and is moved gradually to both sides of wear track. However, there is still room for explanation about the important mechanism responsible for the formation of the bulging. There are brown regions and gray regions in the wear track by surface as shown in Figure 5.2.5. The existence of the two regions in the wear track could be used to formulate a hypothesis, as follows; if the brown region consists of oxidized iron particles, then it can be assumed that the transfer of them on the wear surface took place.

Hypothesis concerning accumulated oxidised iron particles

The height of bulging is approximately 4μm and it has a brown colour, so it is attributed that accumulation of fine oxidised iron particles occurred. Furthermore, the accumulation of debris on the wear track reported stated by Mansori and Paulmier (1999). They point out that perpendicular magnetic field induces the transfer of wear particles, which are produced by abrasive action, to a location of wear track. Besides, Sato et al. also (2000) found that the effect of the magnetic field enhances adsorption of oxygen onto the surface of the ferromagnetic wear particles and increases the trapping of oxidised fine particles on the wear surface.

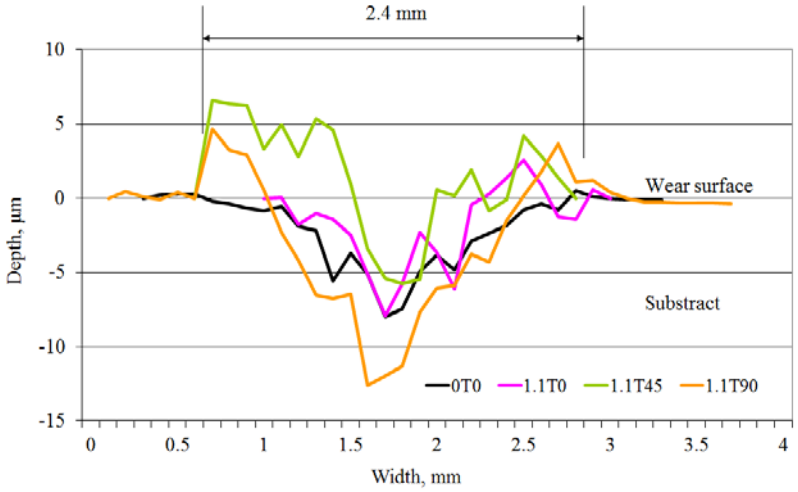

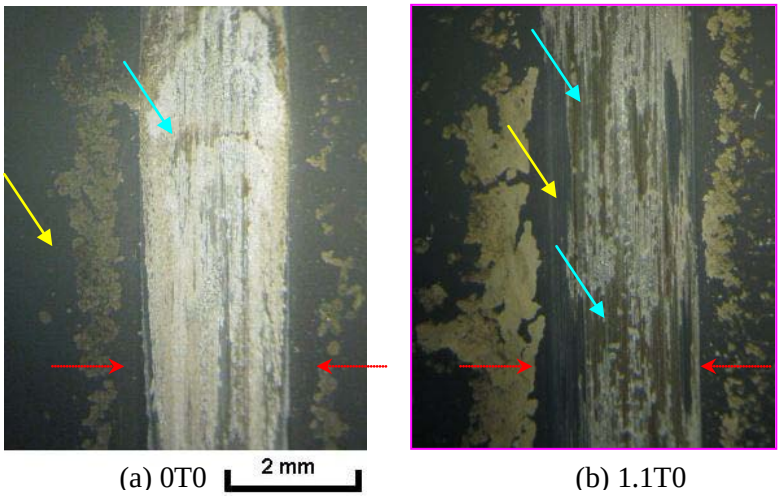

(a) 0T0 (b) 1.1T0

(c) 1.1T45 (d) 1.1T90

: gray area, →: brown area, : measured line

Optical micrograph Wear track, 16x magnifications

Fig 5.2.5 Surface observation of uncoated plate specimen in cross sliding direction after $24x10^3$ strokes

These tests are different from the experimental conditions used in that the sliding wear test is not carried out in perpendicular magnetic field. Therefore, it is assumed that magnetic material is not trapped on the mild steel plate due to the effect of the magnetic field. Comparing, wear surfaces produced in the presence and absence magnetic field, it is seen that individual brown regions on wear surface under the presence of magnetic field are larger than those produced in the absence of magnetic field. Thus, it is possible to make a hypothesis as follows.

Firstly, fine iron particles are produced by abrasive action and, oxygen adsorption by these particles is accelerated due to the effect of magnetic field. The oxidized fine iron particles are estimated to be anti-ferromagnetic materials because the flash temperature is too low to form the ferromagnetic structure as the sliding contact test is carried out at low frequency. Secondly, the wear particles flow and pile up at the weak tangential traction regions. The regions are usually worn down by produced iron and silicon wear particles. Then the production of the oxidized iron particles decreases with a fall of the Hertzian contact pressure, while, the regions are worn down continuously. Finally, the brown region and the bulging disappear from the wear track. In summary, the bulging is formed by accumulation of anti-ferromagnetic material produced by oxidation at low temperature and the oxygen adsorption effect of the magnetic field.

5.2.5 Different magnetic field directions

In the rolling contact test, the demagnetization effect of magnetic field direction which is the opposite angle to the rolling direction it is proposed that it considerably weakens the magnetisation of the discs and influences the wear mechanism (Chikazumi 1964; Iida 2007 pp.119).

However, because the bottom plane of the permanent magnets is arranged toward the surface of the plate specimen, the sliding contact test is not subject to that proposition.

Basically, the different magnetic field directions influence the mild steel plate as follows. The domain wall displacement and the volume increase must slightly increase so that mild steel has single crystal face and is not easily magnetised (see section 2.4). Moreover, the effect of magnetic field is confirmed not to change the micro hardness of mild steel. Furthermore, a relationship between the magnetic field direction and the form of the delamination area is not established (see Figure 5.2.6). Therefore, it is postulated that the influence of the internal magnetic field can be negligible compared with the external magnetic field.

The external magnetic field removes the iron wear particles from the wear track, and the amount of iron wear particles removed is different for different magnetic field directions. Therefore, the different magnetic field directions influence the size of the real contact area, the mass loss and the surface roughness. However, for 1.1T0 and 1.1T45 fields a crack is found which becomes vertically elongated. The crack points to a large single iron wear particle being transfered to the wear surface. It is estimated that the delamination of transfer particle causes a raise of the surface roughness.

Besides, cracks in 1.1T90 field are not found in the delamination area, and mainly thick scratches are on the wear surface. Therefore, it is concluded that the magnetic field

direction increases mass loss and the surface roughness (see Figure 5.2.6).

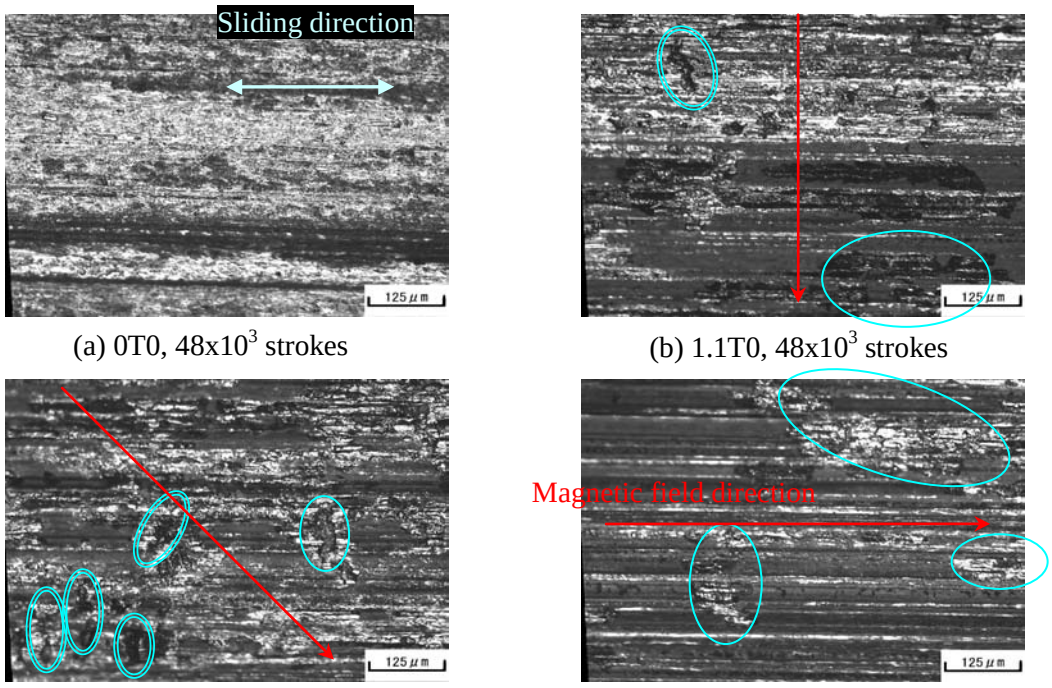

(a) 0T0, $48x10^3$ strokes

(b) 1.1T0, $48x10^3$ strokes

(c) 1.1T45, $48x10^3$ strokes

(d) 1.1T90, $48x10^3$ strokes

Fig 5.2.6 Surface observations of uncoated plate after $48x10^3$ strokes, 200x magnification blue single circle indicates delamination area, blue twice circle indicates cracks.

5.2.6 Questions

Micro hardness of mild steel in the presence of horizontal magnetic field is not changed. However, it is not considered to be applicable to magnetised iron wear particles. For example, if the mild steel plate is in presence of a horizontal magnetic field, the magnetisation field is flowing from the plate to the steel ball. Thus, when an iron wear particle transfers to the wear surface of the plate, it is expected to be caused by that.

It seems that the flow of intensity of magnetic field is similar with vertical magnetic field. Thus, the effect of vertical magnetic field may affect the internal structure of the plate and the iron particle at the minute region where it is nearby the contacting section. In other words, the internal structure change at the minute region reduces the micro hardness. Therefore, it may be the factor increasing the transfer of particles to the wear surface and thus enhancing the delamination area on wear surface.

5.3 Influence of magnetic field on sliding contact for carbon steel coating

5.3.1 Influence of mechanical characteristic by the magnetic field

- The magnetic field reduces the micro-Vickers hardness of the carbon steel coating by approximately 12%.

As mentioned earlier, the hardness of uncoated mild steel plate at the wear region is not affected by the presence of the magnetic field. In contrast, the carbon steel coating with lamellar micro structure consists of carbon steel layer and oxide steel layer. These layers have different crystallographic structures and are estimated to be different in the increment of the magnetic anisotropic energy and the magnetostrictive elongation. Magnetostrictive elongation means the deformation of magnetic material body as shown in Figure 5.3.1. Thus, the fall of hardness of the carbon steel coating suggests that the adhesive strength of the two layers is decreased by influence of magnetic field. In addition, it is attributed that the decline of temporary hardness is caused by deformation of domain structure immediately after it was put under the influence of magnetic field.

Kumagai et al.(1989) report that a similar phenomenon occurs by using alternating current magnetic field. It is the decrease of the hardness of magnetised ferromagnetic material, of uncoated specimen. Additionally, oscillations of domain walls increase mobile dislocation density by alternating current magnetic field. When magnetization is caused by direct current magnetic field it does not affect the change of hardness because domain wall does not displace. The idea, that the alternating current magnetic field

oscillates the *domain* walls and increases mobility of dislocation density and seems reasonable. However, the magnetic field in this study is similar with direct magnetic field. Thus, the lamellar structures of the thermal spay coating, which has sandwich structure consists of oxide layer and steel layer, is believed to be subjected to the phenomena.

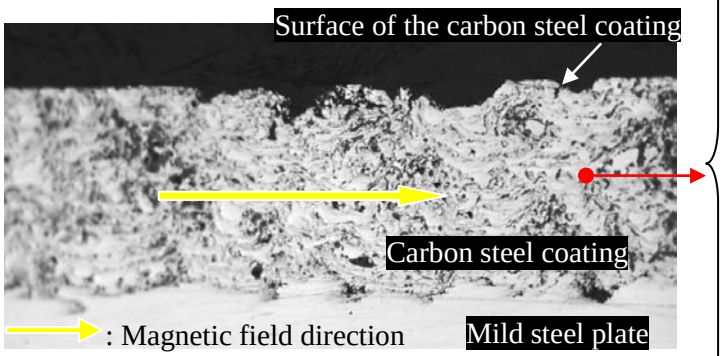

Fig 5.3.1 Cross section of carbon steel coating
Thickness of a carbon steel layer is about 4 - 5μm.

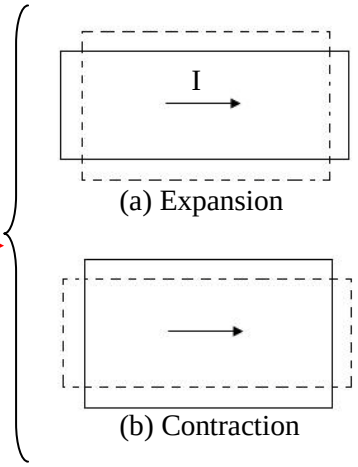

Fig 5.3.2 Deformation of magnetic material body, carbon steel layer and oxide steel layer
I: Intensity of magnetization

5.3.2 Magnetic field effect on carbon steel coating wear

The effect of the magnetic field on the sliding contact of carbon steel coating, and austenite stainless steel coating can be summarized as follows:

- Magnetic field influences the carbon steel coating by a significant decrease of the mass loss and a fall of the surface roughness. Furthermore, it produces a minute wear particle.
- Wear debris produced in the presence and absence of magnetic field consists of oxide iron particles, thus, it is not certain that the effect of oxygen adsorption take place.

The existence of the oxide iron particles suggests that they underwent from severe wear to mild wear process and acceleration of the adsorption oxygen to the oxide film (Hirazuka 1986). Thus, it was suspected that effect of external magnetic field induces the oxidative wear. However, this has not been confirmed by analysis results that the effect of the magnetic field under experimental conditions used induces oxidative wear. In addition, the surface observation of the wear track provides evidence that the oxidative wear did not occur (see Figure 5.3.3). Compared with the wear surface on the ball under absence of magnetic field, there are thinner scratches and delamination areas on the wear surface, as shown in Figure 5.3.3. In addition, the wear surface on the plate specimen under magnetic field appears to have a black region, which is assumed an oxide layer. Thus, it can be said that a progress of wear takes place in the space between steel layer and oxide steel layer. The carbon steel layer wears slowly because an initial crack occurs in oxides surrounding it.

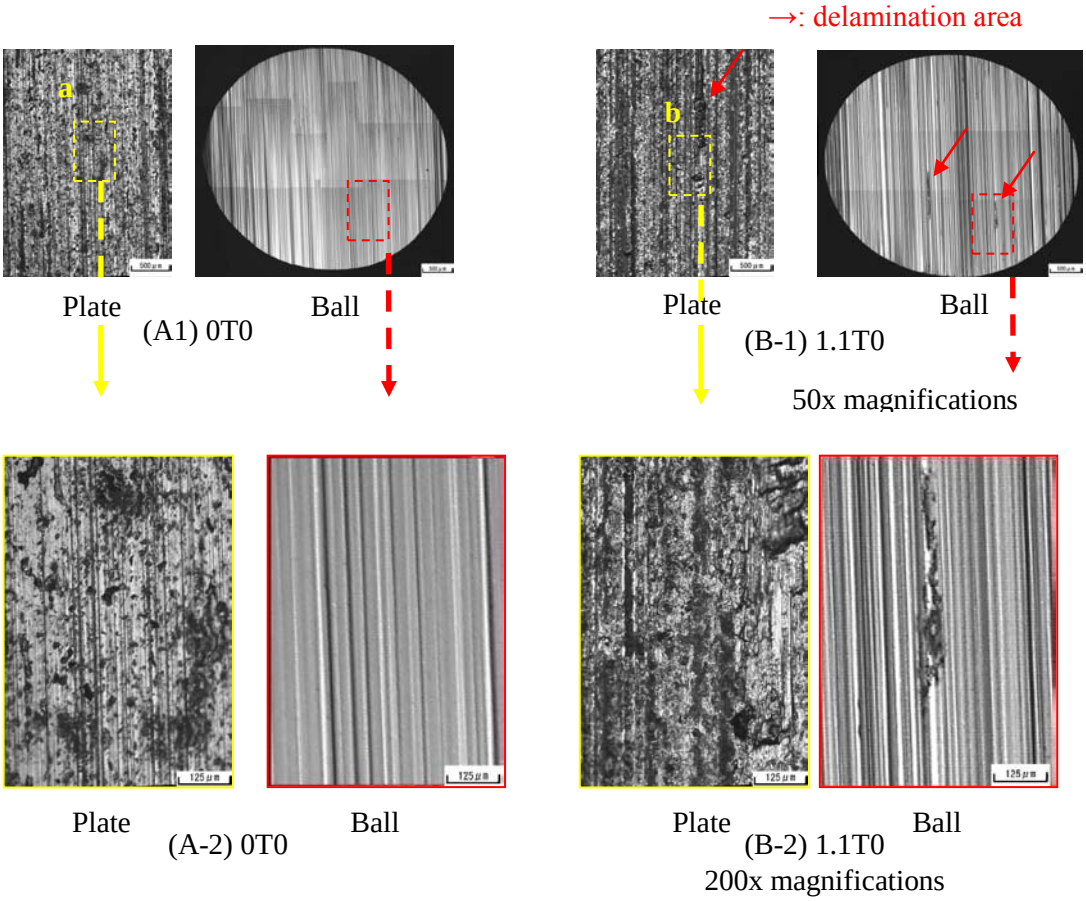

Fig. 5.3.3 Surface observation of the wear surface after $168x10^3$ strokes

5.3.3 Suggested wear mechanism for carbon steel coating in magnetic field

1. The carbon steel coating suffers a decline in hardness immediately after it is placed in the magnetic field.
2. Sliding contact creates a weak point in maximum shear stress distribution within the carbon steel coating under magnetic field; thus, adhesion strength in a space between layers reduces because of the increment of the magnetic anisotropic energy and the magnetostrictive elongation.
3. Sliding contact creates a downward initial crack from a contact surface to the top oxide layer as indicated the location in Figure 5.3.4 (a).
4. The primary crack propagates along a space between layers.
5. The primary crack develops and connects with a subsurface crack where a second layer may be located.
6. Some developing cracks reach the surface and a wear particle is released.
7. The wear undergoes a gradual decrease in the contact area of carbon steel coating. As a result, the contact area appears as a gentle uneven surface and mainly oxide layer (see Figure 5.3.4(b)).

Fig 5.3.4 Mecl el coating

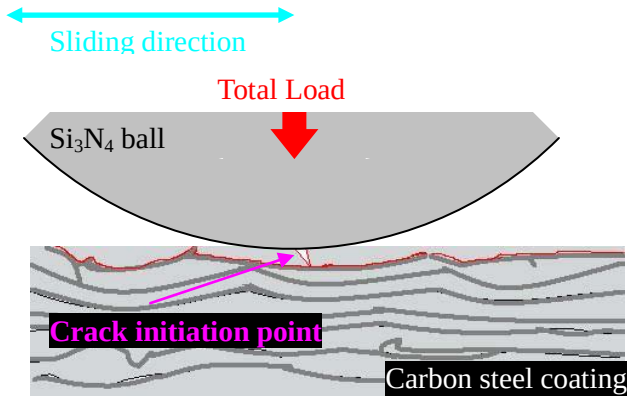

(a). Crack initiation point

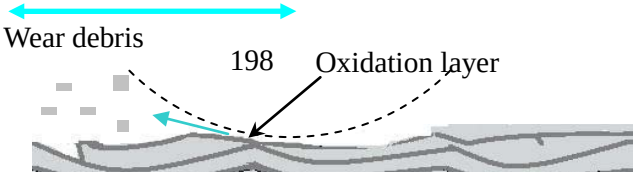

5.4 Effect of magnetic field on lubricated sliding contact

The presence of magnetic field contributes to the wear reduction of lubricated sliding contacts however it does not improve the surface roughness on the wear surface of plate specimen. The question now arises: what was the reason that the redaction of mass loss and the fall of the surface roughness did not happen in the presence of magnetic field? Two factors are offered by experimental results to clarify the cause. One is the iron wear particles removal by the magnetic field from the contact area while the magnetic field influences the wear debris contained in the lubricant. The other factor is lubricated wear mechanism in the presence of magnetic field as it generates delamination area on the wear track of plate specimen only in presence of magnetic field. Additionally, the strength of magnetic flux density is also related to that.

5.4.1 Influence of lubricant by the magnetic field

Generally speaking, generally, adsorption of surface-active substance changes the deformation behaviour of nonferrous metals. In addition, if surface electrical charge on the wear surface of Si_3N_4 ball is nonexistence, Macmillan et al (1974) showed that the fluidity of lubricant is improved due to higher surface tension. Also, there is a reduction of the friction coefficient with the greatest hardness. Therefore, it is postulated that the reduction of mass loss of counter plate specimen is caused by the influence of magnetic field on the electrical charge of the wear surface of Si_3N_4 ball.

The calcium sulphonate surfactants covering the surface of the plate specimen form protective film can be reinserted and reformed to region where the protective film is loose, after the protected surface was worn down by abrasive wear. However, the jagged wear surface region is not protected from oxidation because the calcium sulphonate

surfactants are not inserted at the region (Scherge et al 2006). Therefore, the jagged delamination region is the oxygen state that is easily adsorbed.

5.4.2 Magnetic field effect on wear of lubricated and uncoated surface

It is postulated that the shallow delamination area generation is caused by lack of the calcium sulphonate surfactant at the contact interface. The calcium sulphonate surfactants prevent adsorption of oxygen to the wear surface and wear particles. If the calcium sulphonate surfactants do not cover the wear particles and the surface of specimen, it is estimated that iron wear particles are attracted to the wear surface of the plate specimen. Then, the tangential load creates the shallow delamination area and scratches on the wear track of plate specimen. In particular, the delamination region may be easily oxidised to be increase the surface reactivity of the plate by magnetising it as shown in Figure 5.4.1(Yamamoto and Gondo 1987). The oxidation layer of the delamination area has not been identified by SEM analysis however it can be estimated by the existence of oxidised iron wear particles as shown in Figure 4.3.11 and 4.3.12. Furthermore, transfer particles on the wear track produced in the presence of magnetic field were found as shown in Figure 5.4.2. In addition, it is attributed that the lubricated sliding wear caused the delamination area of elongate shape by the inclusion of the wear debris.

While the influence of magnetic field reduces the mass loss of plate under lubricated sliding, however, high magnetic flux density reduced the effectiveness of wear reduction compared with low magnetic flux density and produced the delamination area on the wear track as a whole. These evidences suggest that the strength of magnetic flux density relates to the trapping iron wear particles. Therefore, the magnetic field

influences the mass loss and the surface roughness.

In the wear particle formation, lubricated sliding wear under the influence at the magnetic field produces the split flaky particles because the iron wear particles of the interface between specimens are compressed to a low angle by the tangential load.

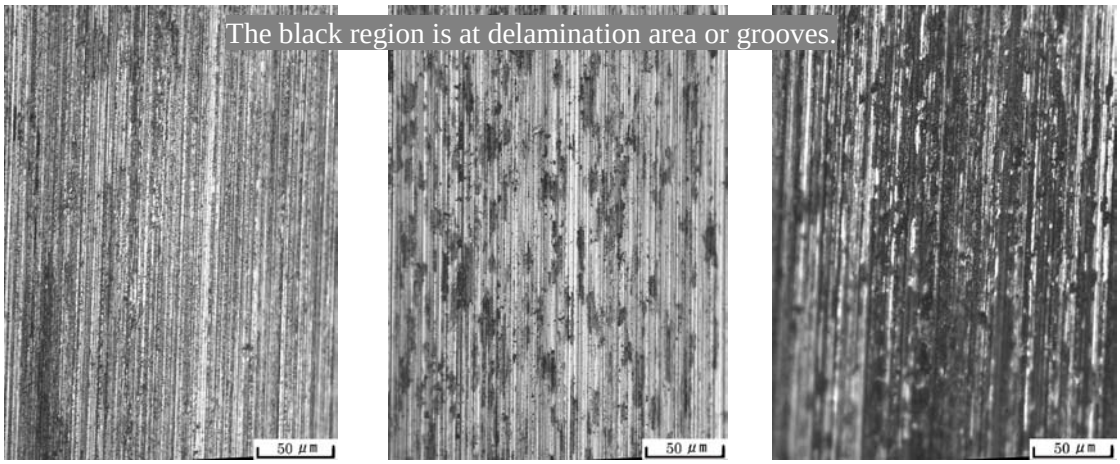

(a) 0T0 (b) 0.4T0 (c) 1.1T0

Fig 5.4.1 Delamination area on the wear track of plate after $72x10^3$ strokes

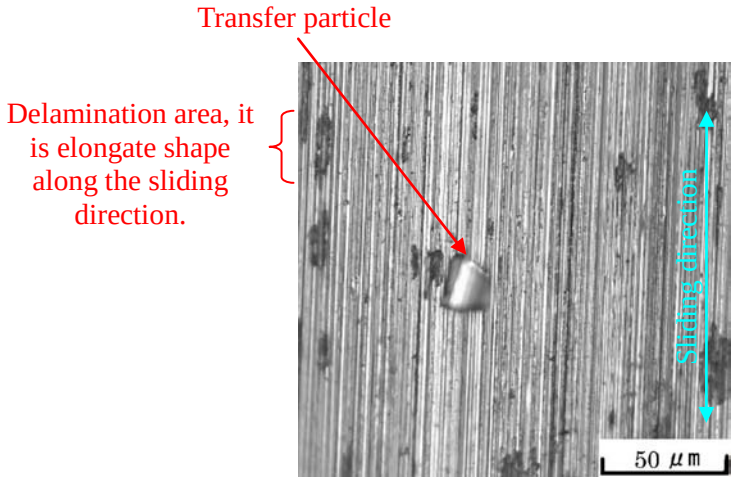

Fig 5.4.2 Transfer particle on wear track produced in low magnetic flux density

5.4.3 Suggested lubricated wear mechanism in the presence of magnetic field

In lubricated sliding contact without magnetic field, wear debris produced are not attracted by the surface of specimens in order to be covered individually by the calcium sulphonate surfactant. In addition, the production of wear debris is continuously accumulating at the interface, and thus accelerates the abrasive action. In the case without the magnetic field, oxygen is not adsorbed to the iron wear particles and the wear surface of the plate specimen.

On the other hand, magnetic field removes the iron wear particles from the interface region between specimens and increases the fluidity of lubricant. Lubricated sliding wear polishes the interface and produces fine wear particles. Also, iron wear particles produced are moved to the outside of wear track by the influence of magnetic field (see Figure 5.4.3a). Scratches on the plate specimen are mainly created by silicon wear particles. Iron wear particle creates a scratch and a delamination region. In addition, the wear surface created by magnetisation attracts the iron wear particles and induces the transfer of the wear particles (see Figure 5.4.3b). However, the calcium sulphonate surfactant (Ca^{++} and $CaCO^{3}$) does not reinsert itself to the delamination region, hence, it is estimated that the region is oxidised. The wear with magnetic field is decreased comparing to that without magnetic field because wear debris are removed from interface region by magnetic field. High magnetic flux density increases the transfer particles on the wear surface of plate specimen. The surface of plate specimen mainly consists of jagged delamination regions and as a result, wear increases.

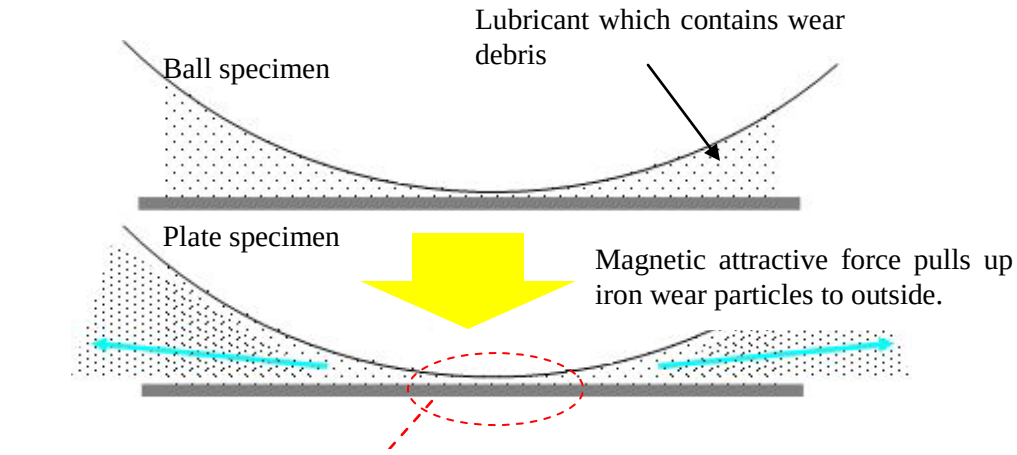

(a) Under presence of magnetic field

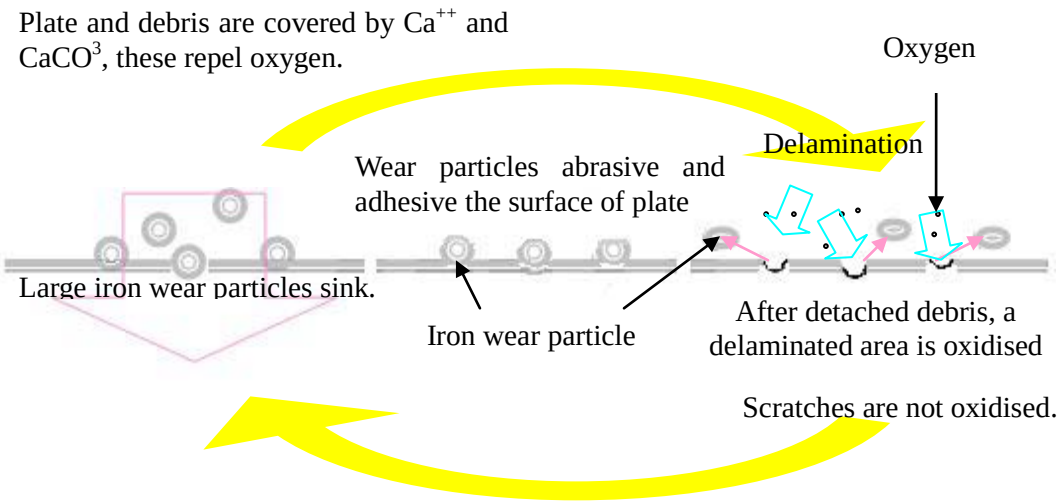

Ca^{++} and $CaCO^3$ adsorb plate and debris and are lost along with body debris**.**

The oxidised delamination region causes wear reduction.

(b) Detail description of the lubricated wear mechanism in presence of magnetic field

Fig 5.4.3 Recommendation of lubricated wear mechanism in the presence of magnetic field

5.5 Effect of magnetic field on high frequency sliding contacts

5.5.1 Comparison between low frequency and high frequency dry sliding experiment

First of all, it is necessary to outline common points between low frequency dry sliding wear experiment and high frequency sliding contact experiment in order to understand the influence of the magnetic field with the high frequency sliding. In sliding test using machine A and B, low frequency without magnetic field alters the surface roughness on the wear track of the plate specimens. The cause can be demonstrated at different frequencies which are 0.3 and 1.75 Hz. However, the surface roughness of the wear track shows a stable tendency (see Figure 5.5.1). And results in adhesive wear transition evidenced by observations of the wear track. Thus, it is assumed that it does not influence sliding wear in the presence of magnetic field. Experimental measurements of surface roughness show a significant different tendency revealed by further tests (see Figure 5.5.1b). It is estimated that the intensity of magnetic field is weak in contact regions shown in Table 5.5.1. Therefore, it is quite likely that the influence of magnetic field on tribological characteristics is small compared with the wear test in presence of magnetic field carried out using test machine A.

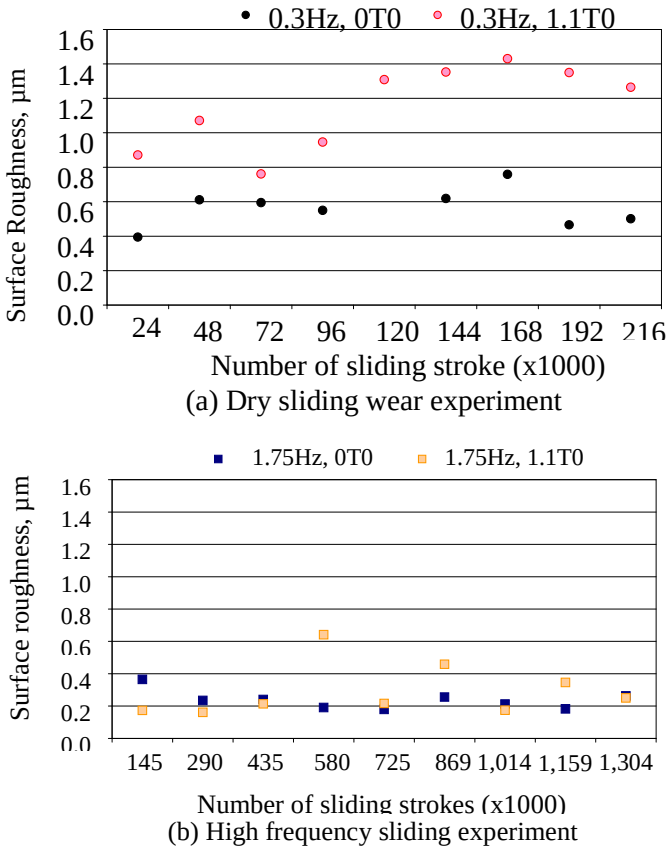

Fig 5.5.1 Surface roughness of plate at low frequency

Table 5.5.1 Magnetic flux density *B* (T) of contact surface or nearby contact surface which uses rare earth magnets, are indicated in Figure 5.5.2

Sliding wear test	Combination of test specimen	A	B	C	D	E
Machine A	Si_3N_4 ball vs. Mild steel plate	0.0001	0	0.92	0	0.0001
Machine B	Si_3N_4 ball vs. Mild steel plate	0	0.33	0.20	0.18	0
	Steel ball vs. Mild steel plate	0	0.25	0.24	0.20	0

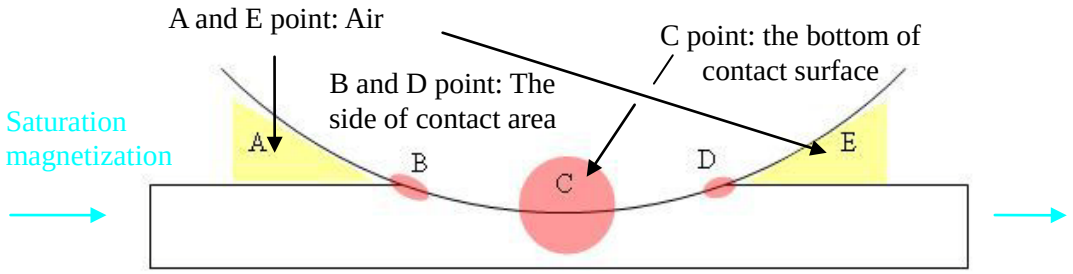

Fig 5.5.2 Distribution map of magnetic flux density at nearby contact surface

5.5.2 Influence of magnetic field combined with high frequency sliding

Using the paramagnetic ball and the ferromagnetic plate, the increase of sliding frequency at the presence of magnetic field is compared with the sliding contact in the absence of magnetic field. Firstly, it brought a larger change in the topography of the wear track. In an intermediate frequency, the oxidation formation on the wear track of the plate specimen appears at high magnetic flux density. However, it is estimated that the formation of brittle oxide layer on the surface is facilitated by the presence of magnetic field because of a deeper wear track. Thus, it is assumed that the influence of magnetic field is manifested by the formation of brittle oxides such as FeO (Stachowiak 2005 p.588).

In addition, magnetic field with the high frequency sliding lowered the surface roughness of the wear track on the plate specimen. Furthermore, it is assumed that high frequency sliding is associated with the mild (oxidative) to severe (adhesive) wear transition reported by Hirazuka et al (1989). In that connection, Zaidi et al (2007) also report the enhancement of the ferromagnetic oxide by carrying out tests on the magnetised sliding contacts with perpendicular magnetic field direction.

Therefore, it is possible to say that high frequency sliding is enhancing the adsorption of oxygen to oxide iron such as FeO because the mild wear is associated with the formation of protective oxides such as Fe_3O_4 (Stachowiak 2005 p.588).

In conclusion, it can be said that the increase in sliding frequency reduces, in principle, the mass loss and lowers the surface roughness of the plate specimen in the presence of magnetic field.

If that is the case, it is justified to say that external magnetic field enhances chemisorptions activity by oxygen and the ferromagnetic material as reported by

Hiratsuka and Sasada (1986). The external magnetic field in high frequency sliding contacts has negligible effects on the wear debris on the wear track. Also, the intensity of magnetisation flow toward the ball from the contact surface of the plate specimen is low (see Table 5.5.1 and Figure 5.5.2). Thus, it is supposed that the influence of internal magnetic field induces the enhancement of the chemisorptions activity of oxygen on a ferromagnetic material.

5.5.3 Wear debris behaviour in the presence of magnetic field

35 degree orientation of the magnetic field combined with high frequency shows increasing wear trend and decreasing *Ra* value. Besides, it forms different appearance of wear surface forward on plate specimen. For instance, it is fine particles aligned in the same direction or it is the black region formation as shown in Figure 4.4.11 to 4.4.13. Thus, it is estimated that these results are attributed to the magnetic field controlling the behaviour of wear debris in the contact area. In other words, it is helping to explain the influence of the magnetic field on the contact area and to elucidate why different magnetic field orientations contribute to forms different appearances of wear track.

In sliding contact of ferromagnetic materials couples at low sliding frequency, the accumulation layer of striped pattern of a wide line was formed on the wear track in the absence of the magnetic field. However, the wear track in the presence of magnetic field is covered in narrow lines consisting of the iron oxide spreading linearly in the sliding direction (see Figure 4.4.23 and 4.4.25).

Therefore, these observations may provide evidence linking the magnetic field to the wear debris behaviour that oxide iron wear particles are moved or attracted toward the permanent magnets along the lines of magnetic force. In other words, it is possible to

say that the magnetic field aligns wear particles, which are estimated to be iron or oxide iron, parallel to wear side of the magnetic field direction.

Meanwhile, high frequency sliding combined with the magnetic field covers the contact area of the plate with oxidised iron caused by gathering oxide iron wear particles (see Figure 4.4.24, 4.4.25 and 5.5.3). It arranges lines of magnetic force through the accumulation of the oxide iron wear particles from the plate specimen in the vertical direction. Therefore, it is estimated that piled oxide iron wear particles did not form a striped pattern.

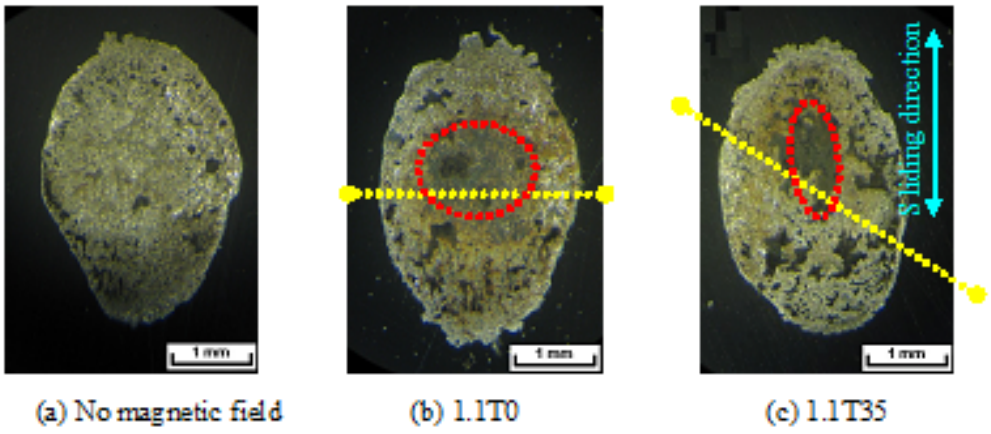

Fig 5.5.3 Comparison of piled wear debris up on the central wear track of the plate specimen, which was produced by the sliding contacts test of paramagnetic/ferromagnetic couples sliding at high frequency

Furthermore, the formation of black or white region consisting of the silicon and iron can be explained based on the reasoning mentioned above. The magnetic field improves the fluidity of wear debris between the contact areas in order to align iron wear particles to the 35 degrees orientation of the magnetic field. Furthermore, the phenomenon may cause rotary motion of silicon wear particles and may be associated with the formation of a dent indicated in Figure 5.5.4. The white and black region formation process is

explained briefly in the next section.

In conclusion, the presence of the magnetic field leads the iron wear debris toward the permanent magnets and alters the fluidity of the wear debris.

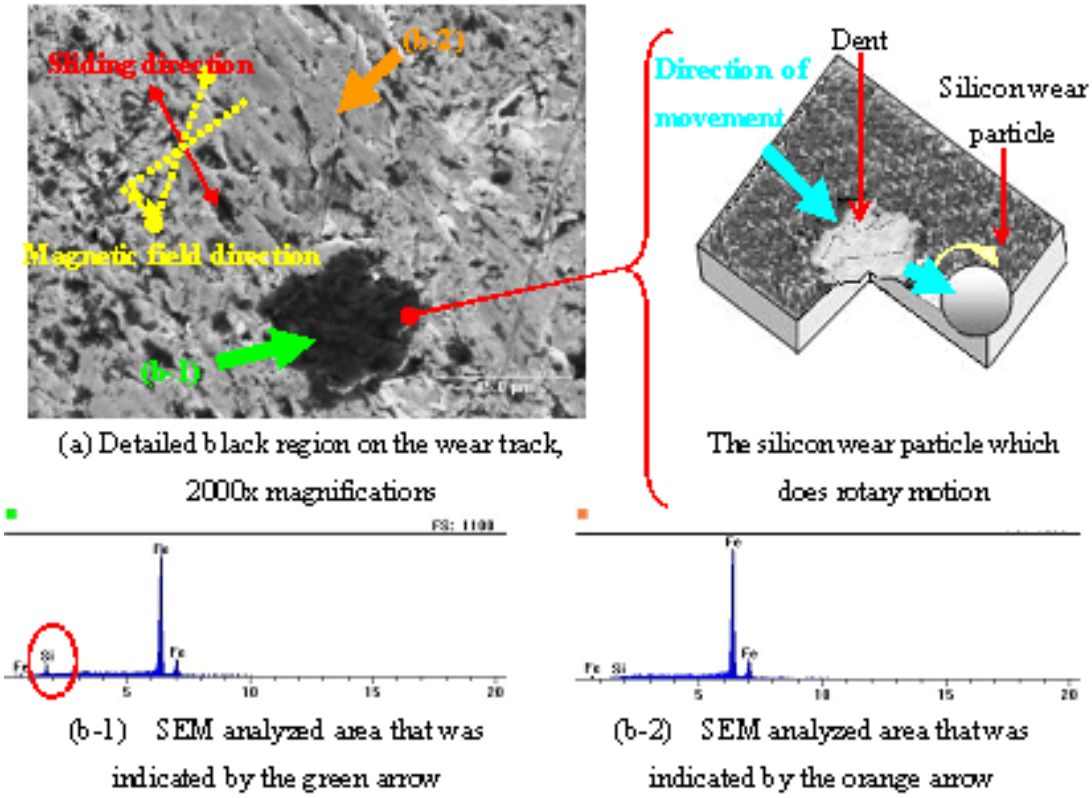

Fig 5.5.4 Detailed black region on the wear track, low frequency sliding contact combines with 35 degree orientation of magnetic field

5.5.4 Suggested mechanism for high frequency sliding contacts in the presence of magnetic field

The mechanism for 0 and 35 degree orientations of magnetic field has common features. Iron wear particles are attracted by the permanent magnets and move along in the magnetic field direction. Meanwhile, silicon wear particles move along in the sliding direction. In other words, the 0 degree orientation of magnetic field forms a right angle to the sliding direction. Thus, the movements of silicon wear particles are hindered by

the interference of iron wear particles being attracted in the magnetic field direction.

Low sliding frequency with magnetic field (see Figure 5.5.5)

At first, the grits, which are forward by silicon wear particles detached from wear surface of the ball specimen, remove the oxide film from the contact area without causing interference with underlying iron (Stachowiak 2005 p.580). However, the movement of grits is interfered with by the iron wear particles. Then, the angle of the pressure changes due to the decrease of the movement of the wear debris forward by grits. Finally, the grits are stuck into the contact area.

Meanwhile, the 35 degree orientations of magnetic field smoothes the movement of wear debris. Therefore, it is estimated that the frictional coefficient is lower compared with 0 degree orientation of magnetic field. Finally, it rolls the grits, and it makes plenty of dents in the contact area by the rolling movement of grits.

Intermediate sliding frequency with magnetic field

The influence of the intermediate sliding frequency with magnetic field consists in that the increase in the frequency grows in thickness of the oxide film (Stachowiak 2005 p.582). On the other hand, some of detaching oxide iron wear particles are piled up for surface asperities of the contact area of the plate specimen and makes the bulge. The bulge is deformed by opposite surface asperities.

In 35 degree orientation of magnetic field plenty of small bulges are formed in the contact area of plate specimen because the bulges are not removed by the grits. On the other hand, the grits cause the rolling movement and make the dents in the contacting asperities. Finally, wear track is created which has plenty of deformed bulge and dents.

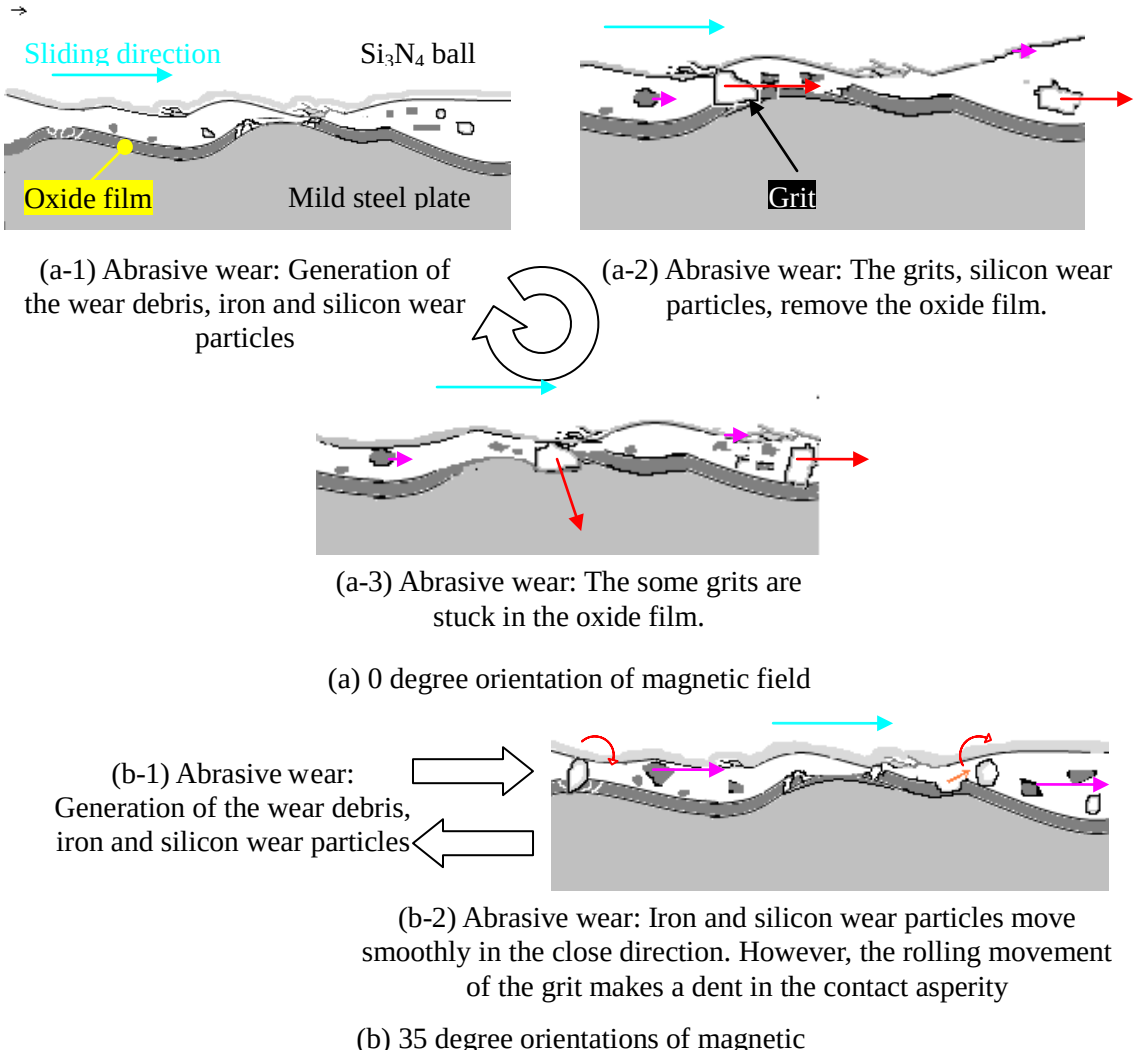

Fig 5.5.5 Mechanism of the low frequency sliding contacts with the magnetic field, the red and purple arrows denote movement behaviour of the grit or iron wear particles.

High sliding frequency with magnetic field

At first, 0 degree orientation of the magnetic field combined with high frequency produces fine wear debris consisting of magnetised oxide iron wear particles and silicon wear particles. Then, the iron oxide wear particles are piled up and a bulge is formed. Finally, the size of the bulge is expanding by the piled iron wear particle and sliding contact. The reason, is that the presence of magnetic field enhances chemical adsorption activity of iron wear particles or oxide iron wear particles and oxygen. Accumulation of magnetised iron oxide particles is tracking the iron wear particles.

For 35 degrees orientation of the magnetic field smooth wear surface and clear lines of the bulge aligned with the sliding direction are formed.

References for chapter 5

Chikazumi, C., (1964) “Physics of magnetism” John Wiley & Sons, Inc

Hirazuka, K., Sasada, T. and Norose, S., (1986) The Magnetic Effect on The Wear of Metals, *wear 110*. pp.251-261.

Hiratsuka, K., Saito, H. and Sasada, T., (1989) The Acceleration of the Severe-mild Wear Transition by the Application of a Magnetic Field, Japanese Society of Iridologist vol.34, 6, pp.430_436.

Iida, Y., Stolarski, T, A. and Sato, K., (2007) Surface damage resulting from rolling contact operating in magnetic field, *JOURNAL OF PHYSICS D: APPLIED PHYSICS Phys. 40*, pp.7629–7637.

Iida, Y., (2007) The Effects of Magnetic Fields on Rolling Contact Fatigue Wear,
A thesis submitted for PhD, Mechanical Engineering, School of Engineering and Design, Brunel University, Pp80-81, 119.

Kumagai, K., Suzuki, K. and Kamiya, O., (1993) Study on Reduction in Wear due to Magnetisation, *Wear*, Vol.162-164, pp.196_201.

Kumagai, K. and Kamiya, O., (1997) Effects of Magnetization on Wear, *Tribology transactions vol 40*, 4, pp.621-626.

Macmillan, N, H., Huntington, R, D. and Westwood, A, R, C., (1974) Chemomechanical control of sliding friction behaviour in non-metals, *Journal of Materials Scienece Volume 9, Number 5*, pp.697_706.

Mansori, M, El. and Paulmier, D., (1999) Effects of selective transfer on friction and wear of magnetised steel-graphite sliding couples, *Applied surface science144-145*, pp.233_237.

Sato, K., Stolarski, T, A. and Iida, Y., (2000) The effect of magnetic field on fretting wear, wear 241, pp99_108.

Sasada, T., Hiratsuka, K. and Saito, H., (1993) Adsorption of Surrounding Gas Molecules on Pure Metal Surfaces During Wear Processes, *Wear*, Vol.135, pp.251_264.

Scherge, M., Martin, M, J. and Pohlmann, K., (2006) Characterization of wear debris of systems operated under low wear-rate conditions *Wear* 260. pp.458_461.

Stachowiak, G, W., (Gwidon W.) (2005) Engineering tribology / Gwidon W. Stachowiak and Andrew W. Batchelor., Oxford: Butterworth-Heinemann, c2005. pp.580, 582, 588_589.

Yamamoto, Y. and Gondo, Seigo., (1987), “Effect of a magnetic field on boundary lubrication”, *Tribology International Volume 20*, Issue 6, pp.342_346.

Zaidi, H., et al (2007) Magnetotribology of ferromagnetic/ferromagnetic sliding couple, Wear 263, pp.1518_1526.

Chapter 6 Conclusions and future study

6.1 Conclusions

The goal of the study is to clarify the effect and mechanism of horizontal magnetic field on tribological characteristics of sliding contacts through experimental approach. In order to accomplish the goal, experimental investigations have been carried out for different directions of magnetic field, different contact conditions, different surface modifications and two sliding frequencies, using a ball-on-plate contact configuration.

In conclusion, the influence of the magnetic field on dry sliding contacts weakens internal structure of uncoated ferromagnetic material however strengthens the following:

- Removal of the iron wear particles from contact zone
- Chemical adsorption activity of iron wear particles or oxide iron wear particles

In low sliding frequency combined with magnetic field,

- The prevailing wear mechanism is weakened due to the low frictional temperature, and the removal of bulging
- The bulging formation process is postulated to be generated by accumulation of anti-ferromagnetic material produced by oxidation at low temperature and the oxygen adsorption due to influence of the magnetic field.
- When the orientation of the magnetic field is parallel to the sliding direction, it increases the surface roughness and the mass losses of the uncoated plate.

In high sliding frequency combined with magnetic field,

- Adsorption of the oxygen is enhanced by oxide iron such as FeO because the mild wear is associated with the formation of protective oxides such as Fe_3O_4.
- The increase in sliding frequency reduces, in principle, the mass loss and lowers the surface roughness of the plate specimen in the presence of magnetic field.
- Enhanced chemisorption activity of oxygen by a ferromagnetic material due to the influence of internal magnetic field is postulated.

In 35 degree orientation of the magnetic field combined with high sliding frequency,

- Trend in wear rate is increased and the *Ra* value is decreased.
- Distinctly different appearances of wear surface are created on plate specimen.
- It is estimated that these results are attributed to the magnetic field controlling the behaviour of wear debris in the contact area. In addition, the presence of the magnetic field alters the “fluidity” of the wear debris, movement.

In dry sliding contact on the carbon steel coating in the presence of magnetic field,

The fall of the micro-Vickers hardness of the carbon steel coating by approximately 12% temporarily in the presence of magnetic field suggests that the adhesive strength of the interface between oxide layer and steel layer is decreased by the influence of magnetic field.

- Magnetic field influences the carbon steel coating by a significant decrease of the mass loss and a fall of the surface roughness.
- Minute wear particles are generated.
- The progress of wear takes place at the interface between steel layer and oxide steel layer.
- The carbon steel layer wears slowly because initial cracks occur in oxides surrounding it.

In the presence of magnetic field on lubricated sliding contact,

- The jagged delamination region is the oxygen state that is easily adsorbed.
- Acceleration of the abrasive action is caused.
- Mass loss of plate specimen is reduced.

It is postulated that the above is caused by the influence of magnetic field on the electrical charge of the wear surface of Si_3N_4 ball.

6.2 Recommendations for Future Work

This study revealed some problems that remain to be solved, and also it identified new problems.

At first, the bulging formation process which is occurring at low sliding frequency combined with magnetic field is not completely clarified whether the accumulation consists of anti-ferromagnetic material or not. If it is anti-ferromagnetic material, it may be effective in preventing of surface activity. Therefore, it is indescribable to identify the mechanism of bulge formation in detail.

This study postulates that the presence of the magnetic field alters the behaviour of wear debris. The increased “fluidity” of wear debris movement may contribute to the control wear. Moreover, this phenomenon might induce the variation of frictional coefficient. Therefore, the frictional coefficient under different orientations of magnetic field ought to be evaluated in experimental research combined with computer simulation.

Finally, the decrease in the adhesive strength of the interface between oxide layer and steel layer of the carbon steel coating is suggested. However, it has not been fully demonstrated through the evaluation of tribological characteristics of a sliding contact under the influence of magnetic field. Therefore, it is suggested that the elucidation of the crack formation mechanism related to the dislocations behaviour into the internal structure of the carbon steel coating is undertaken.

Appendix A Fabrication procedure of thermal spray coating plate and general properties of thermal spray process

Firstly, the surface of a mild steel plate, it is countersunk rectangular plate, was stuck masking tape on both end of the plate. Secondly, it was sandblasted on the surface of the plate in order to clean. The surface treatment was to blow the alumina powder with pressure of 0.6 MPa. Thirdly, the plate was preheated by plasma to improve the adherent strength of coating and substance. Then, it was sprayed iron or austenite stainless steel by APS process. The characteristic of the powders are shown in Figure A-1 and A-2 and Table A-1 and A-2. The parameter of the APS is shown in Table A-3. Finally, the surface was polished with the abrasive paper (number 2400) before the plate specimen is used in sliding contact experiment. The thickness of thermal spray coating respectively is approximately 250 μm. Surface treatment by blast processing and APS process were conducted at Ashikaga Institute of Technology in Japan.

Table A-1 Carbon steel powder, thermal spray powder

Company	: Sulzer Metco
Name	: SULZER 4052 Low Alloy Steel Powder
Magnetism	: Strong
Chemistry	: Fe 1.4Cr 1.4Mn 1.2C
Particle Size	: -38 +15μm (-400 mesh +15μm)
Morphology	: Spheroidal, Gas Atomized

Table A-2 Austenite stainless steel powder, thermal spray powder

Company	: Praxiar
Name	: FE-101
Magnetism	: weak
Chemistry	: Bal.Fe, Cr17%, Ni12%, Mo2.5%
Particle size	: -45 μm/+15μm (-325 mesh/+15μm)
Morphology	: Atomized

Table A-3 Parameters of APS process for iron coating and stainless steel coating

Contents	Unit	Preheating	Thermal spray
Arc gas	(psi), Argon	50	50
Auxiliary gas	(psi), Helium	-	100
Current	(A)	500	800
Power voltage	(V)	30	32
Hopper feed	(rpm)	-	1
Carrier gas	(psi), Argon	-	40
Spraying distance	(mm)	-	100
Spraying pitch	(mm/pitch)	-	4
Traverse speed	(mm/s)	8000	8000

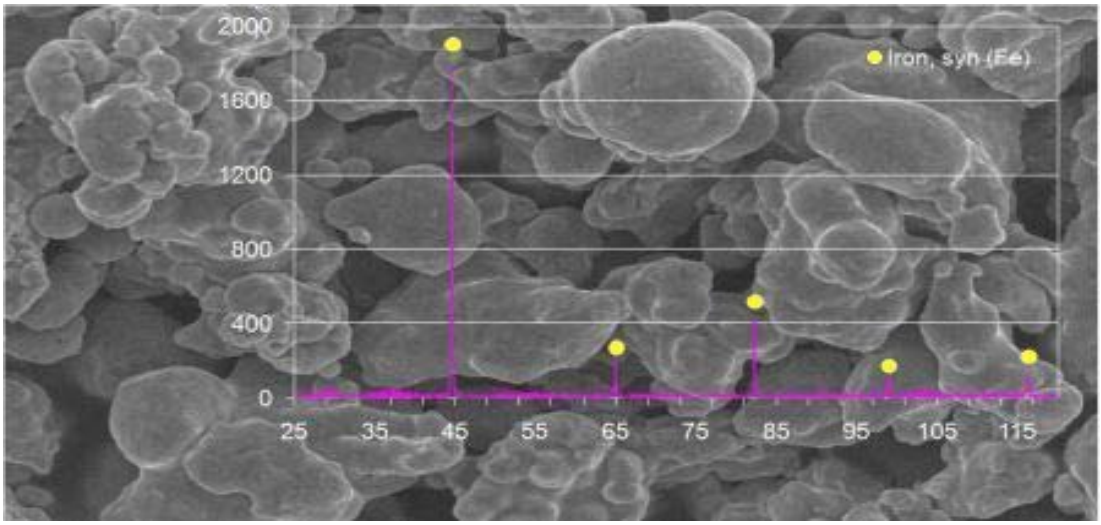

Fig A-1 XRD pattern and SEM image of the carbon steel powder

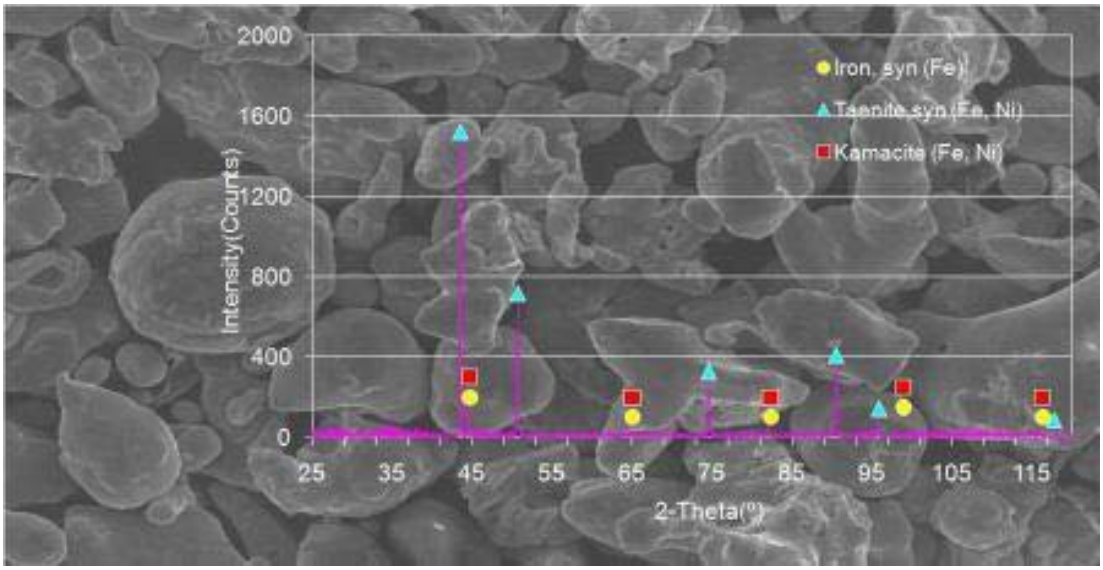

Fig A-2 XRD pattern and SEM image of the austenite stainless steel powder

Appendix B Parameters for the flow of the magnetic field inside the test plate is analysed by Finite Element Analysis (FEA) (see section 3.5)

Table B-1 Model scale (single section)

Zone	Element type	Material property	Size, mm
Air (vacuum)	Plane13	Relative permeability =1	-
Magnetic body, Mild steel	Plane13	B-H loop (see table2)	Length 6, width 5
Magnet, Rare earth magnet	Plane13	Relative permeability =1 Coercive Force of flux density=-873105[A/m]	Length 4, width 20
Infinite boundary	Infin110	Relative permeability =1	-

Notice; defined element types was set up 'Axisymmetric'.

Table B-2 size of elements, (unit is metre)

Zone	Field		Parameters	
Air	X1	X2	-0.5	0.5
	Y1	Y2	-0.5	0.5
Si_3N_4 and Steel ball	Diameter		D=0.00635	
	Positioning		X=0, Y=-0.0001, Z=0	
Specimen	X1	X2	-0.0125	0.0125
	Y1	Y2	-0.00635	-0.00935 (actual data is -0.00835)
Magnet A	X1	X2	0.0175	0.0375
	Y1	Y2	-0.00635	-0.00235
Magnet B	X1	X2	-0.0175	-0.0375
	Y1	Y2	-0.00635	-0.00235

Mesh size
Zone of Si_3N_4 ball is smart size, fine 1. Other zones are fine 6.